Characterization of the Baeyer-Villiger monooxygenase MoxY and closely-related homologues from *Aspergillus flavus*

Carmien Tolmie

Submitted in fulfilment of the requirements for the degree

Magister Scientiae

In the Faculty of Natural and Agricultural Sciences

Department of Microbial, Biochemical and Food Biotechnology

University of the Free State

February 2014

Supervisor: Dr. D. J. Opperman

Co-supervisor: Prof. M. S. Smit

Declaration

It is herewith declared that this dissertation submitted for the degree Magister Scientiae (Biochemistry) at the University of the Free State is the independent work of the undersigned and has not previously been submitted by her at another university or faculty. Copyright of this dissertation is hereby ceded in favour of the University of the Free State.

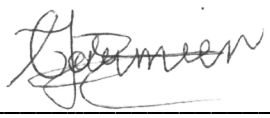

_____

Carmien Tolmie
Department of Microbial, Biochemical and Food Biotechnology
Faculty of Natural and Agricultural Sciences
University of the Free State
South Africa

Acknowledgements

The financial assistance of the National Research Foundation (NRF) towards this research is hereby acknowledged. Opinions expressed and conclusions arrived at, are those of the author and are not necessarily attributed to the NRF.

I would like to thank Prof. C.A. Townsend (John Hopkins University, USA) for supplying the synthetic [1'-^{2}H]HVN

A special thanks to my supervisor, Dr. D.J. Opperman, for his continuous support and enthusiasm – without him this study would not have been possible. Also, to my co-supervisor, Prof. M.S. Smit, for her input in the project.

To my family, friends and lab colleagues, thank you for patiently standing me by through the good times and the bad, and for providing me with the necessary humour and support.

Table of Contents

List of Tables

Chapter 4

Appendix

List of Figures

Non-SI Abbreviations

Abs	Absorbance
$ACMO_{gordon}$	Acetone monooxygenase from *Gordonia sp*. TY-5
AFB_1	Aflatoxin B_1
AFB_2	Aflatoxin B_2
AFG_1	Aflatoxin G_1
AFG_2	Aflatoxin G_2
AFM_1	Aflatoxin M_1
$AKMO_{pseudo}$	Aliphatic ketone monooxygenase from *Pseudomonas fluorescens* DSM50106
ARS	Agricultural Research Service
ATP	Adenosine triphosphate
AVF	Averufin
AVN	Averantin
AVNN	Averufanin
BCA	Bicinchoninic acid
Bicine	*N,N*-Bis(2-hydroxyethyl)glycine
BLAST	Basic Local Alignment Search Tool
bp (b)	Basepairs
BSA	Bovine serum albumin
BV	Baeyer-Villiger
BVMO	Baeyer-Villiger monooxygenase
$BVMO_{Af1}$	BVMO from *Aspergillus fumigatus*
$BVMO_{pseudo}$	BVMO from *Pseudomonas putida* KT2440
cAMP	Cyclic adenosine monophosphate
$CDMO_{rhodoc}$	CDMO from *Rhodococcus ruber* SC1
CDS	Coding sequence
CHES	2-(Cyclohexylamino)ethanesulfonic acid
CHMO	Cyclohexanone monooxygenase
$CHMO_{acinet}$	CHMO from *Acinetobacter sp.* NCIMB 9871 (*Acinetobacter calcoaceticus*)
$CHMO_{rhodoc}$	CHMO from *Rhodococcus sp.* HI-31
CoA	Coenzyme A
$CPDMO_{pseudo}$	Cyclopentadecanone monooxygenase from *Pseudomonas sp.* HI-70
$CPMO_{comamo}$	Cyclopentanone monooxygenase from *Comamonas* sp. NCIMB 9872
CTH	C-terminally His-tagged
CYP450	Cytochrome P450
Da	Daltons
DHDMST	Dihydrodemethylsterigmatocystin
DHHOMST	Dihydro-11-hydroxy-*O*-methylsterigmatocystin
DHOMST	Dihydro-*O*-methylsterigmatocystin
DHST	Dihydrosterigmatocystin
DMST	Demethylsterigmatocystin
DNA	Deoxyribonucleic acid

DNase	Deoxyribonuclease
dNTPs	Deoxyribonucleoside triphosphates
EBI	European Bioinformatics Institute
EDTA	Ethylenediaminetetraacetic acid
EST	Expressed sequence tag
$EtaA_{mycoba}$	BVMO from *Mycobacterium tuberculosis*
FAD	Flavin adenine dinucleotide
FAS	Fatty acid synthase
FID	Flame ionisation detector
FMN	Riboflavin 5'-monophosphate
FMO	Flavin monooxygenase
g	Gravitational force
GC	Gas chromatography
gDNA	Genomic DNA
$HAPMO_{pseudo}$	4-hydroxyacetophenone monooxygenase from *Pseudomonas fluorescens* ACB
HAVN	Hydroxyaverantin
HGT	Horizontal gene transfer
His-tag	$poly(His)_6$-tag
HIV	Human immunodeficiency virus
HOMST	11-hydroxy-*O*-methylsterigmatocystin
HVN	Hydroxyversicolorone
IMAC	Immobilised metal-affinity chromatography
IPTG	Isopropyl β-D-1-thiogalactopyranoside
K_{cat}	Catalytic constant
K_m	Michaelis constant
LB	Luria-Bertani
MKM_{pseudo}	Methyl ketone monooxygenase from *Pseudomonas veronii* MEK700
MFS	Major facilitator superfamily
MO1-MO24	BVMOs from *Rhodococcus jostii* RHA1
MOPS	3-(*N*-Morpholino)propanesulfonic acid
mRNA	Messenger RNA
MS	Mass spectrometry
MUSCLE	Multiple Sequence Comparison by Log-Expectation
MWCO	Molecular weight cut-off
NA	Norsolorinic acid
NAA	Norsolorinic acid anthrone
NAD^+	Nicotinamide adenine dinucleotide (oxidised)
NAD(H)	Nicotinamide adenine dinucleotide (reduced)
$NADP^+$	Nicotinamide adenine dinucleotide phosphate (oxidised)
NADP(H)	Nicotinamide adenine dinucleotide phosphate (reduced)
NCBI	National Center for Biotechnology Information
NMR	Nuclear magnetic resonance
OAVN	Oxoaverantin
OMST	*O*-methylsterigmatocystin
ORF	Open reading frame
$PAMO_{thermo}$	Phenylacetone monooxygenase from *Thermobifida fusca* YX
PCR	Polymerase chain reaction

PDA	Potato dextrose agar
PDB	Potato dextrose broth
PKS	Polyketide synthase
PNK	Polynucleotide kinase
RISC	RNA-induced silencing complex
RNA	Ribonucleic acid
RNAse	Ribonuclease
SAM	*S*-adenosyl-methionine
SDS-PAGE	Sodium dodecyl sulphate polyacrylamide electrophoresis
SEC	Size-exclusion chromatography
siRNA	Small-interfering RNA
$SMO_{rhodoco}$	Steroid monooxygenase from *Rhodococcus rhodochrous*
SMFMO	*Stenotrophomonas maltophilia* flavin monooxygenase
ST	Sterigmatocystin
TLC	Thin-layer chromatography
TIM-barrel	$(\alpha/\beta)_8$-barrel fold
Tris	2-amino-2-hydroxymethyl-propane-1,3-diol
tRNA	Transfer RNA
U	Units
USA	United States of America
UV	Ultraviolet
VA	Versicolorin A
VB	Versicolorin B
VHA	Versiconal hemiacetal acetate
VHOH	Versiconal
V_{max}	Maximum initial velocity
VOAc	Versiconol acetate
VOH	Versiconol
VONE	Versicolorone
WAG	Whelan and Goldman
YMA	Yeast mold agar

Chapter 1

Literature review

1.1. Aflatoxins – an introduction

Aflatoxins are a group of structurally-related, difuranocoumarin-derived mycotoxins produced as secondary metabolites by certain *Aspergillus* fungi (Klich, 2007). The four major aflatoxins are aflatoxin B_1 (AFB_1), aflatoxin B_2 (AFB_2), aflatoxin G_1 (AFG_1) and aflatoxin G_2 (AFG_2) (Fig. 1.1). The 'B' or 'G' designation is derived from the colour of fluorescence under UV light, blue or green, attributed to the presence of a cyclopentanone or lactone ring, respectively (Dutton, 1988). A double-bond in the terminal furan ring distinguishes series 1 from series 2 and results in the differential migration of the compounds during thin-layer chromatography (TLC).

Aflatoxins are mainly produced by fungi classified in the *Flavi* section of the genus *Aspergillus*, including *A. flavus, A. parasiticus, A. nomius*, *A. pseudotamarii* and *A. bombycis* (Peterson *et al*., 2001). However, several non-*Flavi* isolates have been shown to produce aflatoxins, including *A. ochraceoroseus* (Klich *et al*., 2003) and *A. rambelli* (Frisvad *et al*., 2005)*, Emericella venezuelensis* (Frisvad and Samson, 2004), and *E. astellata* (Frisvad *et al*., 2004). The aflatoxin production profiles of the fungi differ significantly with respect to the type of aflatoxin produced, as well as the quantities. *A. flavus* is the most common aflatoxigenic agricultural contaminant and infects numerous crops (Cary and Ehrlich, 2006). Consequently, *A. flavus* has very broad health and economic implications.

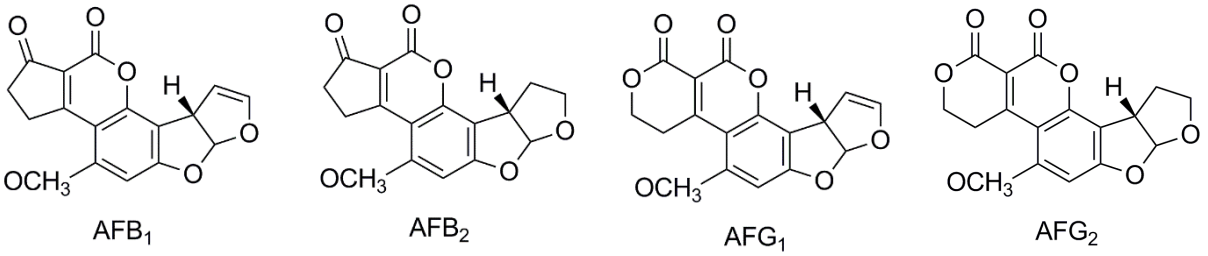

Figure 1.1. Structures of the four major aflatoxins, AFB_1, AFB_2, AFG_1 and AFG_2. The 'B' or 'G' designation is due to the colour of fluorescence under UV light – blue or green, while the '1' or '2' designation is due to the differential migration during TLC (Williams *et al*., 2004).

1.1.1. Impact of aflatoxin contamination on public health

Aflatoxins have been classified as class I carcinogens by the International Agency for Research on Cancer (IARC, 2002) and AFB_1 has been identified as the most potent naturally occurring carcinogen (Squire, 1981). The order of toxicity of the four major aflatoxins is $AFB_1 > AFG_1 > AFB_2 > AFG_2$ (Wogan *et al*., 1971). AFB_1 is oxidised by a liver cytochrome P450 to AFB_1-8,9-*exo*-epoxide that binds DNA to produce a DNA adduct which confers the mutagenic properties on the compound (Wild and Turner, 2002). Lactating mammals that ingest AFB_1 secrete an 11-hydroxylated form of AFB_1, aflatoxin M_1 (AFM_1) into the breast milk (Galvano *et al*., 1996) that carries both the bisfuran and lactone ring originating from AFB_1 which conveys the carcinogenic properties on the compound.

Exposure to aflatoxin causes the disease aflatoxicosis (Williams *et al*., 2004), which can be divided into two categories - acute and chronic aflatoxicosis. Acute aflatoxicosis is due to the ingestion of a large dose of aflatoxin, which results in direct liver damage and illness or death. Chronic aflatoxicosis is caused by long-term exposure to sub-lethal doses of aflatoxins, which result in cancer, mainly of the liver, immune suppression, as well as retardation of growth (Gong *et al*., 2002).

Aflatoxin contamination of foodstuffs are especially of concern in developing countries, including the majority of Africa (Wagacha and Muthomi, 2008). Fungal growth and the consequent mycotoxin contamination of crops is prevalent due to poor agricultural practices and post-harvest treatment of foodstuffs, including storage, transportation, marketing and processing. The majority of households rely on crops susceptible to aflatoxin contamination such as corn as a staple food, resulting in a lifelong exposure to aflatoxins. In addition, co-incidence of hepatitis B with chronic aflatoxicosis increases the risk for hepatocellular carcinoma up to tenfold. Infection with the hepatitis B virus is common for people in the Sub-Saharan regions of Africa (Turner *et al*., 2000; Wagacha and Muthomi, 2008).

1.1.2. Economic impact on the agricultural sector

The agricultural sector suffers severe economic losses annually due to aflatoxin contamination. *A. flavus* and *A. parasiticus* infects a wide range of crops, including corn, peanuts, cotton and tree nuts (Woloshuk and Shim, 2013) and, as mentioned, aflatoxin contamination of a dietary staple such as corn has a widespread impact. In 2006, it was estimated that aflatoxin contamination cost the corn

export markets at least 40 million US dollars in the United States of America (USA), China and Argentina, with a total annual loss of corn amounting to 163 million US dollar in the USA (Wu, 2006).

Farm animals fed with aflatoxin-contaminated grain also suffer the carcinogenic and immunosuppressive effects. These animals often have a shortened lifespan and increased mortality rate due to secondary infections by bacteria, fungi and viruses (Wagacha and Muthomi, 2008). Also, the stunting of growth by aflatoxins results in a decreased weight and yield for meat farms. In the case of dairy cows, the effect of aflatoxin contamination is propagated by the secretion of AFM_1 into milk, which may render the milk unfit for consumption.

In South Africa, the legal limit on AFB_1 in all foodstuffs is 5 $\mu g.kg^{-1}$ with a total aflatoxin limit not exceeding 10 $\mu g.kg^{-1}$ (South African Medical Research Council, 2009). In milk, the maximum level of AFM_1 is 0.05 $\mu g.L^{-1}$. However, as is the case in many developing countries, aflatoxin levels cannot be completely regulated due to the large number of rural farmers and informal markets.

1.2. The aflatoxin biosynthesis gene cluster

Aflatoxins are produced in a polyketide pathway that requires multiple enzymatic steps (Fig. 1.3). Sterigmatocystin (ST) is a penultimate precursor for aflatoxins in the aflatoxin biosynthesis pathway and is produced as a final product by certain fungi, including *A. nidulans* and *A. versicolor* (Schroeder and Kelton, 1975), due to a truncated version of the aflatoxin biosynthesis pathway. ST production proceeds via the same intermediates involved in aflatoxin biosynthesis and the corresponding metabolic conversions are catalysed by homologous enzymes in the aflatoxin and ST pathways.

Over the past three decades, multiple molecular techniques have been employed to investigate the genes involved in aflatoxin and sterigmatocystin biosynthesis (Yu *et al*., 2004). These include the complementation of UV-irradiated mutants blocked in an aflatoxin production step, gene knock-out experiments, purification of native enzymes involved in aflatoxin biosynthesis, as well as recombinant expression of candidate genes. Mutants with impaired aflatoxin biosynthesis genes could often be identified by an altered colony morphology and pigmentation due to the accumulation of coloured aflatoxin intermediates. Key to the exploration of aflatoxin and ST biosynthesis genes was the use of relatively simple aflatoxin/sterigmatocystin inducing and non-inducing media, accomplished by adding a media component such as sucrose (inducing) or peptone (non-inducing) (Shima *et al*., 2009). The induction of aflatoxin/sterigmatocystin production coincides

with the transcriptional activation of the biosynthesis genes and this was used as a criterion for the preliminary identification of the genes involved in the synthesis of aflatoxin/sterigmatocystin.

The genes involved in the aflatoxin biosynthesis pathway are clustered together in a 70 kb region in *Aspergillus parasiticus* (Fig. 1.2). In 2004, the aflatoxin gene cluster had been completely sequenced by Yu and co-workers (GenBank accession number AY371490). The cluster contains 28 open reading frames (ORFs) (Ehrlich, 2009) and is delineated by a sugar utilisation cluster at the 3'end (Yu *et al*., 2000a). The aflatoxin biosynthesis gene clusters of fungi belonging to the *Flavi* section are conserved with respect to the gene positions, order and direction of transcription (Carbone *et al*., 2007).

The naming of the identified aflatoxin biosynthesis genes was based on either the substrate converted or the enzymatic function of the gene, often leading to a single gene receiving multiple names. Yu and co-workers (2004) proposed a new naming scheme for the aflatoxin biosynthesis genes, as *aflA* to *aflY* from the 5' – 3' end. However, the *aflJ* designation existed before the new naming scheme, leading to confusion as to whether the gene corresponds to the new scheme, therefore replacing *estA*, or to the old scheme and being replaced by *aflS.* In 2009, additional open reading frames (ORFs) encoding hypothetical proteins (*hypA – hypE*) were identified in the aflatoxin biosynthesis cluster (Ehrlich, 2009). Expressed sequence tag (EST) data indicated that both *hypB* and *hypC* were only expressed under aflatoxin-inducing conditions (Ehrlich *et al*., 2010).

Similar to the aflatoxin biosynthesis gene cluster, the genes responsible for ST biosynthesis in *A. nidulans* are clustered in a 60 kb region containing 25 ORFs (GenBank accession number U34740.1) (Brown *et al*., 1996). The genes were designated from *stcA* to *stcX* from 5' - 3' of the cluster, with the exception of the pathway regulator, *aflR.* Although the gene products of the sterigmatocystin and aflatoxin biosynthesis clusters are homologous, the gene order and direction of transcription of the two clusters differ (Fig. 1.2). Both clusters contain structural genes encoding the enzymes involved in the biosynthesis pathways, as well as functional genes encoding transcription factors.

The transcription of the genes in the aflatoxin and sterigmatocystin gene clusters are under the positive control of the aflatoxin-pathway associated transcription factor, AflR, which is encoded by the *aflR* gene present in the gene clusters. The *aflR* gene was initially identified as *afl-2* from *A. flavus* as a locus complementing multiple steps in an aflatoxin-blocked mutant (Payne *et al*., 1993) and as *apa-2* from *A. parasiticus* as a locus enhancing the function of existing steps in the pathway (Chang *et al*., 1993). The amino acid sequence contains a sequence-specific DNA-binding binuclear zinc cluster domain ($Zn(II)_2Cys_6$), a common feature of fungal transcription factors, and is similar to

the GAL4 transcriptional activator from *Saccharomyces cerevisiae* regulating the genes involved in galactose metabolism (Woloshuk *et al*., 1994). Recombinantly expressed and purified AflR from *A. nidulans* (Fernandes *et al*., 1998) and *A. parasiticus* (Ehrlich *et al*., 1999) was demonstrated to bind to the palindromic sequence 5'-TCG(N_5)CGA-3' found in the promoters of the cluster genes, with the putative consensus sequence of (5'-TCGSWNNSCGR-3'). The recognition sequence is typically located from position -80 to -600 with the majority ranging from -100 to -200 relative to the translational start site (Yu *et al*., 2004).

Microarray studies with *ΔaflR A. parasiticus* mutants identified 23 genes that were differentially expressed when compared to the wild-type strains (Price *et al*., 2006). Twenty one of the genes were located in the aflatoxin biosynthesis cluster (including *nadA*, *hypA* and *hypB*, previously not assigned to the cluster), while two of the genes are located outside the biosynthesis cluster (*hlyC* and *niiA*). Therefore, AflR regulates the expression of both genes belonging to the aflatoxin biosynthesis cluster, as well as non-cluster genes.

The *niiA* gene is located within the nitrate assimilation cluster. Interestingly, a consensus AflR binding site was identified 2.3 kb upstream from the *niiA* transcription start site, within the coding region of an adjacent gene *niaD*. The *hlyC* gene is located 1.5 Mb from the aflatoxin gene cluster with a putative AflR binding site 1.8 kb upstream from the coding region. No role for *hlyC* has been identified in aflatoxin production, however, it may contribute to pathogenicity in the *Aspergilli.* Although only two non-cluster genes regulated by AflR were identified, these studies were performed using only 40 % of the transcriptome of *A. flavus*, therefore, it is possible that other genes may be regulated by AflR as well.

AflR acts in an autoregulatory fashion by binding to an AflR-recognition sequence in its own gene, *aflR* (Chang *et al*., 1995b; Ehrlich *et al*., 1998). As expected, *aflR* is critical for the biosynthesis of aflatoxins, with *ΔaflR* mutants displaying a loss of aflatoxin production (Price *et al*., 2006). The overall identity between AflR from *A. parasiticus* and *A. nidulans* is only 31 %, however, the amino acids most likely to bind DNA in the metal-binding domain are functionally identical in the two proteins (Ehrlich *et al*., 1999). Also, AflR isolated from *A. flavus* is able to support transcription from the sterigmatocystin biosynthesis cluster in an *aflR* deletion mutant of *A. nidulans* (Yu *et al*., 1996).

The *aflJ* gene has also been implicated in the transcriptional activation of genes belonging to the aflatoxin biosynthesis cluster. The *aflJ* gene is located adjacent to the *aflR* gene with the two genes transcribed divergently. The genes share a 0.7 kb intergenic region, but are transcribed from

independent promoters. Meyers and co-workers (1998) demonstrated that *ΔaflJ* disruption mutants accumulated aflatoxins at 100-fold lower levels and could not convert exogenously supplied pathway intermediates to aflatoxins, although transcripts of the pathway genes were present.

Yeast two-hybrid assays indicated that AflJ interacts with the pathway regulator AflR, and not with the pathway enzymes directly (Chang, 2003). The presence of both *aflR* and *aflJ* demonstrates a synergistic effect in the transcriptional activation of pathway genes and leads to higher levels of pathway intermediates (Du *et al*., 2007). Also, overexpression of the *aflJ* gene enhanced the levels of aflatoxin production significantly. However, *aflJ* alone is not sufficient for the transcriptional activation of the cluster genes and is also not a prerequisite for transcriptional activation of the genes by AflR. AflJ does not control the transcription of *aflR,* while two authors reported contradicting results on the regulation of *aflJ* by AflR (Chang, 2003; Du *et al*., 2007).

The homologous gene in the *A. nidulans* gene cluster displayed 30 % identity and 40 % similarity to AflJ from *A. flavus* (Du *et al*., 2007). No significant homology to any known proteins or peptides were found in numerous databases and no functional domains or motifs could be identified. Finally, the role of AflJ in the pathway is not clear. The lack of a DNA-binding domain and the physical association of AflJ and AflR suggests that AflJ binds to the transcriptional activator AflR to enhance transcription of the pathway genes.

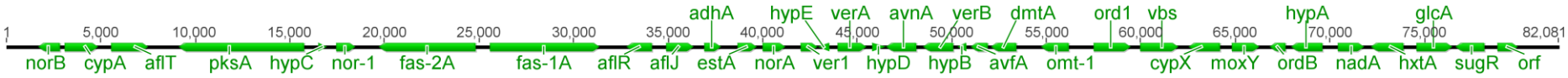

A. parasiticus aflatoxin biosynthesis gene cluster (GenBank accession number AY371490)

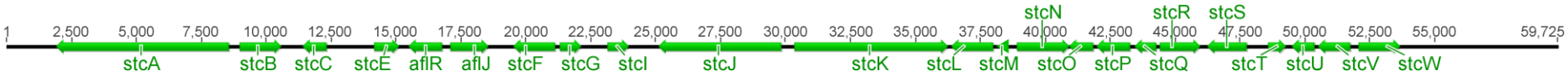

A. nidulans sterigmatocystin biosynthesis gene cluster (GenBank accession number U34740.1)

Figure 1.2. The aflatoxin and sterigmatocystin biosynthesis gene cluster in *A. parasiticus* and *A. nidulans*. The direction of the arrow indicates the direction of transcription, while the size of the arrow is representative of the gene size. The scale is length in basepairs (bp).

1.3. The aflatoxin biosynthesis pathway

The synthesis of aflatoxins proceeds via four major stages (Ehrlich, 2009): firstly, an anthraquinone polyketide is synthesised; secondly, the C_6 'tail' of the anthraquinone moiety is subjected to a series of oxidations; thirdly, the anthraquinone moiety is oxidised and then rearranged to produce the xanthone, ST, and lastly, the xanthone undergoes oxidation and rearrangement to produce the aflatoxin coumarin nucleus. The genes involved in the majority of the enzymatic steps have been identified, although the conversion of certain metabolites remain obscure. The aflatoxin (and sterigmatocystin) biosynthesis pathway is depicted in Fig. 1.3 and each enzymatic step will be discussed in detail. The homologous genes in the aflatoxin and sterigmatocystin gene cluster catalysing the corresponding metabolic steps, as well as the percentage of amino acid identity and similarity, are given in Table 1.1.

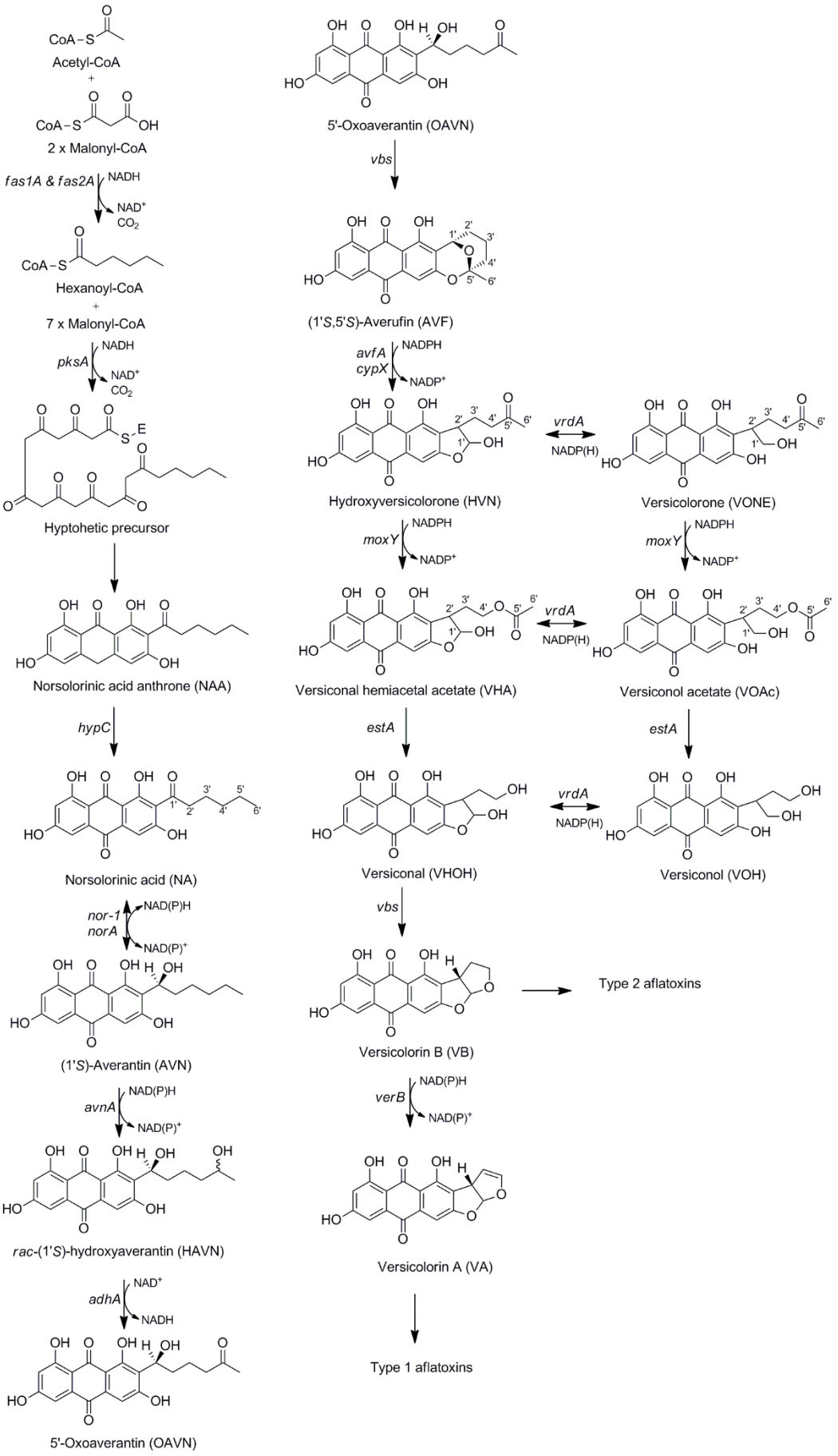
Acetyl-CoA
2 x Malonyl-CoA
fas1A & fas2A
NADH
NAD+
CO2
Hexanoyl-CoA
7 x Malonyl-CoA
pksA
Hyptohetic precursor
Norsolorinic acid anthrone (NAA)
hypC
Norsolorinic acid (NA)
nor-1
norA
NAD(P)H
NAD(P)+
(1'S)-Averantin (AVN)
avnA
rac-(1'S)-hydroxyaverantin (HAVN)
adhA
5'-Oxoaverantin (OAVN)
vbs
(1'S,5'S)-Averufin (AVF)
avfA
cypX
NADPH
NADP+
Hydroxyversicolorone (HVN)
vrdA
NADP(H)
Versicolorone (VONE)
moxY
Versiconal hemiacetal acetate (VHA)
Versiconol acetate (VOAc)
estA
Versiconal (VHOH)
Versiconol (VOH)
Versicolorin B (VB)
Type 2 aflatoxins
verB
Versicolorin A (VA)
Type 1 aflatoxins

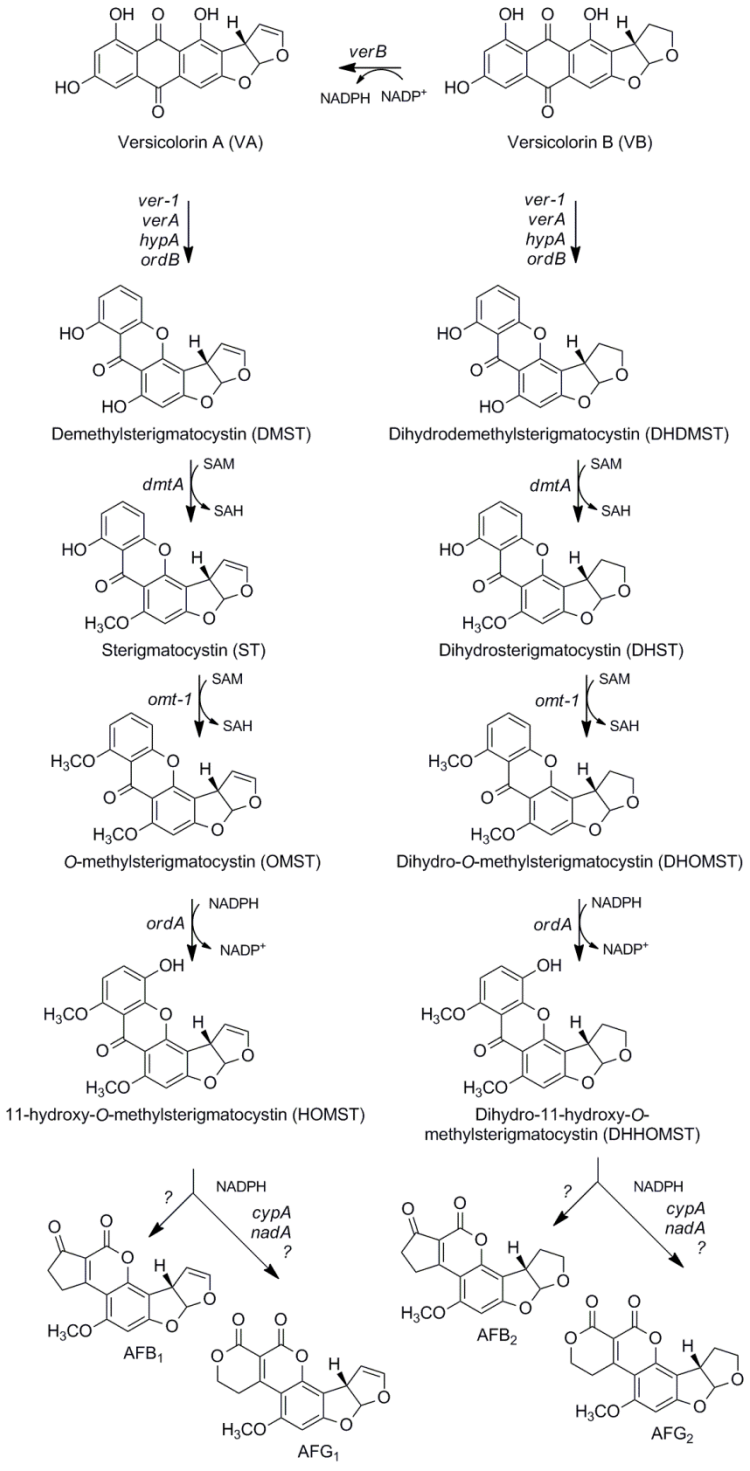

Figure 1.3. The intermediates of the aflatoxin biosynthesis pathway and the genes encoding the enzymes catalysing the metabolic conversions. Sterigmatocystin biosynthesis proceeds via the same metabolic intermediates. '?' indicates that the enzymatic steps are not yet fully clarified and additional genes may be involved in the conversion (Udwary *et al*., 2002; Yabe *et al*., 2003; Yabe and Nakajima, 2004).

Table 1.1. Genes involved in aflatoxin biosynthesis in *A. parasiticus* and *A. flavus* with the corresponding homologues in the sterigmatocystin pathway of *A. nidulans*. The alternative naming scheme of the aflatoxin biosynthesis genes are given, with synonyms of the genes indicated in parenthesis. Genes are located in the aflatoxin or sterigmatocystin biosynthesis gene cluster, unless specified otherwise. The percentage of amino acid identity and similarity between the homologues of the aflatoxin and sterigmatocystin biosynthesis pathways are indicated (where determined), as well as the function of the gene in the synthesis pathway. Adapted from Yu and co-workers (2004).

Aflatoxin Gene (synonyms)	**Alternative naming scheme**	**Sterigmatocystin Gene (synonyms)**	**% aa identity (homology)**	**Function**
aflR (*afl-2; apa-2*)	*aflR*	*aflR*	33 (45)	Transcriptional regulator
fas-1A (*hexB*)	*aflB*	*stcK*	45 (62)	Hexanoate synthase (β subunit)
fas-2A (*hexA*)	*aflA*	*stcJ*	47 (61)	Hexanoate synthase (α subunit)
pksA (*pksL1*)	*aflC*	*stcA (pksST)*	60 (72)	Polyketide synthase
hypC	*aflCa*	*stcM*	28 (50)	NAA → NA
nor-1	*aflD*	*stcE*	56 (73)	NA → AVN
norA	*aflE*	*stcV*	66 (82)	(NA → AVN)
avnA (ord-1)	*aflG*	*stcF*	71 (84)	AVN → HAVN
adhA	*aflH*	*stcG*	64 (83)	HAVN →OAVN
avfA	*aflI*	*stcO*	55 (66)	AVF → HVN
cypX	*aflV*	*stcB*	61 (73)	AVF → HVN
moxY	*aflW*	*stcW*	69 (80)	HVN → VHA VONE →VOAc
estA	*aflJ*	*stcI*	50 (64)	VHA → VHOH VOAc → VOH
vbs	*aflK*	*stcN*	73 (86)	OAVN →AVF VHOH → VB
ver1 (ver1A)	*aflM*	*stcU (verA)*	90 (96)	VA → DMST VB → DHDMST
verA	*aflN*	*stcS (verB)*	64 (75)	VA → DMST VB → DHDMST
hypA	*aflY*	*stcR*	47 (72)	VA → DMST VB → DHDMST
ordB	*aflX*	*stcQ*	54 (68)	VA → DMST VB → DHDMST
dmtA (omtB)	*aflO*	*stcP*	75 (85)	DMST → ST DHDMST → DMST
omt-1 (omtA)	*aflP*			ST → OMST DMST → DHOMST
ord1 (ordA)	*aflQ*			OMST → AFB_1 and AFB_2 OMST → AFG_1 and AFG_2
cypA	*aflU*			OMST → AFG_1 and AFG_2
nadA				OMST → AFG_1 and AFG_2
norB	*aflF*	*stcV*	48 (68)	(uncertain)
vrdA	(Not located in cluster)	EAA66789		Hydroxylase in metabolic grid
aflJ	*aflS*	*aflJ*	34 (60)	Transcriptional activator
aflT	*aflT*			MFS transporter protein
hypB		*stcM*	27 (52)	(uncertain)
hypD		ENU34740 (not located in cluster)		(uncertain)
hypE		L27825 (not located in cluster)		(uncertain)

1.3.1. Synthesis of the anthraquinone moiety, norsolorinic acid

The anthraquinone moiety is produced in a polyketide pathway with the initial reactions analogous to that of fatty acid synthesis, but lacking the reduction and dehydration steps (Bennett and Christensen, 1983). The synthesis of a polyketide is catalysed by a polyketide synthase (PKS) where a starter unit, usually acetyl-CoA, is transferred as acetate to a thiol group in the active site of the enzyme (Dutton, 1988). The primer is sequentially elongated by the addition of acetate groups using malonyl-CoA as a donor molecule with the resulting loss of carbon dioxide.

The hypothetical structure of the norsolorinic acid precursor (Fig. 1.3) contains seven fully oxidised C_2 units and three fully reduced acetate units, which suggests a cooperation between a fatty-acid synthase (FAS) and a PKS (Hitchman *et al*., 2001). Hexanoyl-CoA had been implicated as a six-carbon starter unit in aflatoxin biosynthesis (Townsend *et al*., 1984). Thus, it was proposed that a FAS synthesises the hexanoate primer which is further elongated in an iterative fashion by a PKS (Hitchman *et al*., 2001). Two FAS-encoding genes, as well as a PKS gene, are located in the aflatoxin biosynthesis gene cluster. Evidence had been given in support of a physical association of the FAS and PKS involved in aflatoxin biosynthesis to create a large multi-functional enzyme (Watanabe *et al*., 1996).

1.3.1.1. Fatty acid synthesis of hexanoate

The *fas-1A* and *fas-2A* genes are located side by side in the aflatoxin gene cluster of *A. parasiticus* (Yu *et al*., 2004). The large *fas-1A* gene of 7.5 kb was found to complement a UV-generated mutant, *uvm8*, unable to produce either aflatoxins, or norsolorinic acid (NA) (Mahanti *et al*., 1996). The product of *fas-1A* shares a high degree of identity and similarity with the FAS1 proteins from *Saccharomyces cerevisiae* and *Yarrowia lipolytica,* which encode the β-unit of a FAS, and the amino acid sequence carries domains typically observed in the active sites of fungal FAS β-subunits (Hitchman *et al*., 2001). The *fas-2A* gene constitutes the α-subunit of the FAS and contributes the domains necessary for fatty acid synthesis in cooperation with Fas-1A. The FAS proteins encoded by *fas-1A* and *fas-2A* are collectively referred to as hexanoate synthase due to their dedicated role in synthesis of the hexanoate starter unit for aflatoxin biosynthesis.

1.3.1.2. Elongation of hexanoate by PKS

In two separate studies, a corresponding putative PKS gene involved in aflatoxin biosynthesis was identified in *A. parasiticus*, named *pksL1* (Feng and Leonard, 1995) and *pksA* (Chang *et al*., 1995a). *pksL1* was found to be identical to *pksA* and encoded a large transcript of 7 kb. The gene was identified as a putative PKS by the presence of an acyl carrier protein and synthase domain, characteristic of both PKS and FAS.

Gene disruption experiments indicated that PksL1/A was involved early in aflatoxin biosynthesis, prior to NA formation, as no aflatoxins or aflatoxin intermediates could be detected in *ΔpksL1/A* disruption mutants (Chang *et al*., 1995a; Feng and Leonard, 1995). PksL1/A contains amino acid sequence motifs common to PKSs and FASs, but lacked the domains necessary for the reduction of the *β*-keto group. Therefore, PksL1/A was designated a PKS rather than a FAS.

The *pksL1/A* gene displayed strong sequence similarity to both the *wA* and the *pksST* genes in *A. nidulans* (Yu and Leonard, 1995). Both polypeptides have been identified as a PKS, although their physiological roles differ. WA was responsible for pigment production in the conidial wall, while PksST, also designated as StcA (Brown *et al*., 1996), was involved in the production of ST and located in the sterigmatocystin biosynthesis gene cluster. *pksST/stcA* thus forms the biological counterpart for the *A. parasiticus* PKS gene in sterigmatocystin biosynthesis.

1.3.1.3. Conversion of norsolorinic acid anthrone to norsolorinic acid

Aromatic condensation of the "hypothetical precursor" (Fig. 1.3) yields norsolorinic acid anthrone (NAA), which is oxidised to produce norsolorinic acid (NA), the first stable intermediate in aflatoxin biosynthesis (Yabe *et al*., 1991b). Ehrlich and co-workers (2010) provided evidence that *hypC*, a gene which was identified by EST mapping as belonging to the aflatoxin gene cluster, encodes an anthrone oxidase. *hypC* was recombinantly expressed in *E. coli,* partially purified and assayed for activity against synthetic NAA. HypC was found to fully convert NAA to NA and was subsequently designated as an anthrone oxidase. Orthologs of HypC was found in the genomes of fungi producing metabolites derived from anthrones, including *stcM* of the sterigmatocystin biosynthesis cluster of *A. nidulans* (Brown *et al*., 1996). Comparison of the predicted amino acid sequences led to the identification of a putative active-site region that is similar to the active site found in bacterial anthrone oxidases. Conversely, *hypC* knockout mutants retained the ability to produce both NA and

aflatoxins (Ehrlich *et al*., 2010). Therefore, the conversion of NAA to NA does not absolutely rely on HypC. Under non-enzymatic conditions, NAA is oxidised to NA within 24 hours. Thus, NAA can be converted to NA either non-enzymatically, or the function of *hypC* can be complemented by a yet unidentified gene.

1.3.2. Oxidation of the C_6 tail

1.3.2.1. Oxidation of norsolorinic acid

NA is converted to averantin (AVN) by the product of *nor-1* in the presence of NADPH (Zhou and Linz, 1999), with strict stereospecificity for (1′*S*)-AVN (Yabe *et al*., 1993). Heterologously expressed Nor-1 was shown to catalyse the conversion of the 1'-keto group of NA to the 1'-hydroxyl group of AVN and thus functions as an NADPH-dependent alcohol dehydrogenase. Interestingly, the reaction required an unidentified 'helper' compound present in the cytoplasm of the *E. coli* host. Recombinant inactivation of *nor-1* produces mutants that accumulate NA and aflatoxins (Trail *et al*., 1994). Aflatoxin production is substantially decreased but not eliminated in *Δnor-1* mutants, indicating that the loss of Nor-1 can be bypassed by the use of an alternative enzyme. Incubation of the cytosolic fraction from *A. parasiticus* with racemic AVN and NADPH indicated that the reaction is reversible, utilising only (1′*S*)-AVN as substrate.

The product of the *norA* gene is also able to convert NA to AVN (Cary *et al*., 1996). The *norA* gene shares a high level of sequence similarity with the aryl-alcohol dehydrogenase from *Penicillium chrysosporium*, but not with the alcohol dehydrogenases as in the case of *nor-1.* Also, *norA* shares little sequence homology with *nor-1.* Not surprisingly, knock-out mutants of *norA* in *A. parasiticus* did not affect aflatoxin production significantly, which is most likely due to the presence of a functional *nor-1* gene.

1.3.2.2. Conversion of averantin to hydroxyaverantin

(1′*S*)-AVN is converted to hydroxyaverantin (HAVN) by the product of *avnA* in the presence of NADPH. Genetic disruption of *avnA,* also referred to as *ord-1*, resulted in the accumulation of AVN and a loss of aflatoxin production (Yu *et al*., 1997). Metabolite feeding studies indicated that the pathway was disrupted at the enzymatic step directly following AVN, as feeding of the mutant with

HAVN restored aflatoxin production. The *avnA* sequence encodes a protein which contains conserved motifs characteristic of cytochrome P450 enzymes (CYP450s), including the heme-binding motif crucial for the catalytic activity. Consequently, the *avnA* gene was designated as CYP60A1.

Incubation of microsomes with racemic AVN indicated that (1'*S*)-AVN was selectively converted to HAVN, which is produced as both diastereomers, (1'*S*, 5'*S*) and (1'*S*, 5'*R*) (Yabe *et al*., 1993), with a preference for NADPH over NADH (Yabe *et al*., 1991b).

1.3.2.3. Conversion of hydroxyaverantin to oxoaverantin

Conversion of HAVN to averufin (AVF) had been proposed to occur via two possible routes (Fig. 1.4). ^{13}C-radiolabelling studies indicated that the ether averufanin (AVNN) is an intermediate in aflatoxin biosynthesis (McCormick *et al*., 1987). Bhatnagar and co-workers (1992) suggested that AVNN, produced by dehydration of HAVN, is oxidised to AVF. On the other hand, the 5'-hydroxyl group of HAVN could be oxidised to a keto group to produce an open-chain configuration of AVF, which spontaneously cyclise to produce AVF (Yabe *et al*., 1991b). Both intermediates have been observed in fungal cultures, as well as metabolite feeding studies (Yabe *et al*., 1993; Yu *et al*., 1997). However, in metabolite feeding studies conducted by Yabe and co-workers (1991b), AVNN failed to produce either AVF or aflatoxins. Also, no dehydratase gene has been identified in the aflatoxin biosynthesis cluster, and no dehydratase activity, either non-specific or aflatoxin-associated, has been observed to convert HAVN to AVNN (Chang *et al*., 2000). Therefore, it was concluded that AVNN was produced non-enzymatically by dehydration of HAVN (Chang *et al*., 2000; Sakuno *et al*., 2003).

Incubation of the cytosol of *A. parasiticus* with HAVN and NAD^+ produced (1'*S*, 5'*S*)-AVF exclusively (Yabe *et al*., 1993). Metabolite feeding studies with (1'*S*, 5'*S*)-AVF supported the production of aflatoxins, but no aflatoxins were produced from (1'*S*, 5'*R*)-AVF. Considering the diastereomeric nature of HAVN, production of (1'*S*, 5'*S*)-AVF from (1'*S*, 5'*R*)-HAVN is stereochemically hindered, therefore, it was proposed that the production of AVF from HAVN proceeds via a 5'-keto intermediate and concomitant loss of chirality at that position (Yabe *et al*., 1993). This reaction supports the conversion of HAVN to AVF via OAVN, as initially proposed by Yabe and co-workers (1991b).

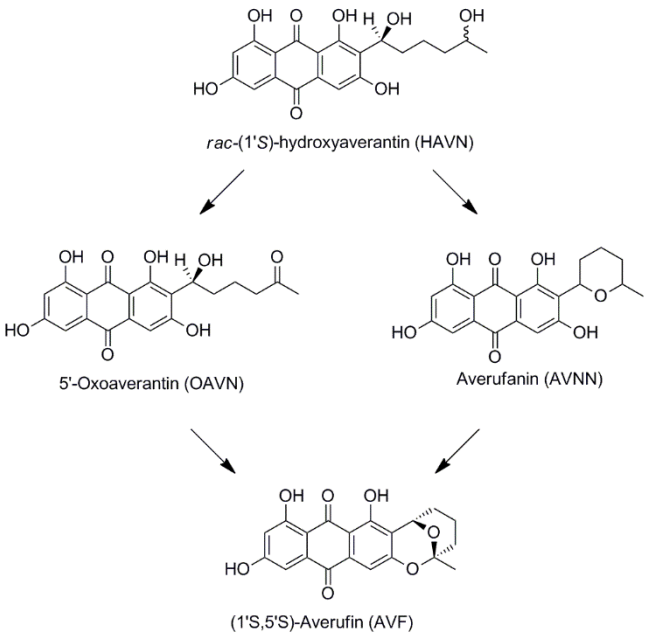

Figure 1.4. The two proposed routes for the conversion of hydroxyaverantin (HAVN) to averufin (AVF). The accepted route for the conversion of HAVN to AVF proceeds via oxoaverantin (OAVN).

Recombinant inactivation of *adhA* in an *A. parasiticus* strain resulted in an accumulation of HAVN, as well as small amounts of *O*-methylsterigmatocystin (OMST), an intermediate produced later in the aflatoxin pathway. This suggests that AdhA functions as a HAVN dehydrogenase to convert the 5'-hydroxyl group to a keto group to produce 5'-oxoaverantin (OAVN). *adhA* encodes a protein that is homologous to short-chain alcohol dehydrogenases, containing a Rossman-fold motif for the binding of a dinucleotide co-factor, as well as a motif characteristic of the alcohol dehydrogenase active site (Chang *et al*., 2000).

Metabolite feeding studies indicated that this reaction is performed selectively with NAD^+ (Yabe *et al*., 1991b). Knock-out mutants of *adhA* indicated that the reaction can be complemented by enzymes with similar activities, and moreover, evidence suggested that complementation can occur with enzymes not associated with aflatoxin biosynthesis (Yabe *et al*., 1991b).

Sakuno and co-workers (2003) purified a protein of approximately 60 kDa from the cytosol of *A. parasiticus* that catalyses the conversion of HAVN to OAVN using NAD^+. The subunits of the enzyme, which functions as a dimer, correspond to the predicted mass of AdhA (29.6 kDa) and peptide mass fingerprinting indicated that the protein was indeed encoded by *adhA.*

1.3.2.4. Conversion of oxoaverantin to averufin

As mentioned, the production of AVF was thought to occur via spontaneous rearrangements of OAVN. However, a dimeric enzyme consisting of two 79 kDa subunits was purified from the cytosol of *A. parasiticus* and demonstrated to catalyse the conversion of OAVN to AVF. The enzymatic reaction occurs through intramolecular ketalisation of the 5'-keto group, the 3'-hydroxyl group and the (1'*S*)-hydroxyl group, and the enzyme adopted the name of OAVN cyclase (Sakuno *et al*., 2003). (1'*S*, 5'*S*)-AVF was exclusively produced and was proven to be the biologically active form of AVF (Yabe *et al*., 1993).

The work of Sakuno and co-workers (2003) thus shed light on the controversy of AVNN as it provided enzymatic evidence for the conversion of HAVN to OAVN by AdhA, and the conversion of OAVN to AVF by OAVN cyclase.

1.3.3. Production of the xanthone, sterigmatocystin

1.3.3.1. Conversion of averufin to hydroxyversicolorone

AVF is converted to hydroxyversicolorone (HVN) by the microsomal fraction of *A. parasiticus* in the presence of NADPH, with strict stereospecificity for (1'*S*, 5'*S*)-AVF (Yabe *et al*., 2003). In a study by Yu and co-workers (2000b), knock-out mutants of the *cypX* gene were found to accumulate AVF, with a loss of aflatoxin production. Feeding experiments with HVN restored the production of aflatoxins, indicating that the metabolic pathway was interrupted between AVF and HVN. CypX displays high homology to the CYP450s and carries the characteristic motifs, including the conserved heme-binding site. *stcB* is the counterpart gene in the *A. nidulans* sterigmatocystin biosynthesis cluster and similarly, *ΔstcB* mutants also accumulated AVF (Keller *et al*., 2000). However, the conversion of AVF to HVN is complex and cannot be performed by the function of a single CYP450.

In addition to *cypX*, the *avfA* gene, which is also located in the aflatoxin biosynthesis cluster, has been implicated in the conversion of AVF (Yu *et al*., 2000c). A non-aflatoxigenic *A. parasiticus* mutant strain that accumulated AVF was complemented with the *avfA* gene which fully restored aflatoxin production. Analysis of the *avfA* gene in the mutant strain identified a point-mutation that resulted in an amino acid substitution that may account for the loss of *avfA* activity. Interestingly, no binding site for the aflatoxin-associated transcription factor, AflR, was observed in the promoter

region of *avfA*, but transcription of *avfA* was still up-regulated in aflatoxin-inducing conditions. It was suggested that *avfA* is co-transcribed with the neighbouring gene, *omtB.*

1.3.3.2. Conversion of hydroxyversicolorone to versicolorin B proceeds via a metabolic grid

HVN is converted to versicolorin B (VB) via a series of reactions that are involved in a complex metabolic grid (Yabe *et al*., 2003). As seen in Fig. 1.3, two parallel pathways diverge from HVN in which the corresponding intermediates exist as hydroxylated or unhydroxylated counterparts. The metabolic counterparts are interconverted enzymatically, thereby laterally connecting the parallel pathways. The relative abundance of metabolites, as well as the amount of aflatoxins produced by feeding studies indicated that the main pathway operates via the hydroxylated metabolites.

The *vrdA* gene encodes a reductase that catalyses the interconversion of HVN and versicolorone (VONE), versiconal hemiacetal acetate (VHA) and versiconol acetate (VOAc), as well as versiconal (VHOH) and versiconol (VOH) (Shima *et al*., 2009; Yabe *et al*., 2003). The VrdA protein was initially purified from the cytoplasm of *A. parasiticus* and demonstrated the ability to convert VHA to VHOc in the presence of NADPH (Matsushima *et al*., 1994). The protein, versiconal hemiacetal acetate reductase, was shown to be encoded by the *vrdA* gene using amino acid sequencing techniques (Shima *et al*., 2009). The *vrdA* gene is not located in or near the aflatoxin biosynthesis gene cluster and does not share similarity with genes within either the aflatoxin or sterigmatocystin biosynthesis cluster in *A. parasiticus* or *A. nidulans*, respectively. However, a homologous gene was identified in *A. nidulans* located elsewhere in the genome, which suggests that the same metabolic grid may operate in sterigmatocystin biosynthesis. Based on sequence similarity, VrdA was classified as an aldo-keto reductase. Aflatoxin biosynthesis in *ΔvrdA* deletion mutants was not impaired, which is not surprising as VrdA does not function in the main pathway for aflatoxin biosynthesis.

The participation of *vrdA* as a structural enzyme in the aflatoxin biosynthesis is proof that genes outside of the aflatoxin gene cluster can be involved in aflatoxin biosynthesis. Although *vrdA* contains the AflR recognition site in the promoter region, the sequence is 5'-$\underline{C}CGN_5CGA$-3' instead of 5'-$\underline{T}CGN_5CGA$-3', as in the case of *aflJ*, which has been proven not to bind AflR. *vrdA* is expressed in the presence and absence of the *aflR* gene, however, expression of *vrdA* was dependent on aflatoxin-inducing media and temperatures. The existence of *vrdA* homologs in non-aflatoxigenic fungi suggests that VrdA is involved in metabolic processes other than aflatoxin biosynthesis.

The side pathway of the metabolic grid may serve as a reservoir for aflatoxin intermediates and function as a complementary pathway when one or more of the reactions in the main pathway is blocked. Additionally, in old cultures the NADPH levels are increased and a shift is observed towards the side pathway, indicating that it might serve as an NADPH sink.

1.3.3.3. Conversion of hydroxyversicolorone to versiconal hemiacetal acetate and conversion of versicolorone to versiconal acetate

HVN is converted to VHA by a cytosolic enzyme in the presence of NADPH (Yabe *et al*., 2003). Similarly, VONE is converted to VOAc in the side-pathway. Sequence analysis indicated that the *moxY* gene encodes a putative flavin-dependant monooxygenase (Yu *et al*., 2000b). The reaction is a Baeyer-Villiger oxidation which converts a ketone to an ester and is catalysed by flavin-dependent enzymes called Baeyer-Villiger monooxygenases (BVMOs, Willetts 1997).

ΔmoxY disruption mutants led to the accumulation of HVN and VONE, with a loss of aflatoxin production (Wen *et al*., 2005). Feeding experiments showed that the *ΔmoxY* mutants were capable of converting VHA and VOAc to aflatoxins, but not HVN or VONE, indicating that the pathway was interrupted at the enzymatic step between HVN and VHA, as well as the parallel step VONE to VOAc. Therefore, MoxY serves as a HVN monooxygenase that converts HVN to VHA, as well as VONE to VOAc.

1.3.3.4. Conversion of versiconal hemiacetal acetate to versiconal and versiconol acetate to versiconol

Treatment of fungal cultures with the organophosphate pesticide dichlorvos resulted in the accumulation of VHA and VOAc, and inhibits the formation of aflatoxins (Yao and Hsieh, 1974). Dichlorvos is an inhibitor of esterases, an enzyme which would be required in the conversion of VHA to VHOH and VOAc to VOH. This conversion is the only known enzymatic step in the aflatoxin biosynthesis pathway that requires the function of an esterase. The gene product of *estA* has significant homology to numerous thioesterases and carboxylesterases (Yu *et al*., 2002). An esterase of 60 kDa which was involved in aflatoxin biosynthesis had been purified from *A. parasiticus* and consists of two 30 kDa isomeric subunits, which is in accordance with the predicted size of EstA.

ΔestA deletion mutants also accumulated significant amounts of VHA and VOAc. Metabolite feeding studies with the *ΔestA* mutants indicated that EstA accounted for 90 % of the esterase activity that converts VHA and VOAc (Chang *et al*., 2004a). Although greatly decreased, the mutants still accumulated downstream aflatoxin intermediates. Therefore, the function of EstA can be complemented by other esterases in the genome.

1.3.3.5. Conversion of versiconal to versicolorin B

VHOH is converted to VB by a cyclase, or dehydrase, encoded by the *vbs* gene (Silva *et al*., 1996; Silva and Townsend, 1997). VHOH cyclase was purified from the *A. parasiticus* cytoplasm and the amino acid sequence was used to identify the *vbs* gene. Furthermore, the function of *vbs* was verified by heterologous expression in *S. cerevisiae.* Interestingly, the *vbs* gene also encodes the OAVN cyclase involved in the conversion of OAVN to AVF (section 1.3.2.4). Therefore, *vbs* is a single gene in the aflatoxin biosynthesis cluster that encodes a cyclase involved in two disconnected aflatoxin biosynthesis reactions. Activity assays with heterologously expressed cyclase indicated that OAVN and VHOH compete for conversion, with the affinity for OAVN being almost ten times higher than for VHOH (Sakuno *et al*., 2005). VHOH cyclase shows stereospecificity for the (1'*R*, 2'*S*) configuration of VHOH (Yabe and Hamasaki, 1993), a stereoisomeric configuration that is propagated throughout the rest of the aflatoxin biosynthesis pathway.

Δvbs disruption mutants accumulated OAVN and various prior intermediates, however, small amounts of VB and aflatoxins were still produced. Therefore, the mutation was considered as 'leaky' and the function of the cyclase could be complemented by another enzyme. It has to be taken into consideration that both OAVN and VHOH are unstable in hydrophobic solutions and spontaneously oxidise to the products. However, this is unlikely to occur in aqueous solution such as the cytoplasm, with a slight possibility of spontaneous oxidation at the membrane surfaces (Sakuno *et al*., 2005).

1.3.3.6. Conversion of versicolorin B to versicolorin A

Bhatnagar and co-workers (1991) used metabolite feeding studies with whole-cells of *A. parasiticus* and *A. flavus* to demonstrate that type "1" and "2" aflatoxins are produced in separate pathways diverging from VB, with the metabolites in the two parallel pathways existing as desaturated counterparts. However, contrary to the metabolic grid between AVF and VB, no interconversion between the metabolites were observed (Bhatnagar *et al*., 1991). The reactions in the parallel pathways are catalysed by the same enzymes with the counterpart metabolites competing as substrates. The route leading to the production of the "1"-type aflatoxins is the preferential pathway, with the enzymes displaying a higher affinity towards the metabolites involved in this route.

In *A. nidulans,* disruption of the *stcL* gene led to a loss of ST production and an accumulation of dihydrosterigmatocystin (DHST), as well as small amounts of VB (Kelkar *et al*., 1997). Upon supplementation with versicolorin A (VA), ST production was restored, indicating that StcL functions in the conversion of VB to VA (Yabe and Hamasaki, 1993). Supplementation of the mutant with NA resulted in the production of DHST, indicating that *stcL* is involved in the production of ST from VB, but not in the production of the dehydrated counterpart DHST. It was concluded that as in *A. parasiticus,* two separate pathways exist for the production of DHST and ST, with a preference for the production of ST. The disconnected nature of the parallel pathways were confirmed as *A. nidulans* was unable to convert DHST to ST. An accumulation of VB in *ΔstcL* mutants could indicate a bottleneck-effect at the branching point due to inefficient processing of VB by the subsequent enzymes, consequent with the observation that the enzymes have a much higher affinity for the dehydrated metabolites when compared to the hydrated counterparts (Bhatnagar *et al*., 1991). StcL displays homology to CYP450s and contains the conserved motifs characteristic of these enzymes, including the heme-binding site. Based on the sequence identity to other fungal CYP450s, StcL was designated as CYP60B.

In *A. parasiticus,* the dehydrogenase activity was demonstrated with the microsomal fraction and in the presence of NADPH. StcL shares 83 % amino acid sequence identity with the gene product of *verB* (Cary and Ehrlich, 2006). On the basis of sequence similarity to *stcL*, the *verB* gene was assigned as the desaturase converting VB to VA in *A. parasiticus.*

1.3.3.7. Conversion of versicolorin A to demethylsterigmatocystin and versicolorin B to dihydrodemethylsterigmatocystin

The conversion of VA to demethylsterigmatocystin (DMST) and VB to dihydrodemethyl-sterigmatocystin (DHDMST) is a complicated metabolic step which requires the cooperation of more than one enzyme. The exact mechanism of the enzymatic steps has not been determined, although several reaction schemes have been suggested (Henry and Townsend, 2005). The authors proposed that the reaction is most likely to occur via oxidation-reduction-oxidation (Fig. 1.5). Firstly, the fused A/B ring is epoxidised, whereafter epoxide-ring opening occurs to produce a stable dienone which is then reduced. The compound undergoes a Baeyer-Villiger type cleavage and is rearranged, dehydrated and decarboxylated to produce DMST. Four genes, *ver-1, verA*, *hypA* and *ordB,* have been shown to play a role in the conversion of VA to DMST and VB to DHDMST.

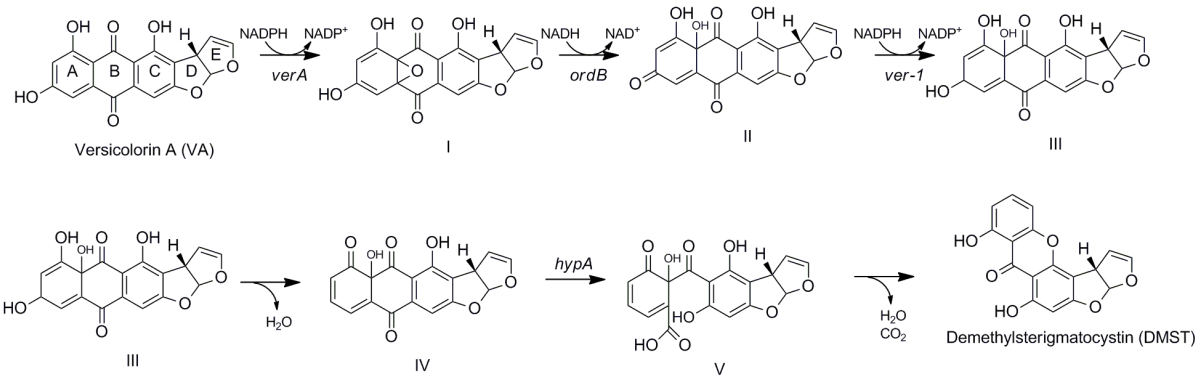

Figure 1.5. The proposed reaction scheme for the conversion of versicolorin A (VA) to demethylsterigmatocystin (DMST) involving the products of the *verA, ordB, ver-1* and *hypA* genes.

1.3.3.7.1. verA / stcS

The *stcS* gene has been implicated in the conversion of VA to DMST and VB to DHDMST in *A. nidulans* (Keller *et al*., 1995). *ΔstcS* disruption mutants resulted in the loss of ST production and metabolite feeding studies confirmed that the blocked enzymatic step occurred after the production of VA and before the production of ST. The predicted amino acid sequence of StcS displayed similarity with CYP450s (Keller *et al*., 1994) and contained the conserved heme-binding motif (Keller *et al*., 1995). Due to a lack of significant homology to other CYP450s (> 40 %), StcS was classified into a new CYP family, namely CYP59. Based on amino acid sequence similarity, the *verA* gene is the

homolog of *stcS* in *A. parasiticus* (Yu *et al*., 2004). VerA was suggested to perform the epoxidation of the A/B ring of VA to produce compound I in Fig. 1.5 (Henry and Townsend, 2005).

1.3.3.7.2. ordB / stcQ

Gene-disruption experiments with *ordB* led to a decrease in aflatoxin production in *ΔordB* mutants, with an accumulation of VA (Cary *et al*., 2006). Metabolite feeding studies with the *ΔordB* mutants indicated that the metabolic block occurred prior to ST production. OrdB is homolgous to AvfA (section 1.3.3.1) and contains a catalytic domain characteristic of NADH-dependent flavin reductases. The homology of AvfA and OrdB indicate that these enzymes may complement the function of each other. Therefore, the 'leaky' nature of *ΔordB* mutants may be due to complementation by an intact *avfA* gene.

Several conserved motifs were identified in OrdB which suggests that OrdB may be involved in the reductive cleavage of an epoxide ring, including a motif required for catalysis by epoxide hydrolases. The predicted product of the epoxide ring cleavage is a hydroxydienone, which is in contrast with the typical diol produced by epoxide hydrolases. The discrepancy in the products may explain the lack of sequence similarity of OrdB to known epoxide hydrolases.

1.3.3.7.3. ver-1 / stcU

Skory and co-workers (1992) isolated and used the *ver-1* gene from *A. parasiticus* to complement the activity of mutants unable to convert VA to ST. The gene restored the production of both type "1" and "2" aflatoxins, indicating that Ver-1 is involved in both legs of the parallel pathway. The amino acid sequence shared identity with reductases and dehydrogenases involved in the conversion of ring structures and contains a dinucleotide-binding motif for NADPH, which is required in the reaction. Based on sequence similarities, it was proposed to encode a ketoreductase and it is suggested that Ver-1 is involved in the reduction of II to III (Fig. 1.5).

Gene disruption of *ver1,* also referred to as *ver1A*, led to the accumulation of VA with a loss of aflatoxin production (Liang *et al*., 1996). Complementation with the *ver1A* gene restored aflatoxin production, confirming the role of Ver1A as a participant in the conversion of VA to ST. The *stcU* gene, also referred to as the *verA,* in *A. nidulans* was isolated as a homolog of the *ver-1* gene (Keller *et al*., 1994). *verA* shared close similarity with *ver1* and also to several NADPH-dependent reductases involved in polyketide synthesis pathways. As in the case with *A. parasiticus, verA* disruption mutants did not produce ST, but accumulated VA. *stcL stcU* double-mutants (corresponding to *verB*

and *ver-1* double mutants in Fig. 1.3) accumulated both VA and VB, with a concomitant loss in ST and DHST production, indicating that both legs of the pathway were blocked. This confirmed that *stcU* is a participant in the conversion of VB to DHST in addition to the conversion of VA to DMST (Kelkar *et al*., 1997).

1.3.3.7.4. hypA / stcR

Disruption of *hypA* resulted in a loss of aflatoxin production and an accumulation of VA (Ehrlich *et al*., 2005). When the *ΔhypA* mutants were supplemented with ST or OMST, aflatoxin production was restored, but no aflatoxins were produced upon supplementation with AVN, AVF or VA, indicating that the pathway was disrupted between VA and ST. The predicted amino acid sequence of HypA has numerous homologs in fungi. Although no conserved protein domains were identified, histidine-rich regions were found that is related to motifs necessary for catalysis in metallooxidases. It was proposed that HypA functions in the Bayer-Villiger type oxidation of IV to V (Fig. 1.5).

1.3.3.8. Conversion of demethylsterigmatocystin to sterigmatocystin and dihydrodemethylsterigmatocystin to dihydrosterigmatocystin

Yabe and co-workers (1989) identified two distinct *O*-methyltransferases, designated as I and II, that catalyse the substrate-specific, sequential methylation of DMST and DHDMST to *O*-methylsterigmatocystin (OMST) and dihydro-*O*-methylsterigmatocystin (DHOMST). Although the enzymes differ in size and physiological properties, both *O*-methyltransferases have a requirement for *S*-adenosyl-methionine (SAM).

The methylation of DMST and ST to DHDMST and dihydrosterigmatocystin (DHST), respectively, is catalysed by *O*-methyltransferase I. Activity studies with purified *O*-methyltransferase I demonstrated that DMST and DHDMST compete as substrates for the same catalytic site, although the enzyme has a higher affinity for DMST (Yabe *et al*., 1989). Partial sequencing of the enzyme led to the identification of *dmtA* as the encoding gene (Motomura *et al*., 1999). The translated amino acid sequence contains the SAM-binding motif and has a predicted molecular mass of 43 kDa, which corresponds to the subunit size of the purified enzyme. The *omtB* gene was cloned simultaneously by Yu and co-workers (2000c) and was shown to be 100 % identical to *dmtA.*

stcP is the homolog of *dmtA/omtB* in the *A. nidulans* ST biosynthesis gene cluster. *ΔstcP* disruption mutants accumulated DMST (Kelkar *et al*., 1996), providing support for the function of StcP as an *O*-

methyltransferase in sterigmatocystin production. The methylation of DMST and DHMST to produce ST and DHST forms the final catalytic step in sterigmatocystin biosynthesis. Therefore, the sterigmatocystin gene cluster is not expected to contain any aflatoxin genes responsible for the final catalytic steps to convert ST and DHST into aflatoxins.

1.3.4. Final rearrangements to produce the coumarin nucleus of aflatoxins

1.3.4.1. Conversion of sterigmatocystin and dihydrosterigmatocystin to *O*-methylsterigmatocystin and dihydro-*O*-methylsterigmatocystin

O-methyltransferase II is responsible for the conversion of ST and DHST to OMST and DHOMST. *omt-1,* also referred to as *omtA*, was identified as the gene encoding *O*-methyltransferase II in *A. parasiticus* by the use of polyclonal antibodies raised against the purified enzyme (Yu *et al*., 1993). As in the case of *O*-methyltransferase I, the predicted amino acid sequence contains the SAM-binding motif.

Feeding experiments with *ΔomtA* disruption mutants indicated that ST could not be converted to OMST or aflatoxins, but retained the ability to convert OMST to aflatoxins (Lee *et al*., 2002). Heterologously expressed *omt-1/A* conferred the ability to convert ST to OMST and DHST to DHOMST on the successful *E. coli* clones. The expressed OmtA was purified and demonstrated to convert ST to OMST in the presence of SAM. The abundance of evidence confirmed the role of *O*-methyltransferase II in aflatoxin biosynthesis.

1.3.4.2. Conversion of *O*-methylsterigmatocystin and dihydro-*O*-methylsterigmatocystin to 11-hydroxy-*O*-methylsterigmatocystin and dihydro-11-*O*-methylsterigmatocystin

The *ord1* gene from *A. flavus* was implicated in the conversion of ST to aflatoxins by complementing a mutant strain lacking the aflatoxin biosynthesis cluster (Prieto *et al*., 1996). Metabolite feeding studies indicated that recombinant *S. cerevisiae* cultures expressing the *ord1* gene was capable of converting OMST to AFB_1. *ordA* was identified as the homolog to *ord-1* in *A. parasiticus* with 97 % amino acid identity (Yu *et al*., 1998). Complementation of an OMST-accumulating *A. parasiticus* mutant with *ordA* restored the production of both B- and G-type aflatoxins.

Radiolabelling experiments indicated that epoxidation of the A-ring of ST could lead to a NIH shift to produce the intermediate 11-hydroxy-*O*-methylsterigmatocystin (HOMST) and the transient production of the intermediate has been observed in metabolite feeding studies (Udwary *et al*., 2002). The conversion of OMST to aflatoxins is associated with the microsomal fraction and requires NADPH (Bhatnagar *et al*., 1991; Yabe *et al*., 1999). The translated amino acid sequence of *ordA* contained sequence motifs characteristic of microsomal CYP450 enzymes, including the heme-binding motif and a hydrophobic N-terminal domain corresponding to a membrane-spanning anchor (Yu *et al*., 1995). Based on similarity to other cytochrome P450s, Ord1 was classified into a new family of CYP450, namely, Cyp64 (Prieto and Woloshuk, 1997). Ord1 does not have significant identity to known fungal CYP450s, including those identified in the *A. nidulans* cluster.

1.3.4.3. Conversion of 11-hydroxy-*O*-methylsterigmatocystin and dihydro-11-*O*-methylsterigmatocystin to AFB_1 and AFB_2

Conversion of OMST to AFB_1 involves oxidative cleavage of the xanthone A-ring, *O*-demethylation, dehydration, decarboxylation and rearrangement to produce the coumarin moiety (Udwary *et al*., 2002). Metabolite feeding studies with the microsomal fraction of cell-free extracts from *S. cerevisiae* heterologously expressing *ordA* confirmed that HOMST can be converted to AFB_1 and dihydro-11-hydroxy-*O*-methylsterigmatocystin (DHHOMST) to AFB_2.

The ability of recombinant OrdA to catalyse the conversion of OMST to AFB_1 implicated that a sole enzyme was responsible for the metabolic step. The stoichiometric loss of carbon dioxide from C_{11} indicates that two cycles of monooxygenase activity was required to convert OMST and DHOMST to aflatoxins, and it was proposed that OrdA performs two consecutive oxidation reactions. The second reaction was postulated to involve oxidative cleavage of the A-ring to produce an open-chain butenyl carboxylic acid intermediate that rearranges to produce AFB_1.

Several schemes were proposed for the rearrangement of the intermediate, but none have been confirmed. OrdA is a membrane-associated protein and was not purified to homogeneity in the previous studies. Thus, it is possible that the conversion of OMST to AFB_1 requires additional enzymes that are supplied by the microsome of the yeast host. It has been speculated by Ehrlich and co-workers (2008) that Nor-1, the norsolorinic acid reductase and product of the *nor-1* gene (section 1.3.2.1), may be involved in a reduction step necessary for B-type aflatoxin biosynthesis.

1.3.4.4. Conversion of 11-hydroxy-*O*-methylsterigmatocystin and dihydro-11-*O*-methylsterigmatocystin to AFG_1 and AFG_2

The conversion of HOMST and DHHOMST to produce G-type aflatoxins is not yet fully understood. Consistent with the proposed separate pathways, OMST is converted to AFB_1 and AFG_1 and DHOMST is converted to AFB_2 and AFG_2 by the cytosolic fraction of *A. parasiticus* in the presence of NADPH (Yabe *et al*., 1999). G-type aflatoxins are produced independently from OMST, as B-type aflatoxins do not support the production of G-type aflatoxins in metabolite feeding studies.

A 220 kDa cytosolic enzyme, as well as the microsomal fraction, are required for AFG_1 production, indicating that a minimum of two enzymes are involved in the metabolic step. As mentioned, the cytochrome P450-encodind *ordA* is invovled in the conversion of OMST and DHOMST to both B- and G-type aflatoxins (Yu *et al*., 1998). However, in the yeast expression system, only AFB_1 and not AFG_1 was produced from OMST. This is consistent with the requirement of more than one enzyme in the catalysis of OMST. Evidence exist that an additional microsomal enzyme is involved in the production of G-type aflatoxins (Yabe *et al*., 1999).

1.3.4.4.1. cypA and norB

Different aflatoxin production profiles of *Aspergillus* species allows elucidation of the differential genes involved in the production of B and G-type aflatoxins. *A. parasiticus* produces both B- and G-type aflatoxins, while *A. flavus* produces B-type aflatoxins exclusively. Comparison of the aflatoxin biosynthesis gene clusters in the two species revealed a deletion in the *A. flavus* cluster spanning a portion of the 5' coding region of *cypA* and *norB,* including the translational start site, as well as the entire intergenic region (Ehrlich *et al*., 2004). The two genes are bidirectionally transcribed from the intergenic region, which contains a binding motif for the aflatoxin-associated transcriptional activator, AflR. Neither *cypA*, nor *norB* was transcribed in aflatoxin-inducing media in *A. flavus.*

The predicted protein sequence of *norB* displays high homology to the fugal aryl alcohol dehydrogenases (Ehrlich *et al*., 2004). NorB also displays 50 % identity and 68 % similarity to NorA, the norsolorinic acid oxidase (section 1.3.2.1) indicating that the enzymes may possibly complement each other. A homologous gene is found in the sterigmatocystin biosynthesis cluster, *stcV.* As *A. nidulans* does not produce aflatoxins, it is likely that StcV functions in a portion of the pathway prior to ST synthesis. Still, the function of these putative aryl alcohol dehydrogenases in aflatoxin biosynthesis is unknown.

The translated amino acid sequence of *cypA* displayed the conserved motifs of CYP450 enzymes, as well as a membrane-binding motif. Due to homology with Tri4, a CYP450 monooxygenase involved in trichothecene biosynthesis in *Fusarium* species, CypA was classified as CYP58B1. Disruption of *cypA* in *A. parasiticus* resulted in a loss of the production of G-type aflatoxins, while the ability to produce B-type aflatoxins was retained. Consistent with the prediction by Yabe and co-workers (1999), CypA is an additional enzyme involved in the production of G-type aflatoxins and the presence of a membrane-spanning region indicates that the enzyme is most likely located in the microsome.

1.3.4.4.2. nadA

The *nadA* gene is located in the sugar-utilisation cluster adjacent to the aflatoxin gene cluster (Yu *et al*., 2000a). However, *nadA* was only transcribed under aflatoxin-inducing conditions and requires the presence of a functional *aflR* gene, suggesting that *nadA* may actually form part of the aflatoxin gene cluster (Cai *et al*., 2008; Price *et al*., 2006). *ΔnadA* deletion mutants accumulated a 360 Da metabolite, NADA, which was only observed under aflatoxin-inducing conditions. G-type aflatoxin production was greatly reduced, but not eliminated, in the *ΔnadA* mutants, while production of B-type aflatoxins remained intact. The instability of NADA and DHNADA may provide an answer to the incomplete inhibition of aflatoxin production. It is notable that *ΔcypA* deletion mutants do not accumulate NADA, indicating that NadA is involved in downstream reactions from CypA.

As described by Yabe and co-workers (1999), cell-free assays of *A. parasiticus* demonstrated that addition of the cytosol fraction to the microsome fraction greatly enhanced the production of G-type aflatoxins. However, addition of the cytosol fraction of *ΔnadA* mutants did not display the same increased production of G-type aflatoxins (Cai *et al*., 2008). The production of B-type aflatoxins was not affected. This indicated that the cytosolic factor required for G-type aflatoxins is most likely NadA. Metabolite feeding studies with the *ΔnadA* mutants indicated that no G-type aflatoxins were produced, while NADA served as a precursor to G-type aflatoxins in wild-type strains. NADA was also spontaneously converted to AFG_1 in the cell-free system, which also indicates that NADA (and DHNADA) are likely to be the last precursors to the G-type aflatoxins. The instability of the metabolites in a cell-free system is not necessarily indicative that the metabolite is unstable in the cellular environment, and it was concluded that NadA plays a major role in the conversion of NADA to AFG_1.

The predicted amino acid sequence of NadA showed significant homology to other NADH oxidases and contains a conserved domain characteristic of Old-Yellow Enzyme-related FMN binding domain reductases (Ehrlich *et al*., 2008).

1.3.5. Genes with uncertain functions in aflatoxin biosynthesis

1.3.5.1. *aflT*

The predicted amino acid sequence of AflT contains multiple transmembrane motifs and shares homology to the major facilitator superfamily (MFS) transporters (Chang *et al*., 2004b). MFS transporters operate in secretion of certain fungal toxins and are implicated in the self-protection of the fungus against the toxin itself. MFS transporters homologous to AlfT have been observed in the gene clusters responsible for toxin synthesis, such as the *dotC* gene in *Dothistroma pini*, which produces the toxin dothistromin that resembles versicolorin B (Bradshaw *et al*., 2002). MFS transporters are integral membrane proteins that use the proton-motive driving force to transport a wide variety of metabolites and anions (Pao *et al*., 1998).

ΔaflT disruption mutants showed no alteration in the distribution of aflatoxins and AflT is unlikely to be involved in the defence against autotoxicity (Chang *et al*., 2004b). Also, numerous metabolite feeding studies with recombinant yeast transformants expressing genes from the aflatoxin biosynthesis pathway indicated that the converted metabolites could be secreted into the medium. Therefore, AflT is not specifically required for the export of aflatoxins and secretion can occur via an unidentified transport system in the yeast cell. Other MFS transporter genes are present in the *A. flavus* genome that can possibly complement the function of *aflT*.

aflT was expressed irrespective of the media used, which is uncommon for enzymes of the aflatoxin biosynthesis pathway. Transcript level of *aflT* did not decrease with the deletion of *aflR* or *alfJ*, and it was reported that no AflR binding motif was observed in the promoter region of *aflT*. Thus, AflT may function as a transporter protein for aflatoxin efflux from the cells, but secretion of aflatoxins is not absolutely dependent on AflT.

1.3.5.2. *hypB*

The *hypB* gene is homologous to *hypC* which functions as an anthrone oxidase to convert NAA to NA (section 1.3.1.3). Contrary to the situation with *hypC,* no precursor metabolite accumulated after the disruption of *hypB* (Ehrlich, 2009). Also, recombinantly expressed HypB was unable to convert NAA to NA upon incubation. An alignment of HypB and HypC with orthologs from numerous fungi identified a putative catalytic site, similar to the site occurring in bacterial anthrone oxidases. It is notable that a highly conserved tryptophan residue is not present in the catalytic site of HypB, providing a possible reason for the inability of HypB to convert NAA. It has been proposed that HypB is involved in the conversion of HOMST to aflatoxins, although this role has to be confirmed (Ehrlich, 2009).

1.3.5.3. *hypD*

The *hypD* gene is predicted to encode an integral membrane binding protein with conserved orthologs in numerous *Aspergillus* species (Ehrlich, 2009). Disruption of *hypD* in *A. parasiticus* led to an increased sporulation with a decrease in aflatoxin production. The exact role of HypD remains unclear, but several possible roles have been suggested. As an integral membrane protein, HypD may function as a permease to allow efflux of aflatoxins from the fungal cells and that the loss of function may result in feedback-inhibition of aflatoxin production. Alternatively, HypD may act as a subunit of a membrane-associated protein, such as the CYP450 OrdA.

1.3.5.4. *hypE*

The *hypE* gene encodes a protein with an ethD domain, which is required for ethyl-t-butyl ether degradation. The predicted sequence of HypE has orthologs in many *Aspergillus* species (Ehrlich, 2009). A possible role for HypE in conjunction with a CYP450 was predicted in the conversion of OMST to aflatoxins, but the function of HypE still has to be verified.

1.3.6. Concluding remarks on the aflatoxin biosynthesis pathway

The in-depth investigation of aflatoxin biosynthesis revealed a complex polyketide-initiated pathway with a metabolic grid and the involvement of parallel pathways. Contrary to the expectations raised by the clustered nature of the genes involved in aflatoxin synthesis, the pathway does not operate as an isolated metabolic entity; firstly, as an enzyme not encoded by the gene cluster participates in the pathway (*vrdA*) and secondly, because the function of numerous genes can be complemented by different genes in the host organism. Also, the ability of one enzyme to catalyse two disconnected metabolic steps (OAVN cyclase) indicates that enzymes encoded by the aflatoxin biosynthesis gene cluster can be involved in more than one step. This complicates the elucidation of the metabolic steps of which the mechanisms are not yet known, such as the conversion of VA to DMST and the production of G-type aflatoxins.

1.4. Current control strategies

Since the discovery of aflatoxins in the 1960s, a multi-disciplinary effort has been underway to address aflatoxin contamination in the field and post-harvest. Post-harvest treatment includes adequate drying and minimising physical damage to crops (Munkvold, 2003). However, contamination often starts at the pre-harvest stage, after which improper handling of the crops post-harvest aggravates the contamination levels. Currently, numerous control strategies are employed to control aflatoxin contamination in the field by either controlling fungal growth or aflatoxin biosynthesis (Klich, 2007).

1.4.1. Good agricultural practices

Good agricultural practices aim at altering the growth conditions so that infection by the fungus is limited or avoided (Munkvold, 2003). Aflatoxins are produced especially when plants are under stress (Klich, 2007) and lowering plant stress can therefore relieve aflatoxin contamination to some extent (Pitt and Hocking, 2006). These methods include planting of regionally adapted cultivars, planting at appropriate seed density, control of weeds, and also, irrigation, when necessary. Fertilisation of crops with nitrogen also leads to consistently lowered levels of aflatoxins. Traditional crop management procedures, such as crop rotation and tillage, have been reported as inefficient to relieve the levels of aflatoxin contamination due to soilborne fungi (McGee, 1996).

The majority of rural farmers in developing countries are ignorant with regards to in-field aflatoxin contamination. Raising awareness on the aflatoxin issue can provide farmers with the knowledge to make informed decisions prior to planting, as well as managing the crops throughout the season. Still, the employment of good agricultural practices is not always feasible, due to the cost of treatments, as in the case of irrigation and fertilization.

1.4.2. Reduction of insect-induced injury

Insect damage has been associated with elevated levels of aflatoxins (Gorman and Kang, 1991; Klich, 2007). Grazing insects cause tissue damage that provide a mode of entry for the fungus, as well as acting as vectors for the delivery of fungal spores. Consequently, control of pests indirectly results in

decreased aflatoxin contamination. Two methods of pest control are currently employed, namely chemical control by means of insecticide and biological control, using transgenic plants.

Chemical control of pests by insecticides has been reported as an efficient method to reduce aflatoxin levels in cotton (Henneberry *et al*., 1978). However, use of insecticides to combat aflatoxin contamination has been proven uneconomical (Dowd, 2003). Also, the use of insecticide is considered environmentally unfriendly and is met with growing scrutiny by the consumers.

Bt crops are transgenic plants carrying genes from the bacterium *Bacillus thuringiensis,* encoding a crystalline protein that is toxic to lepidopteran insects (Romeis *et al*., 2006). Numerous Bt crops are currently used in agriculture, including corn, rice and cotton, with South Africa supporting the cultivation of Bt corn (Wu, 2006). However, the use of Bt corn in the control of aflatoxins has not yielded consistent results, although reduction in aflatoxin levels by Bt crops have been reported (Munkvold, 2003). The lack of aflatoxin control by Bt crops may be due to insect resistance to Bt toxins. Also, it has to be considered that insect damage is not a prerequisite for the infection by *A. flavus* (Klich, 2007).

1.4.3. Breeding of host-plant resistance

Plants with an inherent resistance to *A. flavus* is a highly attractive option from both a biological and economic view. In corn, strains with resistant genotypes have been identified, but they often lack the requirements to fulfil a commercial role (Brown *et al*., 1999; Klich, 2007). Nonetheless, international collaborations exist to develop aflatoxin-resistant, agronomically superior corn cultivars specifically for use in West Africa and the USA. In 2006, proteome analysis of corn was used to identify resistance-associated proteins and genes for use in the breeding of resistant strains (Menkir *et al*., 2006). Still, the breeding of aflatoxin-resistant plants is an ongoing process with no commercially available cultivars which are totally resistant to aflatoxin production. In peanuts, the effort has been largely unsuccessful, with the motivation that *A. flavus* is not a true pathogen of peanuts, but rather exists as a commensal with no apparent pathological effect on the peanut plant (Pitt and Hocking, 2006).

1.4.4. Consumer-targeted control

A novel method for aflatoxin control is the inclusion of an absorbent product in the diet to reduce the bioavailability of aflatoxins. NovaSil™ is a processed clay product that, when ingested, reduces the uptake of aflatoxins in the gastrointestinal track, thereby protecting the individual from the harmful effects (Wang *et al*., 2008). Daily ingestion of NovaSil capsules significantly reduced the aflatoxin biomarkers in blood serum and urine of Ghanians at high risk of aflatoxin exposure upon prolonged use (three months). However, considering the proportions of the aflatoxin problem, providing the population with pharmaceutically-approved adsorbents for a prolonged time is highly unfeasible.

1.4.5. Biocontrol by competitive exclusion

The principle of competitive exclusion involves the use of non-aflatoxigenic *A. flavus* strains to fill the ecological niche, thereby reducing aflatoxin levels but not mould levels (Klich, 2007). Spores of the non-aflatoxigenic strains are applied to the soil to compete with the naturally occurring aflatoxigenic strains of *A. flavus* (Pitt and Hocking, 2006). This method has been employed successfully in field studies of cotton (Cotty, 1994), peanuts (Pitt and Hocking, 2006) and corn (Abbas *et al*., 2011), and several commercial strains are available, including Afla-Guard® for control of aflatoxins in peanuts and corn. This method has been proven highly successful, reducing aflatoxin levels up to 98 %. However, the use of biocompetitive *A. flavus* strains has several drawbacks.

The application of fungal spores of an opportunistic pathogen poses a threat to immunocompromised individuals and therefore requires special care (Pitt and Hocking, 2006). Direct dusting or spraying of the spores are considered an unacceptable health hazard and the problem can be circumvented by growing the competitive strains on a particulate substrate, such as small, non-viable grains, which could be co-dispensed with fertiliser by machines. This approach is once again feasible in developed countries such as Australia and the USA, but is not practical in developing countries. The wide-spread human immunodeficiency virus (HIV) epidemic in Africa renders countless individuals immunocompromised and susceptible to infection by the inhalation of spores. Also, rural farmers seldom possess expensive machinery to dispense fertiliser, if fertiliser is used at all.

In studies focusing on the biocontrol of peanuts, in which both *A. flavus* and *A. parasiticus* are a problem, emphasis was placed on the genetic stability of the competitive strains, ensuring that they would be unable or unlikely to revert back to toxigenicity (Pitt and Hocking, 2006). A very important factor to take into consideration, is the occurrence of horizontal gene transfer.

The horizontal gene transfer (HGT) of isolated genes from bacterial origin has been well documented (Keeling, 2009). The genes involved in the production of aflatoxins as well as sterigmatocystin, which is an aflatoxin intermediate, is located in an isolated gene cluster. In 2011, Slot and Rokas reported the occurrence of an intact sterigmatocystin biosynthesis cluster in the filamentous fungus *Podospora anserina.* The cluster contained 24 genes with intact open reading frames (ORFs) similar in length to the *A. nidulans* sterigmatocystin biosynthesis gene cluster. Expressed sequence tag (EST) studies indicated that 14 of the genes, including the pathway regulator, *aflR*, was expressed and sterigmatocystin production has been observed in *Podospora* sp. (Matasyoh *et al*., 2011). The authors proceeded to provide overwhelming evidence that the entire sterigmatocystin biosynthesis cluster of ~ 57 kb was acquired by *P. anserina* by a single HGT event from an *Aspergillus* donor (Slot and Rokas, 2011).

Fusarium is a fungal genus containing numerous plant pathogens, some of which produce the potent mycotoxin fumonisin (Bennett and Klich, 2003). Ma and co-workers (2010) demonstrated that co-incubation of a pathogenic and a non-pathogenic *Fusarium* strain resulted in the transfer of an entire chromosome, conferring pathogenicity to the recipient strain within 6 – 8 days. Consequently, the possibility of HGT of the aflatoxin biosynthesis gene cluster between the non-aflatoxigenic and aflatoxigenic *A. flavus* strains cannot be discounted, especially as application of the non-aflatoxigenic spores result in prolonged co-incubation of the strains. In addition, if the non-aflatoxigenic strains have a higher growth rate, HGT can lead to the generation of fast-growing toxigenic strains, rendering the use of competitive agents useless and even an increase in aflatoxin levels.

1.4.6. RNA silencing of the aflatoxin-specific pathway regulator gene, *aflR*

An alternative approach for the control of aflatoxins is the use of RNA silencing, which is the interception and degradation of mRNA. The method is based on the digestion of double-stranded RNA by an RNAse III enzyme, Dicer, into 21 – 25 nucleotide small-interfering RNA (siRNA) fragments (Bernstein *et al*., 2001). The siRNA fragments are incorporated into a protein complex called the

RNA-induced silencing complex (RISC) which degrades mRNA sequences with the same sequences as the siRNA by complementary base-pairing (Bernstein *et al*., 2001; Hammond *et al*., 2001). The RNA silencing is achieved by either inserting inverted repeat transgenes into the genomes of organisms, or transfecting the cells with synthesised short-interfering double-stranded RNA molecules. RNA silencing by using inverted repeat transgenes has been used to successfully inhibit production of the aflatoxin- and sterigmatocystin-associated transcription factor, AflR in *A. nidulans* (Hammond and Keller, 2005), *A. parasiticus* and *A. flavus* (McDonald *et al*., 2005), which led to a loss of transcription of the aflatoxin biosynthesis genes and aflatoxin production.

Recently, RNA silencing of the *nor-1* gene, encoding norsolorinic acid oxidase, in addition to the *aflR* gene, by transfection of *A. flavus* and *A. parasiticus* with siRNA was investigated (Abdel-Hadi *et al*., 2011). The method was highly successful with a decrease of 89 % in AFB_1 in *A. flavus* and 77.2 % of AFG_1 in *A. parasiticus*. However, the method is dependent on the use of an effective transfection agent and in-field studies still need to be conducted.

1.5. Conclusions

The devastating effect of aflatoxins has been well-documented over the past few decades. Since the discovery of aflatoxins, a multi-disciplinary effort has resulted in a vast body of knowledge on the phenomenon of aflatoxin contamination. The clustered genes responsible for aflatoxin biosynthesis have been characterised to a great extent, although the function of some are still uncertain. Likewise, the aflatoxin biosynthesis pathway has been elucidated, but the mechanism involved in certain steps remains elusive. The knowledge on the mode of host infection, the environmental effects on aflatoxin production, as well as the function of the aflatoxin genes has led to the development of various control strategies to combat the aflatoxin problem. Still, the quest for improved aflatoxin control strategies continues.

Chapter 2

Introduction to study

2.1. Inhibition of the aflatoxin biosynthetic enzymes – a novel approach

A diverse array of aflatoxin control strategies is currently available to the farmer. Nonetheless, the economic and practical aspects of many of these strategies constrain their use. No control strategy is completely efficient in eliminating aflatoxin contamination and it can be concluded that the problem has to be addressed by using a combination of strategies. A yet under-exploited resource for the development of aflatoxin control strategies is our detailed understanding of the aflatoxin biosynthesis pathway.

A novel strategy for the control of aflatoxins is proposed that targets the synthesis of aflatoxins on the protein level. Complete inhibition of a target enzyme can block the aflatoxin biosynthesis pathway, resulting in loss of aflatoxin production. To date, this method has not yet been employed and provides an opportunity for an alternative strategy in aflatoxin control.

Selecting a suitable enzymatic step for targeted inhibition is no trivial task. The enzymatic reactions involved in aflatoxin synthesis have been characterised to a great extent, providing ample opportunity to select a candidate step for aflatoxin inhibition. Care must be taken to select a suitable target enzyme and a number of factors have to be considered.

Firstly, many of the enzymatic steps are considered as 'leaky', where knock-out of the target gene resulted in decreased levels of aflatoxins, but not a total elimination of aflatoxin production. This indicates that the function of the gene can be complemented by a different gene – albeit in the aflatoxin biosynthesis cluster or located elsewhere in the genome. Inhibition of multiple unknown enzymes may be complicated, rendering these steps less suitable for targeted inhibition.

Secondly, a metabolic step must be chosen prior to the conversions which confer the carcinogenic properties on the aflatoxin metabolites. Inhibition of a target enzyme will most likely cause an accumulation of the substrate metabolite and if the substrate metabolite also conveys the

carcinogenic properties, the effort will be unsuccessful. Therefore, all metabolic steps from the conversion of versicolorin A (VA) and onwards are not suitable for targeted inhibition.

Thirdly, preference must be given to enzymes that do not occur in higher eukaryotes. Inhibition of these enzymes is less likely to affect the native enzymes of plants and animals when compared to families of enzymes which are ubiquitous in all kingdoms of life, such as the cytochrome P450s (CYP450s).

Considering these stringent criteria, a prime candidate for targeted inhibition is MoxY - the enzyme converting hydroxyversicolorone (HVN) to versiconal hemiacetal acetate (VHA), as well as versicolorone (VONE) to versiconol acetate (VOAc). MoxY catalyses a Baeyer-Villiger oxidation which in nature is catalysed by a family of flavin-dependent enzymes called Baeyer-Villiger monooxygenases (BVMOs). The conversion of HVN to VHA is the only reaction in the aflatoxin biosynthesis pathway catalysed by a BVMO. Although a Baeyer-Villiger type reaction has been proposed in the conversion of VA to demethylsterigmatocystin (DMST), the reaction is catalysed by a metallo-oxidase and not a BVMO. BVMOs occur in the genomes of bacteria and fungi, but not in those of higher eukaryotes (Pazmiño and Fraaije, 2007). HVN (and VONE in the side pathway of the metabolic grid) are intermediate metabolites of the aflatoxin biosynthesis pathway that do not yet carry the carcinogenic properties of aflatoxins. In order to understand the function of MoxY as a BVMO, the family of enzymes must be investigated further.

2.2. An introduction to the Baeyer-Villiger monooxygenases (BVMOs)

BVMOs are flavin-dependent enzymes that catalyse the conversion of ketones and cyclic ketones to esters and lactones, respectively. The chemical Baeyer-Villiger reaction was discovered at the turn of the 19th century and has been used in synthetic organic chemistry ever since (Baeyer and Villiger, 1899). Adolf von Baeyer and Victor Villiger reported the conversion of cyclic ketones including menthone, carvomenthone and camphor, to the corresponding lactones using potassium monopersulfate as catalyst. Consequently, the oxidative cleavage of a carbon-carbon bond adjacent to a carbonyl to convert ketones or cyclic ketones to esters or lactones, became known as a Baeyer-Villiger (BV) reaction.

The biochemical BV reaction is nature's counterpart to the chemical reaction, using molecular oxygen as oxidant and the flavin-containing BVMO as catalyst. The ability of microorganisms to perform BV reactions was first discovered in the microbial biotransformation of steroids, where the fungi *Penicillium chrysogenum* and *Cylindrocarpon radicola* converted progesterone to testololactone (Fried *et al*., 1953). The prototype BVMO, cyclohexanone monooxygenase (CHMO) was purified in 1976 from cyclohexanol-grown *Acinetobacter calcoaceticus* (NCIMB 9871) and adopted its name from the oxygenation of the substrate, cyclohexanone (Donoghue *et al*., 1976). The gene encoding the CHMO from *Acinetobacter* sp. ($CHMO_{acinet}$) is located in a gene cluster that encodes a degradation pathway for cyclohexanol, enabling the organism to utilise cyclohexanol as a sole carbon source (Cheng *et al*., 2000). Upon purification of the enzyme, $CHMO_{acinet}$ was found to be promiscuous with regard to substrate acceptance, converting a number of cyclic ketones in addition to cyclohexanone, such as camphor, dihydrocarvone and cuprizone. The study proved that although the BVMO may have a specific role in the metabolism, the catalytic activity is not necessarily constrained to the substrate involved.

The gene of $CHMO_{acinet}$ was cloned in 1988 and enabled the heterologous expression of the protein, which pioneered a number of biocatalytic studies. The substrate scope of $CHMO_{acinet}$ is vast, including cyclic, bicyclic, aromatic and linear ketones, as well as the oxidation of heteroatoms including sulfides. Moreover, the reactions are catalysed with excellent regio- and enantioselectivity, which is far superior to the selectivity attained by attempts with asymmetric chemical catalysis.

The use of BVMOs as biocatalysts has several other advantages over the chemical BV catalysis (ten Brink *et al*., 2004). Peracids are strong oxidants and extensive protection and de-protection steps are necessary to prevent by-product formation (Kamerbeek *et al*., 2003). Furthermore, the intrinsic instability and shock-sensitivity of oxidants is hazardous, especially in large-scale reactions. Also, one equivalent of the corresponding carboxylic acid is produced as waste, which has to be disposed of. Progress has been made to improve the standard BV protocol for a more environmentally friendly reaction, including the use of hydrogen peroxide as an oxidant (Mazzini *et al*., 1996) and alternative catalysts, such as transition metal complexes (Strukul, 1998). Nevertheless, BVMOs as biocatalysts provide a more environmentally friendly alternative and is in accordance with the principles required for 'green chemistry'.

BVMOs are mainly studied for their potential in biocatalysis. In addition to $CHMO_{acinet}$, a great number of BVMOs have been identified, recombinantly expressed and characterised (Leisch *et al*., 2011). The number of characterised BVMOs from bacterial origin greatly surpasses the number from

fungal origin. The first BVMO from the *Aspergilli* to be cloned and heterologously expressed, $BVMO_{Af1}$ from *Aspergillus fumigatus,* was only published in 2013 (Mascotti *et al*., 2013) and no BVMO from *A. flavus* has been cloned to date.

2.3. Classification of BVMOs

BVMOs (E.C. 1.14.13.x) are flavoprotein monooxygenases (FMOs) which belong to the enzyme class oxidoreductases (van Berkel *et al*., 2006; Willetts, 1997). BVMOs can be divided into two subclasses, type I and type II.

Type I BVMOs, also referred to as class B BVMOs, are encoded by a single gene and contain a tightly bound flavin adenine dinucleotide (FAD) co-factor. The enzyme utilises NADPH as co-factor, which remains bound to the enzyme during catalysis. The enzyme consists of two distinct dinucleotide binding domains, each characterised by the presence of a Rossman fold [GXGXX(G/A)] for binding NADPH or FAD, respectively. Type I BVMOs have a strictly conserved sequence motif [FXGXXXHXXXW(P/D)] which is referred to as the 'BVMO fingerprint motif' and can be used in genome mining to identify putative type I BVMOs (Fraaije *et al*., 2002). The majority of the studies performed on BVMOs focused on type I enzymes, which includes $CHMO_{acinet}$.

Type II BVMOs, also referred to as class C BVMOs, are encoded by two genes, producing a monooxygenase and a reductase (van Berkel *et al*., 2006). The co-factor, riboflavin 5'-monophosphate (FMN), is reduced by the reductase, using either NADH or NADPH as electron donor. Also, the core of the monooxygenase adopts a TIM-barrel fold.

2.4. Reaction mechanism

The reaction mechanism of CHMO was elucidated with mechanistic studies using kinetic and spectral data (Sheng *et al*., 2001). The reaction proceeds in a similar fashion to the chemical BV reaction (Fig. 2.1), where the ketone undergoes a nucleophilic attack to produce the tetrahedral 'Criegee'-intermediate, which rearranges to release a carboxylate ion. Migration of a carbon-carbon bond occurs, which results in the production of an ester (Criegee, 1948).

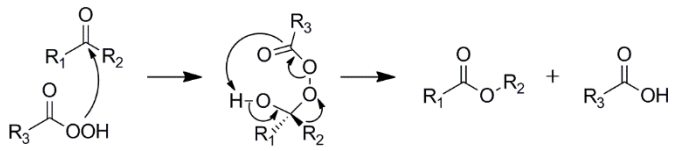

Figure 2.1. Reaction scheme for the chemical Baeyer-Villiger reaction (Kamerbeek *et al*., 2003).

The reaction scheme of CHMO, the model type I BVMO, is depicted in Fig. 2.2. The co-factor NAD(P)H reduces the flavin moiety (FAD) and remains bound to the enzyme, producing a reduced co-factor-protein complex. Molecular oxygen reacts with the reduced FAD to produce a C_{4a}flavin-peroxide species, which launches a nucleophilic attack on the carbonyl group of the ketone substrate. As in chemical BV catalysis, a tetrahedral 'Criegee' intermediate is produced. The intermediate undergoes rearrangement to the ester or lactone, simultaneously producing a flavin hydride. Water is spontaneously eliminated to produce the oxidised FAD, the substrate is released followed by the oxidised $NADP^+$ co-factor.

Besides the oxidation of ketones and lactones, BVMOs can oxidise a variety of heteroatom compounds. The flavin peroxide can exist as both a nucleophile, peroxyflavin, as well as an electrophile, hydroperoxyflavin (Walsh and Chen, 1988). This ambivalent state allows the oxygenation of both electron-rich and electron-deficient substrates (Fig. 2.3). The nucleophilic peroxyflavin is responsible for the Baeyer-Villiger oxidation of ketones and lactones, and is also involved in the oxidation of boron. BVMOs can also perform the asymmetric sulfoxidation of prochiral thioethers (Chen *et al*., 1999), as well as the oxidation of amines (Ottolina *et al*., 1999) and selenides (Walsh and Chen, 1988), which are all proposed to occur via the electrophilic hydroperoxyflavin species. Epoxidation reactions have also been observed for BVMOs, but it is uncertain which peroxyflavin species mediates the reaction (Colonna *et al*., 2002).

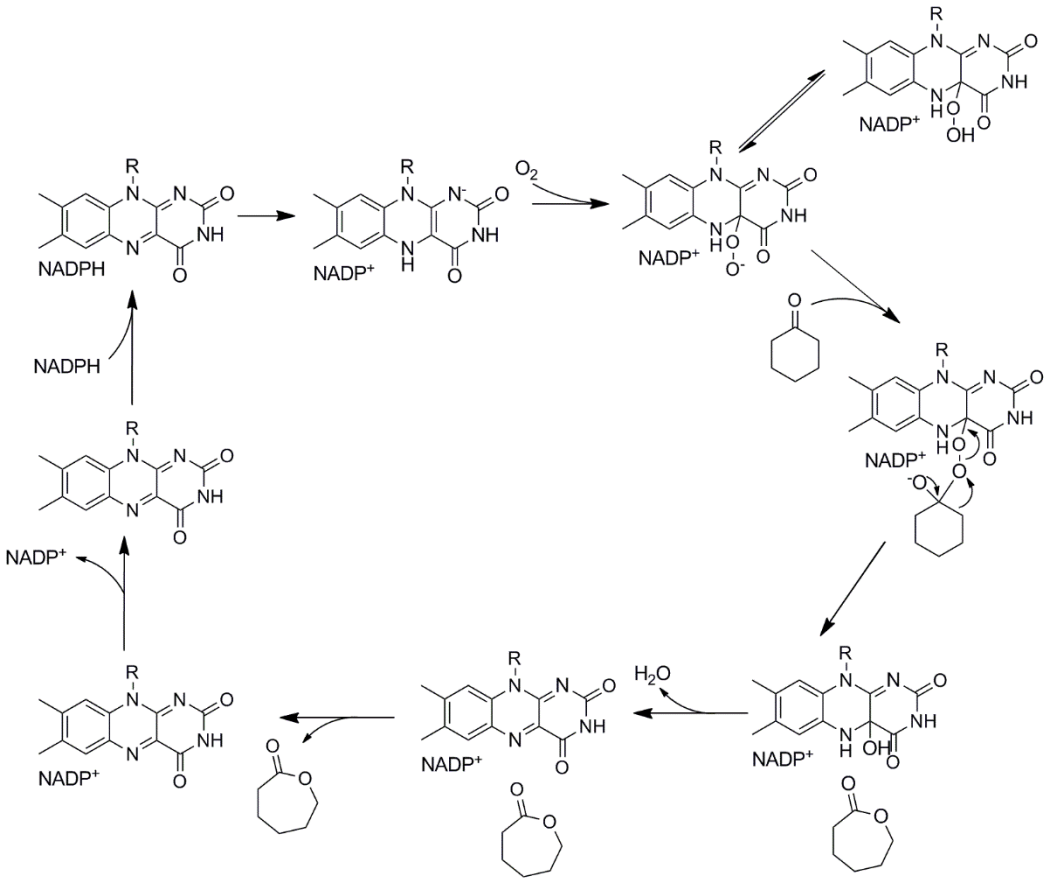

Figure 2.2. Reaction mechanism of the oxidation of cyclohexanone by CHMO (Leisch *et al*., 2011).

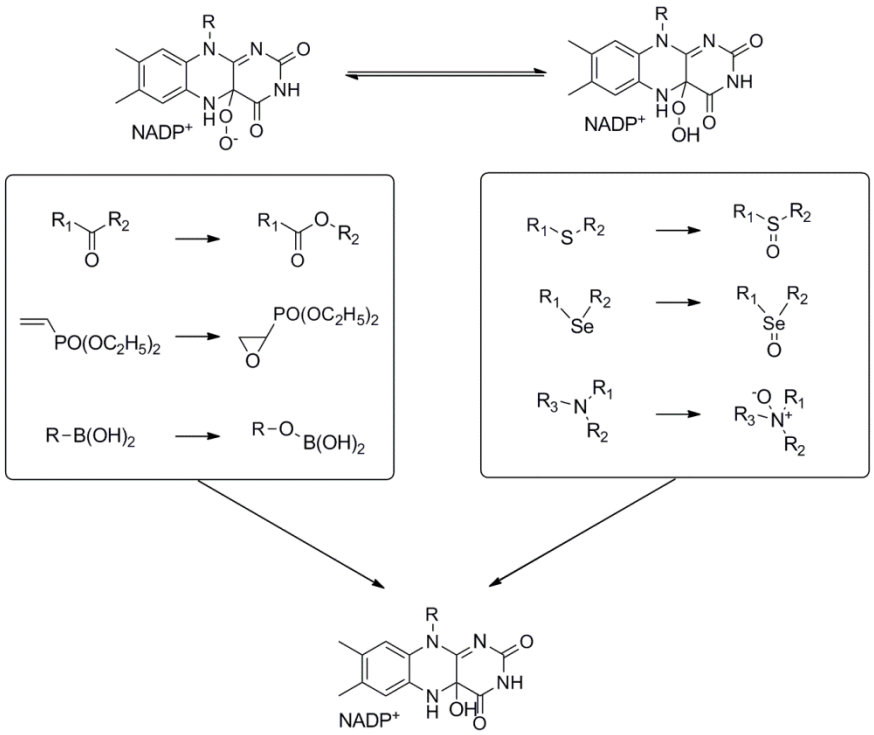

Figure 2.3. The peroxyflavin and hydroperoxyflavin species and the corresponding oxygenation reactions performed by each species (Kamerbeek *et al*., 2003).

2.5. Crystal structures

The availability of three-dimensional structures of BVMOs allows an intimate insight into the architecture and functioning of these enzymes. Crystal structures have been elucidated for a number of bacterial BVMOs, although no structure of a fungal BVMO is available yet.

The first crystal structure of a BVMO to be solved was that of phenylacetone monooxygenase (Malito *et al*., 2004), isolated from the moderate thermophile *Thermobifida fusca* ($PAMO_{thermo}$) (Fraaije *et al*., 2005). The 65 kDa monomeric enzyme is thermostable and oxidises a variety of phenyl-substituted ketones, linear ketones, bicyclic ketones as well as sulfur-containing compounds. $PAMO_{thermo}$ displays the highest affinity towards phenylacetone, from which it has taken its name.

The crystal structure revealed that $PAMO_{thermo}$ consist of two domains, an FAD-binding domain and an NADPH-binding domain, both carrying a Rossman fold characteristic of dinucleotide-binding domains (Fig. 2.4a). The NADP domain contains an α-helical subdomain which interacts with the FAD-binding domain and forms part of the active site.

The structure of CHMO from *Rhodococcus* sp. HI-31 ($CHMO_{rhodoc}$) was elucidated in 2009 (Mirza *et al*., 2009). *Rhodococcus* sp. strain HI-31 was a new environmental isolate utilising cyclohexanone as sole carbon source, as in the case of $CHMO_{acinet}$. The recombinantly expressed $CHMO_{rhodoc}$ shares 55 % sequence identity with $CHMO_{acinet}$ of which, to date, the crystal structure remains elusive. $CHMO_{rhodoc}$ displays the same regio- and enantioselectivity as $CHMO_{acinet}$ with a similar, but extended substrate range. Two crystal structures of $CHMO_{rhodoc}$ were elucidated, each representing the enzyme in different stages of catalysis. This revealed that the NADP domain is rotated during catalysis and that a loop, which is solvent accessible in the one configuration, forms part of the well-defined active site cavity in the other.

The role of the BVMO signature motif was also highlighted in the crystal structures (Fig. 2.4b). The sequence motif consists of 12 residues that form part of the NADP domain. In the $CHMO_{rhodoc}$ structures which are in complex with $NADP^+$, the central histidine is rotated inwards to form hydrogen bonds with a flexible linker segment. The linker connects the NADP and FAD domains and also functions to position the NADPH moiety through stearic interactions. Thus, the signature motif plays a role in the conformational changes adopted by the enzyme and also functions to position the NADPH during catalysis.

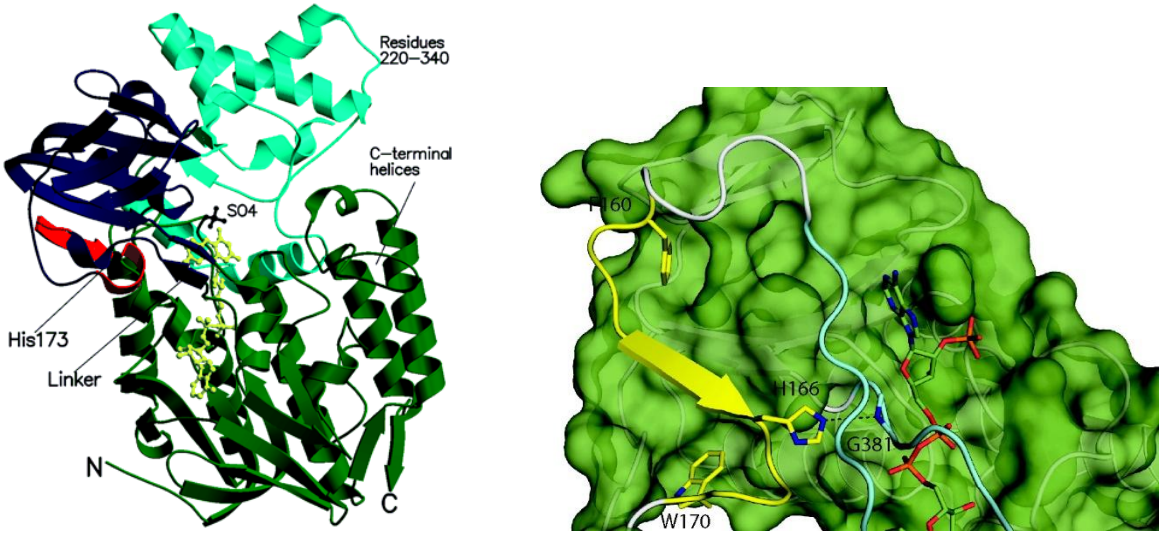

a b

Figure 2.4.a, The crystal structure of phenylacetone monooxygenase ($PAMO_{thermo}$) from *Thermobifida fusca* (Malito *et al*., 2004). The FAD-binding domain is shown in green, and the NADPH-binding domain is shown in blue, with the α-helical subdomain indicated in cyan. The BVMO fingerprint motif is outlined in red, while the bound FAD is depicted in yellow. The critically conserved histidine residue, 173, is indicated as well. **b,** The BVMO signature motif (yellow) of $CHMO_{rhodoc}$. The motif is anchored into the NADPH domain by hydrophobic residues and the central histidine H166 interacts with G381 to facilitate the domain movement during catalysis (Mirza *et al*., 2009).

2.6. Natural roles of BVMOs

As in the case of $CHMO_{acinet}$, many BVMOs fulfil a role in the degradation of alicyclic and aromatic ketones, enabling the utilisation of atypical carbon sources and thereby improving the metabolic flexibility of the host. Other examples include the cyclopentanone monooxygenase from *Pseudomonas* NCIMB 9872 ($CPMO_{comamo}$), also referred to as *Comamonas* sp. (Griffin and Trudgill, 1976) and the cyclododecanone monooxygenase from *Rhodococcus ruber* ($CDMO_{rhodoc}$) (Kostichka *et al*., 2001). The respective BVMO genes are located in gene clusters encoding the enzymes necessary for the degradation of the alcohol carbon source - cyclohexanol, cyclopentanol and cyclododecanol (Cheng *et al*., 2000; Iwaki *et al*., 2002; Kostichka *et al*., 2001). The degradation of the alcohol precursors follows similar pathways in the organisms (Fig. 2.5), and includes the conversion of the alcohol to a cyclic ketone by dehydrogenase activity, the Baeyer-Villiger oxygenation of the ketone to produce a lactone, hydrolytic ring opening by an esterase, followed by dehydration and reduction to produce a diacid which can enter the central metabolism via β-oxidation.

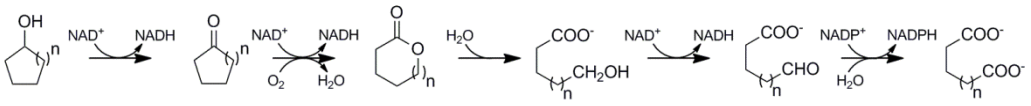

Figure 2.5. Degradation pathway for the metabolism of cyclic alcohols with n = 1, 2 or 8. The genes involved in the degradation pathway are located in a cluster. The cyclic alcohol is converted to a ketone by the function of an alcohol dehydrogenase, whereafter a BVMO converts the alcohol to a lactone; an esterase then functions to open the ring structure, after which the hydroxy acid is oxidized to produce a diacid which can enter the central metabolism via β-oxidation (Cheng *et al*., 2000; Iwaki *et al*., 2002; Kostichka *et al*., 2001).

From the aflatoxin biosynthesis pathway, it is clear that BVMOs do not solely function in catabolic pathways. A number of BVMOs occurring in biosynthetic pathways have been characterised, most of which the genes are located in large gene clusters responsible for the enzymes involved in the pathway. Similar to aflatoxins, many of the compounds are produced via a polyketide-initiated pathway.

Numerous BVMOs have been identified in the synthesis of antibiotics and anti-cancer compounds by the Streptomycetes. Mithramycin is an aureolic acid-type anticancer drug produced by *Streptomyces argillaceus* and various other Streptomycetes (Gibson *et al*., 2005). MtmOIV performs a BV-type oxidative cleavage reaction in one of the metabolic steps involved in mithramycin synthesis. MtmOIV has been purified and demonstrated to catalyse the conversion of premithramycin B to premithramicin B-lactone (Fig. 2.6), confirming the natural role of the enzyme.

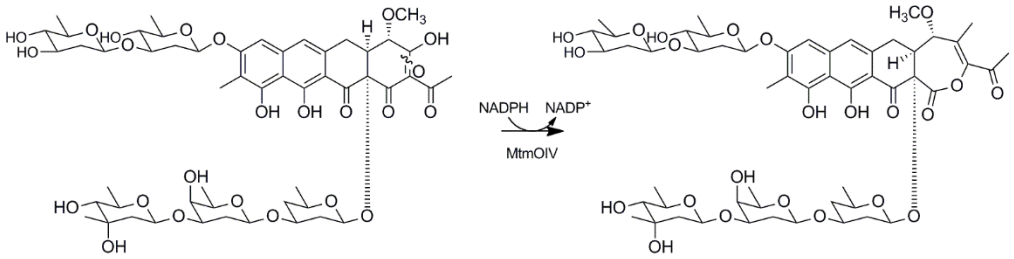

Figure 2.6. The conversion of premithramycin B to premithramycin B-lactone by MtmOIV, the BVMO involved in mithramycin synthesis (Beam *et al*., 2009).

Furthermore, the crystal structure of MtmOIV has been determined and provides evidence for a flavin-catalysed reaction (Beam *et al*., 2009). However, the structure of MtmOIV is highly dissimilar to the structures of $PAMO_{thermo}$ and $CHMO_{rhodoc}$, which is not surprising. MtmOIV, which is encoded by a single gene and uses FAD as co-factor, does not contain the BVMO fingerprint motif and lacks significant sequence homology to well-characterised type I BVMOs (*e.g.* only 8 % sequence identity with $PAMO_{thermo}$). Also, MtmOIV is not related to type II BVMOs. Therefore, MtmOIV represents a new class of BVMO, "O", and belongs to the class A FMOs.

Pentalenolactones are antiviral and antibiotic compounds produced by members of the *Streptomyces*, and are active against DNA viruses, both Gram-positive and Gram-negative bacteria, pathogenic and saprophytic fungi (English *et al*., 1957). In *S. avermitilis,* the genes involved in the synthesis of pentalenolactones are clustered in a 13.4 kb region and contains 13 ORFs (Jiang *et al*., 2009). Genome mining indicated that the gene cluster carries the *ptlE* gene which encodes a type I BMVO. Jiang and co-workers (2009) heterologously expressed *ptlE* and demonstrated that PtlE catalyses the BV oxidation of 1-deoxy-11-oxopentalenic acid to neopentalenolactone D, a compound which was not a known precursor of pentalenolactones (Fig. 2.7). The synthesis of neopentalenolactone D allowed access to a novel family of pentalenolactone derivatives, thereby improving the available structural diversity of the drugs.

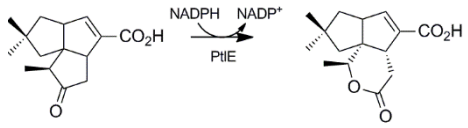

Figure 2.7. The conversion of 1-deoxy-11-oxopentalenic acid to neopentalenolactone D by the type I BVMO PtlE, a reaction that allows access to a novel branch of pentalenolactones (Jiang *et al*., 2009).

Gilvocarcins and jadomycins are anti-tumor drugs which are produced by certain species of the genus *Streptomyces*. The synthesis of gilvocarcins and jadomycins proceeds via a series of oxidations of the precursor angucyclinones (Kharel *et al*., 2007). The genes responsible for gilvocarcin synthesis is located in a cluster of ~32 kb which contains 26 ORFs (Fischer *et al*., 2003). The enzymes GilOII in gilvocarcin synthesis and JadG in jadomycin synthesis are BVMOs which forms part of a multi-oxygenase complex and are responsible for the Baeyer-Villiger oxidation to produce gilvocarcin and jadomycin, respectively (Fig. 2.8). The function of these enzymes has recently been verified by heterologous expression in *E. coli* (Tibrewal *et al*., 2012).

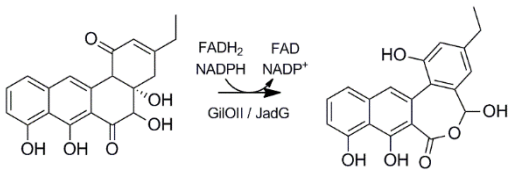

Figure 2.8. The enzymatic reaction performed by GilOII and JadG in gilvocarcin and jadomycin synthesis, respectively (Tibrewal *et al*., 2012).

The genes involved in the biosynthesis of the antibiotic chlorothricin in *Streptomyces antibioticus* are located in a large gene cluster spanning more than 110 kb and containing 42 ORFs (Jia *et al*., 2006). Two genes were identified as encoding FAD-dependent monooxygenases. A BV reaction is involved in the synthesis of a macrocyclic lactone (Fig. 2.9), suggesting that one of the two genes may indeed be a BVMO responsible for the metabolic step.

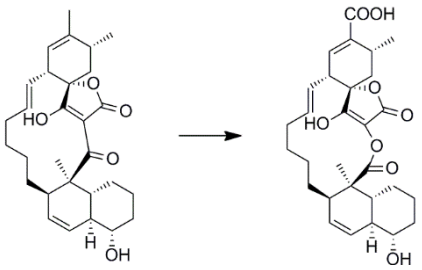

Figure 2.9. A metabolic step in chlorothricin biosynthesis in which a BVMO participates (Jia *et al*., 2006).

2.7. Conclusions and introduction to study

BVMOs represent a well-characterised family of flavin-dependent enzymes. The reaction mechanism has been studied in detail and the three-dimensional structure of the enzymes provides valuable insight to the functioning of BVMOs. Although the majority of studies focus on BVMOs as biocatalysts, the natural roles of BVMOs in their native hosts has been investigated to some extent.

The metabolic step in the aflatoxin pathway that converts hydroxyversicolorone (HVN) to versiconal hemiacetal acetate (VHA), as well as versicolorone (VONE) to versiconol acetate (VOAc), represents a typical BV reaction and the enzyme involved is presumed to be a type I BVMO. The metabolic step represents an ideal candidate for enzyme-targeted aflatoxin inhibition. Before inhibition of the selected metabolic step can be studied, the target enzyme must be characterised in detail.

The first hypothesis to be tested was whether the *moxY* gene from *A. flavus* encodes the BVMO involved in the conversion of HVN to VHA, confirming the natural role of MoxY. Although the *ΔmoxY* gene-knockout mutants were non-leaky, it has to be considered that other BVMO genes may be present in the genome of *A. flavus.* Therefore, the second hypothesis to be tested was whether the function of MoxY can be complemented by the presence of another BVMO in *A. flavus.*

Chapter 3

Heterologous expression and characterisation of MoxY

3.1. Introduction

Hydroxyversicolorone (HVN) was first isolated in 1988 from an UV-irradiated mutant of *Aspergillus parasiticus,* WE-47 (Townsend *et al*., 1988). Yabe and co-workers (1991b; 2003) proceeded to demonstrate that the HVN is converted to versiconal hemiacetal acetate (VHA), an NADPH-dependent reaction that forms part of a complex metabolic grid in the conversion of averufin (AVF) to versicolorin B (VB) (Fig. 1.3). Gene-disruption experiments implicated the product of the *moxY* gene in the conversion of HVN to VHA. Furthermore, MoxY was also involved in the conversion of versicolorone (VONE) to versiconol acetate (VOAc), the hydroxylated counterparts of HVN and VONE that exist in the parallel conversion pathway of the metabolic grid.

The conversion of HVN and VONE to VHA and VOAc, respectively, occur by the insertion of an oxygen atom adjacent to a ketone group to produce the corresponding ester. This metabolic step is a typical Baeyer-Villiger reaction which is catalysed in nature by flavin-containing, nicotinamide co-factor dependent Baeyer-Villiger monooxygenases (BVMOs) (Leisch *et al*., 2011). As described in chapter 2, the BVMO catalysis has been studied in detail, therefore, it is strongly suggested that the conversion of HVN and VONE to VHA and VOAc is performed by a single enzyme, the BVMO MoxY.

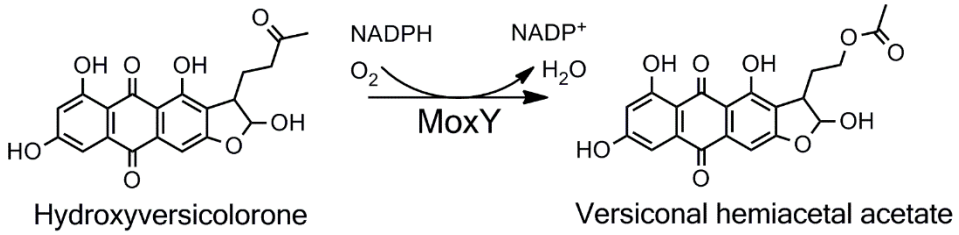

Figure 3.1. Reaction scheme of the conversion of hydroxyversicolorone (HVN) to versiconal hemiacetal acetate (VHA) by MoxY. One atom of molecular oxygen is incorporated into HVN to produce the ester VHA. The other atom is reduced to water with the concomitant oxidation of NADPH.

The proposed reaction of MoxY is illustrated in Fig. 3.1. One atom of molecular oxygen is incorporated into HVN to produce VHA, while the other is reduced to H_2O, with the concomitant oxidation of NADPH.

The aim of this chapter was to recombinantly express the *moxY* gene from *A. flavus* in *Escherichia coli*, to purify the recombinant MoxY and to characterise the purified enzyme. Due to the discrepancies between the predicted intron-exon structure from the National Center for Biotechnology Information (NCBI) database, as well as an alternative up-stream start codon, multiple constructs were created to establish the biologically active form of MoxY.

3.2. Materials and Methods

3.2.1. Strains and plasmids

All strains and plasmids used are listed in Table 3.1. *Aspergillus flavus* NRRL 3357 was obtained from the Agricultural Research Service culture collection (ARS, United States Department of Agriculture). *A. flavus* was cultured aerobically on Potato Dextrose Agar (PDA) or Yeast Mold Agar (YMA) slants at 25°C (Table A1, appendix), whereafter it was maintained at 4°C. *Escherichia coli* TOP10 cells (Life Technologies™) were used as host for genetic manipulation to generate the expression constructs. *E. coli* strains were cultured in Luria-Bertani (LB) medium (Table A1) at 37°C with shaking (200 rpm). Kanamycin (30 µg.ml^{-1}), ampicillin (100 µg.ml^{-1}) or chloramphenicol (34 µg.ml^{-1}) was added to the media to ensure maintenance of the plasmid. The Rosetta-gami™ 2(DE3)pLysS (Novagen) strain served as a source of plasmid pLysSRARE2 (Novagen®).

The pSMART® (Lucigen®) plasmid was used to clone and manipulate the *moxY* gene. pUC57 served as a host plasmid in which commercially synthesised genes were received (GenScript). pET-22b(+) and pET-28b(+) (Novagen®) were used for expression of the MoxY protein in *E. coli* strain BL21-Gold(DE3) (Agilent Technologies).

Table 3.1. Strains and plasmids used in this study.

Strain	Description	Manufacturer
Escherichia coli TOP10	One shot® TOP10 chemically competent cells F⁻ *mcrA* Δ(*mrr-hsd*RMS-*mcr*BC) ϕ80*lac*ZΔM15 Δ*lac*X74 *rec*A1 *ara*D139 Δ(*araleu*)7697 *gal*U *gal*K *rps*L (Str^R) *end*A1 *nup*G	Life Technologies™
Escherichia coli BL21-Gold(DE3)	*E. coli* B F⁻ *ompT hsdS*($r_B^-m_B^-$) *dcm*⁺ Tet^r *gal* λ(DE3) *endA* Hte	Agilent Technologies
Escherichia coli Rosetta-gami™ 2 (DE3) pLysS	Δ (*ara-leu*) *7697* Δ*lacX74* Δ*phoA Pvu*II *phoR araD139 ahpC gale galK rpsL* (DE3) F'[lac_+ $lacI^q$ *pro*] *gor522*::Tn*10 trxB* pRARE2 (Cam^R, Str^R, Tet^R)	Novagen®
pSMART®	pSMART®-HCKan (High copy number) ori Kan^R	Lucigen®
pET-22b(+)	Ap^R, *lac*I, T7*lac* promotor, T7 terminator, f1 ori	Novagen®
pET-28b(+)	Kan^R, T7*lac* promotor, T7 terminator, f1 ori, N-terminal His-tag and thrombin configuration	Novagen®
pLysSRARE2	Cm^R, T7 lysozyme, *argX* tRNA, *proL* tRNA, *leuW* tRNA, *meT* tRNA, *argW* tRNA, *thrT* tRNA, *glyT* tRNA, *tyrU* tRNA, *thrU* tRNA, *argU* tRNA, *ileX* tRNA, p15a ori	Novagen®
pUC57	Ap^R *lacZ rep*(pMB1)	GenScript
pG-KJE8	Cm^R, pACYC ori, *araB, araC, dnaJ, dnaK*, *grpE, groES, groEL, Pzt1, tetR*, rrnBT1T2	Takara Bio Inc.
pGro7	Cm^R, pACYC ori, *araB*, *araC, groES, groEL*	Takara Bio Inc.
pKJE7	Cm^R, pACYC ori, *araB*, *araC, dnaJ, dnaK*, *grpE*	Takara Bio Inc.
pG-Tf2	Cm^R, pACYC ori, *tetR*, *groES, groEL, tig*	Takara Bio Inc.
pTf16	Cm^R, pACYC ori, *araB*, *araC*	Takara Bio Inc.

3.2.2. Isolation of genomic DNA from *Aspergillus flavus* NRRL 3357

A. flavus was cultured in Potato Dextrose Broth (PDB, BD Difco) at 25°C for five days on an orbital shaker (200 rpm). Cells were harvested through centrifugation and high molecular weight genomic DNA (gDNA) was isolated using the ZR Fungal/Bacterial DNA MicroPrep kit (Zymoresearch) according to the manufacturer's instructions.

3.2.3. Cloning of the open-reading frames (ORFs) of *moxY* and *moxYAltNC*

3.2.3.1. Polymerase chain reaction (PCR) amplification of *moxY* and *moxYAltNC*

The *moxY* gene was amplified from the gDNA by PCR. Two different amplicons were generated, namely *moxY*, as the gene was annotated by NCBI, and *moxYAltNC*, a version of *moxY* with an elongated N and C terminus, as depicted in Fig. A1 (appendix).

PCR reactions were performed using a thermal cycler with the KOD Hot Start DNA Polymerase system (Novagen®). The PCR reaction mixture consisted of 5 µl 10X Buffer for KOD Hot Start DNA polymerase, 1.5 mM $MgSO_4$, dNTPs (0.2 mM each), 0.3 µM sense primer (5'), 0.3 µM anti-sense primer (3'), KOD Hot Start DNA polymerase (1 U), template DNA and deionised water, to a total volume of 50 µl. For the initial amplification of the ORFs, 50 ng of gDNA was added to the reaction mixture, whereas 10 ng of DNA was added in subsequent steps where plasmid DNA served as the template.

The thermal cycling procedure was initiated by incubation at 95°C for 2 min to activate the polymerase. The thermal cycle consisted of a denaturing step (95°C for 2 min), annealing of the primer to the template (Table 3.2) and an extension step (70°C for 25 $s.kb^{-1}$). The thermal cycle was repeated 25 times after which a final elongation step of 5 min at 70°C was added to ensure complete elongation of the amplicons.

All primers used in constructing the MoxY expression vectors are listed in Table 3.2. Primers were designed using the Integrated DNA Technologies OligoAnalyzer 3.1 online tool. The *moxY* and *moxYAltNC* genes were amplified from the gDNA of *Aspergillus flavus* using primer set 1 and 2, respectively, with an extension time of 1 min and annealing temperatures of 64°C and 60°C.

Table 3.2. Primer sequences used for PCR amplification of *moxY* and *moxYAltNC*.

Primer Set	Primer	Sequence	T_m (°C)	PCR Annealing Temperature (°C)
1	BVMO_AF_384_F_NdeI	5'-CAT ATG GAC CCG GCC AAC CGC CCG TTG-3'	68.7	64
	BVMO_AF_384_R_XhoI	5'-CTC GAG CTA GCG GTT ACT GTC AGA AAC TCC ATT GG-3'	64.7	
2	BVMO_AF_384_ALTNC_F_NdeI	5'-CAT ATG TCA AAG GTG GAC TAC TCT CAG CC-3'	60.0	60
	BVMO_AF_384_ALTNC_R_HindIII	5'-AAG CTT TTA CGT GAA ACG GAC AAG CGC-3'	61.9	

Underlined sequences indicate introduced restriction sites for *Nde*I, *Xho*I, and *Hind*III

3.2.3.2. Blunt-end ligation of PCR product into pSMART®

The purified PCR product was dried under vacuum in a Speed-Vac concentrator and dissolved in 15 µl of deionised water. Phosphorylation of the PCR product was achieved by incubation with 1 U of polynucleotide kinase (PNK, Thermo Scientific), 2 µl Buffer A and 1 mM ATP in a total volume of 20 µl at 37°C for 20 min. PNK was deactivated by incubation at 72°C for 10 min. The PCR product was ligated into pSMART® by adding 6 µl of the phosphorylated product, 30 ng of pSMART® (Lucigen®, Fig. 3.2), 1 µl of 50 % polyethylene glycol 4 000 (Sigma Aldrich), 1 µl of 10X ligase buffer and 5 Weiss U of T4 DNA ligase to a total volume of 10 µl, and incubating the mixture overnight at 4°C.

In order to verify whether the pSMART® vector contained the inserted *moxY* or *moxYAltNC*, the constructs were digested with restriction enzymes and visualized on an agarose gel. The pSMART®:moxY construct was double-digested with *Nde*I and *Xho*I by incubating 4 µl of plasmid, 1 µl of 10X Buffer R, 10 U of *Nde*I, 5 U of *Xho*I and deionised water to a total volume of 10 µl, at 37°C for 1 h. The pSMART®:moxYAltNC construct was digested with *Eco*RI. The reaction mixture contained 2 µl of the construct, 2 U *Eco*RI, 0.5 µl of 10X *Eco*RI buffer, adjusted to a total volume of 5 µl with deionised water and was incubated at 37°C for 1 h.

3.2.3.3. Transformations

For transformation reactions, 50 µl of chemically competent *E. coli* TOP10 cells (Life Technologies™) were thawed on ice. One microliter of the ligation mixture was added to the cells and incubated on ice for 30 min. The cells were heat-shocked at 42°C for 40 sec and returned to ice for 2 min, after which 250 µl of SOC media (Table A1) was added to the transformation reaction and incubated at 37°C for 1 h. The transformation mixture was plated out on LB plates containing kanamycin (30 $\mu g.ml^{-1}$) and incubated overnight at 37°C.

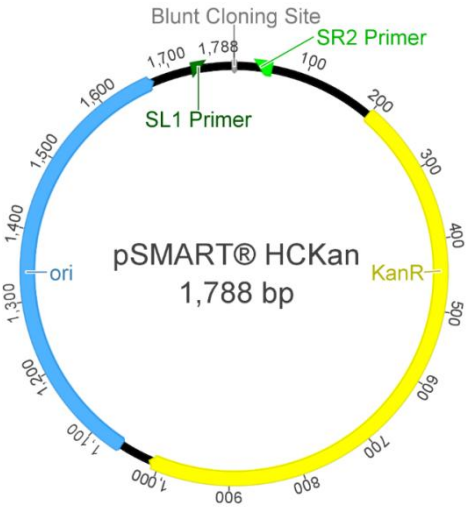

Figure 3.2. Vector map of pSMART® HCKan indicating the kanamycin resistance gene (KanR), the origin of replication (ori), the location of the blunt-cloning site and the binding sites of the sequencing primers, SL1 and SR2 (Lucigen®).

3.2.3.4. Plasmid proliferation

Single colonies of the successful *E. coli* transformants were inoculated into 5 ml LB media supplemented with kanamycin (30 $\mu g.ml^{-1}$) and cultured for 12 - 16 h at 37°C with shaking. Plasmids were isolated using the BioSpin Plasmid DNA Extraction Kit (BioFlux) according to the manufacturer's instructions. The plasmid concentration was determined using a NanoDrop™ ND-1000 spectrophotometer (Thermo Scientific).

3.2.3.5. Intron removal

Introns were removed sequentially from the pSMART®:moxY and pSMART®:moxYAltNC constructs by using inverse PCR with primers annealing to either sides of the intron, effectively amplifying the entire plasmid except the intron. PCR reaction setup and cycling conditions were as described in section 3.2.3.1, with an elongation time of 4 min. The intron-exon structures of the *moxY* and *moxYAltNC* genes are depicted in Fig. A1 (appendix). For removal of the common intron from pSMART®:moxY and pSMART®:moxYAltNC, primer set 3 was used with an annealing temperature of 59°C (Table 3.3). pSMART®:moxYAltNC from which the first intron was successfully deleted, served as template for removal of the second intron. Inverse PCR was performed with primer set 4 and an annealing temperature of 63°C.

Table 3.3. Primer sequences used for intron removal from pSMART®:moxY and pSMART®:moxYAltNC through inverse PCR.

Primer Set	Primer	Sequence	Tm (°C)	PCR Annealing Temperature (°C)
3	BVMO_AF_384_INT_F	5'-GTA CAA GAA CAA CGA GAC GGG TCG-3'	59.4	59
	BVMO_AF_384_INT_R	5'-CAG CTT CGG CAG TTA TCT TTC CAC AC-3'	59.9	
4	BVMO_AF_384_INTA_F	5'-GTA CGA AGA GGT GGG CGG CAA TCC-3'	63.8	63
	BVMO_AF_384_INTA_R	5'-CAT TTC GGG TCG ATC TCC TGT AAG CCC AG-3'	63.5	

After each PCR, contaminating template DNA was removed by *Dpn*I treatment. The PCR reaction mixture was incubated overnight at 37°C with 10 U of *Dpn*I and 4 µl of 10X Tango buffer. To circularise the amplified pSMART® constructs, a one-step phosphorylation and ligation reaction was performed. The PCR product was dried under vacuum in a SpeedVac Concentrator and solubilised in 13 µl deionised water. The product was incubated with 15 U T4 PNK, 7.5 Weiss U T4 DNA ligase, 1 mM ATP and 2 µl 10X T4 DNA ligase buffer for 1 h at 16°C. The reaction mixtures were again transformed into *E. coli* TOP10 cells, after which positive clones were identified by plasmid isolation and DNA sequencing.

3.2.3.6. Analytical techniques

3.2.3.6.1. DNA electrophoresis

The integrity of genomic DNA and DNA fragments was evaluated by electrophoresis on an agarose gel [0.8 % (w/v)] in TAE buffer [Tris (40 mM), acetic acid (20 mM), EDTA (1 mM), pH 8.3; Bio-Rad] for

approximately

45 min at 90 V. GoldView™ (SBS Genetech Co.) was added to facilitate DNA visualization using a ChemiDox™ XRS+ Gel Documentation system (Bio-Rad). Samples were loaded aside GeneRuler™ DNA Ladder (Thermo Scientific) or MassRuler™ DNA Ladder (Thermo Scientific) to estimate the size of the fragments. All PCR products and restriction digestion mixtures were analysed via agarose gel electrophoresis to confirm the success of the cloning steps. PCR clean-up was performed by separating the PCR reaction mixture on an agarose gel, excision of the desired band with a sterile surgical blade and purification from the agarose gel with the BioSpin Gel Extraction Kit (BioFlux), according to the manufacturer's instructions.

3.2.3.6.2. DNA sequencing

In order to verify that all PCR amplification and ligation steps were successful, the plasmids were submitted for DNA sequencing with a 3130*xl* Genetic Analyser (Hitachi). The BigDye® Terminator (v 3.1) Cycle Sequencing Kit (Applied Biosystems®) was used to amplify the insert for sequencing as per manufacturer's instructions, using the primers listed in Table A2 (appendix).

3.2.3.7. Commercial synthesis of *moxY* and *moxYAltNC*

moxY and *moxYAltNC* were commercially synthesised and optimized for expression in *E. coli* by GenScript USA Inc (Figs. A2 and A3, appendix). The genes, respectively referred to as *moxY OPT* and *moxYAltNC OPT*, were received in the pUC57 plasmid (Fig. 3.3) as pUC57:moxY OPT and pUC57:moxYAltNC OPT .

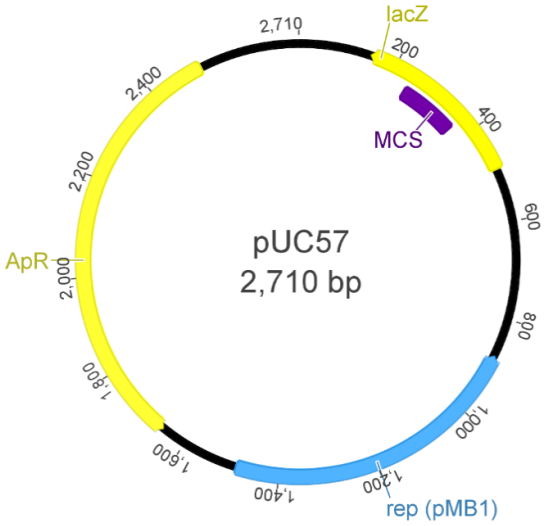

Figure 3.3. Vector map of pUC57 indicating the ampicillin resistance gene (ApR), the pMB1 origin of replication (rep), the *lacZ* coding region and the multiple cloning site (MCS) (GenScript).

3.2.4. Constructs for expression in *E. coli*

3.2.4.1. Sub-cloning of coding sequences (CDSs) from cloning vectors in pET-22b(+) and pET-28b(+)

The coding sequences (CDSs) of *moxY, moxY OPT, moxYAltNC* and *moxYAltNC OPT* were excised from the cloning vectors by means of restriction enzyme double-digestion. All restriction enzymes and restriction enzyme buffers were purchased from Thermo Scientific. The reaction mixture for the excision of *moxY* from pSMART® consisted of 8 µl plasmid, 5 U *Nde*I, 10 U *Xho*I, 2 µl of 10X Buffer R adjusted to a final volume of 20 µl with deionised water. For the excision of *moxY OPT, moxYAltNC* and *moxYAltNC OPT*, the reaction mixture consisted of 4 µl of plasmid, 1 µl of 10X Buffer R, 10 U of *Nde*I, 5 U of *Hind*III, adjusted to a total volume of 10 µl with deionised water. The reaction mixtures were incubated at 37°C for 1 h. pET-22b(+) and pET-28b(+) (Fig 3.4) were similarly digested. The digestion mixtures were separated on an agarose gel and bands corresponding to the desired sizes were excised and purified, as described in section 3.2.3.6.

Cohesive-end ligations were performed in a 1:1 molar ratio to ligate the excised CDSs into the digested pET-22b(+) and pET-28b(+) backbones. The ligation mixtures, comprising of 5 µl of the excised fragment, 3 µl of vector backbone, 5 Weiss U T4 DNA ligase and 1 µl of 10X T4 DNA ligase buffer, was incubated overnight at 16°C. The ligation mixtures were transformed into *E. coli* TOP10 cells and the plasmids isolated as previously described.

In order to verify whether successful clones contained the inserted fragment, restriction enzyme double-digestion was performed. The digestion mixtures, consisting of 4 µl plasmid DNA, 5 U *Xho*I, 10 U *Xba*I, 2 µl of 10X Buffer Tango, adjusted to a total volume of 10 µl with deionised water, were incubated at 37°C for 1 h and visualized by DNA gel electrophoresis. Clones containing the insert were confirmed by DNA sequencing.

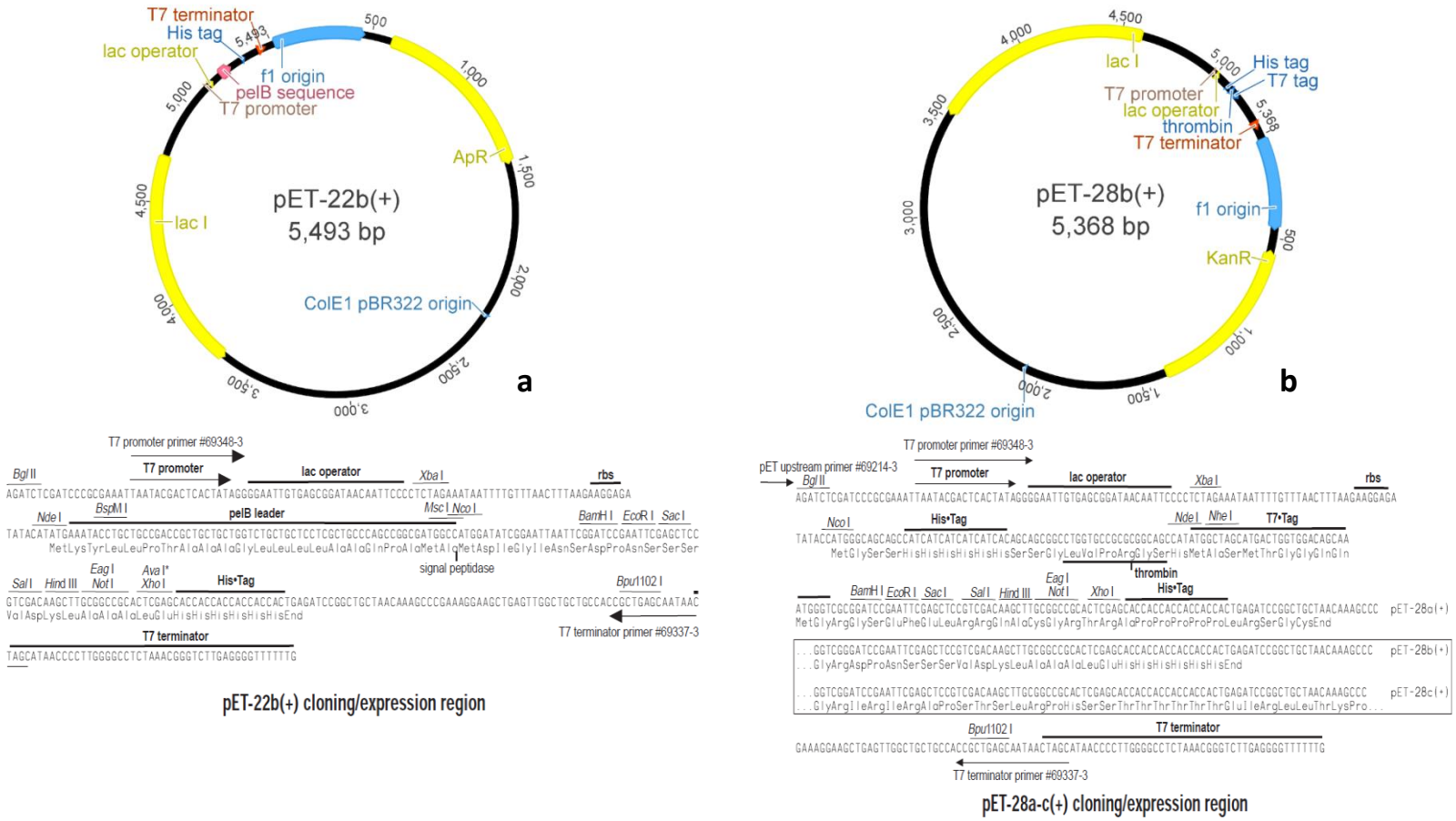

Figure 3.4. Vector map of **a**, pET-22b(+) and **b,** pET-28b(+) indicating the ampicillin (ApR) or kanamycin (KanR) resistance genes, the ColE1 pBR322 origin of replication, the location of the T7 promoter and the *lacI* coding sequence. The sequences of the cloning and expression regions indicates the binding sites of the T7 promoter and T7 terminator sequencing primers, the restriction enzyme recognition sites, as well as the location of the sequence coding for the His-tag (Novagen®).

3.2.4.2. Construction of *moxY* variants with an alternative N or alternative C terminus

A double cross-over method was used to create *moxYAltN* and *moxYAltC* variants by recombination of the pET vectors carrying *moxY* and *moxYAltNC*, as illustrated in Fig. 3.5. The corresponding vectors carrying the *moxY* and *moxYAltNC* genes were digested overnight at 37°C with the reaction setup as listed in Table 3.4, yielding two fragments each. The digested plasmids were separated on an agarose gel and both fragments were purified.

In preparation for the ligation reactions, each fragment was concentrated under vacuum in a SpeedVac concentrator to a volume of 10 µl for the larger fragments and 5 µl for the smaller fragments. Cohesive-end ligations were performed with 10 µl of the large fragment of the first plasmid, 5 µl of the small fragment of the second plasmid, 5 Weiss U T4 DNA ligase and 1 µl of 10X T4 DNA ligase buffer, overnight at 4°C. Plasmids were isolated and subjected to DNA sequencing to confirm the success of the ligation step.

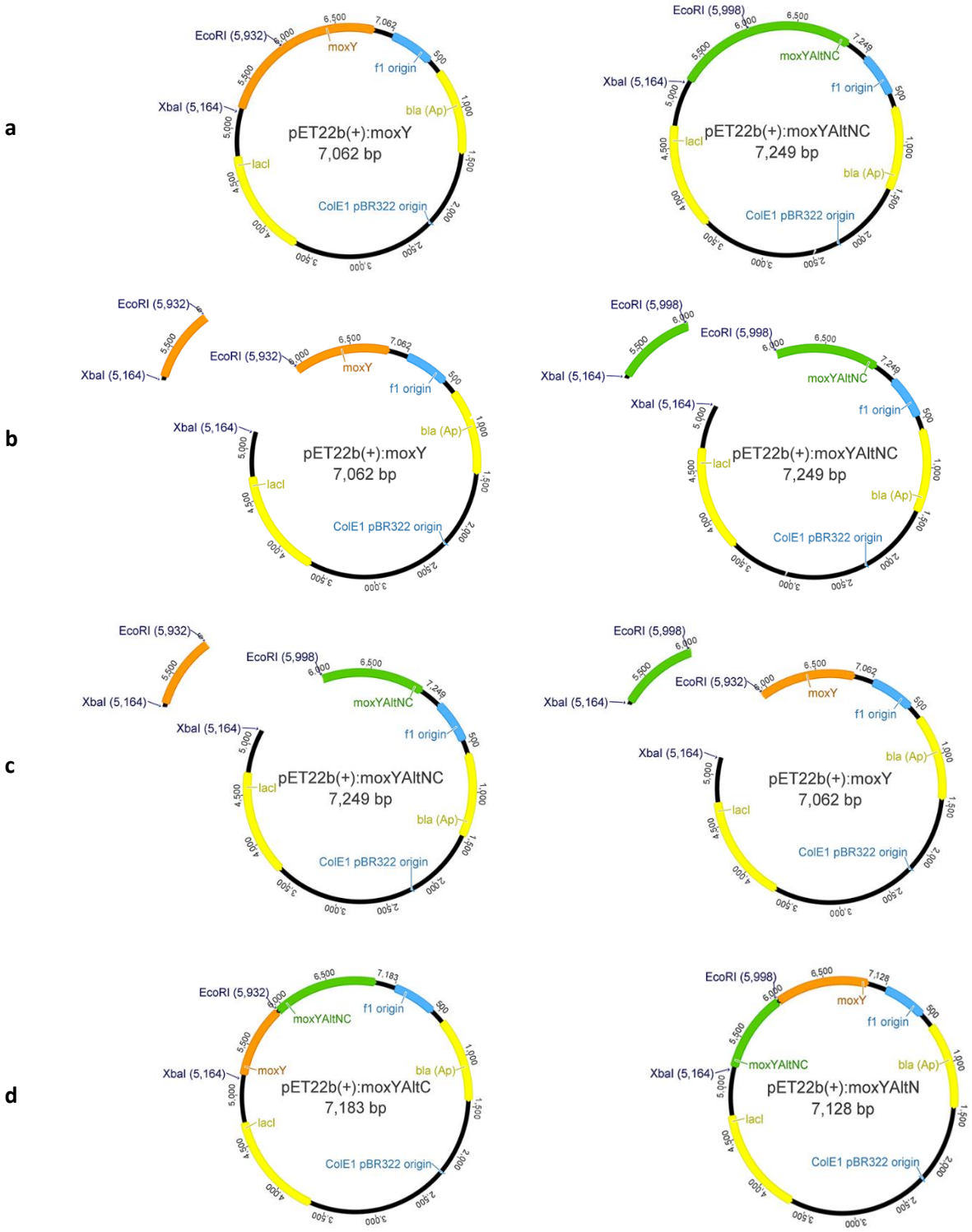

Figure 3.5. The double cross-over strategy to create *moxY* variants with either an alternative N or C terminus; **a,** two corresponding vectors were selected that carry the *moxY* and *moxYAltNC* genes; **b,** corresponding restriction sites were selected in both vectors, one cutting in the vector backbone (*Xba*I) and another cutting in the *moxY* and *moxYAltNC* genes (*Eco*RI), the vectors were double-digested with the restriction enzymes and the fragments purified; **c,** the small fragment of the first vector, carrying the N-terminus and a portion of the coding region, was ligated into the large fragment of the second vector to produce **d,** constructs coding for *moxY* with either an alternative N or alternative C terminus.

Table 3.4. Vector combinations and restriction enzyme digestion setup to generate fragments for the production of *moxYAltN* and *moxYAltC* variants. The vectors produced by ligation of the fragments are indicated in the last column.

Vector combination	Buffer	Restriction enzyme cutting in backbone	Restriction enzyme cutting in gene	Template	Deionised water	Ligated products
pET-22b(+):moxYAltNC	10X Tango	*Xba*I	*Eco*RI			pET-22b(+):moxYAltN
pET-22b(+):moxY	2 µl	1 µl	0.5 µl	4 µl	2.5 µl	pET-22b(+):moxYAltC
pET-28b(+):moxYAltNC	10X Tango	*Xba*I	*Eco*RI			pET-28b(+):moxYAltN
pET-28b(+):moxY	2 µl	1 µl	0.5 µl	4 µl	2.5 µl	pET-28b(+):moxYAltC
pET-22b(+):moxYAltNC OPT	10X Tango	*Xba*I	*Nco*I			pET-22b(+):moxYAltN OPT
pET-22b(+):moxY OPT	1 µl	0.5 µl	0.5 µl	4 µl	4 µl	pET-22b(+):moxYAltC OPT
pET-28b(+):moxYAltNC OPT	10X Tango	*Xba*I	*Sac*I			pET-28b(+):moxYAltN OPT
pET-28b(+):moxY OPT	1 µl	0.5 µl	1 µl	4 µl	3.5 µl	pET-28b(+):moxYAltC OPT

3.2.4.3. Creation of C-terminally His-tagged variants

The pET-22b(+) vector contains a coding sequence for a C-terminal poly(His)$_6$-tag (hereon referred to as a His-tag). C-terminally His-tagged (CTH) variants were created from the pET-22b(+) constructs by inverse PCR, using primers that anneal to either sides of the original stop-codon of the gene. In effect, the entire plasmid was amplified, excluding the stop-codon. The PCR reaction setup and cycling conditions were as described in section 3.2.3.1, with an extension time of 4 min. The plasmid template, primer sets and annealing temperatures are listed in Tables 3.5 and 3.6.

Table 3.5. Primer sets and templates used for the creation of C-terminally His-tagged (CTH) *moxY*-variants by inverse PCR.

Template	Primer set	Variant created
pET-22b(+):moxY	5	pET-22b(+):moxY-CTH
pET-22b(+):moxYAltN	5	pET-22b(+):moxYAltN-CTH
pET-22b(+):moxYAltNC	6	pET-22b(+):moxYAltNC-CTH
pET-22b(+):moxYAltC	6	pET-22b(+):moxYAltC-CTH
pET-22b(+):moxYAltNC OPT	7	pET-22b(+):moxYAltNC OPT-CTH
pET-22b(+):moxYAltC OPT	7	pET-22b(+):moxYAltC OPT-CTH
pET-22b(+):moxY OPT	8	pET-22b(+):moxY OPT-CTH
pET-22b(+):moxYAltN OPT	8	pET-22b(+):moxYAltN OPT-CTH

Table 3.6. Primer sequences used for the creation of the C-terminally His-tagged (CTH) variants.

Primer Set	Primer	Sequence	Tm (°C)	PCR Annealing Temperature (°C)
5	BVMO_AF_384_CTHis_R	5'-GCG GTT ACT GTC AGA AAC TCC ATT GG-3'	59.7	59
	BVMO_AF_ALL_CTHis_F	5'-CAC CAC CAC CAC CAC CAC TGA GAT C-3'	63.1	
6	BVMO_AF_384_ALTC_CTHis_R	5'-CGT GAA ACG GAC AAG CGC CCA G-3'	63.3	63
	BVMO_AF_ALL_CTHis_F	5'-CAC CAC CAC CAC CAC CAC TGA GAT C-3'	63.1	
7	BVMO384_ALTCOPT_CTHisR2	5'-GGT AAA ACG GAC CAG AGC CCA ACC C-3'	63.6	63
	BVMO_AF_ALL_CTHis_F	5'-CAC CAC CAC CAC CAC CAC TGA GAT C-3'	63.1	
8	BVMO384_OPT_CTHisR	5'-GCG ATT ACT ATC TGA CAC GCC ATT GGA CGG-3'	63.7	63
	BVMO_AF_ALL_CTHis_F	5'-GCG ATT ACT ATC TGA CAC GCC ATT GGA CGG-3'	63.7	

The template DNA was removed by *Dpn*I digestion (section 3.2.3.5), after which the PCR product was purified. The plasmids were circularised as described in section 3.2.3.5 and positive clones were identified by DNA sequencing.

3.2.5. Heterologous expression of *moxY* and variants

The pET-22b(+)/pET-28b(+) constructs containing the *moxY* and *moxY* variant genes were transformed into competent *E. coli* BL21-Gold(DE3) cells (Agilent Technologies) for expression. Cyclohexanone monooxygenase (CHMO) from *Acinetobacter calcoaceticus* was expressed in pET-22b(+) as a positive control. Successful transformants were identified through selection on LB agar plates supplemented with 100 $\mu g.ml^{-1}$ ampicillin or 30 $\mu g.ml^{-1}$ kanamycin. At least three colonies were co-inoculated into 5 ml LB media supplemented with the appropriate antibiotics and incubated at 37°C for 12 – 16 h with shaking.

For expression, 2 ml of the culture were used to inoculate 100 ml ZYP5052 auto-induction media (Table A1), also containing the appropriate antibiotics, in a 500 ml Erlenmeyer flask. The flasks were incubated at 25°C in an orbital shaker (200 rpm) for 36 h. Cells were harvested by centrifugation at 7000 x*g* and 4°C for 10 min. One gram of cells (wet weight) was suspended in 10 ml of 50 mM Tris-HCl buffer (pH 8) containing DNase I (Roche) and cOmplete EDTA-free Protease Inhibitor (Roche) or Pierce™ EDTA-free Protease Inhibitor (Thermo Scientific).

3.2.6. Co-expression with pLysSRARE2 and molecular chaperones

The constructs were also co-transformed into *E. coli* BL21(DE3) cells previously transformed with the pLysSRARE2 plasmid (Fig 3.6). pLysSRARE2 was obtained from *E. coli* Rosetta-gami™ 2 (DE3)pLysS (Novagen®) by plasmid extraction using the BioSpin Plasmid DNA Extraction Kit (BioFlux). Chloramphenicol (34 $\mu g.ml^{-1}$) was included for the pLysSRARE2 plasmid.

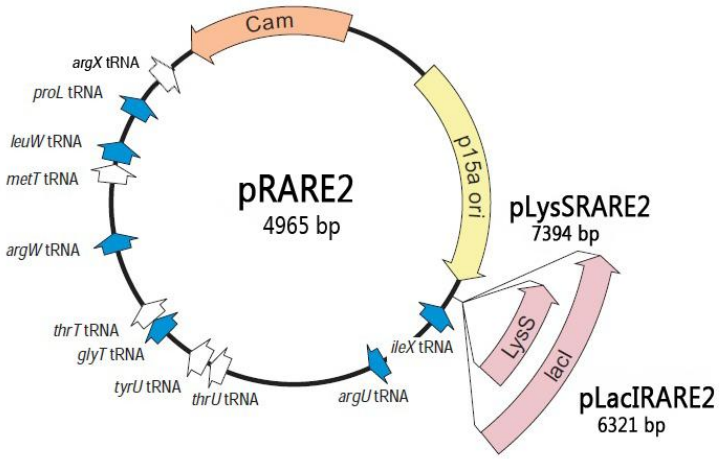

Figure 3.6. Vector map of pLysSRARE2 indicating the chloramphenicol resistance gene (Cam), the p15a origin of replication, the *LysS* coding region and the coding sequences for the tRNA molecules of rare codons in *E. coli* (Novagen®).

The Takara Chaperone Plasmid set consists of five chaperone plasmids (Fig. 3.7) for the purpose of co-expressing a recombinant protein with molecular chaperones. The pET-28b(+):moxYAltN construct was transformed into *E. coli* BL21-Gold(DE3) strains each previously transformed with one of the five molecular chaperone plasmids. All the *moxY* variants were also co-transformed with the pGro7 plasmid. Successful transformants were selected on LB agar plates supplemented with 30 $\mu g.ml^{-1}$ kanamycin and 20 $\mu g.ml^{-1}$ chloramphenicol. At least three colonies were co-inoculated into 5 ml LB (containing 30 $\mu g.ml^{-1}$ kanamycin and 20 $\mu g.ml^{-1}$ chloramphenicol) and incubated for 8 – 12 h at 37°C with shaking.

Two millilitres of the cell culture were used as inoculum for the expression of MoxYAltN using ZYP5052 auto-induction media, as described in section 3.2.5. To induce expression of the molecular chaperones, 0.5 $mg.ml^{-1}$ arabinose and/or 5 $ng.ml^{-1}$ tetracycline was added accordingly (Table 3.1).

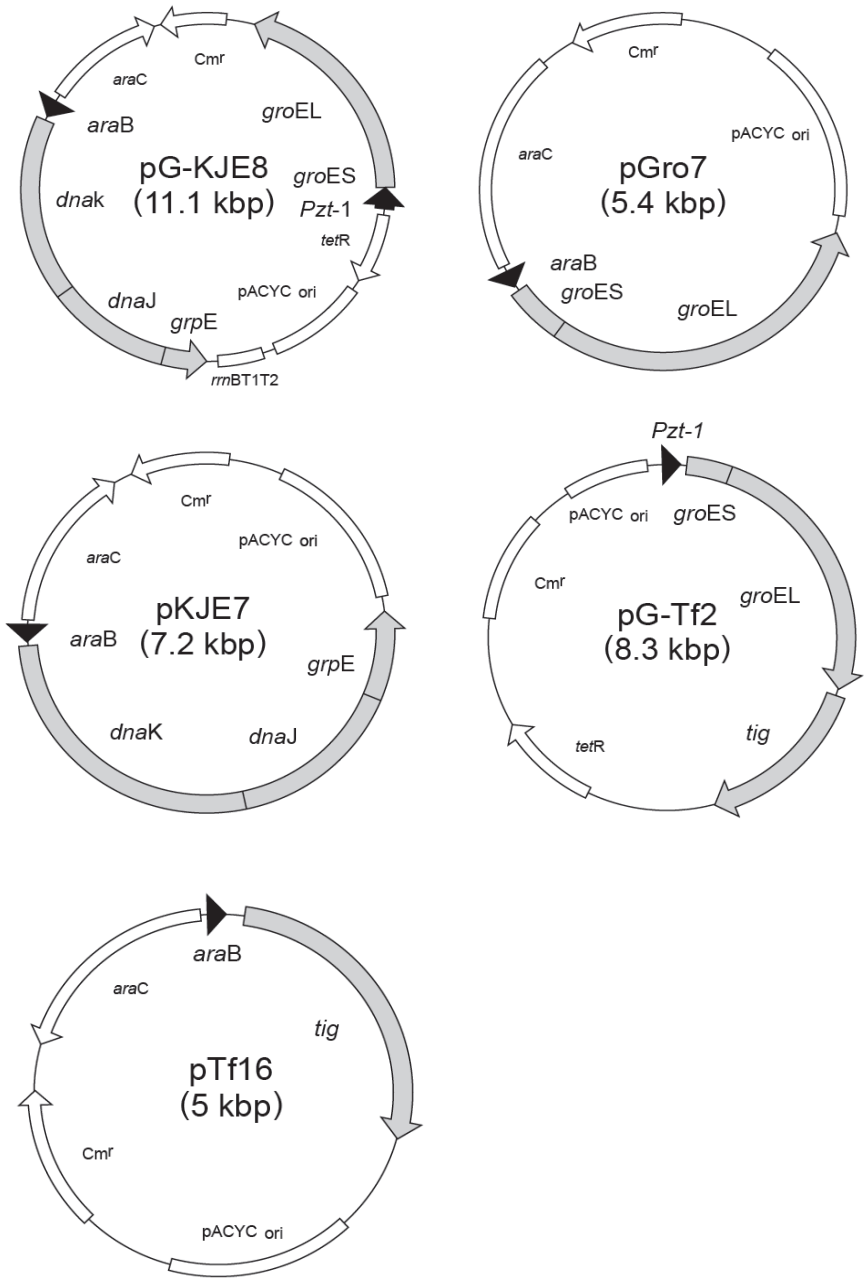

Figure 3.7. The Chaperone Plasmid Set (Takara Bio Inc.) used for co-expression of BVMOs with molecular chaperones indicating the chloramphenicol resistance gene (Cm^r), the origin of replication (pACYC ori), the arabinose (*araB*) and tetracycline (*Pzt-1*) promoters, the *dnaK*, *dnaJ* and *grpE* genes coding for the dnaK-dnaJ-grpE chaperone, the *groES* and *groEL* genes coding for the GroES-GroEL chaperone and the *tig* gene encoding the trigger factor.

3.2.7. Cell disruption

Two methods of cell disruption were used: French press and lysozyme digestion followed by a freeze-thaw cycle. In the French press technique, 7 ml of the above-mentioned cell suspension were lysed using a One Shot cell disrupter (Constant Systems, Ltd.) at 30 kPSI. The fractions were centrifuged at 20 000 x*g* and 4°C for 20 min to remove insoluble proteins, cell debris and unbroken cells. For partial enzymatic digestion of the cell wall, 1 $g.L^{-1}$ lysozyme (Sigma Aldrich) was added to the cell suspension and incubated for 90 min at 25°C. The cells were then frozen at -80°C and thawed completely. The insoluble fraction was removed by centrifugation at 7 000 x*g* and 4°C for 30 min.

3.2.8. Analysis of expression

3.2.8.1. SDS-PAGE

In order to visually analyse the expression levels, sodium dodecyl sulphate polyacrylamide electrophoresis (SDS-PAGE) was performed using the Mini-PROTEAN™ Tetra system (Bio-Rad). The protocol used was as described by Laemmli (1970), using a gel comprised of an 8 % resolving gel and a 4 % stacking gel. Gels were run at 100 V for approximately 1 h using TGS buffer [Tris (25 mM), glycine (192 mM), SDS (0.1 % w/v), pH 8.3; Bio-Rad]. PageRuler™ Prestained Protein Ladder (Thermo Scientific), Precision Plus Protein™ Dual Xtra Standards (Bio-Rad) or Spectra™ Multicolor Broad Range Protein Ladder (Thermo Scientific) was used as molecular weight markers. Coomassie Brilliant Blue R-250 was used to visualise the proteins, using a staining and de-staining procedure described by Fairbanks and co-workers (1971).

3.2.8.2. Activity of MoxY and variants

Preliminary activity assays were used to determine whether MoxY and the MoxY variants expressed as active proteins. Continuous assays were performed by measuring the oxidation of the NADPH co-factor in the presence of selected ketone substrates (Fig. A4, appendix). Substrates were solubilised in acetonitrile with a final acetonitrile concentration of 1 %. Blank rates were determined as the oxidation of NADPH in the absence of substrate.

Activity was evaluated in the total protein fraction from the French-pressed cells, the soluble fraction from the French-pressed cells, as well as the soluble fraction from the lysozyme-treated cells. Activity assays were performed in 96-well flat-bottom microplates (Greiner Bio-one) to allow for parallel screening. The reactions comprised of 50 µl protein fraction, 10 mM substrate and 0.3 mM NADPH in 50 mM Tris-HCl (pH 8.0) to a final volume of 200 µl. The reactions were incubated at 25°C and NADPH oxidation measured continuously for 10 min at 340 nm using a SpectraMax® M2 Multi-Mode Microplate Reader (Molecular Devices). An extinction coefficient of 6.22 $mM.cm^{-1}$ was used for NADPH at 340 nm to calculate the reaction rates (Jablonski and DeLuca, 1977). CHMO from *Acinetobacter calcoaceticus* served as a positive control.

3.2.9. Purification of MoxYAltN

The MoxYAltN protein was over-produced using the pET-28b(+):moxYAltN construct to yield a soluble protein with an N-terminal His-tag. *E. coli* BL21-Gold(DE3) was used to express pET-28b(+):moxYAltN in 2 L (20 x 100 ml) of ZYP5052 auto-induction media in 500 ml Erlenmeyer flasks. Cultures were incubated at 20°C and 200 rpm for 36 h, after which it was harvested by centrifugation at 7 000 x*g* for 10 min (4°C).

3.2.9.1. Cell disruption and ultracentrifugation

Harvested cells were resuspended in 150 ml of 50 mM Tris-HCl (pH 7.4) buffer containing 0.5 M NaCl and 20 mM imidazole in preparation of downstream purification using immobilised metal-affinity chromatography (IMAC). DNase I (Roche) and cOmplete EDTA-free Protease Inhibitor (Roche) or Pierce™ EDTA-free Protease Inhibitor (Thermo Scientific) was added to the cell suspension. Cells were disrupted with the French press (section 3.2.7) and centrifuged at 7 000 x*g* for 1 h (4°C) to separate the soluble fraction from the cell debris, unbroken cells and insoluble particles. The membranes were removed from the soluble fraction by ultracentrifugation at 100 000 x*g* for 90 min (4°C).

3.2.9.2. Immobilised metal-affinity chromatography (IMAC)

Recombinant His-tagged MoxYAltN was purified by immobilised metal-affinity chromatography (IMAC). An ÄKTAprime plus chromatography system (GE Healthcare) was used in all column chromatography steps. Protein eluting from the column was monitored spectrophotometrically by UV absorption at 280 nm.

Supernatants from the ultracentrifuged fractions were loaded onto a 5 ml HisTrap FastFlow (FF) column (GE Healthcare) equilibrated with 50 mM Tris-HCl pH 7.4, 0.5 M NaCl and 20 mM imidazole (5 $ml.min^{-1}$). Ten column volumes of the equilibration buffer served to remove any unbound protein. Bound proteins were eluted in the same buffer (100 ml) with an increasing gradient of imidazole up to 0.5 M. Collected fractions (5 ml) were analysed using SDS-PAGE to evaluate the enzyme purity and for subsequent selective pooling of fractions. FAD (Sigma Aldrich) was added to the pooled fractions obtained after IMAC and incubated overnight at 4°C to ensure maximum co-factor occupancy.

3.2.9.3. Size-exclusion chromatography (SEC)

Size-exclusion chromatography (SEC) was used as a second purification step. Pooled fractions collected from the His-trap were concentrated by ultrafiltration to a total volume of 2 ml with an Amicon® Ultra-15 centrifugal filter device (30 kDa MWCO, Millipore) via centrifugation at 3 500 x*g* for 1 h (4°C). Approximately 200 µl of glycerol was added to the concentrated fraction and loaded onto a Sephacryl S-200 HR column (65 x 2.5 cm, Sigma Aldrich) equilibrated with 10 mM Tris-HCl (pH 8.0) containing 20 mM NaCl. Proteins were eluted with the same buffer at a flow rate of 1 $ml.min^{-1}$. Collected fractions (5 ml) were analysed by SDS-PAGE to determine protein purity.

3.2.9.4. Determination of protein concentration

Protein concentrations were determined using the bicinchoninic acid (BCA) method (Smith *et al*., 1985). The Pierce® BCA Protein Assay Kit (Thermo Scientific) was used according to the manufacturer's instructions with bovine serum albumin (BSA) (supplied with kit) as standard (Fig. 3.8).

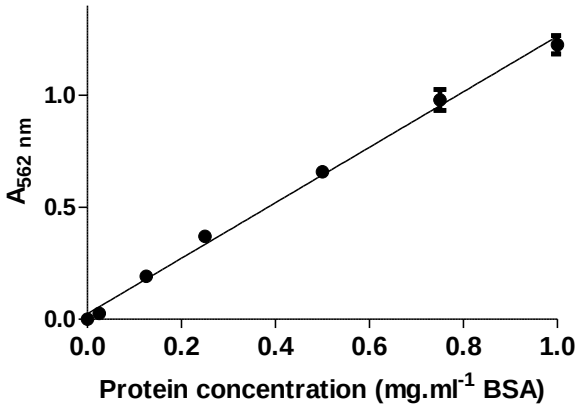

Figure 3.8. Standard curve for the Pierce® BCA Protein Assay Kit (Thermo Scientific) at 37°C using BSA as protein standard. Error bars indicate standard deviation of triplicate values.

3.2.9.5. Activity assays with purified protein

The purified MoxYAltN, supplemented with FAD, was assayed for activity against ketone substrates as in section 3.2.8.2. The reaction volume comprised of 50 µl pure enzyme, 1 mM substrate and 0.3 mM NADPH in a 50 mM Tris-HCl buffer (pH 8.0) to a total volume of 200 µl. The reactions were incubated at 25°C for 10 min and monitored spectrophotometrically.

3.2.10. Characterisation of MoxYAltN

3.2.10.1. Effect of pH on enzyme activity

The effect of pH on the activity of purified MoxYAltN towards phenylacetone was investigated by incubating the mixtures at various pH's ranging from 6.5 – 10.0. The pH range was constructed by adjusting the pH of an equimolar 20 mM MOPS-Bicine-Ches or 50 mM Tris buffer with HCl or NaOH. The reaction mixture consisted of 50 µl purified enzyme, 1 mM phenylacetone and 0.3 mM NADPH in 50 mM Tris buffer to a final volume of 200 µl. Reactions were performed in 96-well microplates at 25°C and monitored spectrophotometrically for 10 min as in section 3.2.8.2. Assays were performed in triplicate and blank rates (represented by oxidation of NADPH by molecular oxygen in the absence of phenylacetone) were taken at each assayed pH value.

3.2.10.2. Effect of buffer concentration on enzyme activity

The effect of an increase in buffer concentration on the enzyme activity of purified MoxYAltN against phenylacetone was determined at various concentrations of Tris, ranging from 50 – 200 mM, at a pH of 8.5. Reactions were performed as described above. Assays were performed in triplicate and blank rates were taken at each assayed concentration.

3.2.10.3. Effect of temperature on enzyme activity

The effect of temperature on enzyme activity of purified MoxYAltN against phenylacetone was determined by incubation at various temperatures ranging from 25 – 40°C. The pH of the buffer (50 mM Tris-HCl) was adjusted to 8.5 for each temperature. The buffer was equilibrated at each temperature and reactions were performed as described above. Assays were performed in triplicate and blank rates were taken at each assayed temperature.

3.2.10.4. Enzyme stability

The stability of the enzyme at increasing temperatures was evaluated by incubating the enzyme at various temperatures ranging from 25 – 42°C. Aliquots were taken at intervals and the activity of the enzyme assayed at 20°C as described above. The reaction mixture consisted of 50 µl purified enzyme, 1 mM phenylacetone and 0.3 mM NADPH in Tris-HCl 200 mM (pH 8.5) to a total volume of 200 µl. All assays were performed in triplicate.

3.2.10.5. Steady-state kinetics

Kinetic constants were determined using purified enzyme by measurement of initial velocities at various concentrations of phenylacetone. Phenylacetone was solubilised in methanol with a final methanol concentration of 1 %. To ensure maximum occupancy of the co-factor, the purified protein was supplemented with FAD in a 1:4 molar ratio. Due to enzyme instability at the optimum temperature of 37°C, reactions were performed at 25°C in 200 mM Tris-HCl buffer (pH 8.5) with 0.2 mg protein in a 1 ml reaction volume.

The continuous oxidation of NADPH was monitored spectrophotometrically at 340 nm over 10 min with a Cary 300 Bio UV-Visible spectrophotometer (Varian). An extinction coefficient of 6.22 $mM.cm^{-1}$ was used for NADPH at 340 nm to calculate the reaction rates (Jablonski and DeLuca, 1977). A blank rate (represented by oxidation of NADPH by molecular oxygen in the absence of phenylacetone) was measured and used to correct the observed rates. Apparent maximum velocities (V_{max}) and apparent Michaelis-constants (K_m) were determined through non-linear regression of Michaelis-Menten plots using GraphPad Prism 5.03 (GraphPad Software Inc.).

3.2.10.6. Reaction of MoxYAltN with hydroxyversicolorone

Synthetic [1'-^{2}H]hydroxyversicolorone (HVN) was obtained from Prof. C. Townsend (John Hopkins University, Maryland, USA). To determine whether MoxYAltN was active towards hydroxyversicolorone, the oxidation of NADPH in the presence of HVN by the enzyme was monitored spectrophotometrically as described above. HVN was incubated with 0.3 mM NADPH and 0.2 mg purified MoxYAltN, supplemented with FAD, in 200 mM Tris-HCl (pH 8.5) for 40 min at 25°C. The substrate and product were extracted with 1 ml ethyl acetate and concentrated under vacuum in a SpeedVac concentrator to a final volume of 50 µl. The mixture was separated using Thin Layer Chromatography (TLC) on Silica 60 or Silica 60 F254 TLC (Merck) plates aside a standard HVN solution and developed using a chloroform:methanol (95:5) mobile phase. The TLC plates were visualised and photographed under white and UV light, respectively.

3.2.10.7. Whole-cell biotransformations

Whole-cell biotransformations were used to investigate the substrate scope of MoxYAltN. The pET-28b(+):moxYAltN construct was co-expressed with the chaperone plasmid (pGro7) in *E. coli* BL21(DE3) as in section 3.2.6. Cells were harvested and 1 g (wet weight) cells resuspended in 10 ml of 200 mM Tris-HCl (pH 8.5) buffer. Whole-cell biotransformations were performed using a 1 ml reaction volume in 60 ml amber vials with non-permeable caps. The reaction mixture comprised of 200 mM Tris-HCl (pH 8.5), 0.5 g cells, 100 mM glucose, 100 mM glycerol and 10 mM substrate. Substrates are depicted in Fig. A4 (appendix). The vials were incubated at 20°C for 2 h with shaking (200 rpm) after which the reactions were stopped and extracted with an equal volume of ethyl acetate (1 ml) containing a 2 mM internal standard (1-undecanol or 3-octanol). Gas chromatography - mass spectrometry (GC-MS) was used to analyse the substrates and products on a Finnigan TRACE GC Ultra (Thermo Scientific) equipped with a FactorFour™ VF-5ms column (60 m x 0.25 mm x 0.25 µm, Varian). Detailed GC programs are given in the appendix (Table A3, appendix).

3.3. Results

3.3.1. Cloning of *moxY* and *moxYAltNC*

3.3.1.1. *In silico* prediction of the *moxY* coding sequence

NCBI database prediction and annotation indicated the *moxY* gene to contain a single intron, located at positions 1 412 – 1 462 basepairs (bp). However, alignment of expressed-sequence tagged (EST) data obtained from cDNA sequencing of *A. flavus* to the *moxY* gene by alignment with Clustal W2 (Fig. 3.9) identified a region, close to the C-terminus, that was differentially spliced and translated. In about half of the available sequences, region 1 689 – 1 746 bp was used as a coding sequence, while it was spliced out as an intron in the other (referred to as AltC).

In addition to the variability in the C-terminus, an alternative start codon was identified 63 bp upstream from the start codon predicted in the NCBI database, giving rise to the possibility that MoxY might exist with an elongated N-terminus (referred to as AltN). Unfortunately, no EST data cover this region to confirm or refute the possibility.

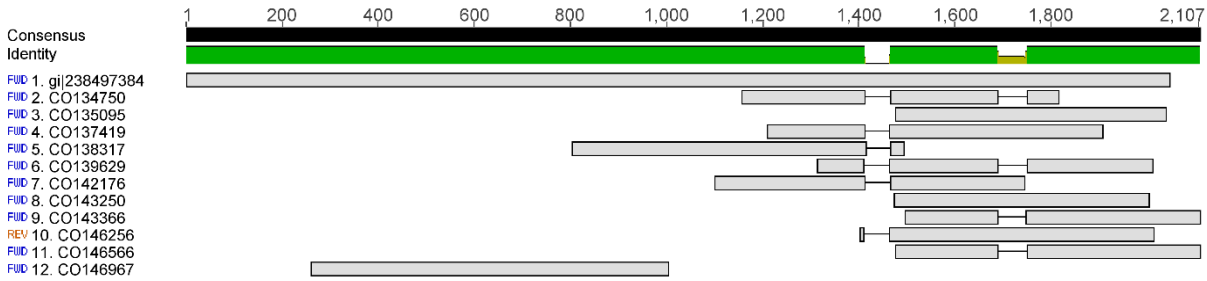

Figure 3.9. Multiple alignment of EST data to the *moxY* gene. The intron at position 1412 – 1462 bp is spliced out in all of the sequences, while the region 1689 – 1746 bp was alternatively spliced and used as coding region in half of the instances, while spliced out as an intron in the other. Alignments were performed with ClustalW2 and visualised with Geneious® v 6.0.3.

3.3.1.2. PCR amplification of *moxY* and *moxYAltNC*

Because the *moxY* gene most likely contained only one or two introns, it was decided to PCR amplify it from gDNA and subsequently remove the introns. Given the uncertainties explained above, two variations of the gene had to be PCR amplified from the genomic DNA: *moxY*, the gene as predicted by the NCBI database, and *moxYAltNC,* the gene with an elongated N-terminus and alternative C-terminus. From these two amplicons, two additional variations of the *moxY* gene could be constructed after removal of the introns by exchange of the N and C termini to produce a *moxY* gene with either the elongated N-terminus (*moxYAltN*) or the alternative C terminus (*moxYAltC*).

Total genomic DNA was isolated successfully from *A. flavus*. Agarose gel electrophoresis (Fig. 3.10) indicated a band greater than 10 kbp, confirming that the gDNA was intact.

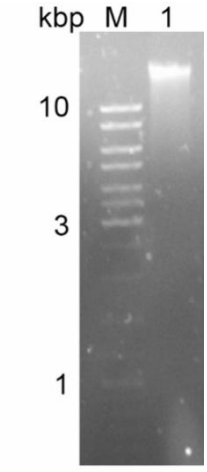

Figure 3.10. Agarose gel electrophoresis of the total genomic DNA from *Aspergillus flavus* NRRL 3357 (lane 1); M, MassRuler™ DNA ladder.

The primers were designed to incorporate restriction sites for either *Nde*I (5') and *Xho*I (3') for *moxY*, or *Hind*III (5') and *Xho*I (3') for *moxYAltNC*, to facilitate downstream directional cloning of the amplicons into the pET expression vectors. The *moxY* and *moxYAltNC* genes were amplified successfully from the gDNA of *A. flavus* with the KOD Hot Start DNA Polymerase system. Agarose gel electrophoresis yielded clear bands of approximately 1 700 bp and 2 000 bp for *moxY* and *moxYAltNC* (Fig. 3.11), respectively, corresponding to the expected size of the products (1 755 bp and 1 987 bp). The KOD Hot Start DNA Polymerase is a DNA polymerase system with high fidelity, high processivity and a fast elongation rate (Novagen®). The system uses an antibody-mediated hot-start to reduce non-specific amplification due to mispriming events during the reaction set-up.

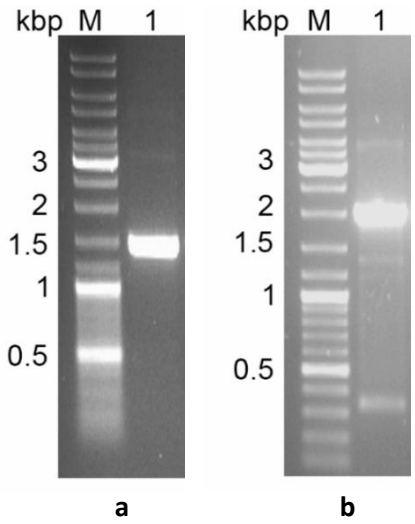

Figure 3.11. Agarose gel electrophoresis of the PCR-amplified *moxY* gene from *Aspergillus flavus* (**a**, lane 1); PCR-amplified *moxYAltNC* gene from *Aspergillus flavus* (**b**, lane 1); M, GeneRuler™ DNA ladder.

KOD Hot Start DNA polymerase produces blunt-ended amplicons. The pSMART® cloning vector is pre-digested with blunt, dephosphorylated ends (Lucigen®) and is thus suitable for blunt-ended cloning of the PCR product generated by the KOD Hot Start system. In addition, the pSMART®-HCKan plasmid has a high copy-number replication origin that produces up to ~300 copies per cell and uses kanamycin (as opposed to ampicillin) as selectable marker, minimizing the growth of satellite colonies.

3.3.1.3. Construction of pSMART®:moxY and pSMART®:moxYAltNC

The amplified *moxY* and *moxYAltNC* genes were blunt-end ligated into the pSMART® vector. Constructs were digested with either *Nde*I and *Xho*I for pSMART®:moxY, or *Eco*RI for pSMART®:moxYAltNC, and separated on an agarose gel to verify whether the constructs contained the inserted genes. The agarose gel indicated two clear bands of ~1 700 bp and ~1 300 bp for pSMART®:moxY (Fig. 3.12a), which corresponds to the 1 752 bp insert and a 1 563 bp fragment of the backbone. Three clear bands of approximately 800, 1 200 and 1 800 bp could be observed for pSMART®:moxYAltNC (Fig. 3.12b). The *moxYAltNC* contains an internal restriction site for *Eco*RI at position 794, therefore, the three bands corresponded to the two *moxYAltNC* fragments and the vector backbone.

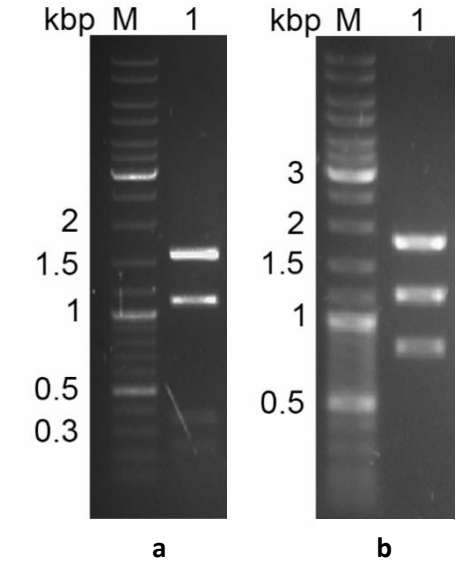

Figure 3.12. Agarose gel electrophoresis of double-digestion of pSMART®:moxY with *Nde*I and *Xho*I to verify whether the construct contains the *moxY* gene (**a**, lane 1) and the digestion of pSMART®:moxYAltNC with *Eco*RI to verify whether the construct contains the *moxYAltNC* gene (**b**, lane 1). M, GeneRuler™ DNA ladder.

3.3.1.4. Intron removal

In Fig. 3.9, it is clear that the region 1 412 – 1 462 bp was spliced out in all of the EST sequences. Therefore, the intron was removed by inverse PCR from both pSMART®:moxY and pSMART®:moxYAltNC. Agarose gel electrophoresis indicated a band of approximately 3 500 bp (Fig. 3.13a), corresponding to the expected PCR product of 3 492 bp from pSMART®:moxY, and a band of approximately 3 700 bp (Fig. 3.13b), corresponding to the expected product of 3 724 bp from pSMART®:moxYAltNC.

The differentially translated region, 1 689 – 1 746 bp, was removed as a second intron from pSMART®:moxYAltNC (from which the first intron had successfully been removed) by inverse PCR. The PCR yielded a product of 3 666 bp which was visualised as a clear band of approximately 3 700 bp on an agarose gel (Fig. 3.13c). DNA sequencing confirmed that the intron removal proceeded without error and that no frame-shift or point mutations were introduced during the amplification and ligation steps.

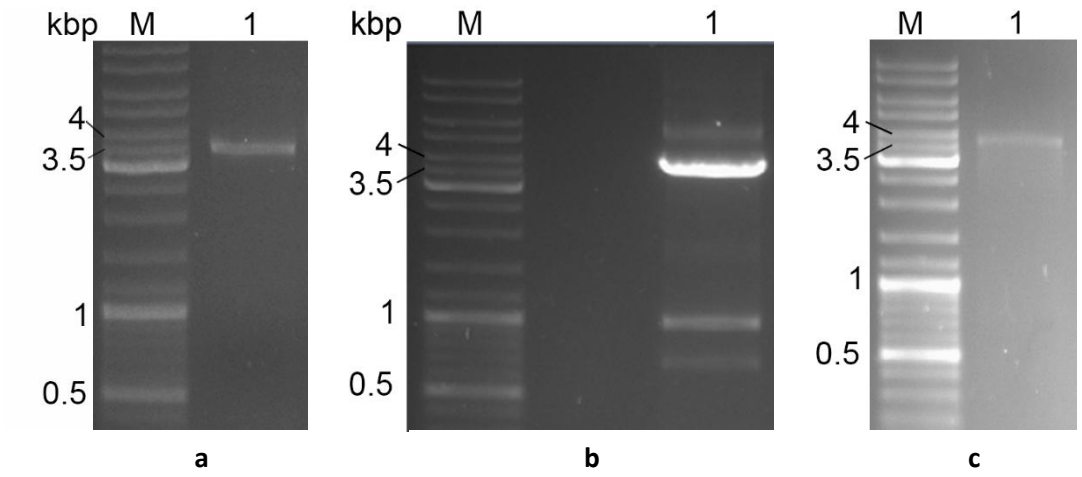

Figure 3.13. Agarose gel electrophoresis of the inverse PCR to remove the first intron from pSMART®:moxY (**a**, lane 1) as well as pSMART®:moxYAltNC (**b**, lane 1), and the second intron from pSMART®:moxYAltNC (**c**, lane 1). M, GeneRuler™ DNA ladder.

3.3.1.5. Commercial synthesis of *moxY OPT* and *moxYAltNC OPT*

The *moxY OPT* and *moxYAltNC OPT* genes were optimised for expression in *E. coli* by GenScript. Alignments of the optimised and native versions of *moxY* and *moxYAltNC* are displayed in Figs. A1 and A2 (appendix), respectively. GenScript uses an OptimumGene™ Gene Design algorithm that can alter a recombinant gene sequence to achieve the highest level of productivity in the chosen expression system. The OptimumGene™ algorithm considers a variety of factors involved in different stages of protein expression including transcription, translation and protein folding. The factors include GC content of the sequence, mRNA secondary structure, codon adaptability, existence of translational pause sites and also various *cis*-elements in transcription and translation.

Advantages of expressing the optimised sequence generally include a significant increase in the recovery of expressed proteins, expression of proteins from very long sequences, as well as expression of sequences containing repetitive regions. *moxY OPT* and *moxYAltNC OPT* were designed to incorporate a 5' *Nde*I site and a 3' *Hind*III site for downstream directional cloning into the pET-22/28b(+) vectors. The sequences of 1 704 and 1 878 bp, respectively, were received in the cloning vector pUC57 and designated as pUC57:moxY OPT and pUC57:moxYAltNC OPT.

3.3.1.6. Sub-cloning of CDSs to the pET expression vectors

In order to extract the coding regions from the cloning vectors, pSMART® and pUC57, the plasmids were double-digested with the restriction enzymes of which the recognition sites had been introduced at the 5' and 3' ends during PCR amplification from the genomic DNA. The pSMART®:moxY vector was digested with *Nde*I and *Xho*I, while the pSMART®:moxY OPT, pSMART®:moxYAltNC and pSMART®:moxYAltNC OPT were digested with *Nde*I and *Hind*III. pET-22b(+) and pET-28b(+) were similarly digested. The restriction digestion mixtures were separated on an agarose gel and bands corresponding to the expected sizes of the following ORFs were excised and purified: the *moxY* and *moxY OPT* fragments of 1 701 bp, the *moxYAltNC* and *moxYAltNC OPT* fragments of 1 875 bp as well as the backbones of pET-22b(+) and pET-28b(+).

The *moxY, moxY OPT*, *moxYAltNC* and *moxYAltNC OPT* fragments were each ligated into the digested pET-22b(+) and pET-28b(+) backbones, respectively. Restriction enzyme double-digestion with *Xho*I and *Xba*I was used to verify whether the ligation was successful. Agarose gel electrophoresis indicated that two bands of approximately 5 500 and 1 700 bp could be observed for all of the constructs (Fig. 3.14), corresponding to the vector backbone and the inserted CDSs, respectively. Clones containing the insert were confirmed by DNA sequencing, indicating that the directional cloning of the CDSs proceeded without error and that no point or frame-shift mutations were introduced during the cloning procedure.

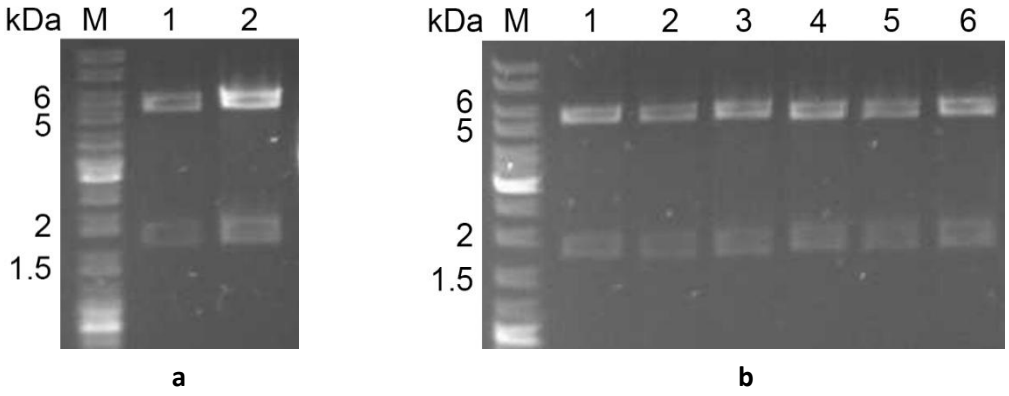

Figure 3.14. Agarose gel electrophoresis of *Xba*I *Xho*I double-digested pET expression constructs to confirm the presence of the *moxY*-variant. **a,** lane 1, pET-22b(+):moxY; lane 2, pET-28b(+):moxY; **b,** lane 1, pET-22b(+):moxYAltNC; lane 2, pET-28b(+):moxYAltNC; lane 3, pET-22b(+):moxY OPT; lane 4, pET-28b(+):moxY OPT; lane 5, pET-22b(+):moxYAltNC OPT; lane 6, pET-28b(+):moxYAltNC OPT; M, GeneRuler™ DNA ladder.

3.3.1.7. Creation of *moxY* variants with either an alternative N or C terminus

The CDS of the *moxYAltNC* encodes a MoxY variant that contains both the alternative N and alternative C terminus. However, it is possible that the active form of the protein exists with only either an alternative N or C terminus. A double cross-over method was used to create *moxYAltN* and *moxYAltC* variants by recombination of the corresponding vectors carrying *moxY* and *moxYAltNC*, as illustrated in Fig. 3.5.

Two identical restriction enzyme sites were selected in the corresponding plasmids: one cutting in the plasmid backbone upstream of the 5' site, and the other at an identical site in both *moxY* and *moxYAltNC*. The smaller fragment contained a portion of the coding region, including the N terminus. The larger fragment contained the rest of the coding region, including the C terminus, as well as most of the plasmid backbone. Therefore, each plasmid acted as a donor of the N-terminus to the other, which acted as an acceptor plasmid already containing the C-terminus. Two bands of ~6 500 and 700 - 900 bp could be observed for each vector on an agarose gel (Fig. 3.15), corresponding to the large and small fragments. Ligating the small fragment of *moxYAltNC* (containing the alternative N-terminus) into the large fragment of *moxY* (containing the 'original' C-terminus) would generate a vector that codes for *moxYAltN*, while ligating the small fragment of *moxY* (containing the 'original' N-terminus) into the large fragment of *moxYAltNC* (containing the alternative C-terminus) would produce *moxYAltC* (Table 3.7). The optimized versions of these genes (*moxYAltN OPT* and *moxYAltC OPT*) were similarly constructed.

Table 3.7. Double cross-over method for the creation of *moxY* variants containing only an alternative N-terminus or an alternative C-terminus.

Donor Plasmid for N-terminus (small fragment)	Acceptor Plasmid for C-terminus (large fragment)	Variant created
pET-22b(+):moxY	pET-22b(+):moxYAltNC	pET-22b(+):moxYAltC
pET-22b(+):moxYAltNC	pET-22b(+):moxY	pET-22b(+):moxYAltN
pET-22b(+):moxY OPT	pET-22b(+):moxYAltNC OPT	pET-22b(+):moxYAltC OPT
pET-22b(+):moxYAltNC OPT	pET-22b(+):moxY OPT	pET-22b(+):moxYAltN OPT
pET-28b(+):moxY	pET-28b(+):moxYAltNC	pET-28b(+):moxYAltC
pET-28b(+):moxYAltNC	pET-28b(+):moxY	pET-28b(+):moxYAltN
pET-28b(+):moxY OPT	pET-28b(+):moxYAltNC OPT	pET-28b(+):moxYAltC OPT
pET-28b(+):moxYAltNC OPT	pET-28b(+):moxY OPT	pET-28b(+):moxYAltN OPT

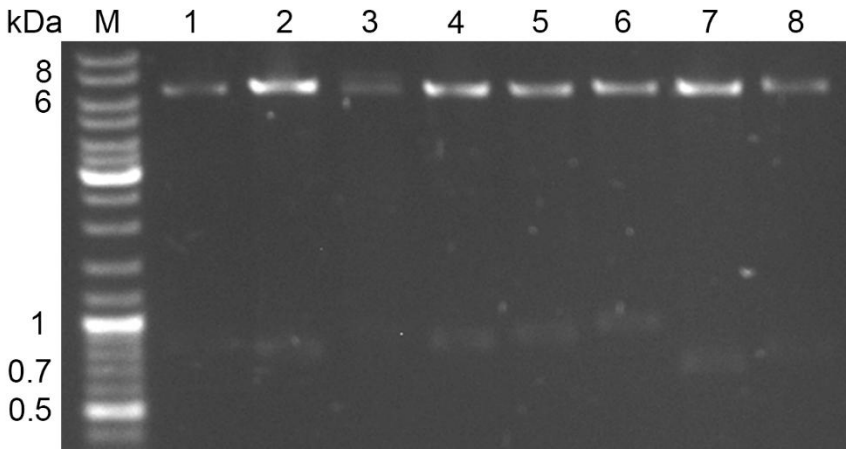

Figure 3.15. Restriction enzyme double-digestion of constructs in preparation for the construction of *moxY* variants with either an alternative N or alternative C terminus. M, GeneRuler™ DNA ladder; lane 1, pET-22b(+):moxY; lane 2, pET-22b(+):moxYAltNC; lane 3, pET-28b(+):moxY; lane 4, pET-28b(+):moxYAltNC; lane 5, pET-22b(+):moxY OPT; lane 6, pET-22b(+):moxYAltNC OPT; lane 7, pET-28b(+):moxY OPT; lane 8, pET-28b(+):moxYAltNC OPT.

Constructs were confirmed by DNA sequencing which verified the ligation steps to have proceeded without error and that no frame-shift mutations were introduced.

3.3.1.8. Creation of C-terminally His-tagged variants

The pET-22b(+):moxY vector allows expression of the *moxY* CDS as a native protein, while the pET-28b(+):moxY vector allows expression of the *moxY* CDS with an N-terminal poly(His)$_6$-tag (His-tag) for downstream protein purification. However, it is unknown how the His-tag will influence the protein folding and activity and/or whether the His-tag will be on the surface of the protein and thus accessible during affinity chromatography. Therefore, C-terminally His-tagged (CTH) variants of the genes were also created to improve the possibility of producing a correctly folded, recombinant protein with an exposed His-tag.

The pET-22b(+) vector encodes an in-frame sequence for a C-terminal His-tag (Fig. 3.4a). However, after cloning of the *moxY* CDS into pET-22b(+), the CDS had been translationally separated from the His-tag by the natural stop codon of the *moxY* gene. Inverse PCR was used to amplify the entire plasmid, except the stop codon, effectively removing the stop codon from the plasmid. Agarose gel electrophoresis (Fig. 3.16) indicated that the inverse PCR was successful as bands of ~7 000 bp, were observed. DNA sequencing verified the removal of the stop codon and that no point or frame-shift mutations were introduced during the PCR and ligation steps.

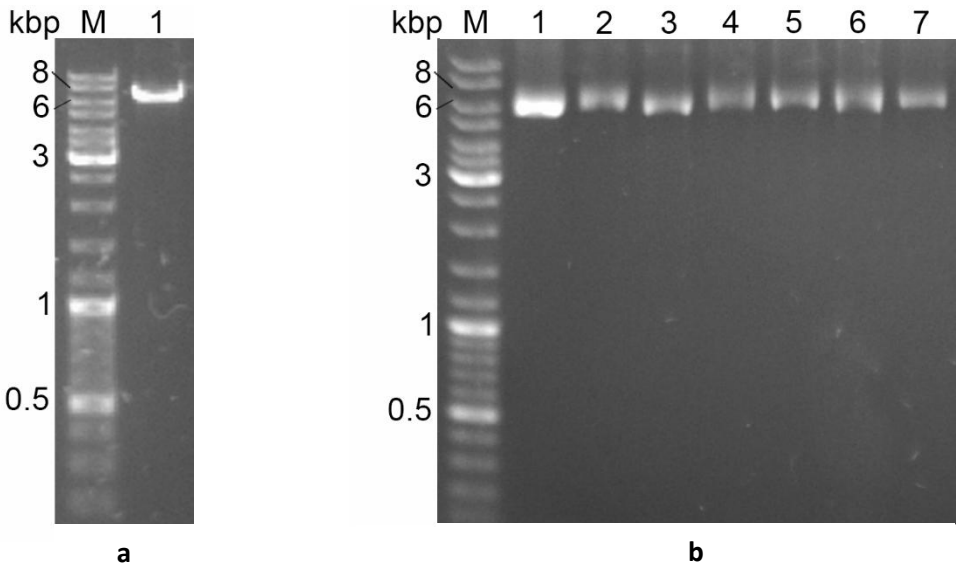

Figure 3.16. Agarose gel electrophoresis of the inverse PCR to create C-terminally His-tagged variants of **a:** pET-22b(+):moxY (lane 1) and **b:** lane 1, pET-22b(+):moxYAltNC; lane 2, pET-22b(+):moxY OPT; lane 3, pET-22b(+):moxYAltNC OPT; lane 4, pET-22b(+):moxYAltC; lane 5, pET-22b(+):moxYAltN; lane 6, pET-22b(+):moxYAltN OPT; lane 7, pET-22b(+):moxYAltC OPT. M, Generuler™ DNA ladder.

3.3.2. Heterologous expression of MoxY and variants

The pET expression constructs were expressed in *E. coli* BL21-Gold(DE3). BL21 strains are constructed from the *E. coli* B strain for the purpose of high-level expression of recombinant proteins (Life Technologies™). One feature contributing to this is the deficiency in proteases as the strains do not carry the gene for either the *lon* protease or the outer membrane protease, OmpT. Therefore, the degradation of the recombinant protein is reduced and the yields are improved. The BL21(DE3) strains carry the DE3 lysogen that encodes the T7 RNA polymerase gene under control of the *lac*UV5 promoter. The *lac*UV5 promoter is a mutated version of the lac promoter which is less sensitive to intracellular levels of cAMP, thereby decreasing the amount of basal expression. Addition of lactose or IPTG to the media will induce the promoter, allowing expression of the T7 polymerase.

Expression of the genes in the pET-vectors is under the control of the *lac* operator. The vectors also contain the coding sequence for the *lac*-repressor, as well as transcription signals for the T7 RNA polymerase; thus, transcription of the target gene will only be obtained in the absence of glucose and the presence of lactose/IPTG. Thus, the recombinant genes can be kept transcriptionally silent until the cell population has reached a sufficient cell density after which transcription can be induced to direct the cells' resources towards expression of the recombinant protein. ZYP5052 auto-induction media contains both glucose and α-lactose. The glucose represses transcription from the T7*lac* promoter present on the pET-22b(+)/pET-28b(+) vectors and simultaneously serves as a carbon source, allowing the cells to proliferate to a substantial density. When the glucose is depleted, the cAMP levels decrease and the established cell population starts expressing the target gene, driven by transcription from the α-lactose-induced T7*lac* promoter (Studier, 2005). Reported benefits of using auto-induction media as opposed to IPTG as inducer, include a higher culture density and increased concentrations of the recombinant protein.

Expression of MoxY and the MoxY variants from *A. flavus* in the *E. coli* host may suffer from codon bias, which is due to the differential preference of amino acid codons. The codon bias of an organism is reflected in the tRNA population in the cells (Dong *et al*., 1996), therefore, codons which are rarely used in *E. coli,* but commonly used in *A. flavus* may lead to a larger demand for a specific tRNA molecule than *E. coli* can provide (Goldman *et al*., 1995; Kane, 1995). This may result in processivity errors, such as translational stalling, premature termination of translation, as well as the introduction of errors in the polypeptide, including frameshifting and amino acid misincorporation (Kurland and Gallant, 1996).

Co-expression with the pLysSRARE2 plasmid was therefore investigated. The pLysSRARE2 plasmid encodes the tRNA molecules that are considered as rare in *E. coli* (Novagen®). The result is an altered tRNA population that may alleviate expression problems associated with codon bias and improve the yield of soluble, recombinant proteins.

The *LysS* gene encodes a bacteriophage T7 lysozyme, which aids in lysis of the cell wall and also acts as a natural inhibitor of T7 RNA polymerase. The gene is under control of a catabolite-sensitive promoter and will be transcribed in the presence of glucose. The T7 lysozyme acts by repressing basal levels of transcription from the T7 promoter on the pET vector and transcription will only commence when the glucose in the growth medium is depleted. In combination with the lactose-induced promoter of pET, a tightly regulated system is achieved where transcription of the target gene is completely repressed until glucose is depleted in the growth medium, allowing sufficient growth of the *E. coli* host before inducing expression of the heterologous gene.

Two different cell lysis methods were also investigated. The French press method of cell lysis involves forcing a cell suspension through a small orifice by using high pressure (Walker, 2010). Cell breakage occurs both due to the shear forces as the cells are forced through the orifice, as well as the rapid drop in pressure when the cells emerge from the orifice, which causes the cells to burst. This method is inexpensive and a large culture volume can be processed. However, a drawback is that the stress placed on the cells can decrease the recovery of the expressed proteins in the soluble fraction.

Lysozyme treatment is an enzymatic method of cell lysis in which the peptidoglycan of the bacterial cell wall is digested (Walker, 2010). Partial digestion of the cell wall is sufficient as the cells are then subjected to a round of freezing and thawing, after which the cell membranes will burst. Enzymatic methods of cell lysis are generally softer techniques in which the recovery of sensitive proteins is superior to that of harsher techniques, such as the French press. Using enzymatic methods of cell lysis is often costly, thereby limiting its application in large-scale purifications.

3.3.2.1. Expression of MoxY

SDS-PAGE was used to evaluate the expression levels in the total and soluble protein fractions with CHMO from *Acinetobacter calcoaceticus* (pET22:CHMO) as positive control. The total protein fraction was represented by the sample obtained after French press lysis, before centrifugation to remove the insoluble portion. The soluble protein fractions were obtained both from the lysozyme-treated cells, as well as the centrifuged fraction obtained from the French-pressed cells.

Initial expression studies of MoxY, as annotated and predicted in the NCBI database, yielded no expression in the pET-22b(+):moxY and pET-22b(+):moxY-CTH constructs (Fig. 3.17a,b). Expression was observed in the constructs in pET-28b(+) which introduces an N-terminal His-tag to the recombinant protein, however, only in the total protein fraction (Fig 3.17a) and not as soluble protein (Fig 3.17b), suggesting incorrectly folded protein located in inclusion bodies. Co-expression with the pLysSRARE2 plasmid did not alter the observed expression pattern. The method of cell-breaking also did not influence the recovery of recombinant protein in the soluble fraction (Fig 3.17b vs Fig 3.18).

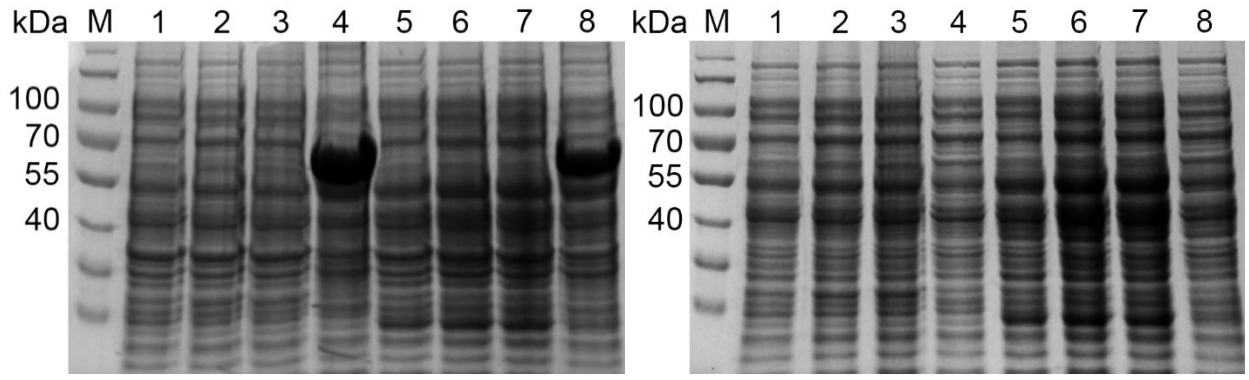

Figure 3.17. SDS-PAGE analysis of the expression of the *moxY* coding sequence. **a,** Total protein fraction; **b,** soluble fraction obtained by French press lysis. M, PageRuler™ Prestained protein ladder; lane 1, pET-22b(+) empty vector control; lane 2, pET-22b(+):moxY; lane 3, pET-22b(+):moxY-CTH; lane 4, pET-28b(+):moxY; lane 5, pET22-b(+) empty vector control + pLysSRARE2; lane 6, pET-22b(+):moxY + pLysSRARE2; lane 7, pET-22b(+):moxY-CTH + pLysSRARE2; lane 8, pET-28b(+):moxY + pLysSRARE2.

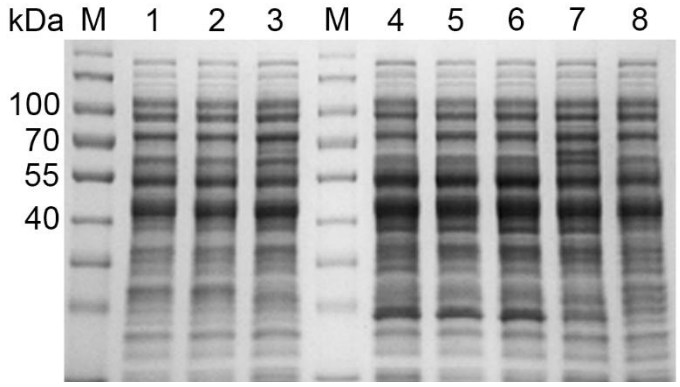

Figure 3.18. SDS-PAGE analysis of the expression of the *moxY* coding sequence. Fractions were obtained from the soluble fraction of cells treated with lysozyme followed by a freeze-thaw cycle. M, PageRuler™ Prestained protein ladder; lane 1, pET-22b(+):moxY; lane 2, pET-22b(+):moxY-CTH; lane 3, pET-28b(+):moxY; lane 4, pET22-b(+) empty vector control + pLysSRARE2; lane 5, pET-22b(+):moxY + pLysSRARE2; lane 6, pET-22b(+):moxY-CTH + pLysSRARE2; lane 7, pET-28b(+):moxY + pLysSRARE2; lane 8, pET-22b(+) empty vector control.

3.3.2.1.1. Expression of MoxY variants in the pET-22b(+) vector

Expression was observed from all the MoxY variants in pET-22b(+), except for MoxYAltC (Fig. 3.19). Soluble expression was only observed for the MoxYAltN, the MoxYAltN co-expressed with the pLysSRARE2 and the MoxYAltN OPT variants, indicating that all the other expressed variants were incorrectly folded and located in inclusion bodies. No improvement in the soluble expression was, however, observed when MoxYAltN was co-expressed with the pLysSRARE2 plasmid and soluble expression levels were lower for the optimized variant. Also, no discernible difference between the yield of soluble MoxYAltN and MoxYAltN OPT could be seen between the lysozyme-treated cells and the French-pressed cells.

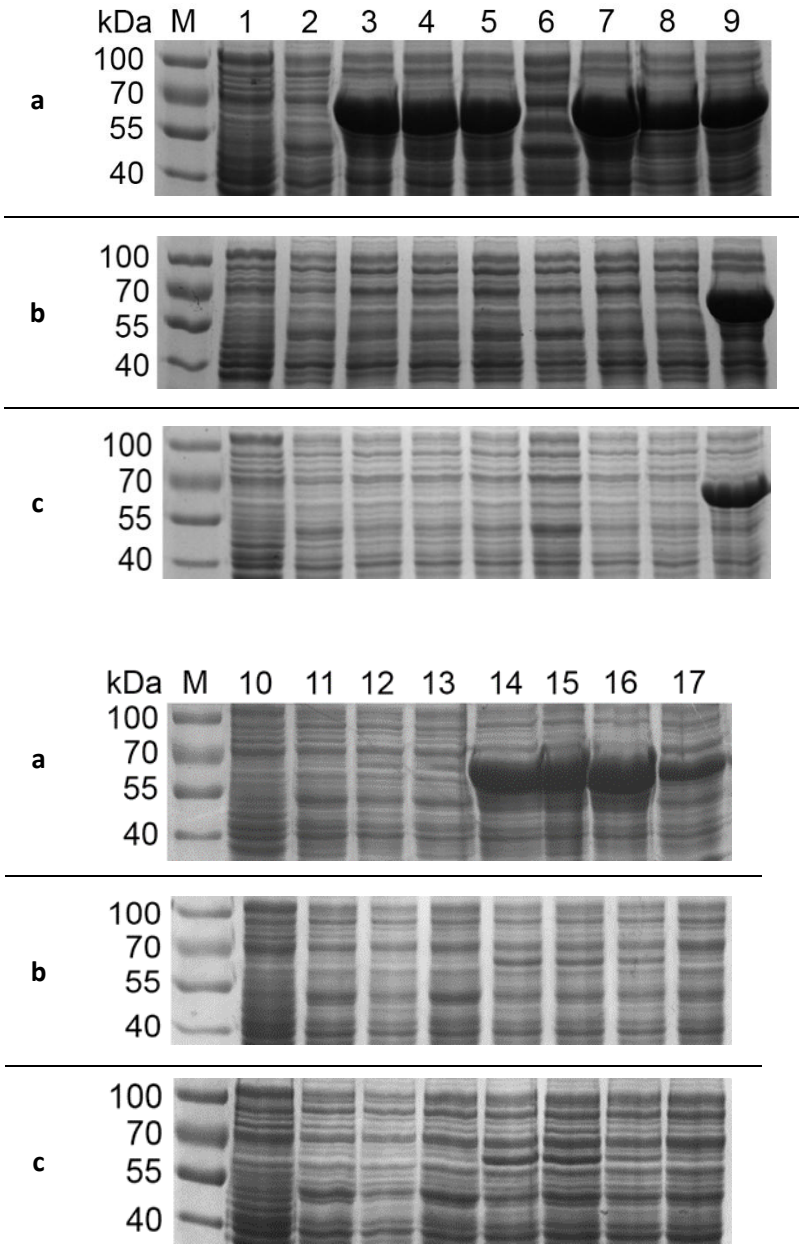

Figure 3.19. SDS-PAGE analysis of the expressed *moxY* variants in the pET-22b(+) vector. **a,** Total protein fraction; **b,** soluble protein fraction obtained from the French-press cell lysis; **c,** soluble protein fraction obtained from lysozyme treatment/freeze-thaw cell lysis. M, PageRuler™ Prestained protein ladder; lanes 1 and 10, pET-22b(+) empty vector control; lanes 2 and 11, pET-22b(+) empty vector control + pLysSRARE2; lane 3, pET-22b(+):moxYAltNC; lane 4, pET-22b(+):moxYAltNC + pLysSRARE2; lane 5, pET-22b(+):moxY OPT; lane 6, pET-22b(+):moxY OPT + pLysSRARE2; lane 7, pET-22b(+):moxYAltNC OPT; lane 8, pET-22b(+):moxYAltNC OPT + pLysSRARE2; lane 9, CHMO positive control; lane 12, pET-22b(+):moxYAltC; lane 13, pET-22b(+):moxYAltC + pLysSRARE2; lane 14, pET-22b(+):moxYAltN; lane 15, pET-22b(+):moxYAltN + pLysSRARE2; lane 16, pET-22b(+):moxYAltN OPT; lane 17, pET-22b(+):moxYAltC OPT.

3.3.2.1.2. Expression of MoxY variants in the pET-28b(+) vector

Expression was observed for all of the MoxY variants in pET-28b(+) (Fig. 3.20). Soluble expression was observed for the MoxYAltN, the MoxYAltN co-expressed with the pLysSRARE2 and MoxYAltN OPT variants. Therefore, all the other variants were expressed as insoluble protein located in inclusion bodies. The two different lysis techniques had no discernible effect on the levels of soluble MoxYAltN and MoxYAltN OPT (Fig. 3.20 b vs c). Also, gene optimization did not improve the levels of soluble protein.

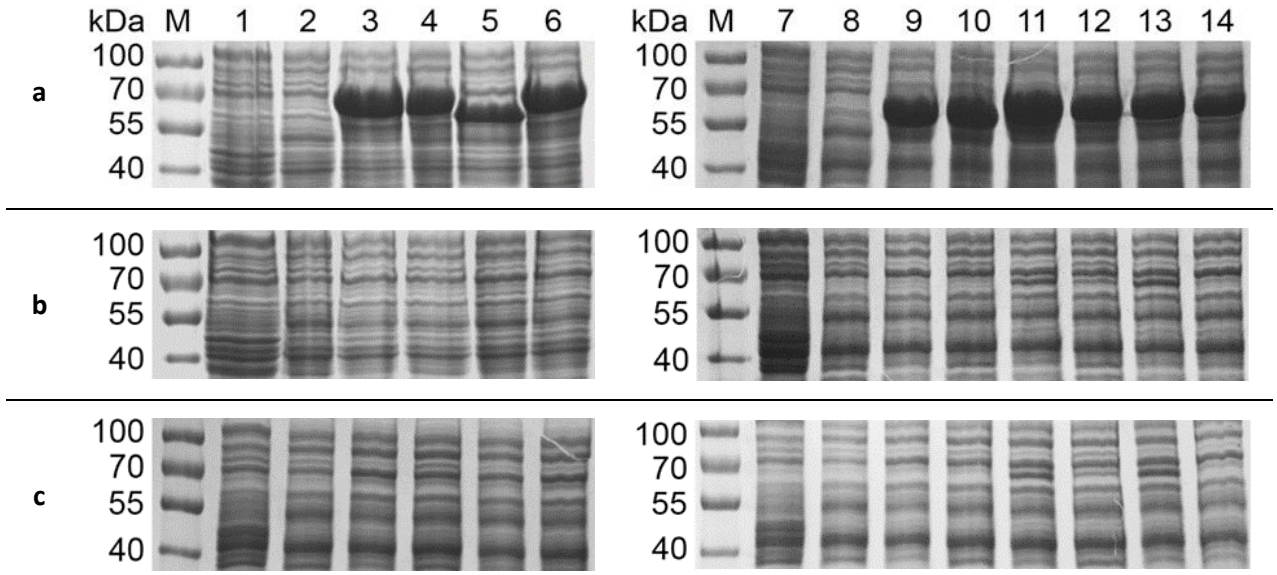

Figure 3.20. SDS-PAGE analysis of the expressed *moxY* variants in the pET-28b(+) vector. **a,** Total protein fraction; **b,** soluble protein fraction obtained from the French-press cell lysis; **c,** soluble protein fraction obtained from lysozyme treatment/freeze-thaw cell lysis. M, PageRuler™ Prestained protein ladder; lanes 1 and 7, pET-28b(+) empty vector control; lanes 2 and 8, pET-28b(+) empty vector control + pLysSRARE2; lane 3, pET-28b(+):moxYAltNC; lane 4, pET-28b(+):moxYAltNC + pLysSRARE2; lane 5, pET-28b(+):moxY OPT; lane 6, pET-28b(+):moxYAltNC OPT; lane 9, pET-28b(+):moxYAltC; lane 10, pET-28b(+):moxYAltC + pLysSRARE2; lane 11, pET-28b(+):moxYAltN; lane 12, pET-28b(+):moxYAltN + pLysSRARE2; lane 13, pET-28b(+):moxYAltN OPT; lane 14, pET-28b(+):moxYAltC OPT.

3.3.2.1.3. Expression of C-terminally His-tagged MoxY and MoxY variants

Expression was observed for all the MoxY variants with a C-terminal His-tag, except for MoxYAltC-CTH when co-expressed with the pLysSRARE2 plasmid (Fig. 3.21). Low levels of soluble expression was observed for MoxYAltN-CTH in the fraction from the lysozyme treated cells, but no soluble protein was recoveredb from the French-pressed cells. Therefore, a softer lysis technique, such as lysozyme treatment, may lead to greater recovery of soluble MoxYAltN-CTH. MoxYAltN-CTH may also be very sensitive to degradation. It is notable that no soluble protein was observed for the optimised variant of MoxYAltN-CTH. Also, no soluble protein was observed when MoxYAltN-CTH was co-expressed with the pLysSRARE2 plasmid. This may be due to an over-alteration of the tRNA population causing a lack in the necessary, non-rare tRNA molecules, leading to amino acid misincorporation and protein misfolding.

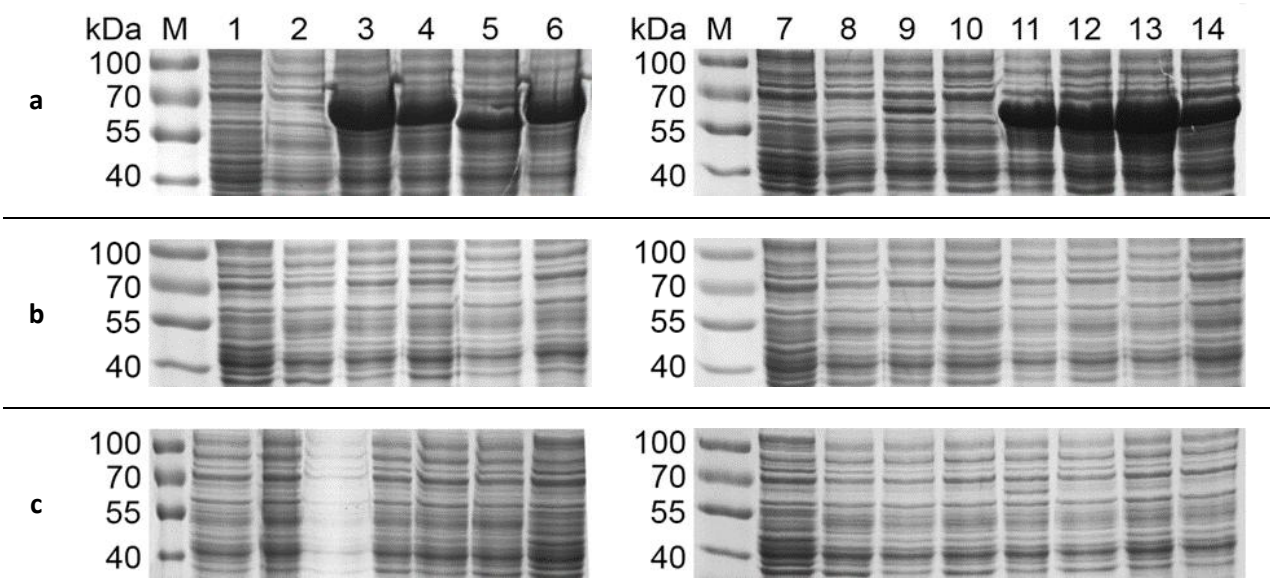

Figure 3.21. SDS-PAGE analysis of the expressed C-terminally His-tagged (CTH) *moxY* variants in the pET-22b(+) vector. **a,** Total protein fraction; **b,** soluble protein fraction obtained from the French-press cell lysis; **c,** soluble protein fraction obtained from lysozyme treatment/freeze-thaw cell lysis. M, PageRuler™ Prestained protein ladder; lanes 1 and 7, pET-22b(+) empty vector control; lanes 2 and 8, pET-22b(+) empty vector control + pLysSRARE2; lane 3, pET-22b(+):moxYAltNC-CTH; lane 4, pET-22b(+):moxYAltNC-CTH + pLysSRARE2; lane 5, pET-22b(+):moxY OPT-CTH; lane 6, pET-22b(+):moxYAltNC OPT-CTH; lane 9, pET-22b(+):moxYAltC-CTH; lane 10, pET-22b(+):moxYAltC-CTH + pLysSRARE2; lane 11, pET-22b(+):moxYAltN-CTH; lane 12, pET-22b(+):moxYAltN-CTH + pLysSRARE2; lane 13, pET-22b(+):moxYAltN OPT-CTH; lane 14, pET-22b(+):moxYAltC OPT-CTH.

3.3.2.2. Activity assays

The activity of MoxY and the MoxY variants were determined for five ketone substrates: acetophenone, phenylacetone, cyclohexanone, 4'-hydroxyacetophenone and 2-decanone (Fig. A4, appendix). The substrates were chosen as they represent a wide range of ketones, namely, aromatic ketones, substituted aromatic ketones, cyclic ketones and linear ketones. Also, the substrates are accepted by well-characterised BVMOs, including CHMO from *Acinetobacter calcoaceticus* ($CHMO_{acinet}$) (Donoghue *et al*., 1976), phenylacetone monooxygenase from *Thermobifida fusca* ($PAMO_{thermo}$) (Fraaije *et al*., 2005), and 4-hydroxyacetophenone monooxygenase from *Pseudomonas fluorescens* ($HAPMO_{pseudo}$) (Kamerbeek *et al*., 2001).

An extinction coefficient of 6.22 $mM.cm^{-1}$ was used for NADPH at 340 nm (Jablonski and DeLuca, 1977) to calculate the reaction rates. The pathlength of 0.58 cm was calculated by the use of a calibration curve with known concentrations of FAD. CHMO from *A. calcoaceticus* served as a positive control for the assays with a netto oxidation rate of 276 $\mu mol.min^{-1}.L^{-1}$ for cyclohexanone. In contrast, no activity against any of the ketone substrates was observed in any of the fractions - total protein fraction, soluble fraction from French-pressed cells or soluble fraction from lysozyme-treated cells – for either MoxY or any of the MoxY variants. This indicated the MoxY and the variants either expressed as inactive proteins, or that the selected substrates were not accepted by the proteins.

3.3.3. Purification of MoxYAltN

3.3.3.1. Immobilised metal-affinity chromatography

Affinity chromatography is a liquid chromatographic technique that uses an immobilised ligand to bind to the desired molecules by selectively interacting with specific chemical groups or larger regions of the molecule (Hage, 1999). The use of affinity chromatography in the purification of recombinant proteins is a widely used technique that enables the purification of a diverse array of proteins (Arnau *et al*., 2006).

IMAC resins contain an immobilised chelating agent which is complexed with metal ions. Separation of proteins by IMAC rests on the differential interaction of the amino acid side chains, as well as the chelated metal ions in the proteins, with the complexed metal ions (Hage, 1999). Purification of

recombinant proteins that carry a histidine affinity tag, generally referred to as a 'His-tag', is the most popular method of protein purification by affinity chromatography. In the case of purification with a His-tag, the IMAC resin, typically consisting of nitriloacetic acid, is complexed specifically with Ni^{2+}. The imidazole side-chain of histidine residues display a high affinity for Ni^{2+}, therefore, proteins with surface-exposed histidine residues will preferentially bind to the column, referred to as a 'His-trap'.

Recombinant proteins can be engineered to contain a His-tag fused to either terminus of the protein. His-tags of varying lengths and sequences have been used in the past (Gaberc-Porekar and Menart, 2001), but the most popular His-tag consist of six consecutive histidine residues. Several commercial expression vectors, including the pET-vectors, contain sequences coding for either N-terminal or C-terminal hexa-histidine tags. Purification of his-tagged proteins is a rapid and simple method, and can be used in a one-step purification procedure to yield protein with more than 95 % homogeneity (Appa Rao *et al*., 1997). However, the use of IMAC in purification is not always suitable for proteins containing metal ions. Also, host organisms that contain proteins naturally rich in surface-exposed histidine residues can complicate the purification procedure by binding of unwanted proteins to the column (Arnau *et al*., 2006).

Recombinant expression of the pET-28b(+):moxYAltN vector yielded the MoxYAltN protein with an N-terminal His-tag. The size of the N-terminally His-tagged MoxYAltN was predicted as 69 kDa, using the coding region of the pET-28b(+):moxYAltN vector with the ProtParam tool from the ExPASy server. SDS-PAGE confirmed the monomeric molecular weight (Fig. 3.20) Purification with nickel-affinity chromatography served as the first step in the purification of MoxYAltN. Figure 3.22 depicts an elution profile of MoxYAltN from a HisTrap FF column. MoxYAltN eluted in the volume of 195 – 265 ml. The collected fractions were run on an SDS-PAGE to verify the homogeneity of the sample (Fig. 3.23), which indicated that the fractions were purified to near-homogeneity. However, several proteins smaller than 40 kDa were still present in low concentrations, and were possibly degradation products of MoxYAltN. Fractions eluting in the volume of 220 – 250 ml were selectively pooled.

Although UV spectra and SDS-PAGE analysis indicated that a bound protein eluted from the column, the collected fractions were colourless. As BVMOs are flavoproteins, it was expected that the fractions would have a characteristic yellow colour. It was thus postulated that the flavin moiety might not be incorporated during expression and protein folding, and that the recombinant protein is present in its apo-form. Alternatively, the flavin co-factor could have been lost during the cell-breaking or purification steps and may explain the lack of activity observed in the activity assays.

MoxYAltN is encoded by a single gene, characteristic of type I BVMOs (Willetts, 1997), therefore it would contain FAD as co-factor. In an attempt to restore the flavin co-factor, an excess of FAD was added to the pooled fractions to ensure maximum co-factor occupancy.

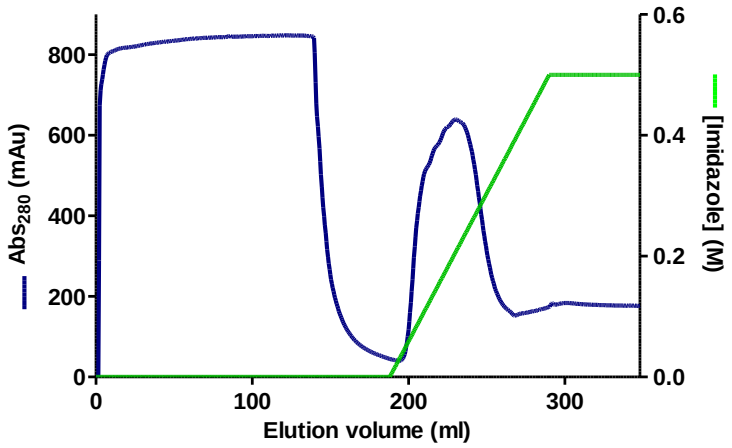

Figure 3.22. Elution profile of MoxYAltN from a FF His-trap column (GE Healthcare) during affinity chromatography. The N-terminally His-tagged MoxYAltN was eluted from the column with an increasing concentration of imidazole. Affinity chromatography was used as the first purification step.

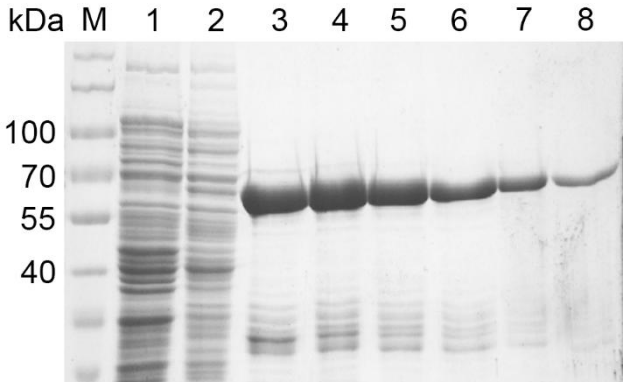

Figure 3.23. SDS-PAGE of the purification of MoxYAltN by IMAC. M, PageRuler™ Prestained protein ladder; lane 1, pET-28b(+) empty vector control; lane 2, pET-28b(+):moxYAltN; lanes 3 – 8, fractions collected from His-trap column at elution volumes 220 – 250 ml.

3.3.3.2. Size-exclusion chromatography

Size-exclusion chromatography (SEC) is a liquid chromatography method that is used to separate molecules based on their relative size, rather than interactions with the stationary phase (Barth *et al*., 1994). The stationary phase consists of gel beads with pores of a defined size. As the molecules move through the column, larger molecules that are unable to penetrate the pores will elute in the interstitial volume. Smaller molecules will penetrate the pores, effectively accessing a larger volume and eluting later than larger molecules (Mori and Barth, 1999).

SEC can also be used for sample clean-up as smaller compounds, such as salts, elute later than proteins. The mobile phase is a buffer of choice, providing a means for buffer exchange, which is often necessary in a multi-step purification setup. Purification of the proteins by IMAC produces samples in a buffer with very high imidazole concentrations. Imidazole in high concentrations can impair the activity of proteins and also interferes with certain protein assays, such as the BCA protein concentration determination (Thermo Scientific). As imidazole absorbs at 280 nm, quantification of protein by UV absorption in buffers with high imidazole concentrations can lead to inaccurate results. SEC thus provided not only a second purification step, but also aided in sample clean-up and buffer exchange to remove the imidazole.

Two migrating yellow bands could be observed on the Sephacryl column during SEC, one corresponding to MoxYAltN eluting in the volume 120 – 200 ml (Fig. 3.24), and the other corresponding to the unbound flavin. Fractions eluting in the volume 140 – 190 ml were selectively pooled and SDS-PAGE indicated that MoxYAltN was purified to near-homogeneity (Fig. 3.25). Contaminating proteins smaller than 40 kDa were still present; however, as size-exclusion chromatography separates proteins based on size, it is likely that the bands arose from degradation of MoxYAltN. For each purification procedure, the concentration of the protein in the pooled fraction was determined by the BCA method, and ranged from 1.63 – 1.70 $mg.ml^{-1}$.

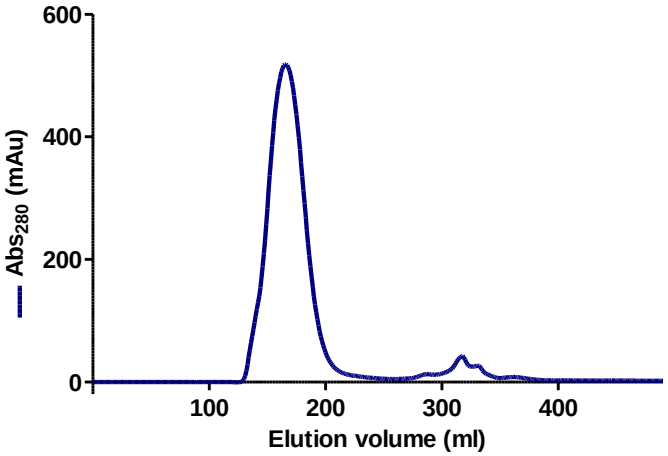

Figure 3.24. Elution of MoxYAltN from a Sephacryl S-200 HR column (Sigma Aldrich) during size-exclusion chromatography. Size-exclusion chromatography was used as a second purification step. The first peak corresponded to the elution of MoxYAltN while the second peak indicated the elution of unbound FAD.

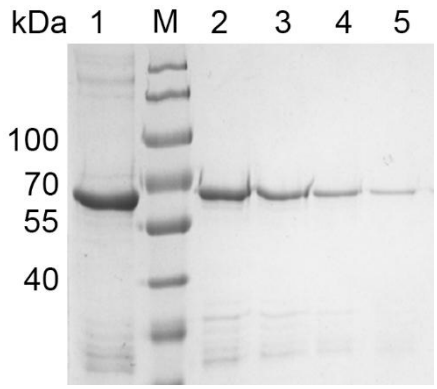

Figure 3.25. SDS-PAGE of the purification of MoxYAltN by size-exclusion chromatography. M, PageRuler™ Prestained protein ladder; lane 1, pooled fractions obtained from IMAC purification; lanes 2 – 5, fractions collected from the Sephacryl S-200 HR column at elution volumes 180 – 200 ml.

3.3.3.3. Activity assays with purified MoxYAltN

The pooled fractions from the SEC step had a light yellow colour, indicating that MoxYAltN retained the FAD co-factor. The purified MoxYAltN was assayed for activity against acetophenone, phenylacetone, 4'-hydroxyacetophenone, cyclohexanone and 2-decanone. Activity was observed with phenylacetone at a rate of 0.023 µmol.min^{-1}.mg^{-1}.

3.3.4. Co-expression with molecular chaperones

3.3.4.1. MoxYAltN

The loss of the FAD co-factor from the recombinant MoxYAltN may be due to improper folding during expression. Recombinant proteins expressed in *E. coli* often fold incorrectly, leading to loss of activity, aggregation and degradation. Molecular chaperones aid in the folding of proteins by binding partially-folded proteins and maintaining them in a soluble, translocation-competent conformation (Thomas *et al*., 1997). By this means, molecular chaperones decrease the likelihood that two or more folding intermediates will associate to produce an improperly folded protein.

The Takara Bio Inc. chaperone plasmid set codes for the DnaK-DnaJ-GrpE and the GroEL-ES molecular chaperone systems. Both chaperone teams belong to the σ^{32} heat-shock regulon which contains about 30 heat-shock proteins. The transcription of heat-shock proteins is transiently upregulated when the cell is subjected to stress, including temperature as well as expression of recombinant proteins. The chaperone plasmid set also encodes the trigger factor, a chaperone-like factor, which binds nascent peptides to improve protein folding. The trigger factor also associates with GroEL to improve peptides binding, thereby aiding in protein folding.

Co-expression of the molecular chaperones with pET-28b(+):moxYAltN improved both the activity and the level of soluble protein (Fig. 3.26). Of interest is also the improvement in activity without the addition of FAD, suggesting that the chaperones indeed aid in the proper folding of MoxYAltN which would improve co-factor binding. The soluble expression levels were improved noticeably by co-expression with pGro7 and pTf16, and to a lesser extent with pG-Tf2. However, co-expression with pGro7 produced the highest level of soluble protein and improved the activity more than five-fold. Therefore, in all further experiments, pET-28b(+):moxYAltN was co-expressed with the pGro7 plasmid. Purified MoxYAltN prepared from *E. coli* co-expressed with the pGro7 plasmid, displayed a light yellow tinge, indicating that the FAD co-factor was retained. Nevertheless, an excess of FAD was added in all the cases before SEC to ensure maximum co-factor occupancy.

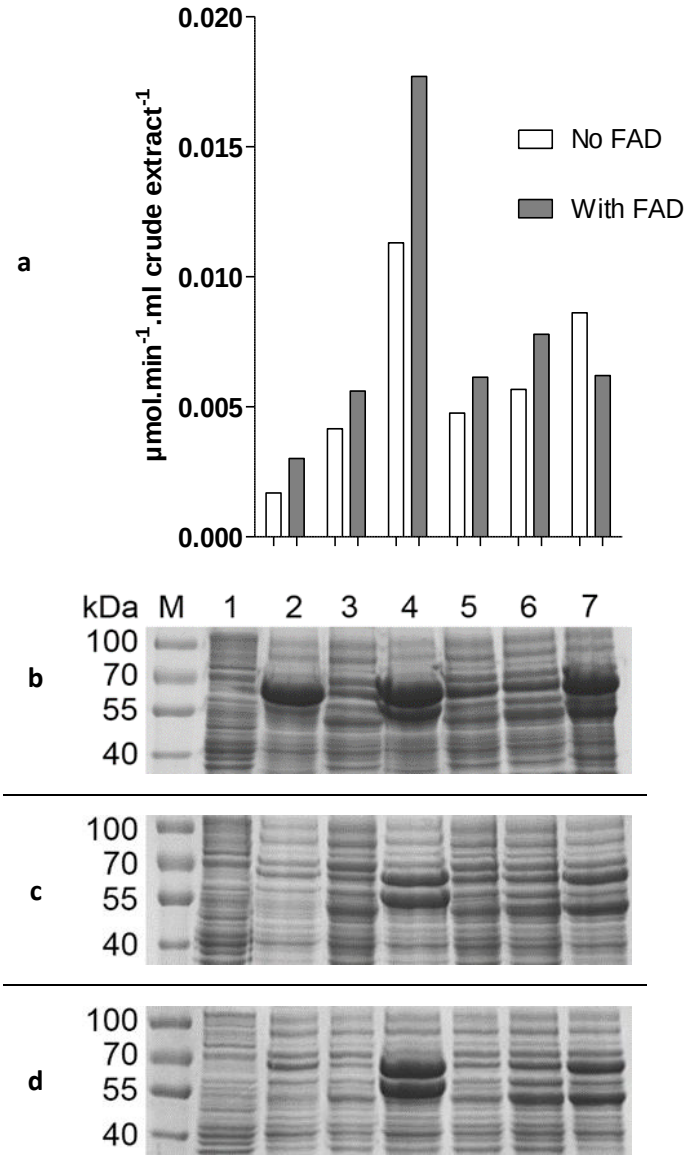

Figure 3.26. a, Activity against phenylacetone of the total protein fractions of pET-28b(+):moxYAltN co-expressed with the chaperone plasmids (Takara Bio. Inc.). White bars represent the fractions before addition of FAD while grey bars represent fractions after the addition of FAD. **b, c & d,** SDS-PAGE analysis of pET-28b(+):moxYAltN co-expressed with molecular chaperones using a chaperone plasmid set (Takara Bio Inc.). **b,** Total protein fraction; **c,** soluble protein fraction obtained from the French-press cell lysis; **d,** soluble protein fraction obtained from lysozyme treatment/freeze-thaw cell lysis. M, PageRuler™ Prestained protein ladder; lane 1, pET-28b(+) empty vector control; lane 2, pET-28b(+):moxYAltN; lane 3, pET-28b(+):moxYAltN + pG-KJE8; lane 4, pET-28b(+):moxYAltN + pGro7; lane 5, pET-28b(+):moxYAltN + pKJE7; lane 6, pET-28b(+):moxYAltN + pG-Tf2; lane 7, pET-28b(+):moxYAltN + pTf16.

3.3.4.2. Alternative MoxY variants

Co-expression of MoxYAltN with pGro7 greatly enhanced both the solubility levels and the activity of the protein. As discussed in section 3.3.2, no or very low levels of soluble protein was detected for the other MoxY variants and no activity was observed in any of the fractions. Therefore, all the MoxY variants in pET-28b(+) was co-expressed with pGro7 with the aim of improving the solubility and activity of the proteins. The pET-28b(+) constructs were chosen for possible further downstream protein purification.

SDS-PAGE analysis indicated that expression was observed for all the constructs (Fig. 3.27). Low levels of soluble expression was observed in the lysozyme-treated fractions for MoxY and MoxY OPT, as well as the MoxYAltC (Fig. 3.28), however, the proteins were not recovered as soluble from the French-pressed cells (data not shown). More importantly, only MoxYAltN and MoxYAltN OPT were active against phenylacetone, even after the addition of FAD. Therefore, it can be assumed that MoxYAltN is the only active recombinant product from the *moxY* gene.

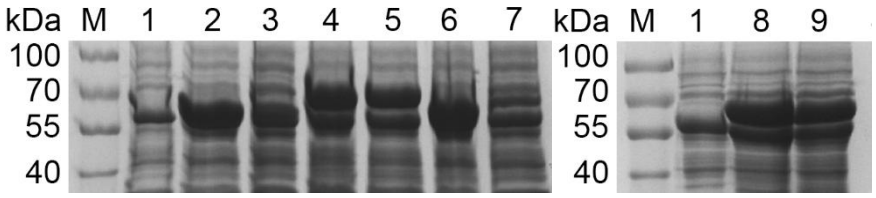

Figure 3.27. SDS-PAGE analysis of the total protein fraction of the MoxY variants in pET-28b(+) co-expressed with the pGro7 molecular chaperone plasmid (Takara Bio Inc). M, PageRuler™ Prestained protein ladder; lane 1, pET-28b(+) empty vector control + pGro7; lane 2, pET-28b(+):moxY + pGro7; lane 3, pET-28b(+):moxYOPT + pGro7; lane 4, pET-28b(+):moxYAltNC + pGro7; lane 5, pET-28b(+):moxYAltNC OPT + pGro7; lane 6, pET-28b(+):moxYAltC + pGro7; lane 7, pET-28b(+):moxYAltC OPT+ pGro7; lane 8, pET-28b(+):moxYAltN + pGro7; lane 9, pET-28b(+):moxYAltN OPT + pGro7.

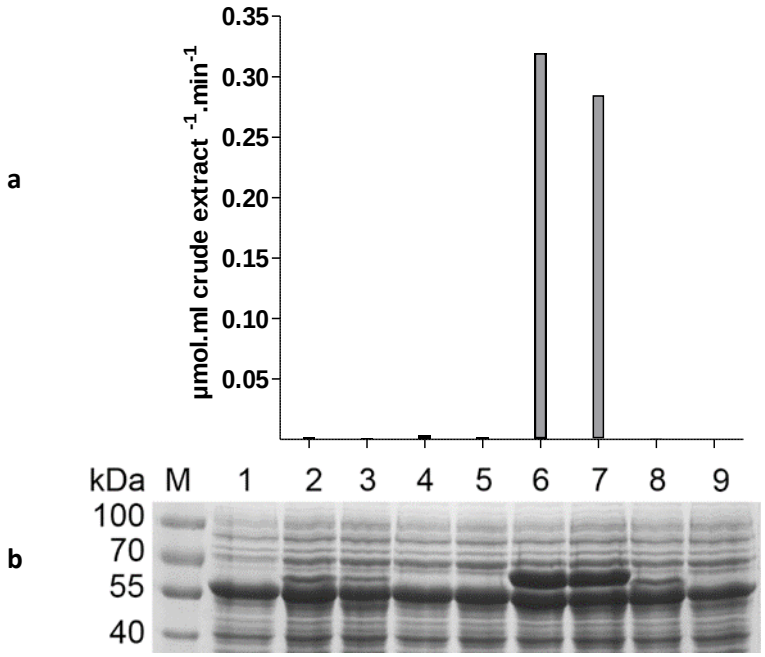

Figure 3.28. a, Activity against phenylacetone of the soluble fractions of the MoxY variants in pET-28b(+) co-expressed with the pGro7 molecular chaperone plasmid (Takara Bio Inc.) obtained by lysozyme lysis/freeze thaw and supplemented with FAD. **b,** SDS-PAGE analysis of the soluble protein fraction of the MoxY variants in pET-28b(+) co-expressed with the pGro7 molecular chaperone plasmid (Takara Bio Inc.); M, PageRuler™ Prestained protein ladder; lane 1, pET-28b(+) empty vector control + pGro7; lane 2, pET-28b(+):moxY + pGro7; lane 3, pET-28b(+):moxYOPT + pGro7; lane 4, pET-28b(+):moxYAltNC + pGro7; lane 5, pET-28b(+):moxYAltNC OPT + pGro7; lane 6, pET-28b(+):moxYAltN + pGro7; lane 7, pET-28b(+):moxYAltN OPT + pGro7; lane 8, pET-28b(+):moxYAltC + pGro7; lane 9, pET-28b(+):moxYAltC OPT + pGro7.

3.3.5. Characterisation of MoxYAltN

3.3.5.1. Effect of pH on enzyme activity

The effect of pH on the activity of purified MoxYAltN towards phenylacetone was investigated by measuring the oxidation of NADPH during conversion of phenylacetone at various pH's ranging from pH 6.5 to 10. Figure 3.29 depicts the effect of pH on the activity towards phenylacetone in a, 20 mM MOPS-Bicine-CHES buffer and b, 50 mM Tris-HCl buffer. Relative activities are shown, with the maximum activity taken as 100 %. Considering Fig. 3.29b, MoxYAltN is active over a wide pH range with less than 15 % variance in activity between pH 7.5 – 9.0. Maximal activity was achieved at pH 8.5 in both buffers. This corresponds well to the optimum pH of characterised BVMOs (Leisch, 2011), including $HAPMO_{pseudo}$, pH 7.5 (Kamerbeek *et al*., 2001), cyclopentanone monooxygenase from *Comamonas* sp. ($CPMO_{comamo}$), pH 7.7 (Griffin and Trudgill, 1976); $PAMO_{thermo}$, pH 8.0 (Fraaije *et al*., 2005), and $CHMO_{acinet}$, pH 9.0 (Donoghue *et al*., 1976).

The optimum pH range of MoxYAltN also corresponds to that of hydroxyaverantin (HAVN) dehydrogenase (pH 7.5 – 8.5, Sakuno *et al*., 2003) and *O*-methyltransferase I (pH 7 – 8.5, Yabe *et al*., 1998), both of which are involved in the aflatoxin biosynthesis pathway. However, this is in contrast with the optimum pH range for oxoaverantin (OAVN) cyclase (pH 6 – 7; Sakuno *et al*., 2005), indicating that the optimum pH values for the enzymes involved in aflatoxin biosynthesis are not strictly conserved.

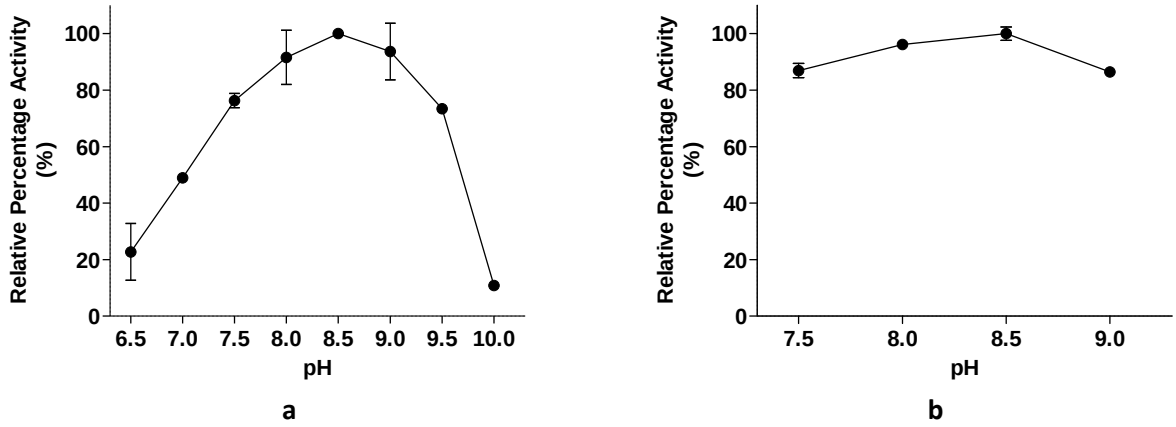

Figure 3.29. Effect of pH on the activity of MoxYAltN towards phenylacetone in **a,** 20 mM MOPS-Bicine-CHES and **b,** 50 mM Tris-HCl. Activity at pH 8.5 was taken as 100 %. Error bars indicate standard deviations.

The activity of MoxYAltN towards phenylacetone was generally higher in 50 mM Tris buffer than in 20 mM MOPS-Bicine-CHES buffer, therefore, Tris buffer was selected as the buffer of choice for all further activity assays.

3.3.5.2. Effect of buffer concentration on enzyme activity

The effect of an increase in the buffer concentration on the activity of MoxYAltN towards phenylacetone was investigated by monitoring the oxidation of NADPH at Tris concentrations ranging from 50 – 200 mM, at pH 8.5. Figure 3.30 depicts the effect of buffer concentration on the activity of MoxYAltN, with the highest activity obtained at 200 mM Tris-HCl. Relative activities are shown, with the maximum activity taken as 100 %. The effect of buffer concentration is quite severe, with a 50 % increase in activity from 50 mM to 200 mM Tris. Therefore, it was concluded that 200 mM is the optimum buffer concentration for the activity of MoxYAltN and 200 mM Tris (pH 8.5) was subsequently used as buffer for all further activity assays

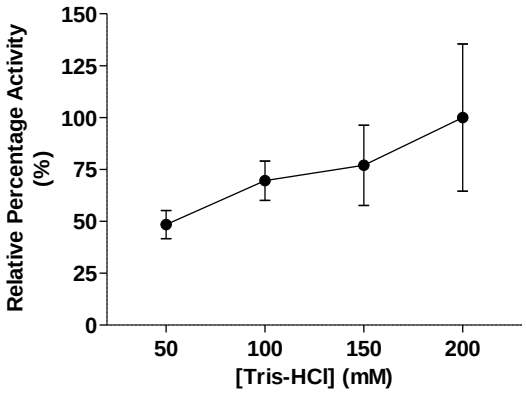

Figure 3.30. Effect of buffer concentration on the activity of MoxYAltN towards phenylacetone. Activity at 200 mM was taken as 100%. Error bars indicate standard deviations.

3.3.5.3. Effect of temperature on enzyme activity

The effect of temperature on the activity of purified MoxYAltN towards phenylacetone was investigated by measuring the oxidation of NADPH at various temperatures ranging from 25 – 40°C. Figure 3.31 depicts the effect of temperature on the enzyme activity in 200 mM Tris-HCl buffer. Relative activities are shown, with the maximum activity taken as 100 %. MoxYAltN was more than

50 % active between 30 – 37°C, with a marked increase at 37°C, the optimum temperature. A sharp decrease was observed when the temperature was raised to 40°C, an indication of possible enzyme instability.

A. flavus can grow at a wide range of temperatures, ranging from 12 – 48°C (Hedayati *et al*., 2007). The optimum growth temperature is 37°C, corresponding to the optimum temperature of MoxYAltN, and is consistent with the organism's capabilities as an opportunistic human pathogen. However, an optimum temperature of 37°C for an enzyme involved in aflatoxin biosynthesis is surprising, as the production of aflatoxins is completely inhibited at 37°C or higher (Bhatnagar *et al*., 2006).

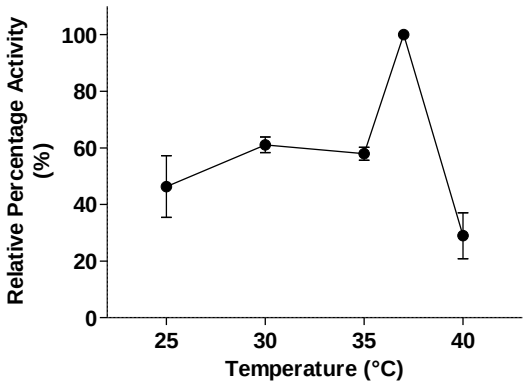

Figure 3.31. Effect of temperature on the activity of MoxYAltN towards phenylacetone. Activity at 37°C was taken as 100 %. Error bars indicate standard deviations.

3.3.5.4. Enzyme stability

In order to investigate the temperature stability of MoxYAltN, activity against phenylacetone was monitored after incubation of the enzyme at various temperatures. Aliquots were taken over time and assayed by following the oxidation of NADPH. Relative activities were determined with the activity before incubation taken as 100%. Incubation at 40°C and 45°C decreases activity to 0 and 20 % within 5 minutes, respectively (data not shown). Figure 3.32 depicts the stability of the enzyme at 35°C and 37°C. Of note is the rapid decrease in activity of MoxYAltN at 37°C, the optimum temperature, with more than 70 % loss of activity over 20 minutes. In contrast to that, when the

incubation temperature is lowered to 35°C, MoxYAltN remains stable for 20 minutes, whereafter the activity decreases. Due to the instability of the enzyme, a reaction temperature of 25°C was chosen for all further assays to minimize inaccuracies caused by loss of enzyme activity.

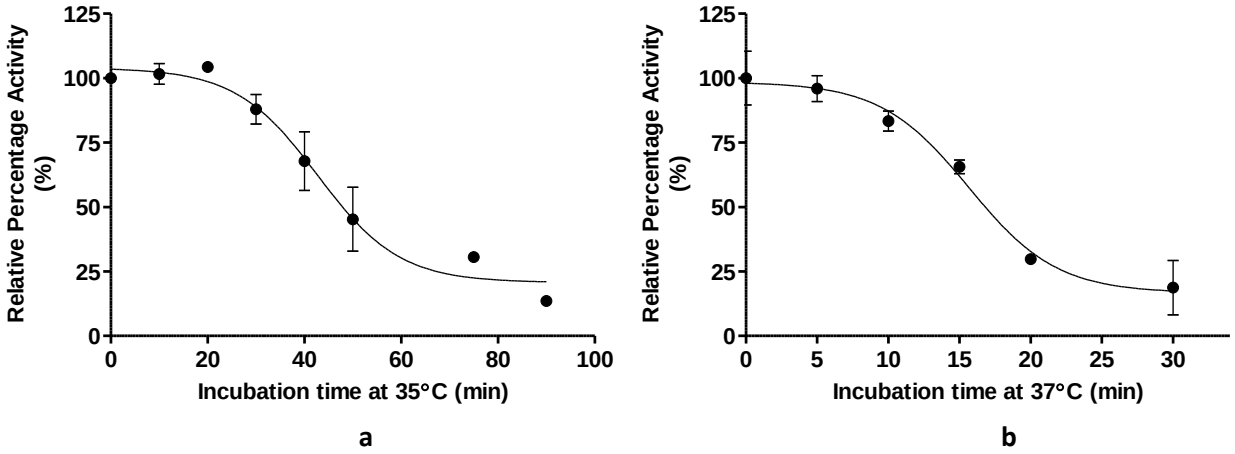

Figure 3.32. Activity of MoxYAltN towards phenylacetone after incubation at **a,** 35°C and **b,** 37°C, the optimum temperature, over time. Activity before incubation was taken as 100%. Error bars indicate standard deviation.

3.3.5.5. Steady-state kinetics

Kinetic constants for the conversion of phenylacetone to phenylacetate by MoxYAltN were determined by measurement of the initial velocities at a range of phenylacetone concentrations. Reactions were performed at 25°C, with the optimum pH and buffer concentrations. In order to ensure that MoxYAltN had full co-factor occupancy, the purified protein was enriched with FAD in a 1:4 molar ratio. Non-linear regression was performed with GraphPad Prism 5.03 to yield a hyperbolic curve with an R^2 of 0.98. Figure 3.33 shows the hyperbolic dependence of the specific activity of MoxYAltN on the phenylacetone concentration. The purified MoxYAltN exhibited Michaelis-Menten kinetics, with an apparent K_m of 19 µM (±1.4 µM) for phenylacetone and a k_{cat} of 0.122 s^{-1}. The wild-type $PAMO_{thermo}$ displayed a K_m of 59 µM for phenylacetone and a k_{cat} of 1.9 s^{-1}. Therefore, although the apparent affinity for phenylacetone is higher for MoxYAltN, $PAMO_{thermo}$ displayed a much higher turnover rate.

The K_m values for the characterised enzymes in the aflatoxin biosynthesis pathway, is highly varied. *O*-methyltransferase I displayed a K_m of 0.94 µM for demethylsterigmatocystin (DMST) and a K_m of 2.5 µM for dihydrodemethylsterigmatocystin (DHDMST) (Yabe *et al*., 1998), OAVN cyclase displayed

a K_m of 2.4 µM for versiconal (VHOH) and a K_m of 20 µM for OAVN (Sakuno *et al*., 2005), and HAVN dehydrogenase displayed a K_m of 83 µM for HAVN. The K_m of MoxYAltN towards phenylacetone, a surrogate substrate, is unexpectedly lower, having a higher affinity as compared to that of HAVN dehydrogenase for HAVN, but comparable to the affinity of OAVN cyclase for OAVN.

The V_{max} of MoxYAltN towards phenylacetone was 0.107 µmol.min^{-1}.mg^{-1} (± 0.002 µmol.min^{-1}.mg^{-1}). The V_{max} is magnitudes lower than the V_{max} of HAVN dehydrogenase, 2.3 µmol.min^{-1}.mg^{-1} for HAVN (Sakuno *et al*., 2003) and *O*-methyltransferase I, 78.1 µmol.min^{-1}.mg^{-1} for DMST and 106.7 µmol.min^{-1}.mg^{-1} for DHDMST (Yabe *et al*., 1998). A plausible explanation for the discrepancy in activity is that phenylacetone is not the natural substrate of MoxYAltN. The kinetics of MoxYAltN towards the natural substrate, HVN, remains to be studied.

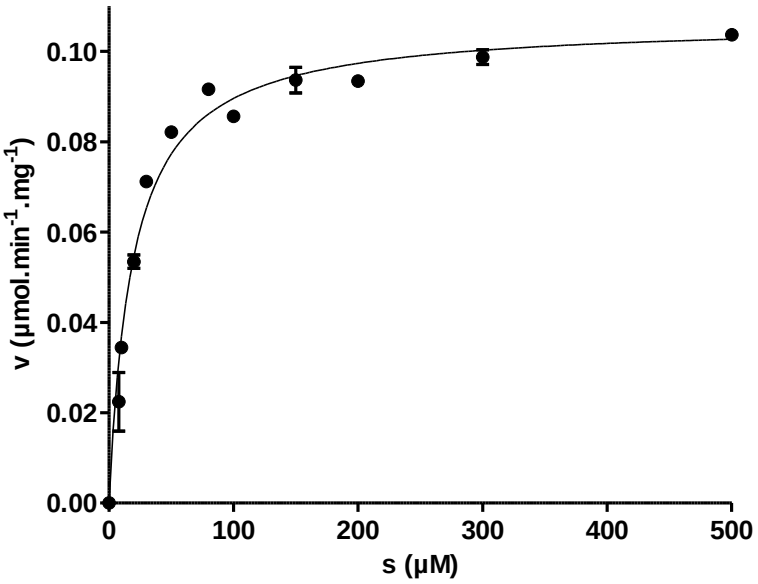

Figure 3.33. Steady-state kinetics of MoxYAltN depicting the dependence of specific activity on the concentration of the substrate, phenylacetone. Error bars indicate standard deviations.

3.3.5.6. Reaction of MoxYAltN with hydroxyversicolorone

In order to determine whether MoxYAltN was active against HVN, the purified enzyme was incubated with [1'-^{2}H]HVN in the presence of NADPH. The reaction was performed at 25°C, at the optimum pH and buffer concentration, with the reaction monitored spectrophotometrically at 340

nm for 40 min. A small, but significant rate was observed against HVN of 2.97 nmol.min^{-1}.mg^{-1} (± 0.212 nmol.min^{-1}.mg^{-1}).

TLC analysis of the synthetic [1'-^{2}H]HVN received from Prof. Townsend indicated that the sample was either impure or partly degraded. The R_f of the synthetic [1'-^{2}H]HVN using the chloroform:methanol mobile phase of 95:5 was, according to literature, expected to be 0.1 (Townsend *et al*., 1988), which is different from the R_f of either spot observed with the sample. This was unexpected and difficult to explain, since NMR spectroscopy analysis had been performed on the sample prior to shipment to confirm the identity as [1'-^{2}H]HVN (Townsend, personal communication).

Comparison of the standard [1'-^{2}H]HVN with the metabolites extracted from the incubation of [1'-^{2}H]HVN with MoxYAltN (Fig 3.34) indicated the presence of an additional compound. Co-spotting of the unincubated and incubated HVN verified that no migration differences occurred during TLC. As MoxYAltN had been demonstrated to be an active BVMO and the 5' carbonyl group is the only ketone group suitable for a BV reaction, it can be assumed that the third spot on the TLC plate is VHA.

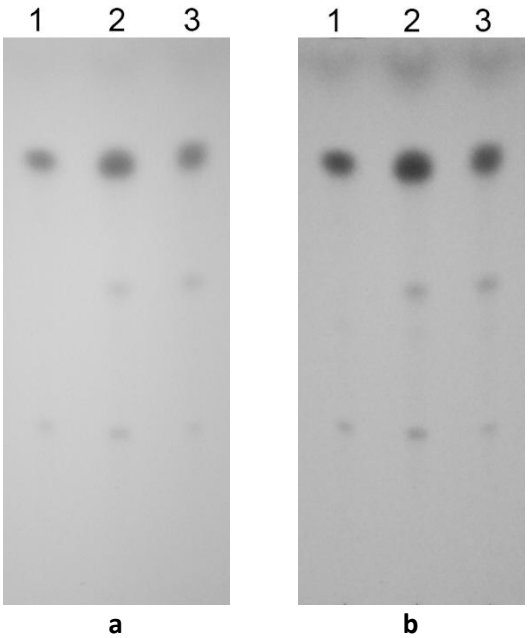

Figure 3.34. TLC analysis of the reaction of the purified MoxYAltN with synthetic [1'-^{2}H]hydroxyversicolorone on **a,** Silica 60 and **b,** Silica F254 gel. Lane 1, [1'-^{2}H]hydroxyversicolorone standard; lane 2, co-spot of lane 1 and 3; lane 3, reaction products and substrates extracted from the incubation of MoxYAltN with [1'-^{2}H]hydroxyversicolorone.

3.3.5.7. Whole-cell biotransformations

The instability of MoxYAltN hampered the screening of an extensive ketone substrate range with purified enzyme. Therefore, whole-cell biotransformations were used to investigate the substrate scope. MoxYAltN was screened for activity against an extended range of ketones as depicted in Fig. A4 (appendix). Activity was observed for a wide range of substrates with the substrates and percentage conversion listed in Table 3.8. Typical GC chromatograms of the substrates and products are illustrated in Fig. A5 (appendix).

A drawback of whole-cell biotransformations is that the native enzymes of the *E. coli* host can interfere with the biotransformation process. When considering Fig. A5b (appendix), a peak corresponding to the alcohol-product can be observed due to the native alcohol dehydrogenase activity in *E. coli* that converts the ketone to the alcohol. Also, short incubation times were used to avoid degradation of the ester or lactone product, which might limit product detection.

Table 3.8. Ketone substrates converted by MoxYAltN during whole-cell biotransformations. The percentage conversion of 10 mM is given after 2 hours, as well as the standard deviation.

Substrate	Conversion (%)
phenylacetone	17.1 ± 1.9
4-phenyl-2-butanone	11.9 ± 1.2
4-(4'-hydroxyphenyl)-2-butanone	7.5 ± 0.3
3-octanone	0.8 ± 0.3
2-decanone	19.3 ± 1.6
2-undecanone	32.1 ± 1.9
2-dodecanone	21.8 ± 2.4
2-phenylcyclohexanone	33.5 ± 8.4
2-indanone	14.8 ± 2.4
(±)-*cis*-bicyclo[3.2.0]hept-2-en-6-one	23.2 ± 4.1

When considering the structure of HVN, the natural substrate for MoxY, or MoxYAltN, in the aflatoxin biosynthesis pathway, it is expected that the enzyme will display a preference for ketones on a linear chain attached to a ring system, as in the case of phenylacetone, 4-phenyl-2-butanone and 4-(4'-hydroxyphenyl)-2-butanone. MoxYAltN also catalyses the conversion of purely linear ketones of varying chain length (C_8 – C_{12}) with the ketone group at position C_2 or C_3. Furthermore, MoxYAltN also converts the substituted aromatic ketone 2-phenylcyclohexanone, and the bicyclic ketones 2-indanone and (±)-*cis*-bicyclo[3.2.0]hept-2-en-6-one. This broad substrate scope is surprising, given the firm physiological role of MoxY/MoxYAltN in the aflatoxin biosynthesis pathway.

3.4. Discussion

MoxYAltN expressed as a soluble protein in all the construction vectors: pET-22b(+), the CTH-variant as well as in pET-28b(+). The MoxYAltN-variant was found as the only variant to display activity towards phenylacetone after supplementation with FAD, and also converted synthetic [1'-^{2}H]HVN to VHA. It was preliminarily concluded that MoxYAltN is the only active recombinant form of the *moxY* gene and is responsible for the conversion of HVN to VHA in the aflatoxin biosynthesis pathway.

An alignment of the amino acid sequences of CHMO from *Rhodococcus* sp. ($CHMO_{rhodoc}$) (Mirza *et al*., 2009), MoxY, MoxYAltN, MoxYAltNC and MoxYAltC from *A. flavus*, along with the predicted amino acid sequences of StcW from *A. nidulans*, as well as MoxY/AflW from *A. parasiticus* and an N-terminal variant of MoxY/AflW, was performed with ClustalO and JalView v. 2 (Fig. 3.35, Waterhouse *et al*., 2009). Similar to the *moxY* gene from *A. flavus*, an alternative translational start site was observed in the *moxY* gene from *A. parasiticus,* leading to an identical elongated N-terminus of 21 amino acids. Interestingly, the predicted amino acid sequence of the *stcW* gene from the sterigmatocystin biosynthesis cluster in *A. nidulans*, also displays an extended N-terminus when compared to MoxY from *A. flavus* and *A. parasiticus*. The extended N-terminus is 24 amino acids in length and displays 23 % identity with the extended N-terminals from *A. flavus* and *A. parasiticus.*

In the aflatoxin biosynthesis pathway, OAVN cyclase which is encoded by the *vbs* gene, is involved in two disconnected enzymatic steps, namely, the conversion of OAVN to averufin (AVF) and VHOH to versicolorin B (VB) (Fig 1.3, Sakuno *et al*. 2005). The OAVN cyclase purified from *A. parasiticus* SU-1 contained an N-terminus that was 41 amino acids longer than that of the OAVN cyclase purified from *A. parasiticus* NIAH-26. Both the full-length and truncated enzymes were able to convert OAVN and VB, indicating that the variability in the N-terminus did not affect either the catalytic efficiency or substrate specificity. This is in contrast to the situation with MoxY, where only the variant with the extended N-terminus was observed as active.

The multiple sequence alignments were also used to investigate whether any residues critical to the catalytic activity was lost in different MoxY variants. Recently, Rebehmed and co-workers (2013) performed a study to verify the critically conserved residues in BVMOs and used the crystal structure of $CHMO_{rhodoc}$ to map the residues. Table 3.9 lists all the critically conserved residues, as well as their localisation, and whether the corresponding residues are conserved in the MoxY variants, MoxY from *A. parasiticus* and StcW from *A. nidulans*.

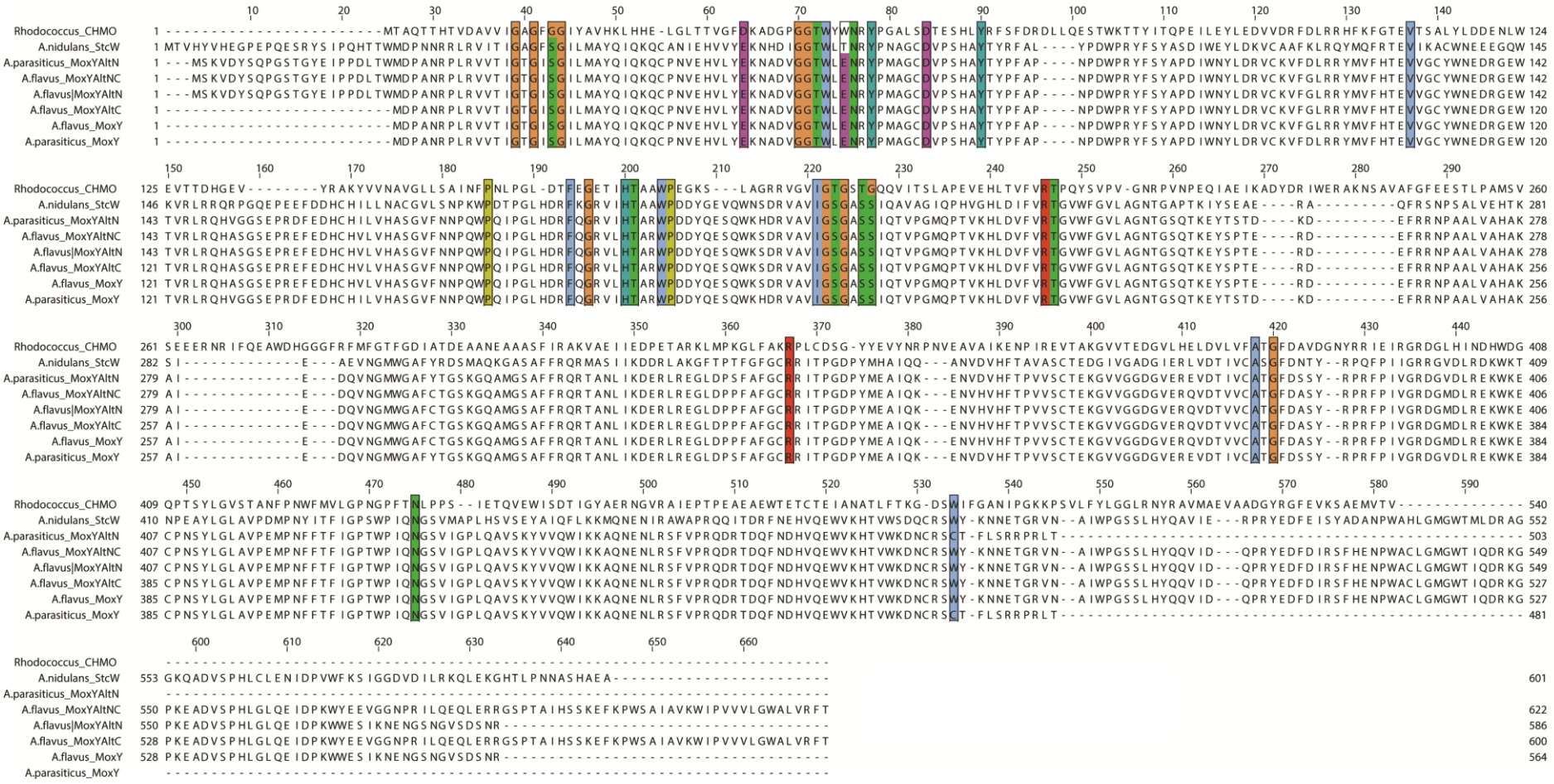

Figure 3.35. Alignment of the amino acid sequences of CHMO from *Rhodococcus* sp. HI-31, the MoxY-variants from *A. flavus* (MoxY, MoxYAltN, MoxYAltNC and MoxYAltC), the MoxY-variants from *A. parasticitus* (MoxY and MoxYAltN) and StcW from *A. nidulans.* The highlighted residues represents regions which are conserved in BVMO enzymes (Rebehmed *et al*., 2013). The alignment was performed with ClustalO, using Jalview version 2.8.

The tryptophan residue at position 50 of $CHMO_{rhodoc}$ interacts through hydrogen-bonding with both hydroxyl groups of the FAD ribose ring. In StcW, the corresponding locus is occupied by a tyrosine residue, which was encountered in 4.3 % of the sequences investigated by Rebehmed and co-workers (2013). However, in all the MoxY sequences from *A. flavus* and *A. parasiticus*, the locus is occupied by a glutamate residue. This difference might lead to a more weakly-bound FAD co-factor and provide an explanation for the loss of FAD during purification.

The other three differences observed between $CHMO_{rhodoc}$ and the MoxY sequences (positions 186, 190, and 492) all belong to the NADPH-binding domain. Position 190 of $CHMO_{rhodoc}$ forms part of the Rossman-fold motif [GXGXX(G/A)], however, in all the cases of the MoxY sequences, as well as StcW, this position is occupied by a serine residue. Position 186 is occupied by a threonine residue in $CHMO_{rhodoc}$ that acts, via its NH group, as a hydrogen donor to the O3B atom of NADPH. The locus is occupied by a serine residue in all the MoxY sequences, as well as StcW, and can be presumed to fulfil the same role. Residue 492 is occupied by tryptophan in $CHMO_{rhodoc}$ that performs hydrogen bonding with its side chain to the O3D atom of NADPH. In MoxY from *A. parasiticus*, this residue is substituted with cysteine, which can stabilise the O3D group via hydrogen interactions with the sulfhydryl group.

Even though the MoxY sequences from *A. flavus* do deviate from the conserved residues, the discrepancies are present in all the MoxY sequences and do not arise due to the elongation of the N-terminus or alternative splicing of the C-terminus. Therefore, the lack of function observed for the MoxY variants (other than MoxYAltN) cannot be attributed to modification of critically conserved amino acids. Although no activity against phenylacetone was observed for MoxYAltC, EST data suggests that this form of the *moxY* gene is expressed *in vivo*. It is possible that MoxYAltC has a catalytic function other than the conversion of HVN in the aflatoxin biosynthesis pathway. Also, activity against phenylacetone is not necessarily a prerequisite for activity against HVN.

Very low levels of soluble protein was present in the lysozyme-treated fractions obtained from co-expression of pET-28b(+):moxYAltC with pGro7 (Fig. 3.28). The soluble fractions were only assayed for activity against phenylacetone. Therefore, it is possible that the enzyme may catalyse the BV oxidation of other ketone substrates or heteroatom oxidations. The possibility necessitates further studies to investigate the activity of this enzyme, preferably by means of both whole-cell biotransformations, as well as substrate screening with purified enzyme.

Table 3.9. Highly conserved residues in the motifs and domains of type I BVMOs. The number of the residue in CHMO from *Rhodococcus* sp. is given in the first columns, while the % conservation of the residue is given in the second columns (Rebehmed *et al*., 2013). The corresponding residue for StcW is given, and whether the residue is conserved in the aflatoxin/sterigmatocystin BVMOs. Deviations from the conserved residues are indicated in brackets.

CHMO residue	% conservation	StcW residue	Conserved	CHMO residue	% conservation	StcW residue	Conserved
Dinucleotide-binding motif (Rossman fold)				**BVMO fingerprint motif**			
G 15	99.1	39	✓	F 160	94.8	190	✓
G 17	99.1	41	✓	G 162	100.0	192	✓
G/A 20	97.4/2.6	44	✓	H 166	94.8	196	✓
				T 167	93.1	197	✓
G 185	100.0	218	✓	W 170	100.0	200	✓
G 187	100.0	220	✓	P/D 171	70.7/28.4	201	✓
G/A 190	62.1/35.5	223	× (S)				
FAD-binding domain				**NADPH-binding domain**			
G/A/S 19	47.0/42.6/9.6	44	✓	P 152	96.6	181	✓
D/E 39	20.0/80.0	64	✓	I 184	94.0	217	✓
G 45	99.1	70	✓	T 186	94.8	219	× (S)
G 46	100.0	71	✓	T/S 189	50.9/49.1	222	✓
T 47	91.3	71	✓	R 209	100.0	242	✓
W 48	100.0	73	✓	T/S 210	81.9/15.5	243	✓
W/F/Y 50	80.9/11.3/4.3	75	✓ StcW × (E)	R 329	100.0	334	✓
N 51	100.0	76	✓	A 379	96.6	382	✓
Y 53	97.4	78	✓	G 381	100.0	384	✓
D 59	100.0	84	✓	W/Y 492	69.8/28.4	496	✓ × (C) MoxY *A. parasiticus*
Y 65	100.0	90	✓				
V 112	82.8	133	✓				
N 436	98.3	437	✓				

3.5. Conclusions

Almost a decade ago, the *moxY* gene of the aflatoxin biosynthesis gene cluster in *A. parasiticus* had been implicated in the conversion of HVN to VHA in the aflatoxin biosynthesis pathway by means of gene-disruption experiments. The *moxY* gene was also demonstrated to be involved in the conversion of VONE to VOAc in the side-pathway of the metabolic grid, representing the parallel reaction to the conversion of HVN to VHA. The homologous gene in *A. flavus* had been identified and encodes a polypeptide that contains the fingerprint motif [FXGXXXHXXXW(P/D)], characteristic of type I BVMOs. The catalytic activity of the *moxY* product is consistent with the activity as a BVMO, namely, the conversion of a ketone to an ester.

Closer inspection of the *moxY* gene in *A. flavus* revealed a translational start site 63 bp prior to the translational start site predicted in the NCBI database, leading to a protein with 21 additional amino acids at the N-terminus. This phenomenon was also observed in the *moxY* homologue in the aflatoxin biosynthesis cluster of *A. parasiticus,* as well as the proposed amino acid sequence of the *stcW* homologue in the *A. nidulans* sterigmatocystin biosynthesis gene cluster. Mapping of EST sequences to the *moxY* gene in *A. flavus* revealed an alternative splicing site near the C-terminus, leading to alternative versions of the MoxY product with and without an elongated C-terminus.

Heterologous expression of the variations of the *moxY* gene and activity screening with surrogate substrates identified MoxYAltN as the only active recombinant form of the MoxY enzyme. Purified MoxYAltN converts synthetic [1'-^{2}H]HVN to VHA in the presence of NADPH, unequivocally confirming the role of the *moxY* gene in the aflatoxin biosynthesis pathway. Interestingly, MoxYAltN has a broad substrate scope including linear, aromatic, substituted aromatic and bicyclic ketones. Considering the firm physiological role of the *moxY* gene in *A. flavus*, this promiscuity towards ketone substrates is surprising.

EST mapping indicated that mRNA for a protein with the alternative C-terminus was present *in vivo*. Therefore, additional studies with the alternative C-variants of the MoxY enzyme are required.

Chapter 4

Recombinant expression and characterisation of the BVMO homologues

4.1. Introduction

In an attempt to devise alternative strategies for aflatoxin inhibition, the biosynthetic pathway was investigated in more detail. The conversion of hydroxyversicolorone (HVN) and versicolorone (VONE) to versiconal hemiacetal acetate (VHA) and versiconol acetate (VOAc) was identified as a key step for possible inhibition, as the enzyme responsible for this step is a Baeyer-Villiger monooxygenase (BVMO) (Wen *et al*., 2005). BVMOs are present in bacterial and fungal genomes, but not in those of higher eukaryotes. A substance selectively inhibiting BVMOs will be less likely to cause inhibition of enzymes in humans, animals and plants, and application to agricultural crops will be more acceptable. As described in chapter 3, the role of the *moxY* gene in the catalysis of HVN to VHA has been firmly established.

Intragenomic complementation of an impaired aflatoxin biosynthesis gene is a recurring theme throughout the experimental research conducted on the aflatoxin biosynthesis pathway. In many instances, gene disruption of an aflatoxin biosynthetic cluster gene produced 'leaky' mutants, where the gene product is non-functional, but aflatoxins were still produced, usually at much lower levels (Ehrlich *et al*. 2010; Sakuno *et al*. 2005; Trail *et al*., 1994). This demonstrated that the blocked enzymatic step could be complemented by another enzyme present in the organism. In the case of *estA*, up to 10 % of the enzymatic activity was attributed to esterases not associated with aflatoxin biosynthesis (Chang *et al*., 2004a).

The availability of the complete genome sequence of *Aspergillus flavus* NRRL3357 allowed genome mining to discover putative BVMOs. Homology searches using the amino acid sequence of cyclohexanone monooxygenase (CHMO) from *Rhodococcus* sp. ($CHMO_{rhodoc}$, Mirza *et al*., 2009) revealed that besides *moxY*, the *A. flavus* genome contained 25 other putative BVMO genes. Therefore, it has to be taken into consideration that the function of MoxY(AltN) can be complemented by one of these BVMOs.

The *moxY* disruption mutants led to a loss of aflatoxin production and were thus not considered as leaky (Wen *et al*., 2005). However, the experiments were performed in tightly-regulated laboratory conditions and the possibility that some of these BVMOs are expressed in field conditions, cannot be disregarded. Also, it has been demonstrated that genes not associated with aflatoxin biosynthesis and not located in or near the aflatoxin biosynthesis gene cluster are regulated by AflR, the aflatoxin-associated transcription factor (Price *et al*., 2006). The microarray studies used to identify these genes used only 40 % of the *A. flavus* transcriptome, therefore, it is possible that the BVMOs may indeed be regulated by AflR and were overlooked.

Mihovilovic and co-workers demonstrated in 2005 that the biocatalytic profiles of BVMOs with respect to the substrate acceptance and enantioselectivity, correspond to the phylogenetic clustering of the enzymes. The so-called "family clustering" of the BVMOs was based on the amino acid identities and would theoretically be indicative of similarity between the biocatalytic properties of closely-related BVMOs. Thus, it is more likely that the BVMOs clustering with MoxY have overlapping biocatalytic profiles and would be able to convert HVN to VHA. In an attempt to systematically determine whether the activity of MoxY could be intragenomically complemented by a BVMO homologue, a phylogenetic analysis was performed to determine the relationship between MoxY and the other 25 BVMOs. The aim of this chapter was to investigate the possible intragenomic complementation of the *moxY* gene by cloning and heterologously expressing the closely-related BVMO homologues of MoxY in *E. coli.*

4.2. Materials and Methods

4.2.1. Identification of BVMO homologues

The amino acid sequence of CHMO from *Rhodococcus* sp. (Mirza *et al*., 2009) was used as a BLASTp query in the National Center for Biotechnology Information (NCBI) database against the whole-genome sequence of *A. flavus* NRRL3357. The predicted BVMOs will be referred to by the last three digits of their accession numbers throughout the chapter. Multiple sequence alignments of the predicted amino acid sequences were performed using the MUSCLE European Bioinformatics Institute (EBI) web tool (http://www.ebi.ac.uk/Tools/msa/muscle) with the default parameters (Edgar, 2004). The best amino acid substitution model was estimated for tree building using the MEGA 5 software (Tamura *et al*., 2011). The Whelan and Goldman (WAG) model (Whelan and Goldman, 2001) was selected with a discrete Gamma distribution with 5 rate categories and by assuming that a certain fraction of sites are evolutionary invariable. An un-rooted maximum likelihood tree was constructed with MEGA 5 using Nearest-Neighbour-Interchange (NNI) with bootstrap support for individual nodes calculated on 500 replicates.

4.2.2. Cloning of BVMO homologues

4.2.2.1. Homologues 087, 653, 868 and 916

The genes coding for the homologues 087, 653, 868 and 916 contained multiple introns and were commercially synthesised by GenScript. The coding sequences (CDSs) were delineated by an *Nde*I recognition site (5') and an *Xho*I recognition site (3'). The CDSs were received in pUC57 (Fig. 3.3) as pUC57:087, pUC57:653, pUC57:868 and pUC57:916.

4.2.2.2. Homologues 338 and 791

The genes encoding the homologues 338 and 791 were PCR amplified from the genomic DNA of *A. flavus* NRRL3357 isolated in section 3.2.2, using the KOD Hot Start DNA Polymerase System (Novagen®). The PCR setup and cycling conditions were as described in section 3.2.3.1, using an extension time of 1 min. Primers were designed using the Integrated DNA Technologies OligoAnalyzer 3.1 online tool. Primer pair 9 (Table 4.1) and an annealing temperature of 63°C was

used to amplify *338*, while primer pair 10 (Table 4.1) and an annealing temperature of 60°C was used to amplify *791*. The PCR products were separated on an agarose gel and bands corresponding to the desired PCR products were excised and purified (section 3.2.3.6).

Table 4.1. Primer sequences used for PCR amplification of *338* and *791*.

Primer Set	Primer	Sequence	T_m (°C)	PCR Annealing Temperature (°C)
9	BVMO_AF_238497338_F_NdeI	5'-CAT ATG CAC CGT CGG AAT CGA CAT CCC TC-3'	63.6	63
	BVMO_AF_238497338_R_XhoI	5'-CTC GAG TCA CTG CTT CAG TGG TTC AGG TAG-3'	62.8	
10	BVMO_AF_238494791_F_NdeI	5'-CAT ATG GCT GCG GTT GAA GTA TCT GTT GTA TC-3'	60.3	60
	BVMO_AF_238494791_R_XhoI	5'-CTC GAG TCA AAC ATC CCA CCA ACC TTC CAT ATA-3'	62.4	

Underlined sequences indicate introduced restriction sites for *Nde*I and *Xho*I

The PCR products were phosphorylated and ligated into pSMART® as described in section 3.2.3.2 to yield pSMART®:338 and pSMART®:791. The resulting plasmids were proliferated and isolated (section 3.2.3.4). In order to verify whether the constructs contained the genes, the plasmids were double digested with *Nde*I and *Xho*I. All restriction enzymes and restriction enzyme buffers were purchased from Thermo Scientific. The reaction mixture consisted of 4 µl plasmid, 5 U *Nde*I, 10 U *Xho*I, 1 µl of 10X Buffer R adjusted to a final volume of 10 µl with deionised water. The mixtures were incubated at 37°C for 1 h and separated on an agarose gel. Positive clones were confirmed by DNA sequencing (section 3.2.3.6.2).

4.2.2.3. Intron removal

The genes *791* and *338* contained two introns each that were sequentially removed by inverse PCR as in section 3.2.3.5. The PCR reaction setup and cycling conditions were as described in section 3.2.3.1, using an elongation time of 4 min. Primer pair 11 (Table 4.2) and an annealing temperature of 60°C was used to remove the first intron from pSMART®:338*,* while primer pair 13 (Table 4.2) and an annealing temperature of 59°C was used to remove the first intron from pSMART®:791. The PCR products were digested with *DpnI* to remove the contaminating template DNA (section 3.2.3.5) and the desired PCR products purified (section 3.2.3.6).

Table 4.2. Primer sequences used for the inverse PCR to remove the introns from pSMART®:338 and pSMART®:791.

Primer Set	Primer	Sequence	T_m (°C)	PCR Annealing Temperature (°C)
11	BVMO_AF_338_INT1_F	5'-CCC ACA TAT ACG CCT TTC CCT TTG AC-3'	59.5	60
	BVMO_AF_338_INT1_R	5'-CTG CCA CGT CAC ATT GTA CTC CAG G-3'	60.8	
12	BVMO_AF_338_INT2_F	5'-TTC TTG AAA GGC AAA AAT AAC GAA GAG GC-3'	58.2	58
	BVMO_AF_338_INT2_R	5'-CAG TTT GTA AGC TTT GTT CGT CCG ATC-3'	58.2	
13	BVMO_AF_791_INT1_F	5'-GAG GCA CAT GGT ACG AAA ACA CAT ATC C-3'	59.4	59
	BVMO_AF_791_INT1_R	5'-CCA CAT CCG CAT TCT TAT CGA AGA TCC-3'	59.2	
14	BVMO_AF_791_INT2_F	5'-TAT GTG GAA CAT CTT GAC GTC CTG ATT AAT GC-3'	60.0	60
	BVMO_AF_791_INT2_R	5'-TAC CCT TCC TAT GCC GAT ATC CCG-3'	59.7	

The purified PCR products were circularised by a one-step phosphorylation and ligation reaction as described in section 3.2.3.5. The resulting plasmids were proliferated and isolated (section 3.2.3.4), and confirmed by DNA sequencing (section 3.2.3.6.1). Positive clones were used as template to remove the second intron. Primer pair 12 (Table 4.2) and an annealing temperature of 58°C was used to remove the second intron from pSMART®:338, while primer pair 14 and an annealing temperature of 60°C was used to remove the second intron from pSMART®:791. The PCR products were again digested with *DpnI*, purified and circularised. Positive clones were identified by plasmid isolation and DNA sequencing.

4.2.3. Constructs for expression in *E. coli*

4.2.3.1. Sub-cloning of CDSs from cloning vectors to pET-22b(+) and pET-28b(+)

The CDSs of *087, 338, 653, 791, 868* and *916* were excised from the cloning vectors by restriction enzyme double-digestion. All restriction enzymes and restriction enzyme buffers were purchased from Thermo Scientific. The reaction mixtures consisted of 8 µl plasmid, 5 U *Nde*I, 10 U *Xho*I, 2 µl of 10X Buffer R in a final volume of 20 µl, for all the constructs. The reaction mixtures were incubated

at 37°C for 1 h. However, pSMART®:791 was first incubated without addition of the *Nde*I for 1 h, after which the *Nde*I was added for 5 min and the mixture placed on ice for a partial digestion of the construct. pET-22b(+) and pET-28b(+) were digested similarly. The digestion mixtures were separated on an agarose gel and bands corresponding to the desired sizes were excised and purified as described previously.

Cohesive-end ligations were performed in a 1:1 molar ratio to ligate the excised CDSs into the digested pET-22b(+) and pET-28b(+) backbones, respectively. The ligation mixtures, comprising of 5 µl of the excised fragment, 3 µl of vector backbone, 5 Weiss U T4 DNA ligase and 1 µl of 10X T4 DNA ligase buffer, were incubated overnight at 16°C. The ligation mixtures were transformed into *E. coli* TOP10 cells and the plasmids isolated as previously described.

In order to verify whether successful clones contained the inserted fragment, restriction enzyme double-digestion was performed. For pET-22/28b(+):087/ 338/ 653/ 868/ 916 the reaction mixture comprised of 4 µl plasmid DNA, 5 U *Nde*I, 10 U *Xho*I and 1 µl of 10X Buffer R in a total volume of 10 µl. The reaction mixture for pET-22/28b(+):791 consisted of 4 µl plasmid DNA, 5 U *Hind*III, 5 U *Xho*I and 1 µl of 10X Buffer R, in a total volume of 10 µl. The mixtures were incubated at 37°C for 1 h and the products were separated on an agarose gel. Positive clones were sequenced to verify the presence of the insert.

4.2.3.2. Creation of C-terminally His-tagged variants

C-terminally His-tagged (CTH) variants were created from the pET-22b(+) constructs by inverse PCR as described in section 3.2.4.3. The PCR reaction setup and cycling conditions were as described in section 3.2.3.1, with an extension time of 4 min. The plasmid template, primer sets and annealing temperatures are listed in Table 4.3 and Table 4.4.

Table 4.3. Primer set and annealing temperatures for the creation of C-terminally His-tagged (CTH) BVMO variants by inverse PCR.

Template	Primer set	Annealing temperature (°C)	Variant created
pET-22b(+):087	15	61	pET-22b(+):087-CTH
pET-22b(+):338	16	61	pET-22b(+):338-CTH
pET-22b(+):653	17	60	pET-22b(+):653-CTH
pET-22b(+):791	18	59	pET-22b(+):791-CTH
pET-22b(+):868	19	56	pET-22b(+):868-CTH
pET-22b(+):916	20	63	pET-22b(+):916-CTH

Table 4.4. Primer sequences used for the creation of C-terminally His-tagged (CTH) BVMO variants by inverse PCR.

Primer Set	Primer	Sequence	T_m (°C)	PCR Annealing Temperature (°C)
15	BVMO_AF_238501087_CTHis_R	5'-ATT TAA ATA TTC TGG TGG TGG CAC CCA CGG-3'	60.9	61
	BVMO_AF_ALL_CTHis_F	5'-CAC CAC CAC CAC CAC CAC TGA GAT C-3'	63.1	
16	BVMO_AF_238497338_CTHis_R	5'-CTG CTT CAG TGG TTC AGG TAG CTC AAC-3'	61.0	61
	BVMO_AF_ALL_CTHis_F	5'-CAC CAC CAC CAC CAC CAC TGA GAT C-3'	63.1	
17	BVMO_AF_238501653_CTHis_R	5'-CCA AAG CCC TCC AAC AAA GTA GTA TGC G-3'	59.9	60
	BVMO_AF_ALL_CTHis_F	5'-CAC CAC CAC CAC CAC CAC TGA GAT C-3'	63.1	
18	BVMO_AF_238494791_CTHis_R	5'-AAC ATC CCA CCA ACC TTC CAT ATA CG-3'	58.6	59
	BVMO_AF_ALL_CTHis_F	5'-CAC CAC CAC CAC CAC CAC TGA GAT C-3'	63.1	
19	BVMO_AF_238481868_CTHis_R	5'-ATG AAC CAT GAA ATC TTC AAA ATC CTC ATC-3'	56.1	56
	BVMO_AF_ALL_CTHis_F	5'-CAC CAC CAC CAC CAC CAC TGA GAT C-3'	63.1	
20	BVMO_AF_238495916_CTHis_R	5'-ACC AGG CCA CAG AGC TGT CAC C-3'	63.8	63
	BVMO_AF_ALL_CTHis_F	5'-CAC CAC CAC CAC CAC CAC TGA GAT C-3'	63.1	

The template DNA was removed by *Dpn*I digestion (section 3.2.3.5), after which the PCR product was purified. The plasmids were circularised as described previously and positive clones were identified by DNA sequencing.

4.2.4. Heterologous expression of BVMO homologues

The created pET-22b(+) and pET-28b(+) constructs were transformed into *E. coli* BL21-Gold(DE3) (Agilent Technologies) as described in section 3.2.3.3. Also, the constructs were transformed into *E. coli* BL21(DE3) cells previously transformed with the pLysSRARE2 plasmid. The constructs were expressed in 100 ml ZYP5052 auto-induction media (Table A1, appendix) for 24 h at 25°C as described in section 3.2.5. The cells were harvested by centrifugation at 7 000 x*g* and 4°C for 10 min. One gram of cells (wet weight) was suspended in 10 ml of 50 mM Tris-HCl buffer (pH 8.0) containing DNase I (Roche) and cOmplete EDTA-free Protease Inhibitor (Roche) or Pierce™ EDTA-free Protease Inhibitor (Thermo Scientific). Cell disruption proceeded via French press as well as lysozyme-

treatment as described in section 3.2.7. Expression levels were visually analysed with SDS-PAGE (section 3.2.8.1) and the activity of the expressed BVMOs were assayed as in section 3.2.8.2.

4.2.5. Co-expression of BVMO homologues with molecular chaperones

The pET-28b(+):087, pET-28b(+):338, pET-28b(+):653, pET-28b(+):791, pET-28b(+):868 and pET-28b(+):916 constructs were transformed into *E. coli* BL21(DE3) strains previously transformed with the pGro7 chaperone plasmid (Takara Bio Inc.). The constructs were co-expressed with the pGro7 chaperone plasmid, described in section 3.2.6. The expression levels were analysed with SDS-PAGE and the activity of the expressed BVMOs assayed (section 3.2.8).

4.2.6. Purification of 338, 653 and 791

The 338, 653 and 791 proteins were over-produced by co-expression of the pET-28b(+):338, pET-28b(+):653 or pET-28b(+):791 constructs with the pGro7 chaperone plasmid to yield soluble proteins with N-terminal His-tags. *E. coli* BL21-Gold(DE3) was used to express the constructs in 1 L (10 x 100 ml) of ZYP5052 auto-induction media in 500 ml Erlenmeyer flasks. The cultures were incubated at 20°C and 200 rpm for 36 h, after which it was harvested by centrifugation at 7 000 x*g* for 10 min (4°C).

The cells were disrupted using lysozyme digestion followed by a freeze-thaw cycle (section 3.2.7) and ultracentrifuged as described in section 3.2.9.1. As a first purification step, immobilised metal-affinity chromatography (IMAC) was employed, as described in section 3.2.9.2. The pooled fractions obtained from the His-trap column were incubated with an excess of FAD, overnight at 4°C, and concentrated to a total volume of 2 ml with an Amicon® Ultra-15 centrifugal filter device (section 3.2.9.3).

Size-exclusion chromatography served as a second purification step, using PD-10 desalting columns (GE Healthcare). The gravity protocol was used to purify the concentrated fractions with a 20 mM Tris-HCl (pH 8.5) buffer, according to the manufacturer's instructions. The purity of the fractions was evaluated using SDS-PAGE after each purification step.

4.2.7. Characterisation of 338, 653 and 791

4.2.7.1. Substrate scope

The substrate scope of 338, 653 and 791 was investigated by whole-cell biotransformations, as described in section 3.2.10.7. Substrates and products were analysed using GC-MS with a FactorFour™ VF-5ms column (60 m x 0.25 mm x 0.25 µm, Varian). GC programs are given in Table A3 (appendix). Chiral analysis of the conversion of (±)-*cis*-bicyclo[3.2.0]hept-2-en-6-one was performed using GC coupled to a flame ionisation detector (GC-FID) with an Astec CHIRALDEX™ G-TA column (30 m x 0.25 mm x 0.12 µm, Sigma Aldrich). The GC program is given in Table A4 (appendix).

The observed activity towards selected substrates was verified using purified 338 and 791. The oxidation of NADPH in the presence of substrate was continuously monitored spectrophotometrically at 340 nm over 10 min with a Cary 300 Bio UV-Visible spectrophotometer (Varian). The reaction mixture contained 1 mM substrate, 0.3 mM NADPH and 0.2 mg purified protein in 200 mM Tris-HCl (pH 8.5) with a total volume of 1 ml. The reactions were performed at 25°C with temperature-equilibrated buffer. An extinction coefficient of 6.22 $mM.cm^{-1}$ was used for NADPH at 340 nm (Jablonski and DeLuca, 1977) to calculate the reaction rates. A blank rate due to the uncoupling of NADPH oxidation and enzyme activity, which results in the unproductive decay of the peroxyflavin species, was measured by incubating the reaction mixture without substrate and used to correct the observed rates.

4.2.7.2. Reaction with hydroxyversicolorone

The reaction of 338, 653 and 791 with hydroxyversicolorone (HVN) was investigated by incubating [1'-^{2}H]HVN with 0.2 mg purified protein and 0.3 mM NADPH at 25°C in 200 mM Tris-HCl buffer (pH 8.5), with a total volume of 1 ml. The oxidation of NADPH in the presence of [1'-^{2}H]HVN was continuously monitored spectrophotometrically at 340 nm over 20 min with a Cary 300 Bio UV-Visible spectrophotometer (Varian). The reaction was incubated for a further 100 min at 25°C. One millilitre of ethyl acetate was used to extract the substrates and products. The organic and aqueous phase was separated by centrifugation at 20 000 x*g* for 15 min. The organic phase was aspirated and concentrated under vacuum in a SpeedVac concentrator to approximately 50 µl. The mixture was spotted onto Silica 60 TLC (Merck) plates aside [1'-^{2}H]HVN and developed using a chloroform:methanol mobile phase of 95:5. The TLC plates were visualised and photographed under white light.

4.3. Results

4.3.1. Cloning of BVMO homologues

4.3.1.1. Identification of BVMO homologues

Genome mining identified 25 putative BVMO genes in addition to *moxY*. Phylogenetic analysis was performed with numerous BVMOs, using the sequences of cyclopentanone monooxygenase from *Comamonas* sp. NCIMB9872 ($CPMO_{comamo}$); methyl ketone monooxygenase from *Pseudomonas veronii* MEK700 (MKM_{pseudo}); acetone monooxygenase from *Gordonia* sp. TY-5 ($ACMO_{gordon}$); cyclohexanone monooxygenase from *Acinetobacter* sp. NCIMB9871 ($CHMO_{acinet}$); cyclohexanone monooxygenase from *Rhodococcus* sp. HI-31 ($CHMO_{rhodoc}$); phenylacetone monooxygenase from *Thermobifida fusca* YX ($PAMO_{thermo}$); steroid monooxygenase from *Rhodococcus rhodochrous* ($SMO_{rhodoco}$); cyclododecanone monooxygenase from *Rhodococcus ruber* SC1 ($CDMO_{rhodoc}$); cyclopentadecanone monooxygenase from *Pseudomonas* sp. HI-70 ($CPDMO_{pseudo}$); 4-hydroxyacetophenone monooxygenase from *Pseudomonas fluorescens* ACB ($HAPMO_{pseudo}$); aliphatic ketone monooxygenase from *Pseudomonas fluorescens* DSM50106 ($AKMO_{pseudo}$); BVMO from *Pseudomonas putida* KT2440 ($BVMO_{pseudo}$); BVMO from *Mycobacterium tuberculosis* ($EtaA_{mycoba}$) and BVMOs from *Rhodococcus jostii* RHA1 (MO1-MO24).

MoxY is not closely related to the well-characterised BVMOs and clusters on a separate branch with six homologues (Fig. 4.1). The six closely-related homologues, 087, 338, 653, 791, 868 and 916, were identified as prime candidates for possible intragenomic complementation of MoxY and were selected for heterologous expression in *E. coli.*

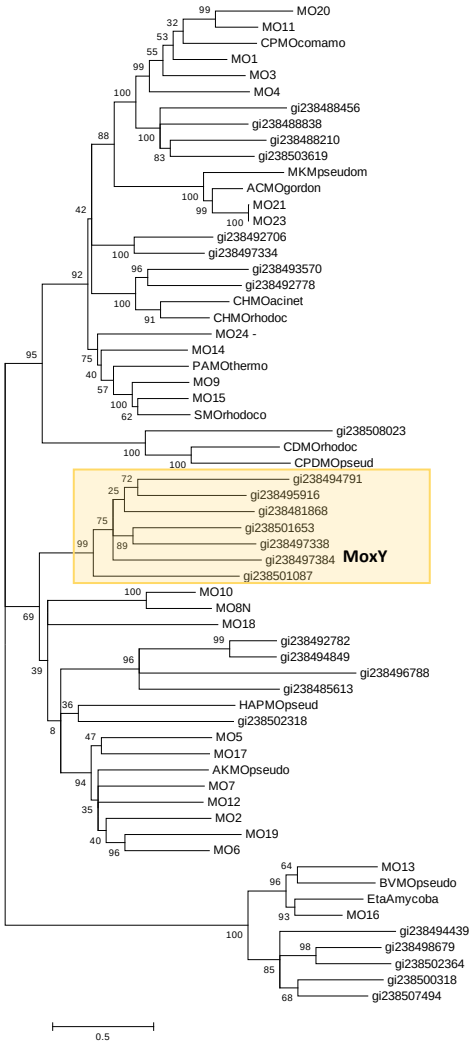

Figure 4.1. Phylogenetic analysis of the putative *Aspergillus flavus* BVMOs with previously cloned and characterised BVMOs. Relationships are shown as an un-rooted maximum likelihood tree (Wheland and Gold model) inferred using Nearest-Neighbour-Interchange with bootstrap support (500 replicates) for individual nodes. Sequences used for comparison are $CPMO_{comamo}$: cyclopentanone monooxygenase from *Comamonas* sp. NCIMB9872; MKM_{pseudo}: methyl ketone monooxygenase from *Pseudomonas veronii* MEK700; $ACMO_{gordon}$: acetone monooxygenase from *Gordonia sp*. TY-5; $CHMO_{acinet}$: cyclohexanone monooxygenase from *Acinetobacter sp.* NCIMB9871; $CHMO_{rhodoc}$: cyclohexanone monooxygenase from *Rhodococcus sp.* HI-31; $PAMO_{thermo}$: phenylacetone monooxygenase from *Thermobifida fusca* YX; $SMO_{rhodoco}$: steroid monooxygenase from *Rhodococcus rhodochrous*; $CDMO_{rhodoc}$: cyclododecanone monooxygenase from *Rhodococcus ruber* SC1; $CPDMO_{pseudo}$: cyclopentadecanone monooxygenase from *Pseudomonas* sp. HI-70; $HAPMO_{pseudo}$: 4-hydroxyacetophenone monooxygenase from *Pseudomonas fluorescens* ACB; $AKMO_{pseudo}$: aliphatic ketone monooxygenase from *Pseudomonas fluorescens* DSM50106; $BVMO_{pseudo}$: BVMO from *Pseudomonas putida* KT2440; $EtaA_{mycoba}$: BVMO from *Mycobacterium tuberculosis*; MO1-MO24: BVMOs from *Rhodococcus jostii* RHA1; gi|: BVMOs from *Aspergillus flavus* NRRL3357. MoxY and the six closely-related homologues are indicated in yellow, with MoxY referred to as gi|238497384.

The genes *087, 653, 868* and *916* contained multiple introns (5 or more). Removal of the introns by inverse PCR would not only be time-consuming, but would also require numerous primer pairs. In addition, the likelihood of introducing point mutations during multiple consecutive rounds of PCR, is markedly higher. Therefore, the genes were commercially synthesised by GenScript. Alignments of the synthesised coding regions and the genes are displayed in Fig. 4.2, showing the multiple introns. The 338 and 791 genes each contained only two predicted introns and were thus deemed suitable for cloning from gDNA.

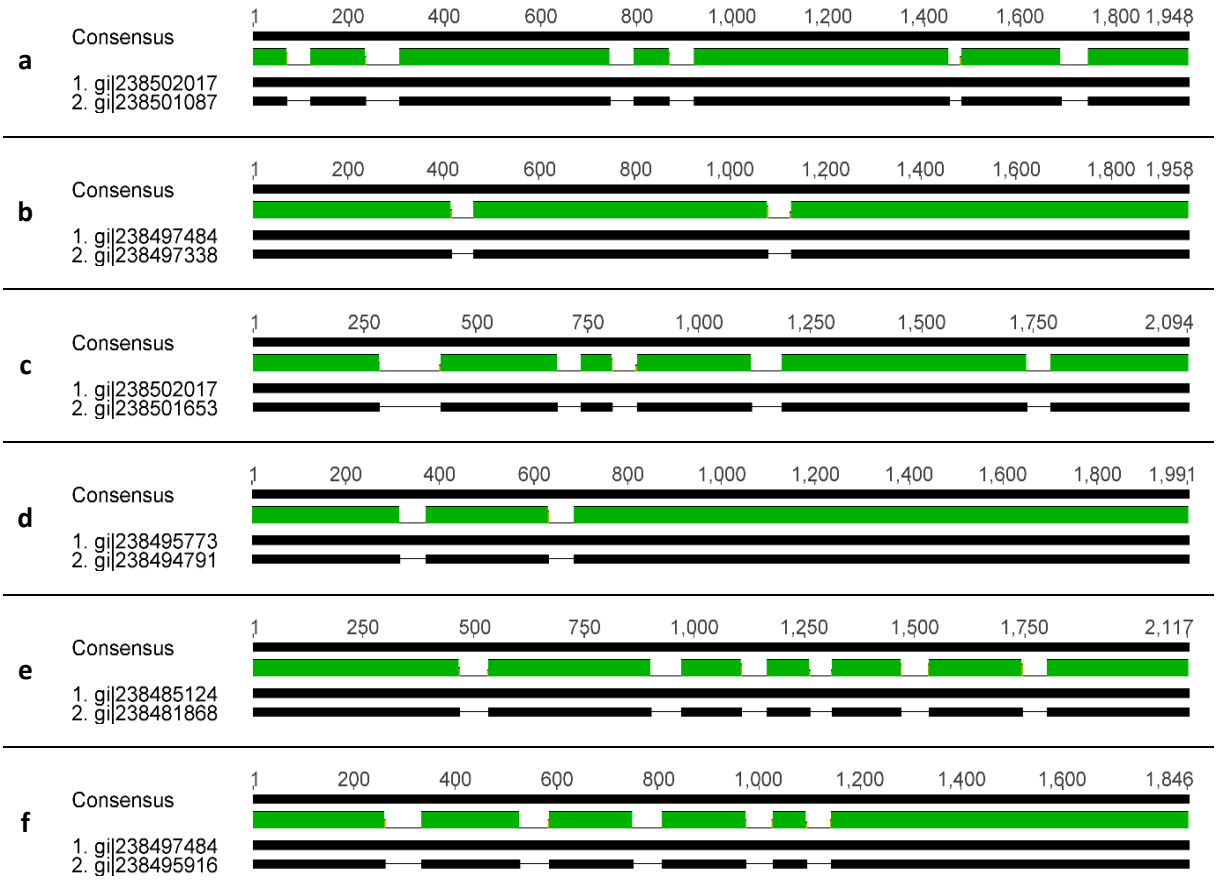

Figure 4.2. Pairwise sequence alignments of the *Aspergillus flavus* genomic DNA (1) and the BVMO homologue mRNA (2), generated using Geneious® v. 6.0.3. The accession numbers of the genomic DNA and mRNA are given in each case. **a,** *087* which contains six introns; **b,** *338* which contains two introns; **c,** *653* which contains five introns; **d,** *791* which contains two introns; **e,** *868* which contains six introns and **f,** *916* which contains five introns. Sequences that contain five or more introns were commercially synthesised for expression by GenScript, while the introns were removed by cloning for *338* and *791.*

4.3.1.2. PCR amplification of 338 and 791

The *338* and *791* genes were successfully amplified from the genomic DNA of *A. flavus* using the KOD Hot Start DNA Polymerase system. The primers used to amplify the genes were designed to introduce restriction enzyme recognition sites for *Nde*I (5') and *Xho*I (3') to the genes for downstream directional cloning into the expression vectors. Agarose gel electrophoreses indicated two clear bands of ~ 2 000 bp (Fig. 4.3), corresponding to the expected amplicons of 1 967 bp for *338* and 2 000 bp for *791.*

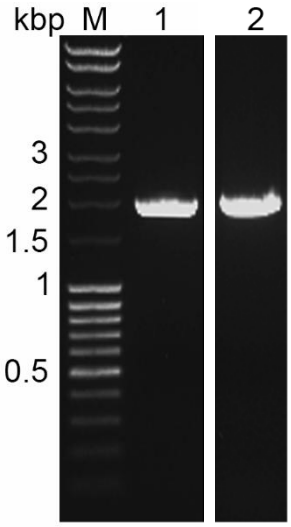

Figure 4.3. Agarose gel electrophoresis of the PCR-amplification of the *338* (lane 1) and *791* (lane 2) genes from the genomic DNA of *Aspergillus flavus*. M, MassRuler™ DNA ladder.

4.3.1.3. Construction of pSMART®:338 and pSMART®:791

The purified *338* and *791* amplicons were blunt-end ligated into the pSMART® cloning vector. Positive clones were double-digested with *Nde*I and *Xho*I to verify that the constructs contained the inserted genes. Agarose gel electrophoresis indicated the presence of three bands of approximately 2 000, 1 500 and 200 bp for the digested pSMART®:338, corresponding to the *338* gene and two fragments of the vector backbone (Fig. 4.4). Four bands of approximately 1 500, 1 300, 500 and 200 bp were observed for the digestion of pSMART®:791, due to the presence of an internal *Nde*I restriction site in the *791* CDS.

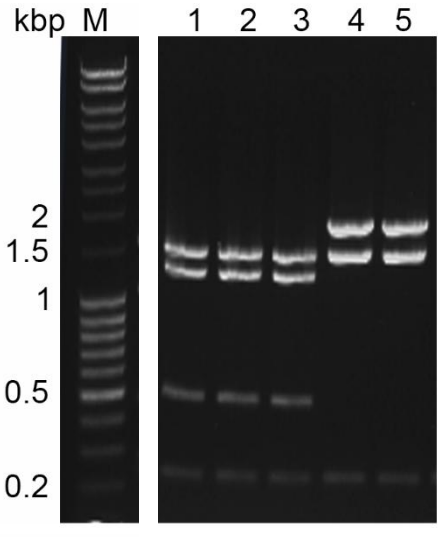

Figure 4.4. Agarose gel electrophoresis of the restriction enzyme double-digestion of pSMART®:338 and pSMART®:791 to verify whether the constructs contained the inserted genes. Lanes 1 – 3, positive clones for pSMART®:791; lanes 4 and 5, positive clones for pSMART®:338. M, MassRuler™ DNA ladder.

4.3.1.4. Intron removal

Intron removal from pSMART®:338 and pSMART®:791 was performed consecutively by using inverse PCR. The removal of the first intron yielded two PCR products of 3 708 and 3 732 bp, respectively, for pSMART®:338 and pSMART®:791. The expected products were represented by clear bands of ~ 3 700 bp (Fig. 4.5a). The success of the intron removal step was verified by DNA sequencing. Constructs from which the intron was successfully removed, were used as template for removal of the second intron. Agarose gel electrophoresis indicated two clear bands of ~ 3 600 bp (Fig. 4.5b), corresponding to the expected PCR products of 3 660 bp for pSMART®:338 and 3 678 bp for pSMART®:791. The plasmids were sequenced to confirm the removal of the introns and to verify that no point or frame-shift mutations were introduced during the PCR and ligation steps.

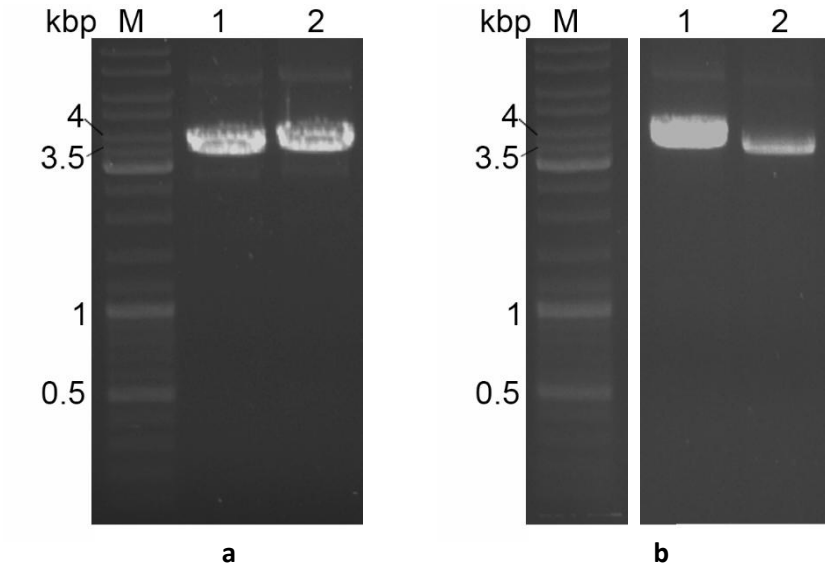

Figure 4.5. Agarose gel electrophoresis of the inverse PCR to sequentially remove the introns from pSMART®:338 (lane 1) and pSMART®:791 (lane 2). **a,** Removal of the first intron and **b,** removal of the second intron. M, GeneRuler™ DNA ladder.

4.3.1.5. Sub-cloning of CDSs to the pET expression vectors

The coding regions were excised from the cloning vectors pSMART® and pUC57 by means of restriction enzyme double digestion. The combination of restriction enzymes, *Nde*I (5') and *Xho*I (3'), corresponded to the sites introduced during PCR amplification of the genes from the genomic DNA, as well as the restriction enzymes introduced during synthesis of the genes by GenScript. Due to the presence of an internal *Nde*I recognition site in *791*, the pSMART®:791 was first fully digested with *Xho*I, after which a partial digestion with *Nde*I was performed. The expression vectors, pET-22b(+) and pET-28b(+), were similarly digested. The restriction enzyme digestion mixtures were separated on an agarose gel. Bands corresponding to the coding regions were excised and gel-purified: 1 653 bp for *087*; 1 869 bp for *338*; 1 734 bp for *653*; 1 887 bp for *791*; 1 764 bp for *868*; 1 566 bp for *916*; as well as the backbones of pET-22b(+) and pET-28b(+).

The isolated coding regions were ligated into the pET-22b(+) and pET-28b(+) vector backbones, respectively. In order to verify whether the ligation was successful, the pET-22b(+) and pET-28b(+) constructs of *087, 338, 653, 868* and *916* were each double-digested with *Nde*I and *Xho*I. The pET-22b(+) and pET-28b(+) vectors containing *791* were double-digested with *Hind*III and *Xho*I, due to the presence of the internal *Nde*I cutting site. Agarose gel electrophoresis indicated two clear bands of approximately 5 500 and 1 800 bp for all of the constructs (Fig. 4.6), corresponding to the inserted coding regions and vector backbones. The plasmids were submitted for DNA sequencing to verify that the ligation steps proceeded without error and that no frame-shift mutations were introduced during the ligation procedure.

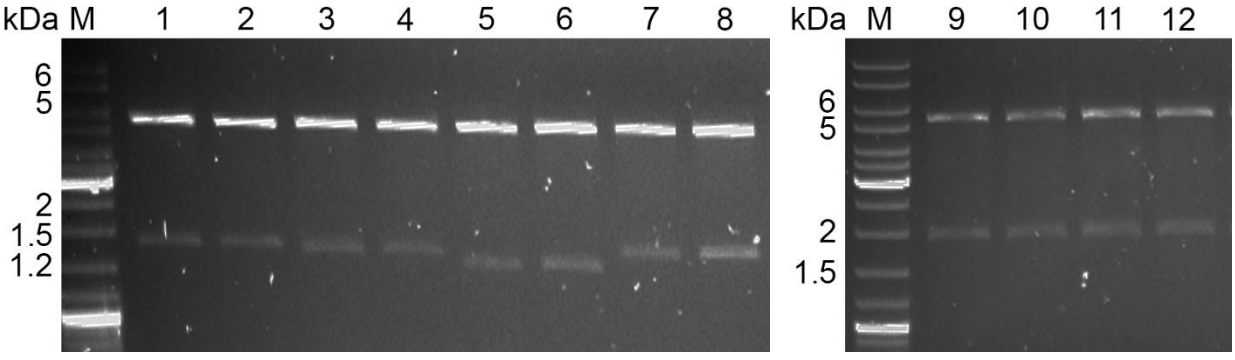

Figure 4.6. Agarose gel electrophoresis of the *Nde*I *Xho*I or *Hind*III *Xho*I double-digested expression vectors to confirm the presence of the BVMO coding regions. Lane 1, pET-22b(+):868; lane 2, pET-28b(+):868; lane 3, pET-22b(+):087; lane 4, pET-28b(+):087; lane 5, pET-22b(+):916; lane 6, pET-28b(+):916; lane 7, pET-22b(+):653; lane 8, pET-28b(+):653; lane 9, pET-22b(+):338; lane 10, pET-28b(+):338; lane 11, pET-22b(+):791; lane 12 pET-28b(+):791. M, GeneRuler™ DNA ladder.

4.3.1.6. Creation of C-terminally His-tagged variants

C-terminally His-tagged (CTH) variants were created from the pET-22b(+):BVMO constructs by deletion of the native stop codon of the genes by using inverse PCR. The resulting pET-22b(+):BVMO-CTH constructs coded for BVMO proteins fused to a C-terminal His-tag. Agarose gel electrophoresis indicated that the inverse PCRs were successful as bands of ~ 7 000 bp were observed (Fig. 4.7). Successful clones were submitted for DNA sequencing to verify that no point or frame-shift mutations were introduced during the PCR and ligation steps.

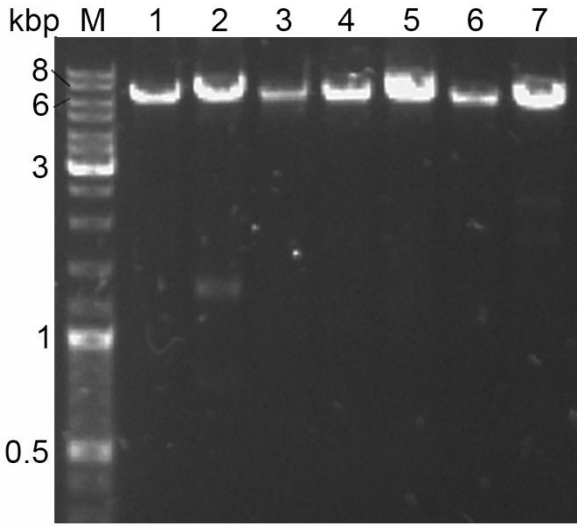

Figure 4.7. Agarose gel electrophoresis of the inverse PCR to create C-terminally His-tagged variants of the BVMO homologues in pET-22b(+). M, Generuler™ DNA ladder; lane 1, pET-22b(+):moxY; lane 2, pET-22b(+):338; lane 3, pET-22b(+):087; lane 4, pET-22b(+):653; lane 5, pET-22b(+):791; lane 6, pET-22b(+):868; lane 7, pET-22b(+):916.

4.3.2. Heterologous expression of BVMO homologues

4.3.2.1. Homologue 087

Expression was observed in the total protein fraction for the pET-22b(+):087, pET-22b(+):087-CTH and the pET-28b(+):087 constructs, as well as with the pLysSRARE2 counterparts (Fig. 4.8). However, expression was markedly decreased when the protein was co-expressed with pLysSRARE2. The lack of expression may be due to the metabolic burden associated with the presence of the pLysSRARE2 plasmid as transcription of the tRNA genes can limit the availability of mRNA for the transcription of the BVMO gene. Also, the tRNA population may be altered to such an extent that the requirement for non-rare tRNA molecules cannot be fulfilled. No recombinant protein was observed in the soluble fraction, therefore, 087 only expressed as an insoluble protein located in inclusion bodies.

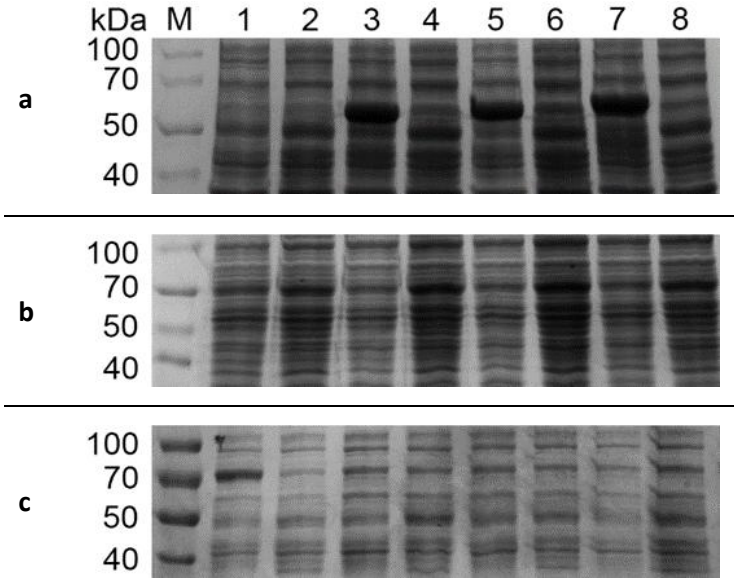

Figure 4.8. SDS-PAGE analysis of the expression of 087. **a,** Total protein fraction, **b,** soluble fraction obtained from the French press and **c,** soluble fraction obtained from the lysozyme-treated cells. M, Spectra™ Multicolor Broad Range Protein ladder; lane 1, pET-22b(+) empty vector control; lane 2, pET-22b(+) empty vector control + pLysSRARE2; lane 3, pET-22b(+):087; lane 4, pET-22b(+):087 + pLysSRARE2; lane 5, pET-22b(+):087-CTH; lane 6, pET-22b(+):087-CTH + pLysSRARE2; lane 7, pET-28b(+):087; lane 8, pET-28b(+):087 + pLysSRARE2.

4.3.2.2. Homologue 338

Soluble expression was observed for 338 in all of the constructs, as well as the pLysSRARE2 counterparts (Fig. 4.9). The recovery of soluble protein was higher in the French-pressed cells when compared to the lysozyme-treated cells.

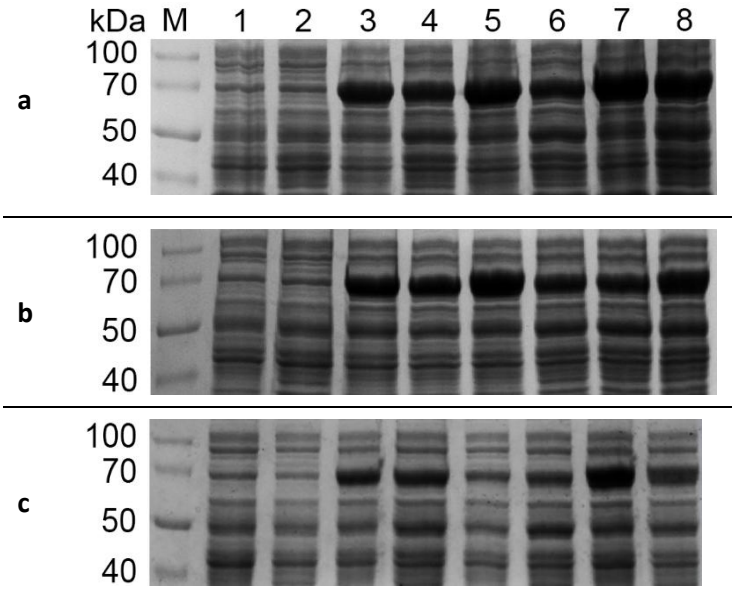

Figure 4.9. SDS-PAGE analysis of the expression of 338. **a,** Total protein fraction, **b,** soluble fraction obtained from the French press and **c,** soluble fraction obtained from the lysozyme-treated cells. M, Spectra™ Multicolor Broad Range Protein ladder; lane 1, pET-28b(+) empty vector control; lane 2, pET-28b(+) empty vector control + pLysSRARE2; lane 3, pET-22b(+):338; lane 4, pET-22b(+):338 + pLysSRARE2; lane 5, pET-22b(+):338-CTH; lane 6, pET-22b(+):338-CTH + pLysSRARE2; lane 7, pET-28b(+):338; lane 8, pET-28b(+):338 + pLysSRARE2.

4.3.2.3. Homologue 653

Similar to 338, soluble expression was observed for 653 in all of the constructs, as well as the pLysSRARE2 counterparts (Fig. 4.10). Levels of soluble protein recovered from the French-pressed and lysozyme-treated cells did not differ notably.

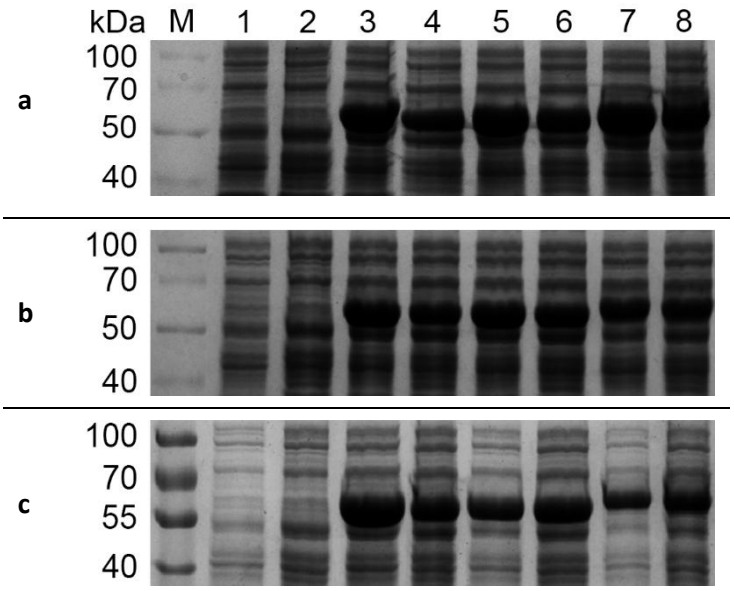

Figure 4.10. SDS-PAGE analysis of the expression of 653. **a,** Total protein fraction, **b,** soluble fraction obtained from the French press and **c,** soluble fraction obtained from the lysozyme-treated cells. M, PageRuler™ Prestained protein ladder; lane 1, pET-22b(+) empty vector control; lane 2, pET-22b(+) empty vector control + pLysSRARE2; lane 3, pET-22b(+):653; lane 4, pET-22b(+):653 + pLysSRARE2; lane 5, pET-22b(+):653-CTH; lane 6, pET-22b(+):653-CTH + pLysSRARE2; lane 7, pET-28b(+):653; lane 8, pET-28b(+):653 + pLysSRARE2.

4.3.2.4. Homologue 791

Expression was observed in the total protein fraction for pET-22b(+):791, pET-28b(+):791 and pET-22b(+):791-CTH (Fig. 4.11). Expression was also observed for pET-22b(+):791 co-expressed with pLysSRARE2, however, at much lower levels, which may once again be due to the metabolic burden associated with the additional pLysSRARE2 plasmid. Soluble expression was observed for pET-22b(+):791 in the fractions obtained from lysozyme-treatment. The presence of a native *E. coli* protein of approximately the same size as 791 complicated the identification of low levels of expressed 791. It is possible that soluble 791 was also present in the pET-22b(+):791, as well as the pLysSRARE2 counterpart fractions obtained from the French press. However, no soluble expression for the pET-22b(+):791 with the pLysSRARE2 counterpart was observed in the fractions obtained by lysozyme treatment. The presence of smaller bands in the soluble fraction may indicate the presence of partially degraded protein.

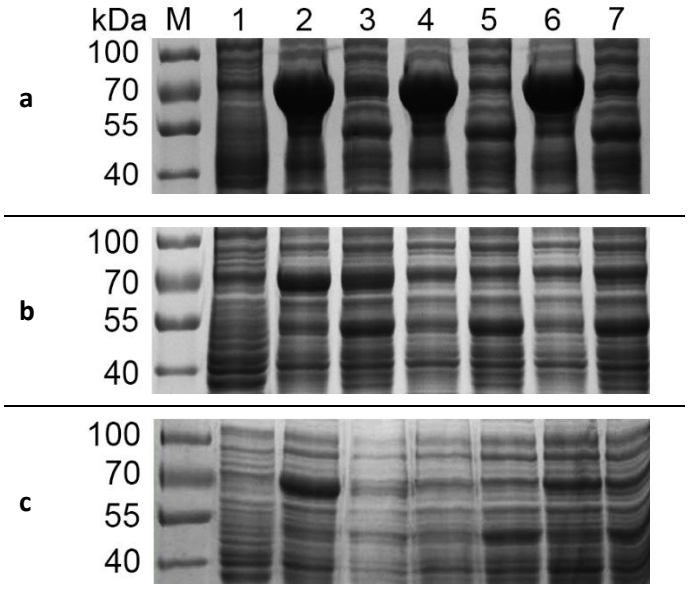

Figure 4.11. SDS-PAGE analysis of the expression of 791. **a,** Total protein fraction, **b,** soluble fraction obtained from the French press and **c,** soluble fraction obtained from the lysozyme-treated cells. M, PageRuler™ Prestained protein ladder; lane 1, pET-22b(+) empty vector control; lane 2, pET-22b(+):791; lane 3, pET-22b(+):791 + pLysSRARE2; lane 4, pET-22b(+):791-CTH; lane 5, pET-22b(+):791-CTH + pLysSRARE2; lane 6, pET-28b(+):791; lane 7, pET-28b(+):791 + pLysSRARE2.

4.3.2.5. Homologue 868

Expression was observed in the total protein fraction for pET-22b(+):868, pET-28b(+):868 and the pLysSRARE2 counterpart, as well as for pET-22b(+):868-CTH and the pLysSRARE2 counterpart (Fig. 4.12). As in the case of 087, no soluble expression was observed, therefore, the 868 was only expressed as an insoluble protein. This indicated that the expressed 868 was probably misfolded and located in inclusion bodies in the insoluble fraction.

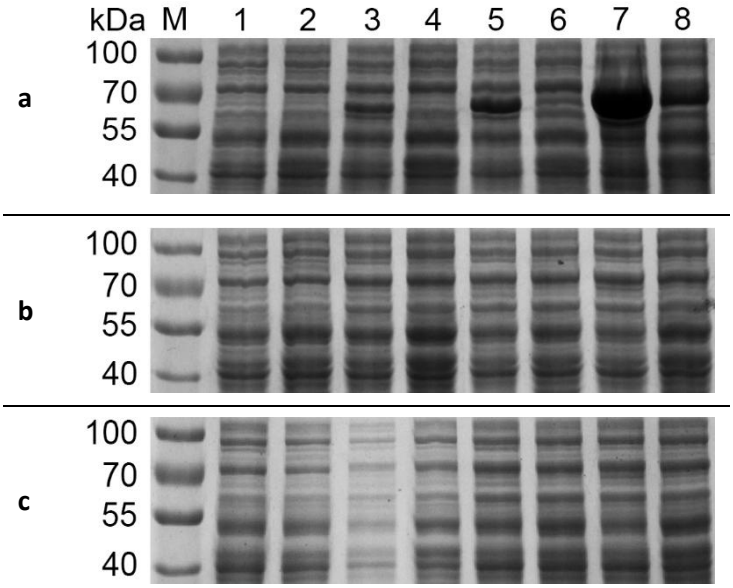

Figure 4.12. SDS-PAGE analysis of the expression of 868. **a,** Total protein fraction, **b,** soluble fraction obtained from the French press and **c,** soluble fraction obtained from the lysozyme-treated cells. M, PageRuler™ Prestained protein ladder; lane 1, pET-22b(+) empty vector control; lane 2, pET-22b(+) empty vector control + pLysSRARE2; lane 3, pET-22b(+):868; lane 4, pET-22b(+):868 + pLysSRARE2; lane 5, pET-22b(+):868-CTH; lane 6, pET-22b(+):868-CTH + pLysSRARE2; lane 7, pET-28b(+):868; lane 8, pET-28b(+):868 + pLysSRARE2.

4.3.2.6. Homologue 916

Expression was observed in the total protein fraction for all of the constructs, except in the case of co-expression of pET-28b(+):916 with pLysSRARE2 (Fig. 4.13). Unfortunately, similar to 087 and 868, no soluble expression was observed for any of the constructs, therefore, 916 only expressed as an insoluble protein.

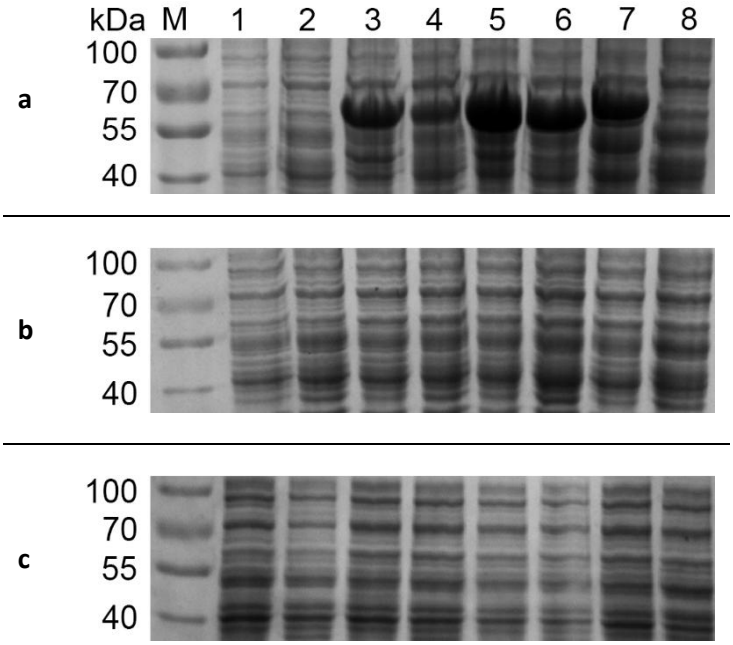

Figure 4.13. SDS-PAGE analysis of the expression of 916. **a,** Total protein fraction, **b,** soluble fraction obtained from the French press and **c,** soluble fraction obtained from the lysozyme-treated cells. M, PageRuler™ Prestained protein ladder; lane 1, pET-28b(+) empty vector control; lane 2, pET-28b(+) empty vector control + pLysSRARE2; lane 3, pET-22b(+):916; lane 4, pET-22b(+):916 + pLysSRARE2; lane 5, pET-22b(+):916-CTH; lane 6, pET-22b(+):916-CTH + pLysSRARE2; lane 7, pET-28b(+):916; lane 8, pET-28b(+):916 + pLysSRARE2.

4.3.2.7. Co-expression with molecular chaperones

The homologues 338 and 653 expressed as soluble proteins from all the expression constructs. Although soluble expression was obtained from the pET-22b(+):791 construct, the construct allows expression of the native protein which is not suitable for purification by IMAC. Although the 087, 868 and 916 homologues did not express as soluble proteins from any of the constructs, expression was observed in the total protein fraction from the pET-28b(+) vector. In an attempt to improve the solubility of the BVMO homologues, all the homologues in the pET-28b(+) vector were co-expressed with pGro7. The pET-28b(+) vector was selected as it allows expression of the protein with an N-terminal His-tag which renders the proteins suitable for downstream purification via IMAC. The pGro7 plasmid was chosen due to the improvement in soluble expression levels and activity observed with MoxYAltN (section 3.3.4).

Co-expression of the homologues with pGro7 improved the expression levels of soluble protein for 338, 653 and 791 (Fig. 4.14). Small amounts of soluble protein was detected for 868 as well. However, no soluble expression was observed for 087 or 916 still. Notably, co-expression of pET-28b(+):791 with the molecular chaperone improved the solubility of the protein strikingly, as no soluble protein was observed in the absence of the molecular chaperone (Fig. 4.11).

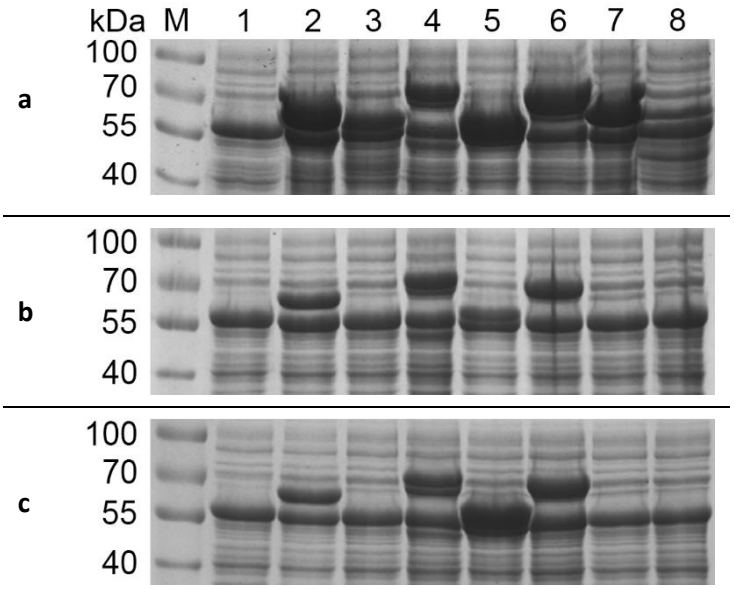

Figure 4.14. SDS-PAGE analysis of the co-expression of the BVMOs in pET-28b(+) with the pGro7 chaperone plasmid. **a,** Total protein fraction, **b,** soluble fraction obtained from the French press and **c,** soluble fraction obtained from the lysozyme-treated cells. M, PageRuler™ Prestained protein ladder; lane 1, pET-22b(+) empty vector control + pGro7; lane 2, pET-28b(+):moxYAltN + pGro7; lane 3, pET-28b(+):087 + pGro7; lane 4, pET-28b(+):338 + pGro7; lane 5, pET-28b(+):653 + pGro7; lane 6, pET-28b(+):791 + pGro7; lane 7, pET-28b(+):868 + pGro7; lane 8, pET-28b(+):916 + pGro7.

4.3.3. Characterisation of 338, 653 and 791

Similar to the assays performed with the MoxY variants, spectrophotometric assays with crude cell-extracts of the homologues were inconclusive. Therefore, whole-cell biotransformations were performed to investigate the activity and substrate scope of the homologues that expressed as soluble proteins at high levels - 338, 653 and 791. An extensive range of ketone substrates were evaluated, as depicted in Fig. A4 (appendix). Activity was observed with 338 and 791 for a number of ketone substrates, as listed in Table 4.5, but no activity was observed with 653.

Table 4.5. Ketone substrates converted by 338 and 791 during whole-cell biotransformations. The percentage conversion of 10 mM substrate is given after 2 hours, as well as the standard deviation.

	338	**791**
Substrate	**Conversion (%)**	**Conversion (%)**
phenylacetone	11.9 ± 0.2	
2-phenylcyclohexanone	7.5 ± 1.0	
thioanisole	5.1 ± 0.1	5.9 ± 3.2
(±)-*cis*-bicyclo[3.2.0]hept-2-en-6-one	23.2 ± 4.1	92.8 ± 3.0

Thioanisole is oxidised by BVMOs to the sulfoxide, as well as the sulfone, as illustrated in Fig. 4.15 (Mascotti *et al.*, 2013). Thioanisole is converted by 338 to only the sulfoxide, while the substrate is converted to both the sulfoxide and the sulfone by 791, in a 4:5 ratio.

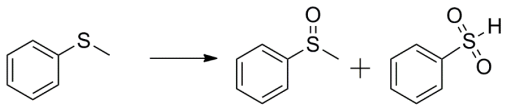

Figure 4.15. Conversion of thioanisole to the corresponding sulfoxide and sulfone by BVMOs (Mascotti *et al.*, 2013).

The oxidation of racemic (±)-*cis*-bicyclo[3.2.0]hept-2-en-6-one (Fig. 4.16) is considered one of the benchmark reactions of BVMOs and is used to evaluate the regio- and enantioselectivity of the catalysts. The racemic compound is transformed into two regio-isomeric compounds, the 'normal' product 2-oxabicyclo[3.3.0]oct-6-en-3-one, which is due to the migration of the more substituted carbon atom, and the 'abnormal' product 3-oxabicyclo[3.3.0]oct-6-en-2-one, which is due to the migration of the less substituted carbon atom (Renz and Meunier, 1999).

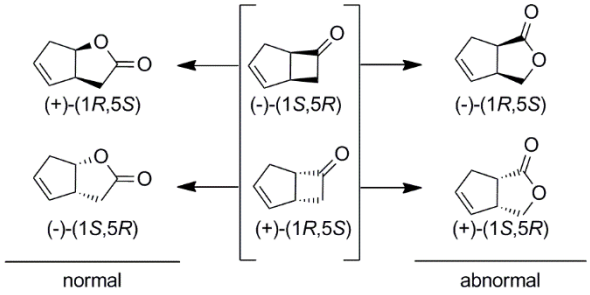

Figure 4.16. Conversion of racemic (±)-*cis*-bicyclo[3.2.0]hept-2-en-6-one by BVMOs. The 'normal' lactone (2-oxabicyclo[3.3.0]oct-6-en-3-one) is produced by migration of the more substituted group while the 'abnormal' product (3-oxabicyclo[3.3.0]oct-6-en- 2-one) is produced by migration of the less substituted group.

In order to evaluate the selectivity of the expressed BVMOs, chiral GC analysis was used to determine which regio- and stereoisomers were produced from (±)-*cis*-bicyclo[3.2.0]hept-2-en-6-one by 338, 791, as well as MoxYAltN, during whole-cell biocatalysis. The regio- and enantiomers are listed in Table 4.6.

Table 4.6. Regio and stereoisomers produced from racemic (±)-*cis*-bicyclo[3.2.0]hept-2-en-6-one by 791 and MoxYAltN during whole-cell biotransformations. The enantiomeric excess for both regio-isomers are indicated (*ee*).

	Normal			**Abnormal**		
	(+)-(1*R*, 5*S*) (%)	(-)-(1*S*, 5*R*) (%)	*ee*	(-)-(1*R*, 5*S*) (%)	(+)-(1*S*, 5*R*) (%)	*ee*
338	1	13	86 %	86		> 99 %
791		47	> 99 %	53		> 99 %
MoxYAltN	1	16	88 %	65	18	57 %

4.3.4. Purification of 338, 653 and 791

In order to determine whether the homologues can complement the function by converting HVN, purification of the proteins were required. Since 338, 653 and 791 expressed very well as soluble proteins from the pET-28b(+) vector, co-expressed with the pGro7 chaperone plasmid, it was decided to purify the three homologues using IMAC and SEC.

4.3.4.1. Purification of 338 by immobilised metal-affinity chromatography

Recombinant expression of the pET-28b(+):338 vector yielded the 338 protein with an N-terminal His-tag. The size of the N-terminally His-tagged 338 was predicted as 72 kDa, using the coding region of the pET-28b(+):338 vector with the ProtParam tool from the ExPASy server. SDS-PAGE confirmed the monomeric molecular weight (Fig. 4.17a). Figure 4.17b depicts an elution profile of 338 from a HisTrap FF column. The N-terminally His-tagged 338 eluted in the volume of 130 – 198 ml and fractions eluting in the volume of 140 – 190 ml were selectively pooled (Fig. 4.17b). The fractions had a yellow colour, characteristic of FAD-binding proteins, indicating that the 338 factor retained the flavin co-factor.

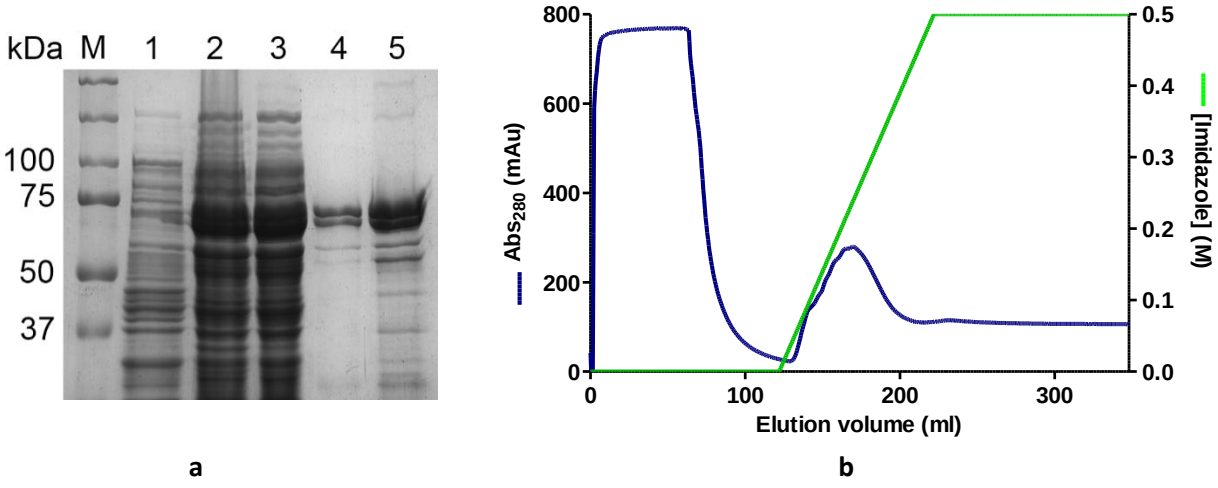

Figure 4.17. a, SDS-PAGE analysis of the purification of N-terminally His-tagged 338. pET-28b(+):338 was co-expressed with the pGro7 chaperone plasmid. M, Precision Plus Protein™ Dual Xtra Standards protein ladder; lane 1, pET-28b(+) empty vector control; lane 2, soluble fraction; lane 3, ultracentrifuged fraction; lane 4, pooled His-trap fractions; lane 5, pooled SEC fractions. **b,** Elution of 338 from a FF His-trap column (GE Healthcare) during affinity chromatography.

SDS-PAGE analysis indicated that two distinct bands were present in the purified fractions, differing slightly in molecular mass (Fig. 4.17a). This may be due to the presence of a 338 protein with an incomplete C-terminus, which would still bind to the His-trap column via the N-terminal His-tag. Faint bands of smaller contaminating proteins were also still visible.

4.3.4.2. Purification of 653 by immobilised metal-affinity chromatography

The 653 protein expressed from the pET-28b(+):653 vector contained an N-terminal His-tag with a total size of 67 kDa (ProtParam, ExPASy). The N-terminally His-tagged 653 protein eluted in the volume of 130 – 190 ml from the HisTrap FF column (Fig. 4.18b) and the monomeric nature of the protein was confirmed by SDS-PAGE (Fig. 4.18a). Fractions eluting in the volume 130 – 180 ml were selectively pooled. The pooled fractions had a brilliant yellow colour, indicating that the FAD co-factor was retained during the purification step. SDS-PAGE demonstrated that the 653 protein was purified to near homogeneity, although faint bands of contaminating proteins were still visible (Fig. 4.18a).

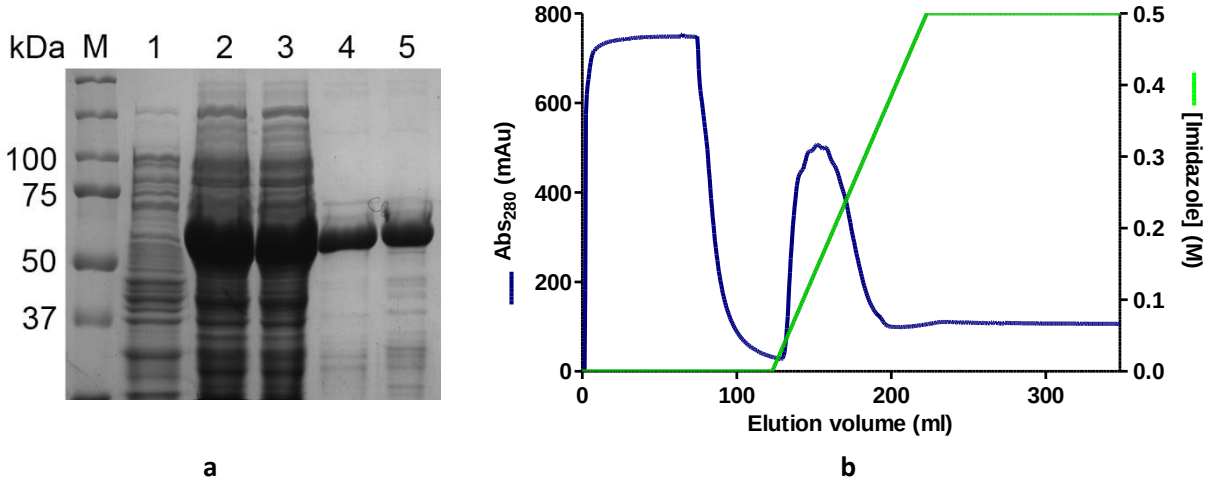

Figure 4.18. a, SDS-PAGE analysis of the purification of N-terminally His-tagged 653. pET-28b(+):653 was co-expressed with the pGro7 chaperone plasmid. M, Precision Plus Protein™ Dual Xtra Standards protein ladder; lane 1, pET-28b(+) empty vector control; lane 2, soluble fraction; lane 3, ultracentrifuged fraction; lane 4, pooled His-trap fractions; lane 5, pooled SEC fractions. **b,** Elution of 653 from a FF His-trap column (GE Healthcare) during affinity chromatography.

4.3.4.3. Purification of 791 by immobilised metal-affinity chromatography

The recombinantly expressed 791 contained an N-terminal His-tag and had a monomeric mass of 72 kDa (ProtParam, ExPASy), as confirmed by SDS-PAGE (Fig. 4.19a). The elution profile of the N-terminally His-tagged 791 from the HisTrap FF column is illustrated in Fig. 4.19b. The protein eluted in the volume of 118 – 187 ml and fractions eluting in the volume 125 – 175 ml were selectively pooled and the homogeneity of the sample evaluated using SDS-PAGE (Fig. 4.19a). The fractions had a brilliant yellow colour, indicating that the FAD co-factor was retained during purification. SDS-PAGE showed that, similar to 653, the protein was significantly purified, although several faint bands of contaminating proteins were still present.

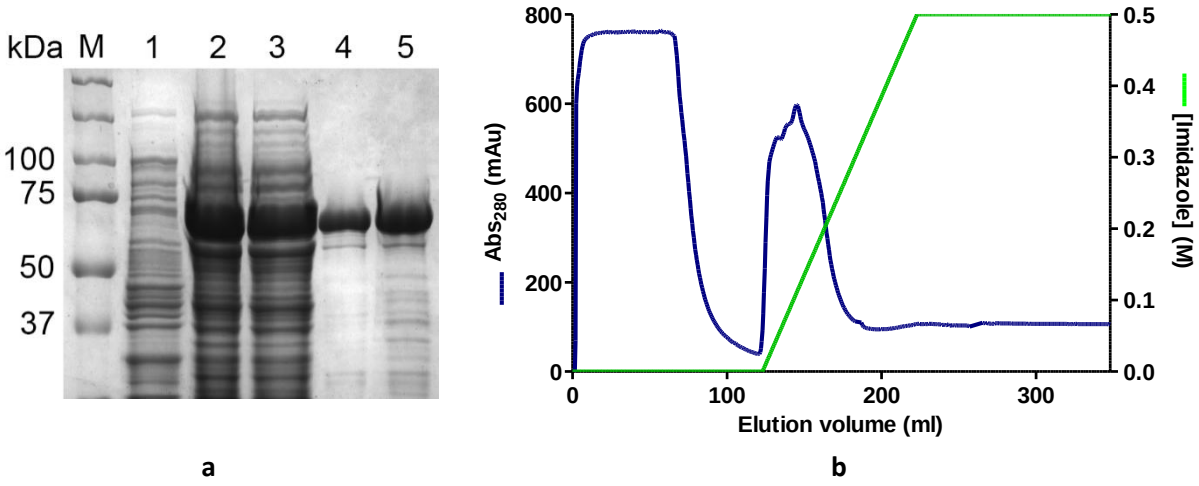

Figure 4.19. a, SDS-PAGE analysis of the purification of N-terminally His-tagged 791. pET-28b(+):791 was co-expressed with the pGro7 chaperone plasmid. M, Precision Plus Protein™ Dual Xtra Standards protein ladder; lane 1, pET-28b(+) empty vector control; lane 2, soluble fraction; lane 3, ultracentrifuged fraction; lane 4, pooled His-trap fractions; lane 5, pooled SEC fractions. **b,** Elution of 791 from a FF His-trap column (GE Healthcare) during affinity chromatography.

4.3.4.4. Purification of 338, 653 and 791 by size-exclusion chromatography

The pooled fractions of 338, 653 and 791 obtained from the His-trap purification step were incubated with an excess of FAD to ensure maximum co-factor occupancy. The pooled fractions were further purified using SEC with PD-10 desalting columns (GE Healthcare). The PD-10 columns have an exclusion limit of 5 kDa and will therefore aid as a means of buffer exchange rather than removal of contaminating proteins. As described in section 3.3.3.2, removal of the imidazole is

necessary for downstream assays. The homogeneity of the fractions obtained from the PD-10 columns were evaluated by means of SDS-PAGE (Figs. 4.17a, 4.18a and 4.19a).

4.3.4.5. Activity assays with purified protein

In order to evaluate the activity of 338 and 791 as isolated enzymes, assays were performed with the purified proteins using the ketones identified as substrates by whole-cell biotransformations.

Table 4.7. Specific activity of purified 338 and 791.

Substrate	338	791
	Specific activity ($nmol.min^{-1}.mg^{-1}$)	**Specific activity ($\mu mol.min^{-1}.mg^{-1}$)**
phenylacetone	1.8 ± 0.8	
2-phenylcyclohexanone	1.9 ± 0.9	
thioanisole	2.6 ± 0.8	0.592 ± 0.018
(±)-*cis*-bicyclo[3.2.0]hept-2-en-6-one	7.7 ± 1.8	0.138 ± 0.004

The rates observed for 338 were relatively low, in the $nmol.min^{-1}.mg^{-1}$ range (Table 4.7). When compared to the yields during whole-cell biotransformations (Table 4.5), it is clear that the enzyme functions better in the protected environment that the whole-cell provides. It is also possible that the FAD co-factor is lost to some extent during purification, as the colour of the purified 338 is much less intense when compared to both 653 and 791. The conversion rates of thioanisole and (±)-*cis*-bicyclo[3.2.0]hept-2-en-6-one by 791 was very high (Table 4.7), with the conversion rate of thioanisole more than four times higher than that of (±)-*cis*-bicyclo[3.2.0]hept-2-en-6-one. Interestingly, the percentage conversion for (±)-*cis*-bicyclo[3.2.0]hept-2-en-6-one during whole-cell biotransformations is considerably higher (92.8 %) when compared to thioanisole (5.9 %).

4.3.5. Reaction with hydroxyversicolorone

The ability of 338, 653 and 791 to convert HVN was evaluated by incubating the enzymes with [1'-^{2}H]HVN in the presence of NADPH. The incubation of the homologues with [1'-^{2}H]HVN was monitored spectrophotometrically at 340 nm for 20 min. No significant reaction rate was observed for any of the three homologues.

TLC analysis indicated that the minor compound present in the [1'-^{2}H]HVN was completely converted to a product with a very low R_f value (Fig. 4.20). Incubation of the [1'-^{2}H]HVN in the absence of enzyme served as a negative control to prove that this reaction occurred non-enzymatically. Co-spotting of the unincubated and incubated [1'-^{2}H]HVN verified that no migration errors occurred during TLC. When compared to the TLC analysis performed on the incubation of [1'-^{2}H]HVN with MoxYAltN, no production of VHA was observed by 338, 653 or 791. Two possible scenarios exist – firstly, that the minor compound of [1'-^{2}H]HVN is the true form of [1'-^{2}H]HVN and was unstable during storage, which implies that no conversion of [1'-^{2}H]HVN by the homologues would be detected or secondly, that the minor compound is a byproduct and that neither one of the homologues is capable of converting [1'-^{2}H]HVN to VHA.

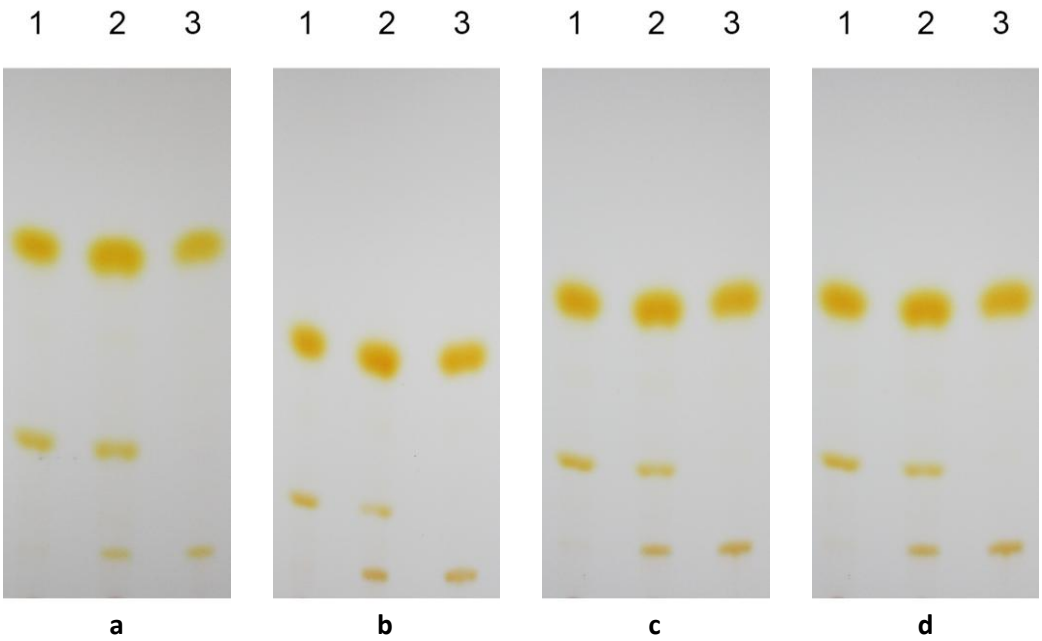

Figure 4.20. TLC analysis of the incubation of [1'-^{2}H]hydroxyversicolorone with **a,** no enzyme; **b,** 338; **c,** 653 and **d,** 791. Lane 1, unincubated [1'-^{2}H]hydroxyversicolorone, lane 2, co-spot of lane 1 and 3; lane 3, reaction products and substrates extracted from the incubation of [1'-^{2}H]hydroxyversicolorone with either no protein (**a**) or the respective homologues (**b, c** and **d**).

4.4. Discussion

Genome-mining of the *A. flavus* genome and phylogenetic analysis revealed six BVMO homologues closely related to MoxY. Three of these BVMO homologues (338, 653 and 791), expressed as soluble, recombinant proteins, with activity observed for 338 and 791. Whereas 338, similar to MoxYAltN, was active towards more structurally diverse ketones, including the aromatic ketone phenylacetone, substituted aromatic ketone 2-phenylcyclohexanone and the bicyclic ketone (±)-*cis*-bicyclo[3.2.0]hept-2-en-6-one, 791 was only able to convert (±)-*cis*-bicyclo[3.2.0]hept-2-en-6-one (Fig. 4.21). Unlike MoxYAltN, both 338 and 791 were able to catalyse the sulfooxidation of thioanisole, with 791 able to overoxidise the sulfoxide product to a sulfone. No activity was observed against linear ketones with either 338 or 791, while MoxYAltN was active against a range of linear ketones.

As (±)-*cis*-bicyclo[3.2.0]hept-2-en-6-one was the only common substrate for MoxYAltN, 338 and 791, chiral GC analysis was performed to evaluate the enantio- and regioselective conversion of the substrate. 791 produces the normal and abnormal lactone in a 1:1 ratio. MoxYAltN and 338 produces the abnormal product in a 1:4 ratio, however, 338 yields an optically pure lactone while MoxYAltN produces a racemate. 791 produces the normal and abnormal product in equal amounts as optically pure lactones with the preferential use of (-)-(1*S*, 5*R*)-*cis*-bicyclo[3.2.0]hept-2-en-6-one, indicating that 791 may be suitable for the dynamic kinetic resolution of the racemic substrate, although this necessitates further time-dependent studies. Therefore, the biocatalytic profiles of MoxYAltN, 338 and 791 with respect to the conversion of (±)-*cis*-bicyclo[3.2.0]hept-2-en-6-one, differ significantly.

Phylogenetic analysis (Fig. 4.1) indicated that MoxY and the homologues were clustered in a distinct group. Therefore, based on the "family clustering" principle, it is expected that the enzymes display similar biocatalytic profiles. In the study by Mihilovic and co-workers (2005), the catalytic profiles of BVMOs were investigated specifically with regard to the enantioselective conversion of (±)-*cis*-bicyclo[3.2.0]hept-2-en-6-one. Two distinct biocatalytic profiles were observed - the production of both regio-isomers (normal and abnormal) in a 1:1 ratio with high optical purity, such as in the case of $CHMO_{rhodoc}$, as opposed to the predominant production of the normal product in a racemic form, as in the case of $CPMO_{comamo}$. The differential catalysis of (±)-*cis*-bicyclo[3.2.0]hept-2-en-6-one corresponded to the phylogenetic clustering of the proteins, with the two different catalytic profiles represented on two different branches of a phylogenetic tree.

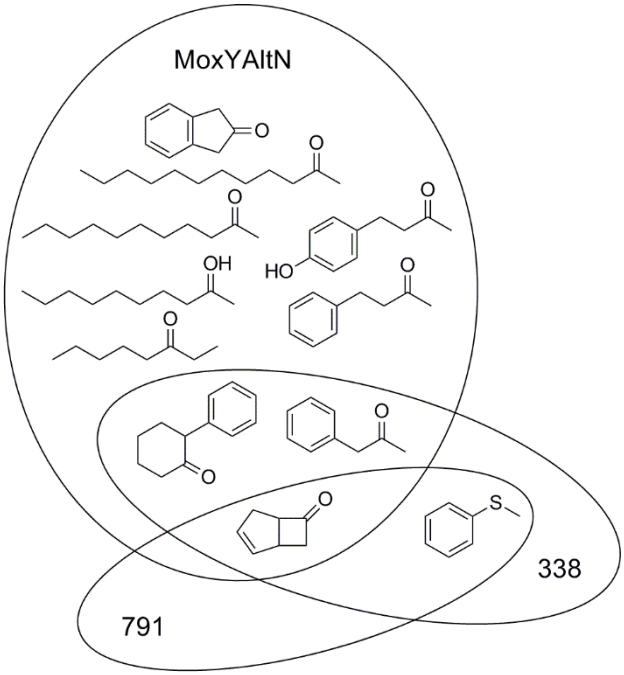

Figure 4.21. The ketone substrates accepted by MoxYAltN, 791 and 338.

The phylogenetic tree generated from the putative BVMOs in *A. flavus*, as well as the well-characterised BVMOs such as $CHMO_{rhodoc}$ (Fig. 4.1), indicated that MoxY(AltN) and the six homologues clustered together on a separate branch and were not closely-related to any of the well-characterised BVMOs. Table 4.8 compares the enantio- and regioselectivity of the conversion of (±)-*cis*-bicyclo[3.2.0]hept-2-en-6-one by 338, 791, MoxYAltN, $CHMO_{rhodoc}$, $CPMO_{comamo}$ (Mihovilovic *et al*., 2005) and $BVMO_{Af1}$ from *A. fumigatus* (Mascotti *et al*., 2013).

Table 4.8. Enantioselective conversion of (±)-*cis*-bicyclo[3.2.0]hept-2-en-6-one by 791, MoxYAltN, CHMO from *Rhodococcus* sp. ($CHMO_{rhodoc}$), CPMO from *Comamonas* sp. ($CPMO_{comamo}$) and $BVMO_{Af1}$ from *A. fumigatus*. The ratio of normal to abnormal lactone is shown, as well as the enantiomeric excess (*ee*) values.

	Ratio normal:abnormal	***ee*** **(-)-(1*S*,5*R*)**	***ee*** **(-)-(1*R*,5*S*)**	**Reference**
338	14:86	86	>99	
791	47:53	>99	>99	
MoxYAltN	18:82	88	56	
$CHMO_{rhodoc}$	50:50	99	>99	(Mihovilovic *et al*., 2005)
$CPMO_{comamo}$	97:3	0	>99	(Mihovilovic *et al*., 2005)
$BVMO_{Af1}$	50:50	>99	>99	(Mascotti *et al*., 2013)

The biocatalytic profile of 791 is similar to that of $CHMO_{rhodoc}$ as well as $BVMO_{Af1}$, producing the normal and abnormal lactones in a 1:1 ratio with high optical purity. In contrast, MoxYAltN has a highly dissimilar profile. While the ratio of regio-isomers produced by 338 is similar to MoxYAltN, 338 displays a higher enantioselectivity with respect to the abnormal product. Therefore, although 338, 791 and MoxYAltN are closely related phylogenetically, their substrate acceptance profile and enantioselectivity differ considerably, indicating that the substrate binding pockets of the enzymes are likely to differ significantly.

In an attempt to determine whether the absence of any observed activity for 653 is due to the lack of conservation in critical amino acids, a multiple sequence alignment was performed with the homologues and $CHMO_{rhodoc}$ (Fig. 4.22, Rebehmed *et al*., 2013). The conservation of the amino acids are shown in Table 4.9. The residues corresponding to the Rossman-folds or dinucleotide binding motifs are 100 % conserved in all of the homologues. However, in the FAD and NADPH-binding domains, numerous substitutions can be observed, as well as in the BVMO fingerprint motif.

In the FAD-binding domain, position 50 is occupied by a tryptophan residue in $CHMO_{rhodoc}$. The tryptophan residue performs hydrogen bonding with the hydroxyl groups of the FAD ribose ring. In 338, this residue is occupied by a valine, which will not be able to perform hydrogen bonding. Therefore, it might be expected that the FAD co-factor is more weakly bound, and can provide an explanation for the low enzymatic rate observed with 338. Similar to MoxYAltN, the position is occupied by an asparagine residue in the other homologues.

Position 59 is occupied in 100 % of the sequences by an aspartic acid, however, in 653, this locus is occupied by a glutamic acid. It is, however, the backbone NH group of this residue that performs hydrogen bonding with the O4 ketone of the FAD isoalloxazine ring. The side chain of the aspartic acid forms part of the active site pocket of $CHMO_{rhodoc}$. As glutamic acid is one carbon longer, it might result in a smaller active site. In general, substitutions at the other loci will be able to fulfil the roles of the conserved residues with respect to hydrogen bonding to the FAD co-factor.

Numerous substitutions are observed in the NADPH-binding domain. Of importance is the deviation from the critically conserved residues at position 209 and 210 by the homologues. In 100 % of the sequences investigated by Rebehmed and co-workers (2013), position 209 is occupied by an arginine residue and 210 by either a threonine or a serine. These residues interact with the phosphate group on the NADPH moiety by both electrostatic interactions and hydrogen bonding. It has been shown that the corresponding loci in the *Stenotrophomonas maltophilia* flavin monooxygenase (SMFMO) is

occupied by a glutamine and a histidine, respectively (Jensen *et al*., 2012). The substitutions at these positions relax the co-factor specificity for NADPH and allows catalysis with the non-phosphorylated counterpart, NADH, in addition to NADPH. In 087, these loci are occupied by an alanine and a histidine, respectively, indicating that when successfully expressed, the 087 protein may be either flexible with respect to NAD(P)H co-factor specificity, or non-functional, as alanine cannot interact electrostatically with the phosphate group for NADPH binding. The residue at position 210 is only conserved in the 868 protein. In 338 and 916, this locus is occupied by a glutamic acid and in 653 and 791, the locus is occupied by an asparagine. The threonine in $CHMO_{rhodoc}$ at position 210 acts in hydrogen bonding with the phosphate group on the NADPH moiety. As both glutamic acid and asparagine have side-chains amenable to hydrogen bonding, it can be expected that the residues will fulfil the same role as the threonine and serine. This is verified by the activity of both 791 (substituted with an asparagine) and 338 (substituted with a glutamic acid) and serves to indicate that the conservation at this locus is not critical for activity.

The multiple sequence alignment does not provide an answer for the lack of activity observed for 653. The bright orange colour of the purified protein indicated that the co-factor was retained and it suggested that rather than being inactive, the protein has a very specific substrate profile for ketones that were not screened in the whole-cell biotransformations. To reinforce this notion, it should be considered that for 791, activity was only observed against two of the 28 substrates screened. Therefore, the activity of 653 should be investigated towards a broader substrate range, including multiple heteroatom compounds.

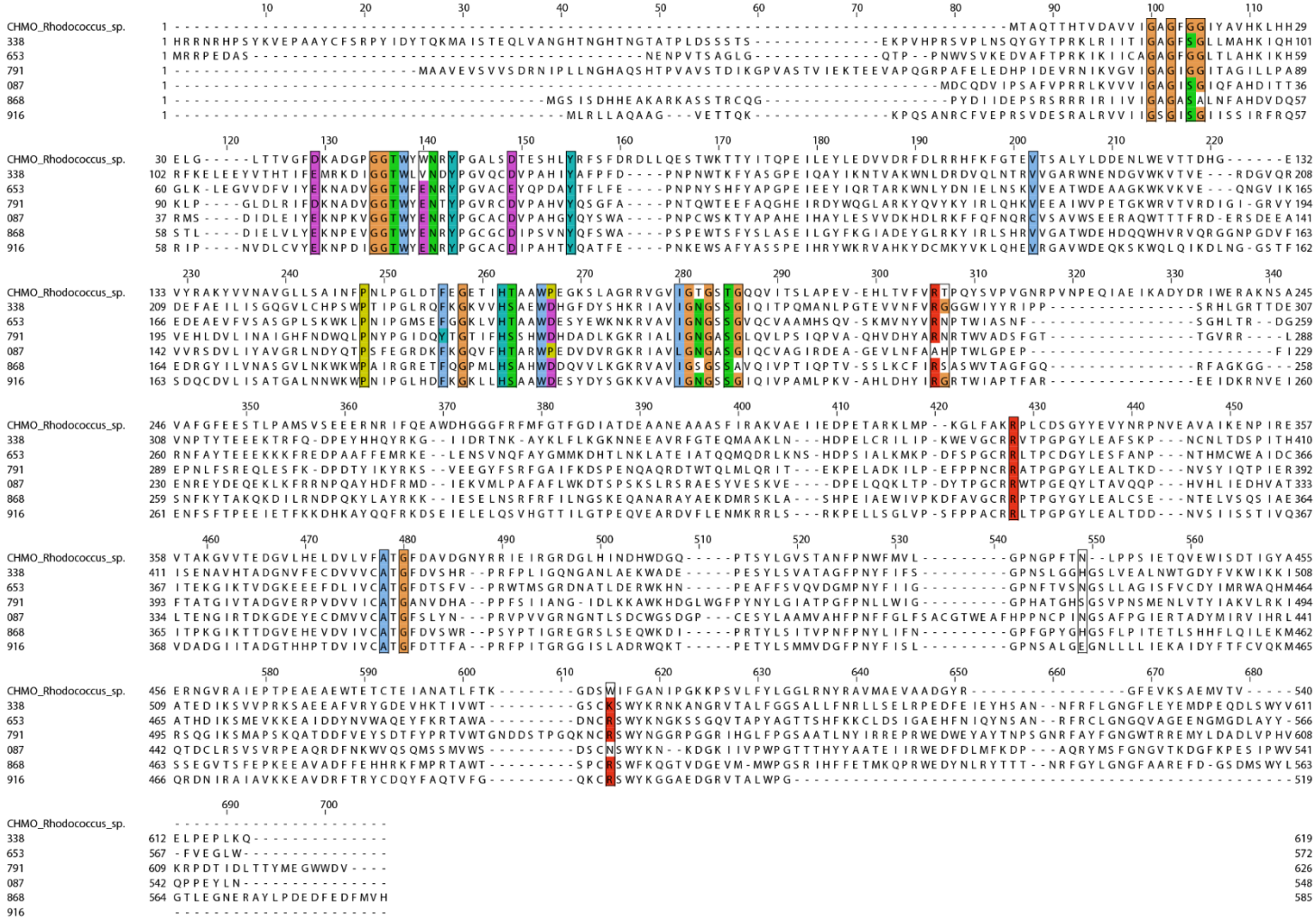

Figure 4.22. Alignment of the amino acid sequences of CHMO from *Rhodococcus* sp. HI-31, and six-closely related BVMO homologues from *A. flavus* (087, 338, 653, 791, 868 and 916). The alignment was performed with ClustalWS, using Jalview version 2.8.

Table 4.9. Highly conserved residues in the motifs and domains of type I BVMOs. The number of the residue in CHMO from *Rhodococcus* sp. is given in the first column, while the % conservation of the residue is given in the second column (Rebehmed *et al*., 2013). Deviations from the conserved residues are indicated in brackets, while deviation in all sequences but one is designated as 'other'.

CHMO residue	% conservation	Conserved	CHMO residue	% conservation	Conserved
Dinucleotide-binding motif (Rossman fold)			**BVMO fingerprint motif**		
G 15	99.1	✓	F 160	94.8	✓ × (Y) 791
G 17	99.1	✓	G 162	100.0	✓
G/A 20	97.4/2.6	✓	H 166	94.8	✓
G 185	100.0	✓	T 167	93.1	✓ × (S) 338, 791, 868, 916
G 187	100.0	✓	W 170	100.0	✓
G/A 190	62.1/35.5	✓	P/D 171	70.7/28.4	✓
FAD-binding domain			**NADPH-binding domain**		
G/A/S 19	47.0/42.6/9.6	✓	P 152	96.6	✓
D/E 39	20.0/80.0	✓	I 184	94.0	✓ × (L) 087
G 45	99.1	✓	T 186	94.8	× (S) 868 × (N) Other
G 46	100.0	✓	T/S 189	50.9/49.1	✓
T 47	91.3	✓	R 209	100.0	✓ × (A) 087
W 48	100.0	✓	T/S 210	81.9/15.5	✓ × (G) 338, 916 (N) 653, 791 (H) 087
W/F/Y 50	80.9/11.3/4.3	× (V) 338 (E) Other	R 329	100.0	✓
N 51	100.0	✓	A 379	96.6	✓
Y 53	97.4	✓	G 381	100.0	✓
D 59	100.0	✓ × (E) 653	W/Y 492	69.8/28.4	✓ × (K) 338 × (R) 653, 791, 498, 501
Y 65	100.0	✓			× (N) 868
V 112	82.8	✓ × (C) 087			
N 436	98.3	✓ × (H) 338, 868 × (S)791 × (E) 916			

A differential migration pattern is observed when comparing the substrate and products involved in the reaction of [1'-^{2}H]HVN with MoxYAltN and the reaction of [1'-^{2}H]HVN with the three homologues. No VHA was detected in any of the incubations with the homologues and non-enzymatic breakdown of the minor compound present in [1'-^{2}H]HVN was observed. If the minor compound is [1'-^{2}H]HVN, conversion of [1'-^{2}H]HVN by the homologues would not be detected. In contrast, if the compound is a byproduct, the homologues were unable to convert the [1'-^{2}H]HVN to VHA. The TLC results remain inconclusive and the intragenomic complementation of MoxYAltN by the homologues remain uncertain.

4.5. Conclusions

A. flavus is a rich source of BVMO enzymes, containing a total of 26 putative BVMOs of which the physiological role of only *moxY*, as a participant in the aflatoxin biosynthesis pathway, is known. The enzymatic step catalysed by MoxY(AltN) in aflatoxin biosynthesis is an ideal candidate for inhibition to relieve the production of aflatoxin biosynthesis, as BVMOs occur only in bacteria and fungi, and not in higher eukaryotes. However, it is a common phenomenon that impaired enzymatic steps in the aflatoxin biosynthesis pathway can be complemented intragenomically by the function of other native enzymes. Therefore, for inhibition of MoxYAltN to be successful, intragenomic complementation of the enzymatic step by one of the numerous native BVMOs in *A. flavus*, has to be investigated.

The family clustering principle of BVMOs suggests that phylogenetically closely-related BVMOs share similar catalytic profiles with regard to substrate acceptance and enantioselectivity. Therefore, the six closest homologues to MoxY(AltN) were investigated by heterologous expression in *E. coli.*

The ability of BVMO homologues to complement the activity of MoxYAltN remains uncertain. However, inspection of the substrate scope of the BVMOs may provide valuable insight into the probability of complementation by a specific enzyme. An overlapping substrate scope could be an indicator of possible intragenomic complementation of MoxYAltN by the specific BVMO. MoxYAltN, 338 and 791 share a common substrate, (±)-*cis*-bicyclo[3.2.0]hept-2-en-6-one, of which the enantio- and regioselective conversion by BVMOs is well-characterised. Contrary to expected, the enantioselectivity of the two enzymes differ drastically, with 791 sharing a profile with $CHMO_{rhodoc}$ of which it is phylogenetically distantly related. Therefore, although clustered together, MoxYAltN and the homologues do not necessarily have similar biocatalytic abilities. Based on the nature of the substrate scopes, neither 338 nor 791 is a strong candidate for the intragenomic complementation of MoxYAltN as their active site topology is likely to differ.

These results serve to demonstrate that family clustering of related enzymes is not absolutely indicative of overlapping biocatalytic profiles, therefore, more distantly related, putative BVMOs in *A. flavus* also has to be considered for possible complementation of MoxYAltN. Nevertheless, the study confirms the success of genome mining to discover novel BVMO biocatalysts.

Chapter 5

Conclusions and future outlook

The genome of *Aspergillus flavus* is rich in putative BVMOs, containing a total of 26 BVMO genes of which the function of only one is known, *moxY.* The role of the *moxY* gene, located in the aflatoxin biosynthesis gene cluster of *Aspergillus flavus,* has been confirmed as encoding a type I BVMO that catalyses the NADPH-dependent conversion of hydroxyversicolorone to versiconal hemiacetal acetate. The coding region of the *moxY* gene as predicted by the NCBI database represents a truncated version of the gene, with the actual coding translational start site located 63 bp upstream from the indicated start site. This results in an elongated N-terminus which corresponds to the N-terminus of the homologue in the *A. nidulans* sterigmatocystin biosynthesis gene cluster, StcW. The presence of an elongated N-terminus is also present in the *moxY* gene of the aflatoxin biosynthesis gene cluster in *A. parasiticus.*

EST data indicates that the *moxY* gene contains a region in the C-terminus that is differentially spliced. Although no activity was observed for MoxY variants containing the alternative C terminus, further studies are required to verify whether the protein is functional, as this form of MoxY exists in nature.

MoxY(AltN) represents an ideal candidate for targeted enzyme inhibition in an attempt to metabolically block aflatoxin biosynthesis as a novel strategy for aflatoxin control. Two different strategies in studying the inhibition of MoxY(AltN) is possible – *in vitro* and *in silico*.

In vitro studies will involve the manual screening of possible inhibitors by evaluating the effect of selected compounds on the reaction of purified MoxYAltN with substrates. As MoxYAltN accepts a range of ketone substrates, the effect of possible inhibitors can be investigated by monitoring the reaction of MoxYAltN with a surrogate substrate, such as phenylacetone. This is useful as the reaction rate, as measured spectrophotometrically, of MoxYAltN with hydroxyversicolorone is relatively low. In addition, spectrophotometric screening of a large number of possible inhibitors will proceed much faster than TLC analysis. The action of successful inhibitors on the reaction of MoxYAltN with HVN can then be verified via TLC analysis. Nonetheless, manual screening of inhibitors is a labour-intensive approach, which limits the number of compounds that can be tested for inhibition.

In silico screening of inhibitors requires a three-dimensional structure of MoxYAltN. This necessitates crystallisation in order to obtain an X-ray crystal structure for MoxYAltN. Once solved, the crystal structure can be used to screen for possible inhibitors against a small molecule database, thereby allowing the evaluation of a very large number of compounds. The efficacy of compounds identified as possible inhibitors can be verified *in vitro* using purified enzyme. In addition, the crystal structure can allow rational design of small molecules that fit into the active site, which can be synthesised and tested for their ability to inhibit the activity of MoxYAltN. To date, no structure of a fungal BVMO is available. Consequently, the structure of MoxYAltN will represent a great advance in the field of BVMOs.

The ability of closely-related homologues to complement the activity of MoxYAltN with respect to the conversion of HVN was investigated. However, the results remain inconclusive. The homologues were selected on the basis of phylogenetic clustering as closely-related BVMOs have been shown to have similar biocatalytic profiles.

MoxYAltN was promiscuous with regard to the ketone substrates accepted and converted a wide range of structurally diverse substrates. This is surprising, given the firm physiological role of MoxYAltN. Moreover, the substrate acceptance profile of MoxYAltN is much wider than that of the successfully expressed homologues. MoxYAltN and the homologues shared only one common substrate, (±)-*cis*-bicyclo[3.2.0]hept-2-en-6-one, a substrate of which the enantio- and regioselective conversion by BVMOs is well-characterised. Phylogenetically related BVMOs have been shown to share similar biocatalytic profiles with respect to the conversion of (±)-*cis*-bicyclo[3.2.0]hept-2-en-6-one. However, this is not the case with MoxYAltN and the homologues, which displays different catalytic profiles in each case. Therefore, phylogenetic clustering of enzymes is not absolutely indicative of overlapping biocatalytic profiles and more distantly related BVMOs have to be considered as candidates for possible intragenomic complementation of the activity of MoxYAltN.

A three-dimensional structure of MoxYAltN will also aid in the identification of BVMOs that can complement the activity of MoxYAltN. Generating homology models of the BVMOs by using the MoxYAltN structure can allow direct comparison of the active sites rather than the overall similarity of the enzymes. BVMO homologues with similar active sites to MoxYAltN are much more likely to convert HVN, thereby complementing the activity of MoxYAltN. The inhibition of these enzymes must be studied as well to ensure complete inhibition of the metabolic step converting HVN to VHA in the aflatoxin biosynthesis pathway.

Appendix

Table A1. Composition of media used in this study.

Media	Components	Concentration
Potato Dextrose Agar (PDA)	PDB (Potato Dextrose Broth)	24 $g.L^{-1}$
	Agar	15 $g.L^{-1}$
Yeast Mold Agar (YMA)	Yeast extract	3 $g.L^{-1}$
	Malt extract	3 $g.L^{-1}$
	Peptone	5 $g.L^{-1}$
	Dextrose	10 $g.L^{-1}$
	Agar	15 $g.L^{-1}$
Luria-Bertani (LB)	Tryptone	10 $g.L^{-1}$
	Yeast extract	5 $g.L^{-1}$
	NaCL	5 $g.L^{-1}$
SOC	Tryptone	20 $g.L^{-1}$
	Yeast extract	5 $g.L^{-1}$
	NaCl	10 mM
	KCl	2.5 mM
	MgCl	10 mM
	$MgSO_4$	10 mM
	Glucose	20 mM
ZYP5052 Auto-induction media	Tryptone	10 $g.L^{-1}$
	Yeast extract	5 $g.L^{-1}$
	$(NH_4)_2SO_4$	25 mM
	KH_2PO_4	50 mM
	Na_2HPO_4	50 mM
	Glycerol	5 $g.L^{-1}$
	Glucose	0.5 $g.L^{-1}$
	α-lactose	2 $g.L^{-1}$
	$MgSO_4$	2 mM

Table A2. Sequencing primers used in DNA sequencing reactions.

Plasmid	Primer	Sequence
pSMART®	SL1	5’-CAG TCC AGT TAC GCT GGA GTC-3’
	SR2	5’-GGT CAG GTA TGA TTT AAA TGG TCA GT-3’
pET-22b(+)	T7 promoter	5’-TAA TAC GAC TCA CTA TAG GG-3’
pET-28b(+)	T7 terminator	5'-GCT AGT TAT TGC TCA GCG G-3'

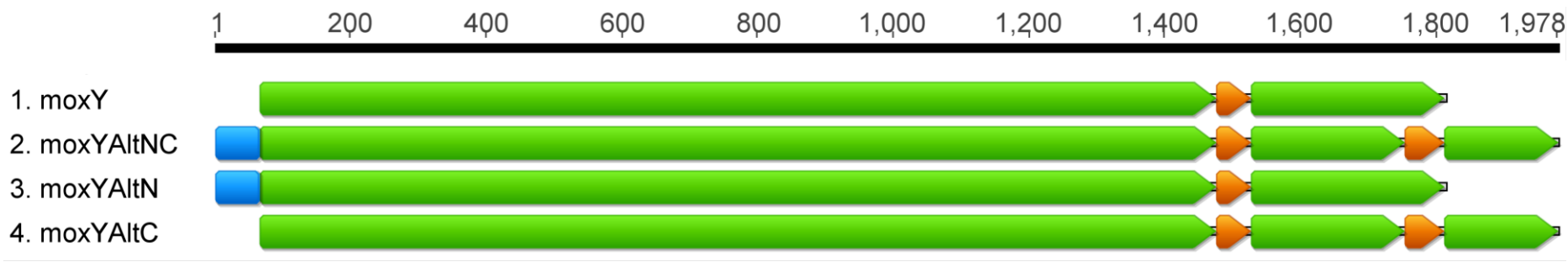

Figure A1. Alignment of the *moxY, moxYAltN, moxYAltC* and *moxYAltNC* genes. The coding regions are indicated in green, while the exons are indicated in orange. The elongated N-terminus of *moxYAltN* and *moxYAltNC* is shown in blue. The *moxY* and *moxYAltNC* genes were PCR-amplified from the genomic DNA of *Aspergillus flavus*, while the *moxYAltC* and *moxYAltN* variants were created by a cross-over recombination of *moxY* and *moxYAltNC* in corresponding expression vectors.

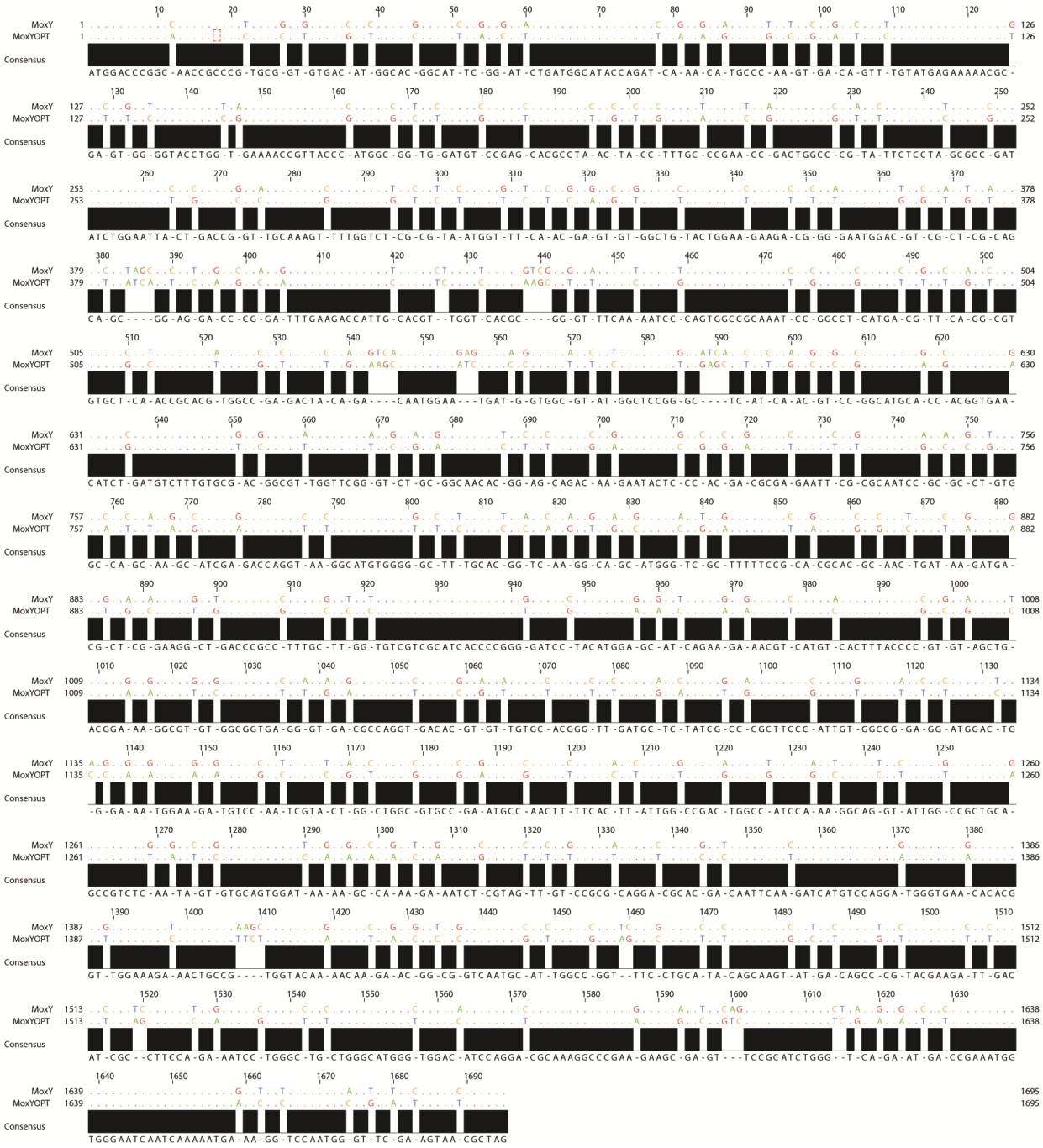

Figure A2. Alignment of unoptimised and optimised sequences of *moxY.* Optimised genes were synthesised by GenScript. Alignment was performed with ClustalO and visualised with JalView v 2.

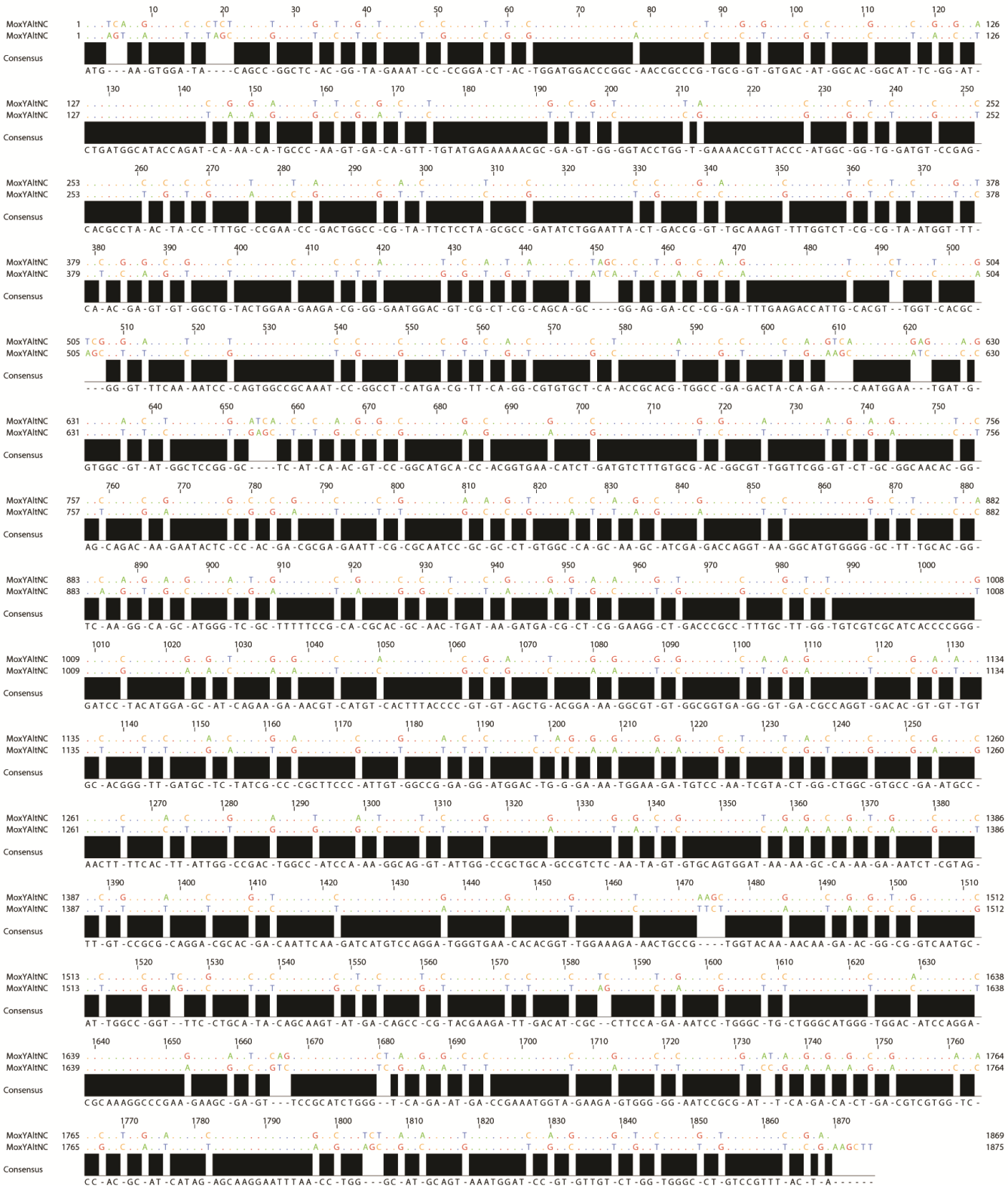

Figure A3. Alignment of unoptimised and optimised sequences of *moxYAltNC.* Optimised genes were synthesised by GenScript. Alignment was performed with ClustalO and visualised with JalView v 2.

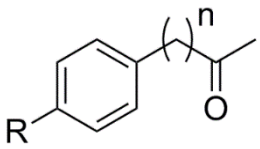

Substrate	R	n
acetophenone	H	0
4’-hydroxyacetophenone	OH	0
phenylacetone	H	1
4-phenyl-2-butanone	H	2
4’-(4-hydroxyphenyl)-2-butanone	OH	2
4’-(4-methoxyphenyl)-2-butanone	OCH_3	2

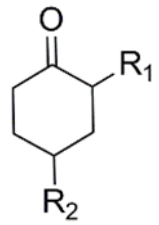

Substrate	R_1	R_2
2-phenylcyclohexanone	Ph	H
4-propylcyclohexanone	H	Pr
4-ethylcyclohexanone	H	Eth

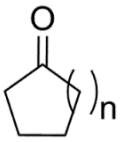

Substrate	n
cyclopentanone	1
cyclohexanone	2
cyclooctanone	4
cyclododecanone	8

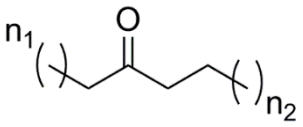

Substrate	n_1	n_2
2-octanone	0	4
3-octanone	1	3
2-decanone	0	6
2-undecanone	0	7
2-dodecanone	0	8

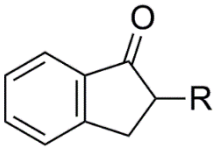

Substrate	R
2-indanone	H
2-methylindanone	CH_3

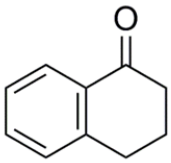

β-tetralone

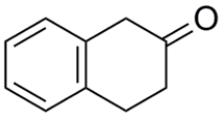

α-tetralone

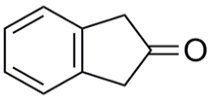

1-indanone

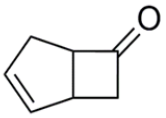

(±)-*cis*-bicyclo[3.2.0.]hept-2-en-6-one

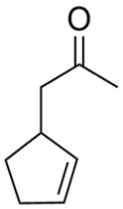

2-cyclopentenyl-1-acetone

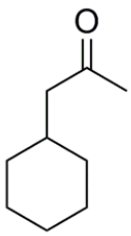

1-cyclohexylacetone

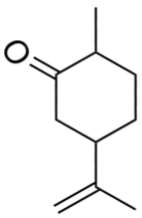

dihydrocarvone

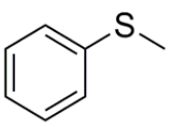

thioanisole

Figure A4. Selected ketone substrates for BVMO activity assays and whole-cell biotransformations.

Table A3. GC programs for the separation of substrates and products extracted from whole-cell biotransformations. A Finnigan TRACE GC Ultra (Thermo Scientific) equipped with a FactorFour™ VF-5ms column was used (60 m x 0.25 mm x 0.25 µm, Varian). Retention times for the substrate(s) and product(s) are indicated. n.d. = not detected.

Program[a]	**Substrate**	**Retention time (min)**	
		Substrate	Product(s)
80/2/15/185/0	cyclopentanone	1.92	6.03
60/1/10/110/4/25/200/2	cyclohexanone	2.82	6.2
60/1/10/110/4/25/200/2	cyclooctanone	5.05	5.2
80/2/15/250/0	cyclododecanone	8.92	n.d.
60/1/10/110/4/25/200/2	2-phenylcyclohexanone	12.96	14.45
60/1/10/110/4/25/200/2	4-propylcyclohexanone	6.66	12.01
60/1/10/110/4/25/200/2	4-ethylcyclohexanone	5.16	10.62
80/2/15/250/0	2-octanone	3.45	3.67
80/2/15/250/0	3-octanone	3.34	3.54
80/2/15/250/0	2-decanone	5.63	5.80
80/2/15/250/0	2-undecanone	6.67	6.81
80/2/15/250/0	2-dodecanone	7.64	7.73
60/2/8/140/0/15/220/2	acetophenone	5.92	5.71
60/2/8/140/0/15/220/2	4'-hydroxyacetophenone	11.65	10.62
60/2/8/140/0/15/220/2	phenylacetone	7.33	7.94
60/2/8/140/0/15/220/2	4-phenyl-2-butanone	9.45	9.59
60/2/8/140/0/15/220/2	4-(4-methoxyphenyl)-2-butanone	12.91	12.99
60/5/5/160/0/25/250/2	4-(4-hydroxyphenyl)-2-butanone	23.07	23.23
60/5/5/160/0/25/250/2	2-cyclopentenyl-1-acetone	6.65	n.d.
60/5/5/160/0/25/250/2	1-cyclohexylacetone	10.54	n.d.
80/2/15/260/5	(±)-*cis*-bicyclo[3.2.0]hept-2-en-6-one	2.94	5.64, 5.69 (abnormal, normal)
60/2/5/165/0	α-tetralone	15.32	n.d.
60/2/5/165/0	β-tetralone	15.00	n.d.
60/2/5/165/0	1-indanone	12.85	15.57
60/2/5/165/0	2-indanone	11.52	17.99
60/2/5/165/0	2-methyl-1-indanone	13.51	n.d.
80/2/15/260/5	dihydrocarvone	5.78, 5.84	n.d.
60/2/8/140/0/15/220/2	thioanisole	6.52	10.83, 11.85 (sulfoxide, sulfone)

[a]Initial temp (°C)/ time (min)/ slope (°C.min^{-1})/ temperature (°C)/ time (min)/ slope (°C.min^{-1})/ temperature (°C)/ time

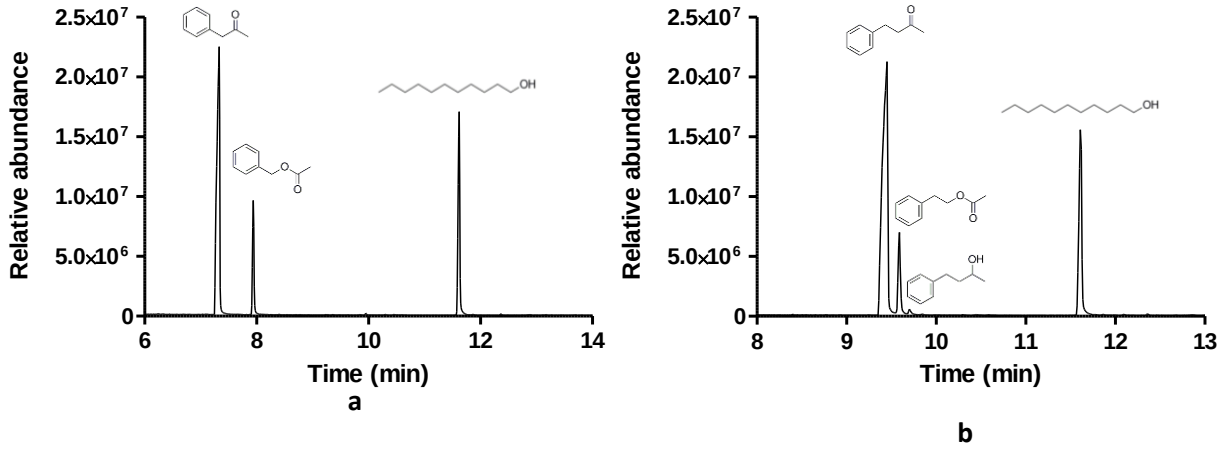

Figure A5. GC-MS chromatograms of the substrates and products extracted after whole-cell biotransformations with **a,** phenylacetone and **b,** 4-phenyl-2-butanone. The structures of the eluting compounds are indicated above the peaks.

Table A4. GC program for the separation of (±)-*cis*-bicyclo[3.2.0]hept-2-en-6-one and products extracted from whole-cell biotransformations. A Finnigan TRACE GC Ultra (Thermo Scientific) equipped with an Astec CHIRALDEX™ G-TA column (30 m x 0.25 mm x 0.12 µm, Sigma Aldrich) was used and compounds were detected by FID. Retention times for the substrates and products are indicated.

Program[a]	**Retention time (min)**	**Compound**	
80/7/10/125/15/15/160/1			
	6.7	(-)-(1*S*,5*R*)-bicyclo[3.2.0]hept-2-en-6-one	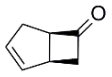
	7.3	(+)-(1*R*,5*S*)-bicyclo[3.2.0]hept-2-en-6-one	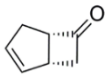
	21.7	(-)-(1*R*,5*S*)-3-oxabicyclo[3.3.0]oct-6-en-2-one	
	22.5	(+)-(1*R*,5*S*)-2-oxabicyclo[3.3.0]oct-6-en-3-one	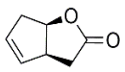
	24.4	(-)-(1*S*,5*R*)-2-oxabicyclo[3.3.0]oct-6-en-3-one	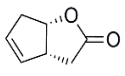
	25.0	(+)-(1*S*,5*R*)-3-oxabicyclo[3.3.0]oct-6-en-2-one	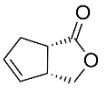

[a]Initial temp (°C)/ time (min)/ slope (°C.min^{-1})/ temperature (°C)/ time (min)/ slope (°C.min^{-1})/ temperature (°C)/ time

Summary

Aflatoxins are carcinogenic mycotoxins produced by certain species of the *Aspergilli*, with the most prominent producers being *Aspergillus flavus* and *A. parasiticus.* Exposure to aflatoxins causes liver cancer, immune suppression, retardation in growth and in extreme cases, even death. *A. parasiticus* and *A. flavus* infect a wide range of crops, including corn, cotton, peanuts and tree nuts. Consequently, aflatoxin contamination has a severe impact on public health, as well as the agricultural sector.

Several control strategies are currently in place to combat aflatoxin contamination. Although great progress has been made in developing innovative methods for aflatoxin control, no strategy is completely efficient in eliminating aflatoxin contamination. Also, the application of the strategies is often limited by practical and economic factors. This necessitates the development of further aflatoxin control strategies.

A yet under-exploited resource is the aflatoxin biosynthesis pathway. Aflatoxins are synthesised in a complex polyketide-initiated pathway that requires multiple enzymatic steps. The genes encoding the aflatoxin biosynthetic enzymes are located in a cluster which contains both the regulatory and structural genes. A novel approach to aflatoxin control is the direct inhibition of a target enzyme in the aflatoxin biosynthesis pathway. An ideal candidate is the Baeyer-Villiger monooxygenase (BVMO), MoxY, that catalyses the conversion of hydroxyversicolorone to versiconal hemiacetal acetate. BVMOs are flavin-containing proteins that catalyse the oxidation of ketones or cyclic ketones to esters or lactones, respectively. BVMOs occur only in the genomes of bacteria and fungi, rendering the MoxY enzyme as a suitable candidate for targeted enzyme inhibition.

In silico analysis of the *moxY* gene indicated that MoxY may exist with an elongated N-terminus or an alternative C-terminus, due to alternative splicing of the mRNA. In addition to cloning the *moxY* gene, variations of the *moxY* gene were created that encode a protein with both the alternative termini or either an alternative N-terminus or an alternative C-terminus.

The MoxY variants were heterologously expressed in *E. coli* and MoxY with an elongated N-terminus (MoxYAltN) was found to be the only active recombinant form of the MoxY enzyme. MoxYAltN is promiscuous with regard to the substrate accepted, converting linear, aromatic, substituted aromatic and bicyclic ketones. MoxYAltN was purified and the kinetic parameters determined with

respect to the reaction with a surrogate substrate, phenylacetone. Purified MoxYAltN was demonstrated to convert synthetic [1'-^{2}H]hydroxyversicolorone to versiconal hemiacetal acetate, confirming the role of MoxYAltN in the aflatoxin biosynthesis pathway.

Intragenomic complementation of an impaired aflatoxin biosynthetic step is a common theme that has emerged from the experimental study of the aflatoxin biosynthetic pathway. Therefore, the complementation of the activity of MoxY(AltN) by another BVMO in the *A. flavus* genome was investigated. The genome contains 26 putative BVMOs and phylogenetic analysis indicted that six of these are closely-related to MoxY, which were selected for heterologous expression in *E. coli*. Three of the homologues expressed as soluble proteins and activity was observed for two. The substrate profiles of the homologues differ significantly from that of MoxYAltN, with the only common substrate converted being (±)-*cis*-bicyclo[3.2.0]hept-2-en-6-one.

The enantio- and regioselective conversion of (±)-*cis*-bicyclo[3.2.0]hept-2-en-6-one by BVMOs is a well-characterised reaction. Chiral analysis indicated divergent biocatalytic profiles of MoxYAltN and the two homologues with respect to the conversion of (±)-*cis*-bicyclo[3.2.0]hept-2-en-6-one, which suggests that the substrate binding pockets of the enzymes are likely to differ.

The ability of the homologues to complement the activity of MoxY(AltN) by converting [1'-^{2}H]hydroxyversicolorone remains uncertain. However, the differential substrate profiles demonstrate that phylogenetic clustering is not an absolute indication of overlapping biocatalytic abilities. Therefore, more distantly related BVMOs in *A. flavus* have to be considered as candidates for intragenomic complementation as well.

Key terms: Aflatoxin biosynthesis, gene cluster, *Aspergillus flavus*, *moxY/aflW* gene, hydroxyversicolorone, Baeyer-Villiger monooxygenase, genomic complementation.

Opsomming

Aflatoksiene is kankerwekkende mikotoksiene wat geproduseer word deur sekere lede van die *Aspergilli*. Die mees prominente aflatoksienproduseerders is *Aspergillus parasiticus* en *A. flavus*, fungi wat ‘n groot verskeidenheid landbouprodukte infekteer, insluitend mielies, katoen, grondboontjies en ander neute. Blootstelling aan aflatoksiene lei tot aflatoksikose, wat lewerkanker, immuunonderdrukking en vertraagde groei veroorsaak, en kan selfs lewensgevaarlik wees. Gevolglik het aflatoksienkontaminasie ‘n groot impak op die menslike gesondheid, asook op die ekonomie.

Huidig is daar ‘n verskeidenheid strategieë vir die beheer van aflatoksiene. Alhoewel aflatoksienkontaminasie tot ‘n groot mate bekamp kan word, is daar nie ‘n strategie wat ten volle suksesvol is om aflatoksienproduksie te elimineer nie. Sommige strategieë is ook nie toepasbaar nie as gevolg van die praktiese en ekonomiese faktore verbonde daaraan. Daarom is dit nodig om nuwe aflatoksien beheermetodes te ontwikkel.

Die aflatoksien biosintese weg bied ‘n ryk bron vir die ontwikkeling vir nuwe strategieë. Aflatoksiene word gesintetiseer deur ‘n poliketied-geïnisieerde metaboliese weg wat bestaan uit veelvuldige ensiemstappe. Die ensieme word gekodeer deur gene wat saam gegroepeer is en die groep sluit beide strukturele en regulatoriese gene in. ‘n Nuwe, innoverende metode vir die beheer van aflatoksiene is die inhibisie van ‘n spesifieke teikenstap in die aflatoksien sintese weg. ‘n Ideale stap is die omskakeling van hidroksiversikoloroon na versikoloroon hemiasetal asetaat, ‘n reaksie wat gekataliseer word deur MoxY, ‘n Baeyer-Villiger monooksigenase (BVMO). BVMOs is flavien-afhanklike ensieme wat die omskakeling van ketone na esters en sikliese ketone na laktone kataliseer. BVMO’s kom egter net in die genome van bakterieë en fungi voor, dus is die MoxY-gekataliseerde reaksie ‘n ideale kandidaat vir geteikende ensieminhibisie.

In silico analise van die *moxY* geen het aangedui dat MoxY moontlik bestaan met ‘n verlengde N-terminus en ‘n alternatiewe C-terminus wat ontstaan as gevolg van alternatiewe splitsing van die mRNA. Die *moxY* geen is gekloneer en variasies van die *moxY* geen is gemaak wat die kodeer vir ‘n MoxY proteïen met beide die alternatiewe termini, asook ‘n proteïen met net die alternatiewe N- of C-terminus.

Die variante van MoxY was uitgedruk as heteroloë proteïene in *E. coli*. Slegs MoxYAltN, die variant met die verlengde N terminus, het uitgedruk as ‘n oplosbare, aktiewe, rekombinante proteïen. Die

MoxYAltN is ‘n promiskue ensiem wat diverse substrate omskakel, waaronder lineëre, aromatiese, gesubstitueerde aromatiese en bisikliese ketone. MoxYAltN is gesuiwer en kineties gekarakterieseer met betrekking tot die surrogaatsubstraat, fenielasetoon. Verder is die omskakeling van sintetiese [1’-^{2}H]hidroksiversikoloroon deur gesuiwerde MoxYAltN gedemonstreer, wat die rol van MoxYAltN in die aflatoksien sintese weg bevestig.

Die intra-genomiese komplementasie van ‘n nie-funksionele ensiematiese stap in die aflatoksien biosintese weg is gereeld waargeneem; daarom moet daar bepaal word of die aktiwiteit van MoxYAltN deur ‘n ander BVMO in *A. flavus* gekomplementeer kan word. Die genoom bevat 26 moontlike BVMO gene en ses van die BVMO’s is filogeneties naby-verwant aan MoxY. Die ses is gekies vir heteroloë uitdrukking in *E. coli*, waarvan drie uitgedruk het as oplosbare proteïene en twee aktiwiteit getoon het. Die substraatprofiele van die homoloë verskil baie van dié van MoxYAltN, met (±)-*cis*-bisiklo[3.2.0]hept-2-en-6-oon as die enigste gemene substraat.

Die regio- en enantiospesifieke omskakeling van (±)-*cis*-bisiklo[3.2.0]hept-2-en-6-oon deur BVMO’s is ‘n deuglik-bestudeerde reaksie. Chirale analise het aangedui dat die omskakelingsprofiel van (±)-*cis*-bisiklo[3.2.0]hept-2-en-6-oon deur MoxYAltN en die homoloë nie ooreenstem nie, wat wys daarop dat die substraatbindingsetels van die ensieme heel waarskynlik verskil.

Dit bly egter onseker of die homoloë wel [1’-^{2}H]hidroksiversikoloroon kan omskakel. Die uiteenlopende substraatprofiele van MoxYAltN en die homoloë dui daarop dat filogenetiese verwantskap nie noodwendig dui op ‘n oorvleueling in biokatalitiese vermoëns nie. Dus moet BVMO’s wat filogeneties minder verwant is aan MoxY, ook in ag geneem word as potensiële kandidate vir intragenomiese komplementasie.

References

Abbas HK, Zablotowicz RM, Horn BW, Phillips NA, Johnson BJ, Jin X, Abel CA. 2011. Comparison of major biocontrol strains of non-aflatoxigenic *Aspergillus flavus* for the reduction of aflatoxins and cyclopiazonic acid in maize. *Food Addit. Contam. Part A. Chem. Anal. Control. Expo. Risk Assess.* **28**:198–208.

Abdel-Hadi AM, Caley DP, Carter DRF, Magan N. 2011. Control of aflatoxin production of *Aspergillus flavus* and *Aspergillus parasiticus* using RNA silencing technology by targeting *aflD* (*nor-1*) gene. *Toxins* **3**:647–59.

Appa Rao KBC, Garg LC, Panda AK, Totey SM. 1997. High-level expression of ovine growth hormone in *Escherichia coli*: single-step purification and characterization. *Protein Expr. Purif.* **11**:201–8.

Arnau J, Lauritzen C, Petersen GE, Pedersen J. 2006. Current strategies for the use of affinity tags and tag removal for the purification of recombinant proteins. *Protein Expr. Purif.* **48**:1–13.

Baeyer A, Villiger, V. 1899. Einwirkung des Caro'schen reagens auf ketone. *Ber. Dtsch. Chem. Ges.* **32**:3625-33.

Barth HG, Boyes BE, Jackson C. 1994. Size exclusion chromatography. *Anal. Chem.* **66**:595R–620R.

Beam MP, Bosserman MA, Noinaj N, Wehenkel M, Rohr J. 2009. Crystal structure of Baeyer-Villiger monooxygenase MtmOIV, the key enzyme of the mithramycin biosynthetic pathway. *Biochemistry* **48**:4476–87.

Bennett JW, Christensen SB. 1983. New perspectives on aflatoxin biosynthesis. *Adv. Appl. Microbiol.* **29**:53–92.

Bennett JW, Klich M. 2003. Mycotoxins. *Clin. Microbiol. Rev.* **16**:497–516.

Bernstein E, Caudy AA, Hammond SM, Hannon GJ. 2001. Role for a bidentate ribonuclease in the initiation step of RNA interference. *Nature* **409**:363–6.

Bhatnagar D, Cary JW, Ehrlich KC, Yu J, Cleveland TE. 2006. Understanding the genetics of regulation of aflatoxin production and *Aspergillus flavus* development. *Mycopathologia* **162**:155-66.

Bhatnagar D, Cleveland TE, Kingston DG. 1991. Enzymological evidence for separate pathways for aflatoxin B_1 and B_2 biosynthesis. *Biochemistry* **30**:4343–50.

Bhatnagar D, Ehrlich KC, Cleveland TE. 1992. Oxidation-reduction reactions in biosynthesis of secondary metabolites. In: Bhatnagar D, Lillehoj EB, Arora DK, editors. Handbook of Applied Mycology, volume 5. Mycotoxins in ecological systems. New York: Marcel Dekker, Inc. p 255–86.

Bradshaw RE, Bhatnagar D, Ganley RJ, Gillman CJ, Monahan BJ, Seconi JM. 2002. *Dothistroma pini*, a forest pathogen, contains homologs of aflatoxin biosynthetic pathway genes. *Appl. Environ. Microbiol.* **68**:2885–92.

Brown DW, Yu JH, Kelkar HS, Fernandes M, Nesbitt TC, Keller NP, Adams TH, Leonard TJ. 1996. Twenty-five coregulated transcripts define a sterigmatocystin gene cluster in *Aspergillus nidulans*. *Proc. Natl. Acad. Sci. U. S. A.* **93**:1418–22.

Brown RL, Chen ZY, Cleveland TE, Russin JS. 1999. Advances in the development of host resistance in corn to aflatoxin contamination by *Aspergillus flavus*. *Phytopathology* **89**:113–7.

Cai J, Zeng H, Shima Y, Hatabayashi H, Nakagawa H, Ito Y, Adachi Y, Nakajima H, Yabe K. 2008. Involvement of the *nadA* gene in formation of G-group aflatoxins in *Aspergillus parasiticus*. *Fungal Genet. Biol.* **45**:1081–93.

Carbone I, Ramirez-Prado JH, Jakobek JL, Horn BW. 2007. Gene duplication, modularity and adaptation in the evolution of the aflatoxin gene cluster. *BMC Evol. Biol.* **7**:111.

Cary JW, Wright M, Bhatnagar D, Lee R, Chu FS. 1996. Molecular characterization of an *Aspergillus parasiticus* dehydrogenase gene, *norA*, located on the aflatoxin biosynthesis gene cluster. *Appl. Environ. Microbiol.* **62**:360–6.

Cary JW, Ehrlich KC. 2006. Aflatoxigenicity in *Aspergillus*: molecular genetics, phylogenetic relationships and evolutionary implications. *Mycopathologia* **162**:167–77.

Cary JW, Ehrlich KC, Bland JM, Montalbano BG. 2006. The aflatoxin biosynthesis cluster gene, *aflX*, encodes an oxidoreductase involved in conversion of versicolorin A to demethylsterigmatocystin. *Appl. Environ. Microbiol.* **72**:1096–101.

Chang PK, Cary JW, Yu J, Bhatnagar D, Cleveland TE. 1995a. The *Aspergillus parasiticus* polyketide synthase gene *pksA*, a homolog of *Aspergillus nidulans wA*, is required for aflatoxin B_1 biosynthesis. *Mol. Gen. Genet.* **248**:270–7.

Chang PK, Cary JW, Bhatnagar D, Cleveland TE, Bennett JW, Linz JE, Woloshuk CP, Payne GA. 1993. Cloning of the *Aspergillus parasiticus apa-2* gene associated with the regulation of aflatoxin biosynthesis. *Appl. Environ. Microbiol.* **59**:3273–9.

Chang PK, Ehrlich KC, Yu J, Bhatnagar D, Cleveland TE. 1995b. Increased expression of *Aspergillus parasiticus aflR*, encoding a sequence-specific DNA-binding protein, relieves nitrate inhibition of aflatoxin biosynthesis. *Appl. Environ. Microbiol.* **61**:2372–7.

Chang PK, Yu J, Ehrlich KC, Boue SM, Montalbano BG, Bhatnagar D, Cleveland TE. 2000. *adhA* in *Aspergillus parasiticus* is involved in conversion of 5'-hydroxyaverantin to averufin. *Appl. Environ. Microbiol.* **66**:4715–9.

Chang PK, Yabe K, Yu J. 2004a. The *Aspergillus parasiticus estA*-encoded esterase converts versiconal hemiacetal acetate to versiconal and versiconol acetate to versiconol in aflatoxin biosynthesis. *Appl. Environ. Microbiol.* **70**:3593–9.

Chang PK, Yu J, Yu JH. 2004b. *aflT*, a MFS transporter-encoding gene located in the aflatoxin gene cluster, does not have a significant role in aflatoxin secretion. *Fungal Genet. Biol.* **41**:911–20.

Chang PK. 2003. The *Aspergillus parasiticus* protein AFLJ interacts with the aflatoxin pathway-specific regulator AFLR. *Mol. Genet. Genomics* **268**:711–9.

Chen G, Kayser MM, Mihovilovic MD, Mrstik ME, Martinez CA, Stewart JD. 1999. Asymmetric oxidations at sulfur catalyzed by engineered strains that overexpress cyclohexanone monooxygenase. *New J. Chem.* **23**:827–32.

Cheng Q, Thomas SM, Kostichka K, Valentine JR, Nagarajan V. 2000. Genetic analysis of a gene cluster for cyclohexanol oxidation in *Acinetobacter* sp. strain SE19 by in vitro transposition. *J. Bacteriol.* **182**:4744–51.

Colonna S, Gaggero N, Carrea G, Ottolina G, Pasta P, Zambianchi F. 2002. First asymmetric epoxidation catalysed by cyclohexanone monooxygenase. *Tetrahedron Lett.* **43**:1797–9.

Cotty PJ. 1994. Influence of field application of an atoxigenic strains of *Aspergillus flavus* on the populations of *A. flavus* infection cotton balls and on the aflatoxin content of cottonseed. *Phytopathology* **84**:1270–7.

Criegee R. 1948. Die umlagerung der dekalin-peroxydester als folge von kationischem sauerstoff. *Justus Liebigs Ann. Chem.* **560**:127–35.

Dong H, Nilsson L, Kurland CG. 1996. Co-variation of tRNA abundance and codon usage in *Escherichia coli* at different growth rates. *J. Mol. Biol.* **260**:649–63.

Donoghue NA, Norris DB, Trudgill PW. 1976. The purification and properties of cyclohexanone oxygenase from *Nocardia globerula* CL1 and *Acinetobacter* NCIB 9871. *Eur. J. Biochem.* **63**:175–92.

Dowd PF. 2003. Insect management to facilitate preharvest mycotoxin management. *Toxin Rev.* **22**:27–350.

Du W, Obrian GR, Payne GA. 2007. Function and regulation of *aflJ* in the accumulation of aflatoxin early pathway intermediate in *Aspergillus flavus*. *Food Addit. Contam.* **24**:1043–50.

Dutton MF. 1988. Enzymes and aflatoxin biosynthesis. *Microbiol. Rev.* **52**:74–295.

Edgar RC. 2004. MUSCLE: multiple sequence alignment with high accuracy and high throughput. *Nucleic Acids Res.* **32**:1792–7.

Ehrlich KC, Montalbano BG, Cary JW. 1999. Binding of the C6-zinc cluster protein, AFLR, to the promoters of aflatoxin pathway biosynthesis genes in *Aspergillus parasiticus*. *Gene* **230**:249–57.

Ehrlich KC. 2009. Predicted roles of the uncharacterized clustered genes in aflatoxin biosynthesis. *Toxins* **1**:37–58.

Ehrlich KC, Chang PK, Yu J, Cotty PJ. 2004. Aflatoxin biosynthesis cluster gene *cypA* is required for G aflatoxin formation. *Appl. Environ. Microbiol.* **70**:6518–24.

Ehrlich KC, Li P, Scharfenstein L, Chang PK. 2010. HypC, the anthrone oxidase involved in aflatoxin biosynthesis. *Appl. Environ. Microbiol.* **76**:3374–7.

Ehrlich KC, Montalbano B, Boué SM, Bhatnagar D. 2005. An aflatoxin biosynthesis cluster gene encodes a novel oxidase required for conversion of versicolorin A to sterigmatocystin. *Appl. Environ. Microbiol.* **71**:8963–5.

Ehrlich KC, Montalbano BG, Bhatnagar D, Cleveland TE. 1998. Alteration of different domains in AFLR affects aflatoxin pathway metabolism in *Aspergillus parasiticus* transformants. *Fungal Genet. Biol.* **23**:279–87.

Ehrlich KC, Scharfenstein LL, Montalbano BG, Chang PK. 2008. Are the genes *nadA* and *norB* involved in formation of aflatoxin G_1? *Int. J. Mol. Sci.* **9**:1717–29.

English AR, McBride TJ, Lynch JE. 1957. PA 132, a new antibiotic. II. *In vitro* and *in vivo* studies. *Antibiot. Annu*.682–7.

Fairbanks G, Steck TL, Wallach DFH. 1971. Electrophoretic analysis of the major polypeptides of the human erythrocyte membrane. *Biochemistry* **10**:2606–17.

Feng GH, Leonard TJ. 1995. Characterization of the polyketide synthase gene (*pksL1*) required for aflatoxin biosynthesis in *Aspergillus parasiticus*. *J. Bacteriol.* **177**:6246–54.

Fernandes M, Keller NP, Adams TH. 1998. Sequence-specific binding by *Aspergillus nidulans* AflR, a C6 zinc cluster protein regulating mycotoxin biosynthesis. *Mol. Microbiol.* **28**:1355–65.

Fischer C, Lipata F, Rohr J. 2003. The complete gene cluster of the antitumor agent gilvocarcin V and its implication for the biosynthesis of the gilvocarcins. *J. Am. Chem. Soc.* **125**:7818–9.

Fraaije MW, Wu J, Heuts DPHM, van Hellemond EW, Spelberg JHL, Janssen DB. 2005. Discovery of a thermostable Baeyer-Villiger monooxygenase by genome mining. *Appl. Microbiol. Biotechnol.* **66**:393–400.

Fraaije MW, Kamerbeek NM, van Berkel WJH, Janssen DB. 2002. Identification of a Baeyer–Villiger monooxygenase sequence motif. *FEBS Lett.* **518**:43–7.

Fried J, Thoma RW, Klingsberg A. 1953. Oxidation of steroids by microorganisms. III. Side-chain degradation, ring D-cleavage and dehydrogenation in ring A. *J. Am. Chem. Soc.* **75**:5764–5.

Frisvad JC, Samson RA, Smedsgaard J. 2004. *Emericella astellata*, a new producer of aflatoxin B_1, B_2 and sterigmatocystin. *Lett. Appl. Microbiol.* **38**:440–5.

Frisvad JC, Samson RA. 2004. *Emericella venezuelensis*, a new species with stellate ascospores producing sterigmatocystin and aflatoxin B_1. *Syst. Appl. Microbiol.* **27**:672–80.

Frisvad JC, Skouboe P, Samson RA. 2005. Taxonomic comparison of three different groups of aflatoxin producers and a new efficient producer of aflatoxin B_1, sterigmatocystin and 3-*O*-methylsterigmatocystin, *Aspergillus rambellii* sp. nov. *Syst. Appl. Microbiol.* **28**:442–53.

Gaberc-Porekar V, Menart V. 2001. Perspectives of immobilized-metal affinity chromatography. *J. Biochem. Biophys. Methods* **49**:335–60.

Galvano F, Galofaro V, Galvano G. 1996. Occurrence and stability of aflatoxin M_1 in milk and milk products: a worldwide review. *J. Food Prot.* **59**:1079–90.

Gibson M, Nur-e-alam M, Lipata F, Oliveira MA, Rohr J. 2005. Characterization of kinetics and products of the Baeyer-Villiger oxygenase MtmOIV, the key enzyme of the biosynthetic pathway toward the natural product anticancer drug mithramycin from *Streptomyces argillaceus*. *J. Am. Chem. Soc.* **127**:17594–5.

Goldman E, Rosenberg AH, Zubay G, Studier FW. 1995. Consecutive low-usage leucine codons block translation only when near the 5' end of a message in *Escherichia coli*. *J. Mol. Biol.* **245**:467–73.

Gong YY, Cardwell K, Hounsa A, Egal S, Turner PC, Hall AJ, Wild CP. 2002. Dietary aflatoxin exposure and impaired growth in young children from Benin and Togo: cross sectional study. *BMJ* **325**:20–1.

Gorman DP, Kang MS. 1991. Preharvest aflatoxin contamination in maize: resistance and genetics. *Plant Breed.* **107**:1–10.

Griffin M, Trudgill PW. 1976. Purification and properties of cyclopentanone oxygenase of *Pseudomonas* NCIB 9872. *Eur. J. Biochem.* **63**:199–209.

Hage DS. 1999. Affinity chromatography: a review of clinical applications. *Clin. Chem.* **45**:593–615.

Hammond SM, Boettcher S, Caudy AA, Kobayashi R, Hannon GJ. 2001. Argonaute2, a link between genetic and biochemical analyses of RNAi. *Science* **293**:1146–50.

Hammond TM, Keller NP. 2005. RNA silencing in *Aspergillus nidulans* is independent of RNA-dependent RNA polymerases. *Genetics* **169**:607–17.

Hedayati MT, Pasqualotto AC, Warn PA, Bowyer P, Denning DW. 2007. *Aspergillus flavus*: human pathogen, allergen and mycotoxin producer. *Microbiology* **153**:1677–92.

Henneberry TJ, Bariola LA, Russell T. 1978. Pink bollworm: chemical control in Arizona and the relationship to infestations, lint yield, seed damage and aflatoxin in cotton seed. *J. Econ. Entomol.* **71**:440–2.

Henry KM, Townsend CA. 2005. Ordering the reductive and cytochrome P450 oxidative steps in demethylsterigmatocystin formation yields general insights into the biosynthesis of aflatoxin and related fungal metabolites. *J. Am. Chem. Soc.* **127**:3724–33.

Hitchman TS, Schmidt EW, Trail F, Rarick MD, Linz JE, Townsend CA. 2001. Hexanoate synthase, a specialized type I fatty acid synthase in aflatoxin B_1 biosynthesis. *Bioorg. Chem.* **29**:293–307.

International Agency for Research on Cancer (IARC). 2002. The evaluation of carcinogenic risks to humans: traditional herbal medicines, some mycotoxins, napthalene and styrene. IARC Monograph volume 82. Lyon: IARC p 171-300.

Iwaki H, Hasegawa Y, Wang S, Kayser MM, Lau PCK. 2002. Cloning and characterization of a gene cluster involved in cyclopentanol metabolism in *Comamonas* sp. strain NCIMB 9872 and biotransformations effected by *Escherichia coli*-expressed cyclopentanone 1,2-monooxygenase. *Appl. Environ. Microbiol.* **68**:5671–84.

Jablonski E, DeLuca M. 1977. Purification and properties of the NADH and NADPH specific FMN oxidoreductases from *Beneckea harveyi*. *Biochemistry* **16**:2932–6.

Jensen CN, Cartwright J, Ward J, Hart S, Turkenburg JP, Ali ST, Allen MJ, Grogan G. 2012. A flavoprotein monooxygenase that catalyses a Baeyer-Villiger reaction and thioether oxidation using NADH as the nicotinamide cofactor. *Chembiochem* **13**:872–8.

Jia XY, Tian ZH, Shao L, Qu XD, Zhao QF, Tang J, Tang GL, Liu W. 2006. Genetic characterization of the chlorothricin gene cluster as a model for spirotetronate antibiotic biosynthesis. *Chem. Biol.* **13**:575–85.

Jiang J, Tetzlaff CN, Takamatsu S, Iwatsuki M, Komatsu M, Ikeda H, Cane DE. 2009. Genome mining in *Streptomyces avermitilis*: a biochemical Baeyer-Villiger reaction and discovery of a new branch of the pentalenolactone family tree. *Biochemistry* **48**:6431–40.

Kamerbeek NM, Moonen MJH, van der Ven JGM, van Berkel WJH, Fraaije MW, Janssen DB. 2001. 4-Hydroxyacetophenone monooxygenase from *Pseudomonas fluorescens* ACB. *Eur. J. Biochem.* **268**:2547–57.

Kamerbeek NM, Janssen DB, van Berkel WJH, Fraaije MW. 2003. Baeyer–Villiger monooxygenases, an emerging family of flavin-dependent biocatalysts. *Adv. Synth. Catal.* **345**:667–8.

Kane JF. 1995. Effects of rare codon clusters on high-level expression of heterologous proteins in *Escherichia coli*. *Curr. Opin. Biotechnol.* **6**:494–500.

Keeling PJ. 2009. Functional and ecological impacts of horizontal gene transfer in eukaryotes. *Curr. Opin. Genet. Dev.* **19**:613–9.

Kelkar HS, Skloss TW, Haw JF, Keller NP, Adams TH. 1997. *Aspergillus nidulans stcL* encodes a putative cytochrome P-450 monooxygenase required for bisfuran desaturation during aflatoxin/sterigmatocystin biosynthesis. *J. Biol. Chem.* **272**:1589–94.

Kelkar HS, Keller NP, Adams TH. 1996. *Aspergillus nidulans stcP* encodes an *O*-methyltransferase that is required for sterigmatocystin biosynthesis. *Appl. Environ. Microbiol.* **62**:4296–8.

Keller NP, Segner S, Bhatnagar D, Adams TH. 1995. *stcS*, a putative P-450 monooxygenase, is required for the conversion of versicolorin A to sterigmatocystin in *Aspergillus nidulans*. *Appl. Environ. Microbiol.* **61**:3628–32.

Keller NP, Kantz NJ, Adams TH. 1994. *Aspergillus nidulans verA* is required for production of the mycotoxin sterigmatocystin. *Appl. Environ. Microbiol.* **60**:1444–50.

Keller NP, Watanabe CM, Kelkar HS, Adams TH, Townsend CA. 2000. Requirement of monooxygenase-mediated steps for sterigmatocystin biosynthesis by *Aspergillus nidulans*. *Appl. Environ. Microbiol.* **66**:359–62.

Kharel MK, Zhu L, Liu T, Rohr J. 2007. Multi-oxygenase complexes of the gilvocarcin and jadomycin biosyntheses. *J. Am. Chem. Soc.* **129**:3780–1.

Klich MA. 2007. *Aspergillus flavus*: the major producer of aflatoxin. *Mol. Plant Pathol.* **8**:713–22.

Klich MA, Cary JW, Beltz SB, Bennett CA. 2003. Phylogenetic and morphological analysis of *Aspergillus ochraceoroseus*. *Mycologia* **95**:1252–60.

Kostichka K, Thomas SM, Gibson KJ, Nagarajan V, Cheng Q. 2001. Cloning and characterization of a gene cluster for cyclododecanone oxidation in *Rhodococcus ruber* SC1. *J. Bacteriol.* **183**:6478–86.

Kurland C, Gallant J. 1996. Errors of heterologous protein expression. *Curr. Opin. Biotechnol.* **7**:489–93.

Laemmli UK. 1970. Cleavage of structural proteins during the assembly of the head of bacteriophage T4. *Nature* **227**:680–5.

Lee L, Chiou C, Linz JE. 2002. Function of native OmtA *in vivo* and expression and distribution of this protein in colonies of *Aspergillus parasiticus*. *Appl. Environ. Microbiol.* **68**:5718–27.

Leisch H, Morley K, Lau PCK. 2011. Baeyer-Villiger monooxygenases: more than just green chemistry. *Chem. Rev.* **111**:4165–222.

Liang SH, Skory CD, Linz JE. 1996. Characterization of the function of the *ver-1A* and *ver-1B* genes, involved in aflatoxin biosynthesis in *Aspergillus parasiticus*. *Appl. Environ. Microbiol.* **62**:4568–75.

Ma L, van der Does HC, Borkovich KA, Coleman JJ, Daboussi M, Di Pietro A, Dufresne M, Freitag M, Grabherr M, Henrissat B, Houterman PM, Kang S, Shim W, Woloshuk C, Xie X, Xu JR, Antoniw J, Baker SE, Bluhm BH, Breakspear A, Brown DW, Butchko RAE, Chapman S, Coulson R, Coutinho PM, Danchin EGJ, Diener A, Gale LR, Gardiner DM, Goff S, Hammond-Kosack KE, Hilburn K, Hua-Van A, Jonkers W, Kazan K, Kodira CD, Koehrsen M, Kumar L, Lee YH, Li L, Manners JM, Miranda-Saavedra D, Mukherjee M, Park G, Park J, Park S, Proctor RH, Regev A, Ruiz-Roldan MC, Sain D, Sakthikumar S, Sykes S, Schwartz DC, Turgeon BG, Wapinski I, Yoder O, Young S, Zeng Q, Zhou S, Galagan J, Cuomo CA, Kistler HC, Rep M. 2010. Comparative genomics reveals mobile pathogenicity chromosomes in *Fusarium*. *Nature* **464**:367–73.

Mahanti N, Bhatnagar D, Cary JW, Joubran J, Linz JE. 1996. Structure and function of *fas-1A*, a gene encoding a putative fatty acid synthetase directly involved in aflatoxin biosynthesis in *Aspergillus parasiticus*. *Appl. Environ. Microbiol.* **62**:191–5.

Malito E, Alfieri A, Fraaije MW, Mattevi A. 2004. Crystal structure of a Baeyer-Villiger monooxygenase. *Proc. Natl. Acad. Sci. U. S. A.* **101**:13157–62.

Mascotti ML, Ayub MJ, Dudek H, Sanz MK, Fraaije MW. 2013. Cloning, overexpression and biocatalytic exploration of a novel Baeyer-Villiger monooxygenase from *Aspergillus fumigatus* Af293. *AMB Express* **3**:33.

Matasyoh JC, Dittrich B, Schueffler A, Laatsch H. 2011. Larvicidal activity of metabolites from the endophytic *Podospora* sp. against the malaria vector *Anopheles gambiae*. *Parasitol. Res.* **108**:561–6.

Matsushima K, Ando Y, Hamasaki T, Yabe K. 1994. Purification and characterization of two versiconal hemiacetal acetate reductases involved in aflatoxin biosynthesis. *Appl. Environ. Microbiol.* **60**:2561–7.

Mazzini C, Lebreton J, Furstoss R. 1996. Flavin-catalyzed Baeyer-Villiger reaction of ketones: oxidation of cyclobutanones to γ lactones using hydrogen peroxide. *J. Org. Chem. Soc.* **61**:8–9.

McCormick SP, Bhatnagar D, Lee LS. 1987. Averufanin is an aflatoxin B_1 precursor between averantin and averufin in the biosynthetic pathway. *Appl. Environ. Microbiol.* **53**:14–6.

McDonald T, Brown D, Keller NP, Hammond TM. 2005. RNA silencing of mycotoxin production in *Aspergillus* and *Fusarium* species. *Mol. Plant. Microbe. Interact.* **18**:539–45.

McGee DC. 1996. Populations of *Aspergillus flavus* in the Iowa cornfield ecosystem in years not favorable for aflatoxin contamination of corn grain. *Plant Dis.* **80**:742-6.

Menkir A, Brown RL, Bandyopadhyay R, Chen ZY, Cleveland TE. 2006. A USA-Africa collaborative strategy for identifying, characterizing, and developing maize germplasm with resistance to aflatoxin contamination. *Mycopathologia* **162**:225–32.

Meyers DM, Obrian G, Du WL, Bhatnagar D, Payne GA. 1998. Characterization of *aflJ*, a gene required for conversion of pathway intermediates to aflatoxin. *Appl. Environ. Microbiol.* **64**:3713–7.

Mihovilovic MD, Rudroff F, Grötzl B, Kapitan P, Snajdrova R, Rydz J, Mach R. 2005. Family clustering of Baeyer-Villiger monooxygenases based on protein sequence and stereopreference. *Angew. Chem. Int. Ed. Engl.* **44**:3609–13.

Mirza IA, Yachnin BJ, Wang S, Grosse S, Bergeron H, Imura A, Iwaki H, Hasegawa Y, Lau PCK, Berghuis AM. 2009. Crystal structures of cyclohexanone monooxygenase reveal complex domain movements and a sliding cofactor. *J. Am. Chem. Soc.* **131**:8848–54.

Mori S, Barth HG. 1999. Size exclusion chromatography. Berlin: Springer. 234 p.

Motomura M, Chihaya N, Shinozawa T, Hamasaki T, Yabe K. 1999. Cloning and characterization of the *O*-methyltransferase I gene (*dmtA*) from *Aspergillus parasiticus* associated with the conversions of demethylsterigmatocystin to sterigmatocystin and dihydrodemethylsterigmatocystin to dihydrosterigmatocystin in aflatoxin. *Appl. Environ. Microbiol.* **65**:4987–94.

Munkvold GP. 2003. Cultural and genetic approaches to managing mycotoxins in maize. *Annu. Rev. Phytopathol.* **41**:99–116.

Ottolina G, Bianchi S, Belloni B, Carrea G, Danieli B. 1999. First asymmetric oxidation of tertiary amines by cyclohexanone monooxygenase. *Tetrahedron Lett.* **40**:8483–6.

Pao SS, Paulsen IT, Saier MH. 1998. Major facilitator superfamily. *Microbiol. Mol. Biol. Rev.* **62**:1–34.

Payne GA, Nystrom GJ, Bhatnagar D, Cleveland TE, Woloshuk CP. 1993. Cloning of the *afl-2* gene involved in aflatoxin biosynthesis from *Aspergillus flavus*. *Appl. Environ. Microbiol.* **59**:156–62.

Pazmiño DET, Fraaije MW. 2007. Discovery, redesign and applications of Baeyer-Villiger monooxygenases. In: Matsuda T, editor. Future directions in biocatalysis. Amsterdam: Elsevier Sciences. p 107-28.

Peterson SW, Ito Y, Horn BW, Goto T. 2001. *Aspergillus bombycis*, a new aflatoxigenic species and genetic variation in its sibling species, *A. nomius*. *Mycologica* **93**:689–703.

Pitt JI, Hocking AD. 2006. Mycotoxins in Australia: biocontrol of aflatoxin in peanuts. *Mycopathologia* **162**:233–43.

Price MS, Yu J, Nierman WC, Kim HS, Pritchard B, Jacobus CA, Bhatnagar D, Cleveland TE, Payne GA. 2006. The aflatoxin pathway regulator AflR induces gene transcription inside and outside of the aflatoxin biosynthetic cluster. *FEMS Microbiol. Lett.* **255**:275–9.

Prieto R, Woloshuk CP. 1997. *ord1*, an oxidoreductase gene responsible for conversion of *O*-methylsterigmatocystin to aflatoxin in *Aspergillus flavus*. *Appl. Environ. Microbiol.* **63**:1661–6.

Prieto R, Yousibova GL, Woloshuk CP. 1996. Identification of aflatoxin biosynthesis genes by genetic complementation in an *Aspergillus flavus* mutant lacking the aflatoxin gene cluster. *Appl. Environ. Microbiol.* **62**:3567–71.

Rebehmed J, Alphand V, de Berardinis V, de Brevern AG. 2013. Evolution study of the Baeyer-Villiger monooxygenases enzyme family: functional importance of the highly conserved residues. *Biochimie* **95**:1394–402.

Renz M, Meunier B. 1999. 100 years of Baeyer–Villiger oxidations. *European J. Org. Chem.* **1999**:737–50.

Romeis J, Meissle M, Bigler F. 2006. Transgenic crops expressing *Bacillus thuringiensis* toxins and biological control. *Nat. Biotechnol.* **24**:63–71.

Sakuno E, Wen Y, Hatabayashi H, Arai H, Aoki C, Yabe K, Nakajima H. 2005. *Aspergillus parasiticus* cyclase catalyzes two dehydration steps in aflatoxin biosynthesis. *Appl. Environ. Microbiol.* **71**:2999–3006.

Sakuno E, Yabe K, Nakajima H. 2003. Involvement of two cytosolic enzymes and a novel intermediate, 5'-oxoaverantin, in the pathway from 5'-hydroxyaverantin to averufin in aflatoxin biosynthesis. *Appl. Environ. Microbiol.* **69**:6418–26.

Schroeder HW, Kelton WH. 1975. Production of sterigmatocystin by some species of the genus *Aspergillus* and its toxicity to chicken embryos. *Appl. Microbiol.* **30**:589–91.

Sheng D, Ballou DP, Massey V. 2001. Mechanistic studies of cyclohexanone monooxygenase: chemical properties of intermediates involved in catalysis. *Biochemistry* **40**:11156–67.

Shima Y, Shiina M, Shinozawa T, Ito Y, Nakajima H, Adachi Y, Yabe K. 2009. Participation in aflatoxin biosynthesis by a reductase enzyme encoded by *vrdA* gene outside the aflatoxin gene cluster. *Fungal Genet. Biol.* **46**:221–31.

Silva JC, Minto RE, Barry CE, Holland KA, Townsend CA. 1996. Isolation and characterization of the versicolorin B synthase gene from *Aspergillus parasiticus*. Expansion of the aflatoxin B_1 biosynthetic gene cluster. *J. Biol. Chem.* **271**:13600–8.

Silva JC, Townsend CA. 1997. Heterologous expression, isolation, and characterization of versicolorin B synthase from *Aspergillus parasiticus*. A key enzyme in the aflatoxin B_1 biosynthetic pathway. *J. Biol. Chem.* **272**:804–13.

Skory CD, Chang PK, Cary J, Linz JE. 1992. Isolation and characterization of a gene from *Aspergillus parasiticus* associated with the conversion of versicolorin A to sterigmatocystin in aflatoxin biosynthesis. *Appl. Environ. Microbiol.* **58**:3527–37.

Slot JC, Rokas A. 2011. Horizontal transfer of a large and highly toxic secondary metabolic gene cluster between fungi. *Curr. Biol.* **21**:134–9.

Smith PK, Krohn RI, Hermanson GT, Mallia AK, Gartner FH, Provenzano MD, Fujimoto EK, Goeke NM, Olson BJ, Klenk DC. 1985. Measurement of protein using bicinchoninic acid. *Anal. Biochem.* **150**:76–85.

South African Medical Research Council. 2009. Guidelines on mycotoxin control in South African foodstuffs: From the application of the Hazard Analysis and Critical Control Point (HACCP) systems to new national mycotoxin regulations. MRC policy brief October 2009. MRC: Tygerberg p 1-2.

Squire RA. 1981. Ranking animal carcinogens: a proposed regulatory approach. *Science* **214**:877–80.

Strukul G. 1998. Transition metal catalysis in the Baeyer-Villiger oxidation of ketones. *Angew. Chemie Int. Ed.* **37**:1198–209.

Studier FW. 2005. Protein production by auto-induction in high-density shaking cultures. *Protein Expr. Purif.* **41**:207–34.

Tamura K, Peterson D, Peterson N, Stecher G, Nei M, Kumar S. 2011. MEGA5: molecular evolutionary genetics analysis using maximum likelihood, evolutionary distance, and maximum parsimony methods. *Mol. Biol. Evol.* **28**:2731–9.

Ten Brink GJ, Arends IWCE, Sheldon RA. 2004. The Baeyer-Villiger reaction: new developments toward greener procedures. *Chem. Rev.* **104**:4105–24.

Thomas JG, Ayling A, Baneyx F. 1997. Molecular chaperones, folding catalysts, and the recovery of active recombinant proteins from *E. coli*. *Appl. Biochem. Biotechnol.* **66**:197–238.

Tibrewal N, Pahari P, Wang G, Kharel MK, Morris C, Downey T, Hou Y, Bugni TS, Rohr J. 2012. Baeyer-Villiger C-C bond cleavage reaction in gilvocarcin and jadomycin biosynthesis. *J. Am. Chem. Soc.* **134**:18181–4.

Townsend CA., Christensen SB, Trautwein K. 1984. Hexanoate as a starter unit in polyketide biosynthesis. *J. Am. Chem. Soc.* **106**:3868–9.

Townsend CA, Plavcan KA, Pal K, Brobst SW, Irish MS, Ely EW, Bennett JW. 1988. Hydroxyversicolorone: isolation and characterization of a potential intermediate in aflatoxin biosynthesis. *J. Org. Chem.* **53**:2472–7.

Trail F, Chang PK, Cary J, Linz JE. 1994. Structural and functional analysis of the *nor-1* gene involved in the biosynthesis of aflatoxins by *Aspergillus parasiticus*. *Appl. Environ. Microbiol.* **60**:4078–85.

Turner PC, Mendy M, Whittle H, Fortuin M, Hall AJ, Wild CP. 2000. Hepatitis B infection and aflatoxin biomarker levels in Gambian children. *Trop. Med. Int. Health* **5**:837–41.

Udwary DW, Casillas LK, Townsend CA. 2002. Synthesis of 11-hydroxyl *O*-methylsterigmatocystin and the role of a cytochrome P-450 in the final step of aflatoxin biosynthesis. *J. Am. Chem. Soc.* **124**:5294–303.

Van Berkel WJH, Kamerbeek NM, Fraaije MW. 2006. Flavoprotein monooxygenases, a diverse class of oxidative biocatalysts. *J. Biotechnol.* **124**:670–89.

Wagacha JM, Muthomi JW. 2008. Mycotoxin problem in Africa: current status, implications to food safety and health and possible management strategies. *Int. J. Food Microbiol.* **124**:1–12.

Walker J. 2010. Protein structure, purification, characterisation and function analysis. In: Walker J. and Wilson K, editors. Principles and techniques of biochemistry and molecular biology. Cambridge: Cambridge University Press. p 300-351.

Walsh CT, Chen YCJ. 1988. Enzymic Baeyer-Villiger oxidations by flavin-dependent monooxygenases. *Angew. Chemie Int. Ed. English* **27**:333–43.

Wang P, Afriyie-Gyawu E, Tang Y, Johnson NM, Xu L, Tang L, Huebner HJ, Ankrah N, Ofori-Adjei D, Ellis W, Jolly PE, Williams JH, Wang JS, Phillips TD. 2008. NovaSil clay intervention in Ghanaians at high risk for aflatoxicosis: II. Reduction in biomarkers of aflatoxin exposure in blood and urine. *Food Addit. Contam. Part A. Chem. Anal. Control. Expo. Risk Assess.* **25**:622–34.

Watanabe CM, Wilson D, Linz JE, Townsend CA. 1996. Demonstration of the catalytic roles and evidence for the physical association of type I fatty acid synthases and a polyketide synthase in the biosynthesis of aflatoxin B_1. *Chem. Biol.* **3**:463–9.

Waterhouse AM, Procter JB, Martin DMA, Clamp M, Barton GJ. 2009. Jalview Version 2 - a multiple sequence alignment editor and analysis workbench. *Bioinformatics* **25**:1189–91.

Wen Y, Hatabayashi H, Arai H, Kitamoto HK, Yabe K. 2005. Function of the *cypX* and *moxY* genes in aflatoxin biosynthesis in *Aspergillus parasiticus*. *Appl. Environ. Microbiol.* **71**:3192–8.

Whelan S, Goldman N. 2001. A general empirical model of protein evolution derived from multiple protein families using a maximum-likelihood approach. *Mol. Biol. Evol.* **18**:691–9.

Wild CP, Turner PC. 2002. The toxicology of aflatoxins as a basis for public health decisions. *Mutagenesis* **17**:471–81.

Willetts A. 1997. Structural studies and synthetic applications of Baeyer-Villiger monooxygenases. *Trends Biotechnol.* **15**:55–62.

Williams JH, Phillips TD, Jolly PE, Stiles JK, Jolly CM, Aggarwal D. 2004. Human aflatoxicosis in developing countries: a review of toxicology, exposure, potential health consequences, and interventions. *Am. J. Clin. Nutr.* **80**:1106–22.

Wogan GN, Edwards GS, Newberne PM. 1971. Structure-activity relationships in toxicity and carcinogenicity of aflatoxins and analogs. *Cancer Res.* **31**:1936–42.

Woloshuk CP, Foutz KR, Brewer JF, Bhatnagar D, Cleveland TE, Payne GA. 1994. Molecular characterization of *aflR*, a regulatory locus for aflatoxin biosynthesis. *Appl. Environ. Microbiol.* **60**:2408–14.

Woloshuk CP, Shim WB. 2013. Aflatoxins, fumonisins, and trichothecenes: a convergence of knowledge. *FEMS Microbiol. Rev.* **37**:94–109.

Wu F. 2006. Mycotoxin reduction in Bt corn: potential economic, health, and regulatory impacts. *Transgenic Res.* **15**:277–89.

Yabe K, Ando Y, Hamasaki T. 1991a. A metabolic grid among versiconal hemiacetal acetate, versiconol acetate, versiconol and versiconal during aflatoxin biosynthesis. *J. Gen. Microbiol.* **137**:2469–75.

Yabe K, Ando Y, Hashimoto J, Hamasaki T. 1989. Two distinct *O*-methyltransferases in aflatoxin biosynthesis. *Appl. Environ. Microbiol.* **55**:2172–7.

Yabe K, Chihaya N, Hamamatsu S, Sakuno E, Hamasaki T, Nakajima H, Bennett JW. 2003. Enzymatic conversion of averufin to hydroxyversicolorone and elucidation of a novel metabolic grid involved in aflatoxin biosynthesis. *Appl. Environ. Microbiol.* **69**:66–73.

Yabe K, Hamasaki T. 1993. Stereochemistry during aflatoxin biosynthesis: cyclase reaction in the conversion of versiconal to versicolorin B and racemization of versiconal hemiacetal acetate. *Appl. Environ. Microbiol.* **59**:2493–500.

Yabe K, Matsushima K, Koyama T, Hamasaki T. 1998. Purification and characterization of *O*-methyltransferase I involved in conversion of demethylsterigmatocystin to sterigmatocystin and of dihydrodemethylsterigmatocystin to dihydrosterigmatocystin during aflatoxin biosynthesis. *Appl. Environ. Microbiol.* **64**:166–71.

Yabe K, Matsuyama Y, Ando Y, Nakajima H, Hamasaki T. 1993. Stereochemistry during aflatoxin biosynthesis: conversion of norsolorinic acid to averufin. *Appl. Environ. Microbiol.* **59**:2486–92.

Yabe K, Nakajima H. 2004. Enzyme reactions and genes in aflatoxin biosynthesis. *Appl. Microbiol. Biotechnol.* **64**:745–55.

Yabe K, Nakamura M, Hamasaki T. 1999. Enzymatic formation of G-group aflatoxins and biosynthetic relationship between G- and B-group aflatoxins. *Appl. Environ. Microbiol.* **65**:3867–72.

Yabe K, Nakamura Y, Nakajima H, Ando Y, Hamasaki T. 1991b. Enzymatic conversion of norsolorinic acid to averufin in aflatoxin biosynthesis. *Appl. Environ. Microbiol.* **57**:1340–5.

Yao RC, Hsieh DPH. 1974. Step of dichlorvos inhibition in the pathway of aflatoxin biosynthesis. *Appl. Microbiol.* **28**:52–7.

Yu J, Butchko RA, Fernandes M, Keller NP, Leonard TJ, Adams TH. 1996. Conservation of structure and function of the aflatoxin regulatory gene *aflR* from *Aspergillus nidulans* and *A. flavus*. *Curr. Genet.* **29**:549–55.

Yu J, Cary JW, Bhatnagar D, Cleveland TE, Keller NP, Chu FS. 1993. Cloning and characterization of a cDNA from *Aspergillus parasiticus* encoding an *O*-methyltransferase involved in aflatoxin biosynthesis. *Appl. Environ. Microbiol.* **59**:3564–71.

Yu J, Chang PK, Bhatnagar D, Cleveland TE. 2000a. Cloning of a sugar utilization gene cluster in *Aspergillus parasiticus*. *Biochim. Biophys. Acta* **1493**:211–4.

Yu J, Chang PK, Bhatnagar D, Cleveland TE. 2000b. Genes encoding cytochrome P450 and monooxygenase enzymes define one end of the aflatoxin pathway gene cluster in *Aspergillus parasiticus*. *Appl. Microbiol. Biotechnol.* **53**:583–90.

Yu J, Chang PK, Bhatnagar D, Cleveland TE. 2002. Cloning and functional expression of an esterase gene in *Aspergillus parasitcus*. *Mycopathologia* **156**:227–34.

Yu J, Chang PK, Cary JW, Bhatnagar D, Cleveland TE. 1997. *avnA*, a gene encoding a cytochrome P-450 monooxygenase, is involved in the conversion of averantin to averufin in aflatoxin biosynthesis in *Aspergillus parasiticus*. *Appl. Environ. Microbiol.* **63**:1349–56.

Yu J, Chang PK, Cary JW, Wright M, Bhatnagar D, Cleveland TE, Payne GA, Linz JE. 1995. Comparative mapping of aflatoxin pathway gene clusters in *Aspergillus parasiticus* and *Aspergillus flavus*. *Appl. Environ. Microbiol.* **61**:2365–71.

Yu J, Chang PK, Ehrlich KC, Cary JW, Bhatnagar D, Cleveland TE, Payne GA, Linz JE, Woloshuk CP, Bennett JW. 2004. Clustered pathway genes in aflatoxin biosynthesis. *Appl. Environ. Microbiol.* **70**:1253–62.

Yu J, Chang PK, Ehrlich KC, Cary JW, Montalbano B, Dyer JM, Bhatnagar D, Cleveland TE. 1998. Characterization of the critical amino acids of an *Aspergillus parasiticus* cytochrome P-450 monooxygenase encoded by *ordA* that is involved in the biosynthesis of aflatoxins B_1, G_1, B_2, and G_2. *Appl. Environ. Microbiol.* **64**:4834–41.

Yu J, Leonard TJ. 1995. Sterigmatocystin biosynthesis in *Aspergillus nidulans* requires a novel type I polyketide synthase. *J. Bacteriol.* **177**:4792–800.

Yu J, Woloshuk CP, Bhatnagar D, Cleveland TE. 2000c. Cloning and characterization of *avfA* and *omtB* genes involved in aflatoxin biosynthesis in three *Aspergillus* species. *Gene* **248**:157–67.

Zhou R, Linz JE. 1999. Enzymatic function of the Nor-1 protein in aflatoxin biosynthesis in *Aspergillus parasiticus. Appl. Environ. Microbiol.* **65**:5639-41.